NUMERICAL SIMULATION OF AN ENGLISH EQUESTRIAN SADDLETREE

Abdul-Hakeem .O. Noibi (MSc BSc)

A thesis submitted in partial fulfilment of the requirements of the University of Wolverhampton for the degree of Master of Philosophy

October 2011

This work or any part thereof has not previously been presented in any form to the University or to any other body whether for the purposes of assessment, publication or for any other purpose (unless otherwise indicated). Save for any express acknowledgments, references and/or bibliographies cited in the work, I confirm that the intellectual content of the work is the result of my own efforts and of no other person.

Signature ……

Date ……...

Dedicated to the memory of my parents

ABSTRACT

The manufacture of horse riding saddlery in the UK is centred in Walsall in the West Midlands. The local industry faces stiff competition from cheap imports in local markets and dwindling exports to international markets. To continue to provide affordable high end products, which the local industry is reputed for, it is essential to develop an understanding of the functional and performance requirements of the saddletree based on scientific and engineering methods thereby laying a foundation for a methodical approach to product development.

Through the measurement of surface data from a physical artefact, a 3 dimensional CAD geometrical replica of the English jumping saddletree was developed. Assumptions for the loading and boundary conditions identical to the user environment were obtained from available literature on the movements of the horseback, parameters for a jumping horse, saddletree test data, and, interface contact measurements acquired using a pressure mat. In addition, material properties data were obtained from available literature.

Nonlinear static numerical models were subsequently developed and parametric studies were performed to determine the relationship between the deformation of the saddletree and the bending loads. Furthermore, nonlinear transient dynamic numerical models were developed and parametric studies performed to determine the response of the pommel to impact loads.

The models were found to be sensitive to loading, material, and geometric

parameters. From cantilever tests, the stiffness of the saddletree was found to be between 3.63 N/mm and 4.68 N/mm, and the steel reinforcement plates increased the stiffness by a factor of up to 2.3 times. Simply supported, the stiffness of the saddletree was between 526.62 N/mm and 596.16 N/mm, and the steel reinforcement plates increased the stiffness by a factor of up to 5.5 times. In addition, the simply supported models were sensitive to the wood laminate stacking sequence. Furthermore, the dynamic models showed that the steel reinforcement plates dampened the oscillations in the pommel after impact with a rigid body at 7 m/s, 8.5 m/s, and 10 m/s.

The numerical cantilever models were validated with experimental data while interface pressure mat measurements validated interface contact stresses between the deformable bodies and the rigid body surfaces. Interface pressure mat results exhibited pressure hot spots and uneven load distributions underneath the saddletree. Peak and average pressures were 82.7 KPa and 15.4 KPa respectively, representing 16.2 % and 10.0 % error in comparison with the contact stresses obtained from the numerical models. Compression-flexure tests complemented the dynamic models. The steel reinforcement plates were observed to protect the pommel from delamination which was the principal failure mode of the wooden pommel; however, the reinforced pommel failed in flexure.

From the simulations and tests performed, it was evident that there is a stiffness mismatch between the saddletree and the horseback which is undesirable. In addition to this significant conclusion, it has been shown that the steel reinforcement plates have a significant effect on the stiffness of the saddletree and do not protect it from

failing. Hence, their continued use in the design and manufacturing of the English jumping saddletree is not recommended. Invaluable knowledge gained from the research allowed the definition of the performance attributes in a materials selection process ensuring the choice of potential material candidates to guarantee the optimal performance of the saddletree. Finally, the findings were incorporated in the development of a new concept design for next generation English saddletrees.

ACKNOWLEDGEMENT

I am sincerely grateful to Professor F. Richard Hall, whose invaluable contribution, encouragement, and support facilitated the development of my understanding of the subject. My appreciation also goes to Professor A. Pollard and Phil Wilson for their contribution; to the Centre of Engineering Excellence and the School of Technology (formerly known as SEBE) for providing some financial support for my research.

I am grateful to Julian Spence for providing the initial training on the use of the simulation software and his support in ensuring access to relevant software, and to the staff of MSC.Software for their support.

I would like to express my appreciation to Professor Kevin Kibble, Colin Durnall, and Kevin Worrall for their assistance in performing the laboratory experiments.

In addition, I wish to recognise Bob Wood at Loughborough University for his contribution at the conception of the research; Ian Rae at Lariot, Frank Baines at Frank Baines Saddlery, and, Duncan Kent at E. Jeffries & Sons Ltd for their support.

I am without a doubt grateful to my wife, children, brother, and sisters for their understanding and support. I recognise and appreciate their tolerance during this period.

Finally, I express my gratitude to all those who supported and encouraged me to complete this research study.

TABLE OF CONTENT

LIST OF FIGURES

LIST OF TABLES

NOMENCLATURE

Π_P (J)	Total potential energy
Π (J)	Strain energy
$\cup_e$ (J)	The elastic potential energy (or strain energy) $\cup_e = \frac{1}{2}\left(kx^2\right)$
ϕ_B^e	Shape factor for beams under elastic bending loads, $\phi_B^e = \frac{4\pi I}{A^2}$
A (m^2)	Area
a'_{n+1}	Estimate of acceleration at step $n + 1$
σ_L (Pa)	Stress in longitudinal direction
σ_T (Pa)	Stress in transverse direction
σ_{LT} (Pa)	Shear stress along longitudinal-transverse direction
σ_{LL}(Pa)	Stress in longitudinal direction
σ_{TT} (Pa)	Stress in transverse direction
σ_{LT} (Pa)	Shear stress along longitudinal-transverse direction
σ_f (Pa)	The flexural stress $\sigma_f = \frac{3Pl}{2bd^2}$
ρ (kg/m^3)	Density
δ_{max} (m)	The maximum deflection at the tip of a cantilever beam, $\delta_{max} = \frac{PL^3}{3E_f I_{yy}}$
υ_{LR}	Poisson's ratios longitudinal-radial plane
υ_{LT}	Poisson's ratios longitudinal-tangential plane
υ_{RT}	Poisson's ratios radial-tangential plane
υ_{21}	Poisson's ratios YX-axes

υ_{31}	Poisson's ratios ZX-axes
υ_{32}	Poisson's ratios ZY-axes
υ_{RL}	Poisson's ratios radial- longitudinal plane
υ_{TL}	Poisson's ratios tangential-longitudinal plane
υ_{TR}	Poisson's ratios tangential-radial plane
C	Damping matrix of the structure
d	Displacement parameters
d_{n+1}	Estimate of displacement at step $n + 1$
E_L (Pa)	Young's modulus longitudinal direction
E_R (Pa)	Young's modulus radial direction
E_T (Pa)	Young's modulus tangential direction
E_{11} (Pa)	Young's modulus X-axis
E_{22} (Pa)	Young's modulus Y-axis
E_{33} (Pa)	Young's modulus Z-axis
E_f (Pa)	Effective flexural modulus of the beam, $E_f = \frac{8}{h^3}\sum_{j=1}^{N/2}(E_x)_j\left(Z_j^3 - Z_{j-1}^3\right)$
f (N)	Applied load
F_n^{ext}	Vector of externally applied loads, the equation of motion for the explicit methods is, $F_n^{ext} = Ma_n + Cv_n + Kd_n$
F_{n+1}^{ext}	Vector of externally applied loads at step $n + 1$, the equation of motion for the implicit methods is, $F_{n+1}^{ext} = Ma_{n+1}^{'} + Cv_{n+1}^{'} + Kd_{n+1}$
$F_{n+1}^{residual}$	Vector of residual loads at step $n + 1$
F_n^{int}	Vector of internal loads
G_{LR} (Pa)	Shear modulus longitudinal-radial plane

G_{LT} (Pa)	Shear modulus longitudinal-tangential plane
G_{RT} (Pa)	Shear modulus radial-tangential plane
G_{12} (Pa)	Shear modulus XY-axes
G_{31} (Pa)	Shear modulus ZX-axes
G_{23} (Pa)	Shear modulus YZ-axes
I_{yy}	Moment of inertia about the neutral axis, $I_{yy} = \int z^2 dA = \frac{bh^3}{12}$
j	Number of ply
K	Stiffness matrix
$[K]d = f$	The governing equation for static problems derived from the principle of minimum potential energy
N	Total number of plies.
M	Mass matrix of the structure
m (kg)	Mass
mgh	Potential energy
$\frac{1}{2}mv^2$	Kinetic energy
v (m^3)	Volume
W_P	Work done
X_T (Pa)	Tensile strength parallel to the grain
X_C (Pa)	Compressive strength parallel to the grain
Y_T (Pa)	Tensile strength perpendicular to the grain
Y_C (Pa)	Compressive strength perpendicular to the grain
$S_{/\!/}$ (Pa)	Shear strength parallel to the grain
$S_{\perp}$ (Pa)	Shear strength perpendicular to the grain
t_{n+1} (s)	time of an explicit algorithm

T (s)	Impact time
Δt	Time step
v'_{n+1}	Estimate of velocity at step $n + 1$
x	Spring extension
Z (m)	Distance from the neutral surface

CHAPTER ONE

INTRODUCTION

1.1 BACKGROUND INFORMATION

Equestrianism has developed over many centuries (Evans, et al., 1990; Roe, et al., 2003; Wood and Newbold, 2004). Horse riding is a popular leisure activity (Carrillo, et al., 2007; Moss, et al., 2002; Roe, et al., 2003; Wood and Newbold, 2004); and, equestrian sports are to be found in most parts of the world (Balendra, et al., 2007; Iba, et al., 2001). The past century has seen an explosion in the popularity of equestrian sports (Back and Clayton, 2001). Overall participation, especially in terms of leisure riders is growing and anecdotal evidence suggests that there are more horse-owning leisure riders than ever before in Britain (Henley Centre, 2004).

The horse industry makes a valuable contribution to the economies of many countries. In the UK, it is said that the industry serves an estimated 1.4 million horses, and has a gross output of £ 3.4 billion (BHIC, 2005). Likewise, the horse industry in the United States of America is estimated to include 6.9 million horses and worth $25.3 billion (Malinowski and Luba, 2004). In Australia, the horse industry was estimated to have contributed over $ 6.3 billion to the GDP (Gordon, 2001).

Production within the horse industry encompasses a wide range of activities. The focus of this research is on an element of saddlery, which is a vital aspect of the horse industry (Henley Centre, 2004). Although horses can be ridden without tack, a saddle and stirrups provide extra support for the rider (Robinson, 2001). Historically,

the first improvement upon bareback riding was achieved with the horse-cloth (also referred to as a shabrack); this was to be later transformed by the saddle (Waterer, 1975). Although the early designs appear to have been adapted to satisfy the needs of the rider, saddle designs have evolved with the aim of distributing the rider's weight evenly on the horse's back (Robinson, 2001). Saddle designs have evolved over the past centuries into three basic designs: English, Western, and Australian, as well as a significant number of experimental designs (Liswaniso, 2001). There are three principal types of English saddle covering the major disciplines of dressage, eventing and arena jumping (Edwards, 1990). The jumping saddle was selected for this research.

1.2 THE SADDLETREE

The saddletree may be described as the framework on which a riding saddle is made (Hayes, 2008; BS 6635: 2003; BS 7875:1996; Synder-Smith and Bauer, 2006; Liswaniso, 2001; Swain, 2002; Beatie, 1981; Bayliss, 1958). It constitutes the internal "skeleton" of a saddle construction, giving the saddle both strength and flexibility (Belton, 2006). It provides the inherent stability for the saddle and contributes in giving the rider a stable seating position on the horse (Ness, 2006; Hitchen, 2006). In addition, the saddletree is meant to protect contact with the horse's spine, and to distribute the weight of the rider (Billington, 2006). The saddletree comprises three principal parts conveniently defined as the head (pommel section), cantle, and, the opposite side rails which connect the cantle and the head (Nicholls, 1935).

1.3 EVOLUTION OF THE SADDLETREE DESIGN

Evolution and change are inherent in the life of a product design (Palani Rajan, et al., 2005). Edwards (1990, 1994) suggested that the saddletree was introduced at the beginning of the Christian era. Its design has evolved mainly to the credit of horseback warriors, and craftsmen. During the early modern period, specifically the period from the mid-15th century to 1714, English saddles developed from medieval or sub-medieval designs into designs recognisable as the predecessor of the modern English riding saddle (Gilmour, 2004). A comparison between the saddletree used in modern English saddles and one used in English saddles as far back as 1740 may reflect the type of progression that occurred in the design of the product from its inception till date.

Figures 1.3.1 to 1.3.10 present some available illustrations of saddletrees used from the 11th century AD. Debatably, they express an idea of the design evolution of the product.

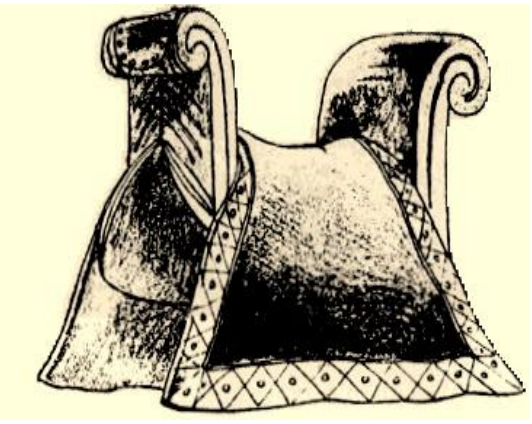

Figure 1.3.1 11th Century saddle (Source: Waterer, 1975)

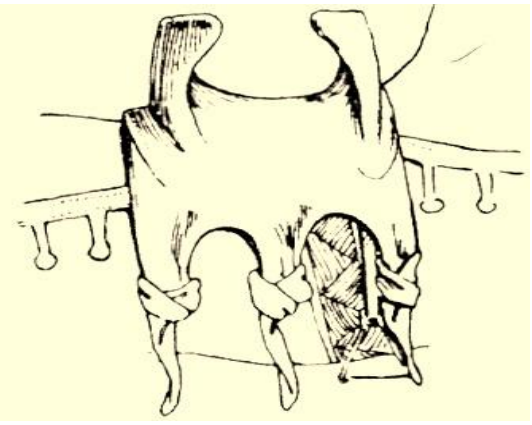

Figure 1.3.2 13th Century Jousting saddle (Source: Waterer, 1975)

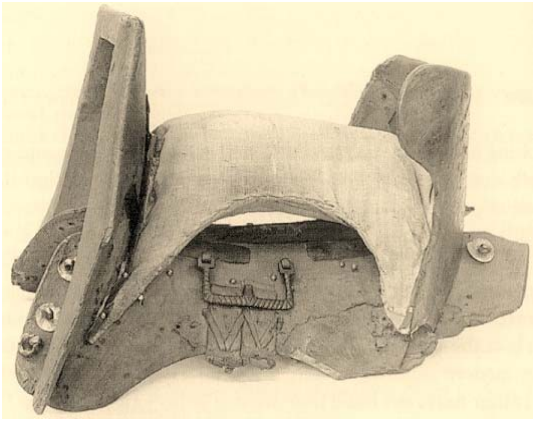

Figure 1.3.3 Saddletree reputed to have been carried at the funeral of Henry V in 1422 (Source: Waterer, 1975; Hickling in Gilmour, 2004)

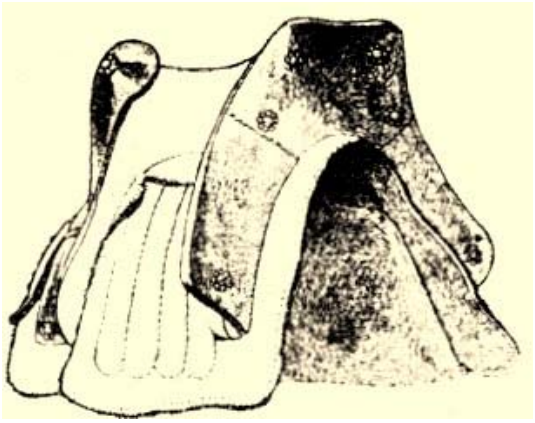

Figure 1.3.4 16th Century French Jousting Saddle (Source: Waterer, 1975)

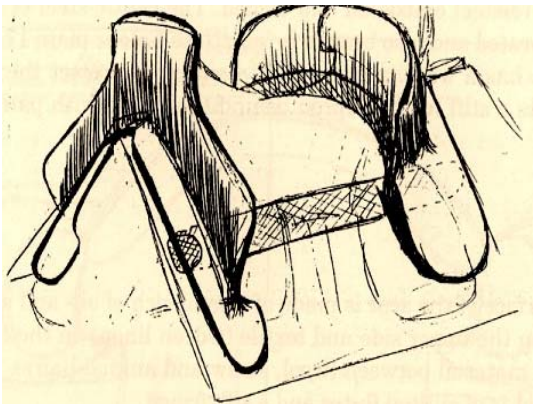

Figure 1.3.5 16th Century saddle in the Wallace Collection (Source: Blouet and Beaumont in Gilmour, 2004)

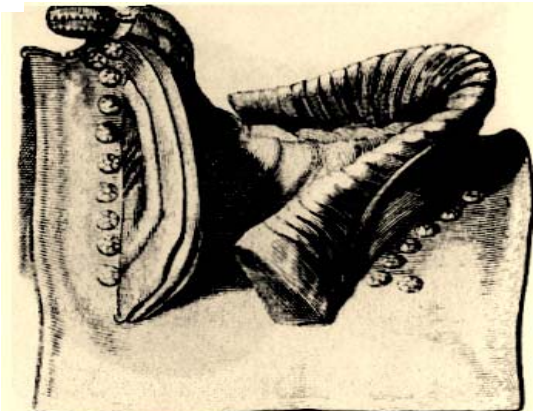

Figure 1.3.6 1658 type of saddle advocated by The Duke of Newcastle, William Cavendish (Source: Waterer, 1975)

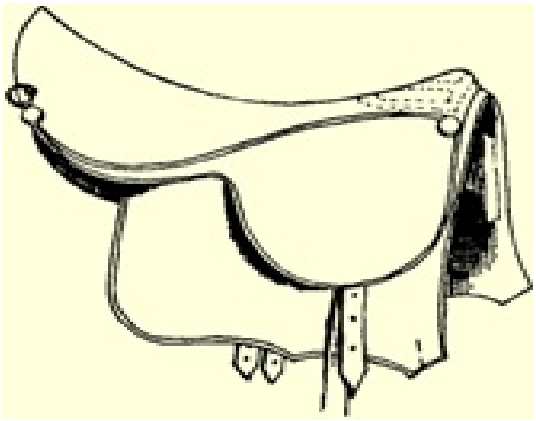

Figure 1.3.7 English saddle about 1740 (Source: Waterer, 1975)

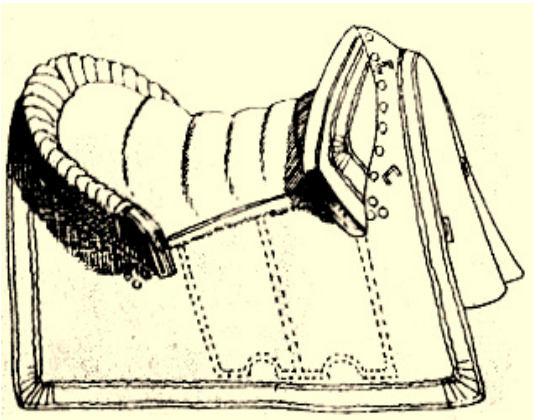

Figure 1.3.8 French royal saddle about 1740 (Source: Waterer, 1975)

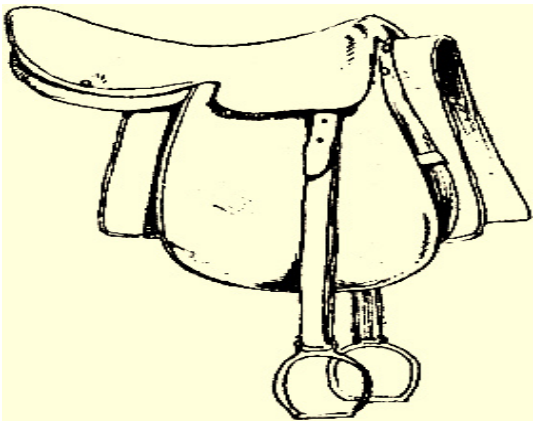

Figure 1.3.9 English riding saddle about 1800 (Source: Waterer, 1975)

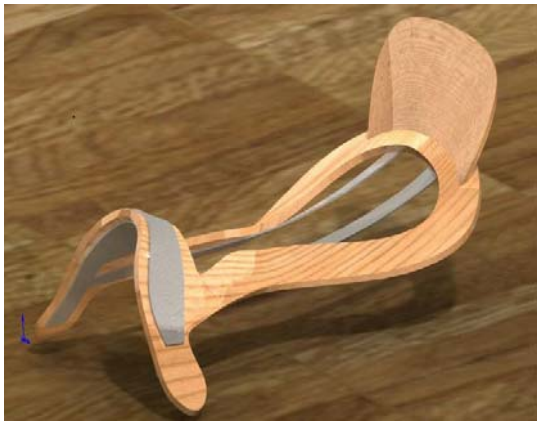

Figure 1.3.10 Saddletree of contemporary English saddle

The development of the tree pre-1740 illustrated that it was probably designed to secure a rider. The design would have suited warriors on horsebacks. It would also have been suitable for jousting tournaments. Riding for hunting, pleasure and leisure may have propelled the transition to the 1740 models and those after. The desire to reduce weight coupled with the need to enhance body-to-body communication between the horse and the rider may also have contributed to reducing the size of the wood used to make the saddletree.

The knowledge that defects inherent in solid wood are better distributed in plywood, veneer plywood, core plywood, or composite plywood (Kollmann, et al., 1975) may have contributed to replacing the solid wood with laminates. There is a dearth of knowledge on the design history, methodology, processes and intention of the craftsmen that designed the saddletree. Available patents are devoid of scientific evidence to support inventions in the industry.

As the thickness of the saddletree reduced, metal parts, including the cap plate, gullet plate, and spring steel were later added to reinforce the saddletree made from

wooden laminates (see figure 1.3.11).

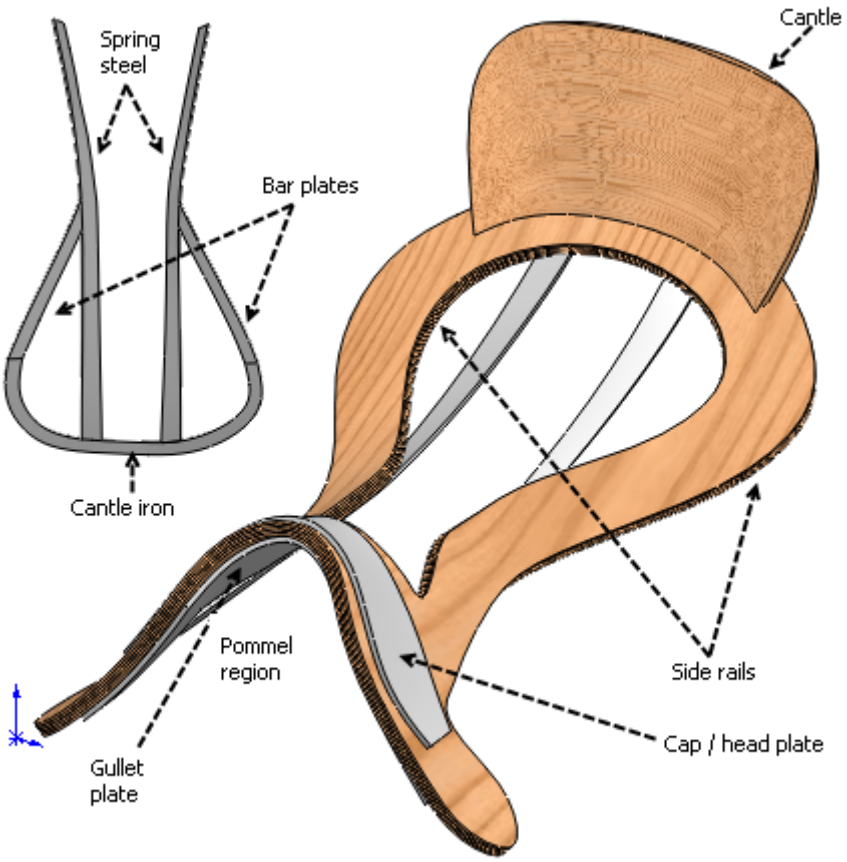

Figure 1.3.11 Parts of an English jumping saddletree

1.4 RESEARCH DRIVERS

Various factors contribute to a product's evolution (Palani Rajan, et al., 2005), redesign and/or remanufacture (Qureshi et al., 2006); here, the following are the key drivers of this research leading to an evolution of the saddletree design:

1.4.1 Economic factors

The manufacture of horse riding saddles in the UK is centred in Walsall in the West Midlands. Following the Second World War, the most significant innovations and advances in the design of the English saddletree and saddles had been credited to Walsall saddlers, who created a niche for designing and manufacturing 'high-end'

saddlery products (Edwards, 1990). A strengths, weaknesses, opportunities and threats (SWOT) analysis conducted in the early stage of this research (see Appendix 1) illustrated that the local industry is facing stiff competition in its local and international markets particularly from growing international manufacturers with a cheaper labour force. To maintain its share of a competitive market (Qureshi, et al., 2006), the UK saddlery and harness industry must combine improved, innovative and optimized designs, materials, and cost saving manufacturing technologies (Palani Rajan, et al., 2005; Qureshi, et al., 2006).

1.4.2 Technological factors

Horse back riding is reputed to be the least technologically advanced sport, (Schneller and Subic, 2000). For centuries, people have ridden horses and have used a multitude of different saddles, but with little scientific understanding of the effect of the saddle on the horse; the loading or pressure distribution on a particular part of the horse's back could have direct clinical significance (Liswaniso, 2001). Although there are difficulties in establishing a specific diagnosis (Jeffcott, 1979), a loaded saddle has been suspected to contribute to soft tissue injuries (De Cocq, et al., 2004).

Furthermore, the functional requirements of the saddletree and its component parts, and the relationship between the saddletree and its component parts, in particular, the steel reinforcement plates remain unknown therefore hampering innovation and advancement in its design and manufacture. There is a dearth of quantitative insight in product function and quality (Wood and Newbold, 2004). In Barton v. Irish (Unpublished Minnesota Court of Appeals, 2002), it was established that a defective saddle containing sharp metal pieces dug into the horse's back and caused it to throw

the rider off. Without a detailed knowledge of the functional requirements of the saddletree and its component parts, it remains questionable why such metal reinforcements are required.

Product functionality and performance can be improved as a result of consumer feedback (Palani Rajan, et al., 2005; Qureshi, et al., 2006) and knowledge acquired from research and development. Knowledge obtained by performing physical experimental tests (Stump, et al., 2002) and simulations (Bailetti and Litva, 1995) with the aim of understanding the product's performance (Otto and Wood, 1996, 1998) in a user environment can be documented and applied in developing new concepts (Kurtoglu and Campbell, 2009) either at subsystem, configuration, component or parametric level (Otto and Wood, 1996, 1998).

In addition, the manufacture of saddlery is devoid of quality control resulting in saddles with twisted trees, flaps and panels installed asymmetrically (Harman, 1995). To continue to provide high end products, which the local industry is reputed for, it is necessary to continuously encourage the industry by transferring innovative knowledge and services from universities and other sectors. Companies that apply innovative methods in designing and manufacturing have a higher competitive rate earning than others that do not (Naveiro and Pereira, 2008).

1.5 AIM AND OBJECTIVES

- **Aim:**

Through the development of numerical models, to simulate the behaviour of an English jumping saddletree with a view to understanding its complex performance

characteristics and sensitivity to variables such as loading, material variations, and geometric variations. This will provide a more scientific approach to be able to support future improvements to saddletree design.

- **Objectives**:

(i) To develop numerical models of the English equestrian saddletree.

BS 6635:2003 – "Manufacture of saddle trees made from wood - Specification" defines the geometry of English saddletrees. The standard requires that the saddletree is symmetric in accordance with table 1.5.1 and figure 1.5.1.

Table 1.5.1 Measurements for the symmetry of saddletrees

Component Symmetry	Points of reference (L= left, R= Right)
Head	Y to AL = Y to AR
Bar position	X to BL = X to BR
Waist	Y to CL = Y to CR
Seat	Y to DL = Y to DR
Cantle	Y to EL = Y to ER
Bar pitch	Z to GL = Z to GR
Bar height	Z to HL = Z to HR
Waist height	Z to JL = Z to JR (as at C)
Seat rail height	Z to KL = Z to KR (as at D)

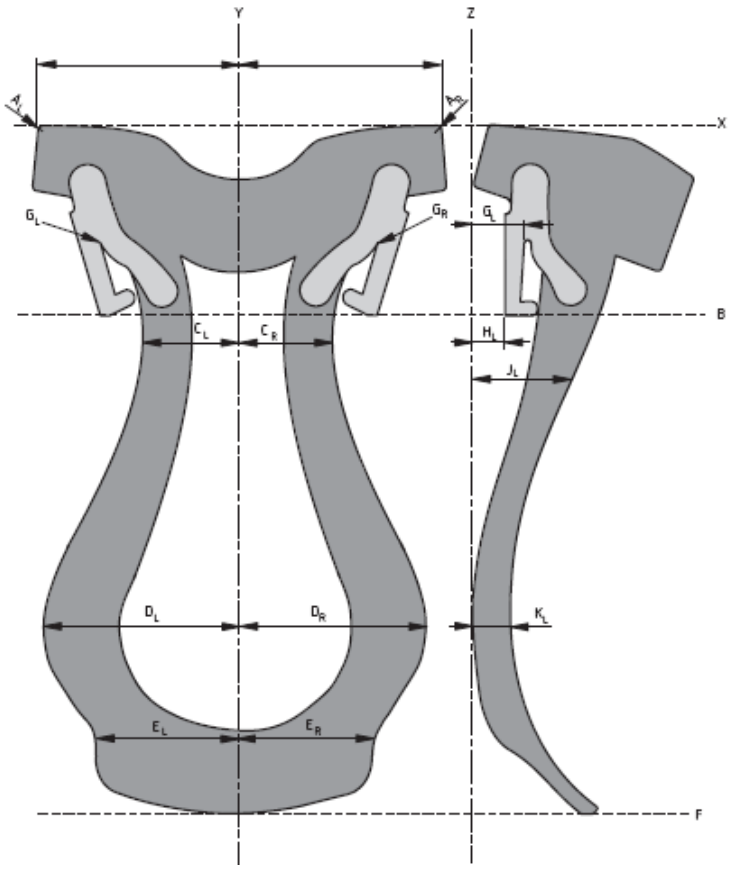

Figure 1.5.1 Symmetry in a saddletree
(Source: BS 6635:2003)

Unfortunately, due to the manual methods used in the current design and manufacturing processes, the manufactured product is asymmetric. Hence, surface data measured from a manufactured product will be used to define the geometry of the saddletree, which will be further used to develop the numerical model.

Continuum composite elements are used to simplify the laminate models. To further simplify the models, the rivets which were used to fasten the metallic reinforcements to the wooden frame will be replaced with contact – glue all boundary conditions.

(ii) To perform parametric studies of the sensitivity of the behaviour of the saddletree to various variables such as loading, material variations, and

geometric variations:-

The numeric model will be simulated under two different load types namely point and uniformly distributed loads to investigate its bending stiffness. Load will be applied to the cantle region while the model is cantilevered at a part of the head (pommel section). The simulations will provide an opportunity to investigate the following:

- The effects of the steel reinforcement plates on the wood only product;
- The effects of the material layout – solid wood and laminated plies;
- The effects of thickness variation of the saddletree.

In addition, numerical models in contact with rigid body supports underneath the saddletree located towards the front and rear sections will be simulated. The models will be loaded through another rigid body model identical to the seating posture of a rider. The simulations will provide an opportunity to study the following:

- The effects of the steel reinforcement plates on the wood only product;
- The effects of the laminate stacking sequence on the stiffness of the saddletree.

Further, a simplified model of the pommel section will be simulated under impact loading conditions. This will provide an opportunity to investigate the following:

- The effects of the steel reinforcement plates on the wood only structure;
- The effects of the material layout – solid wood and laminated plies;
- The effects of varying the impact velocity.

(iii) To improve the understanding of saddletree performance and its interaction with the equine back.

Understanding the sensitivity of the behaviour of the saddletree relative to important variables will contribute to the knowledge in this area of research, where to date there has been little scientific analysis. Models developed and the understandings gained such as the stiffness values from these models will be used to recommend some structural design changes and possibly, the utilisation of new materials to provide improved conformity to the motions and constraint of both the rider and the horse.

1.6 RESEARCH FRAMEWORK

Otto and Wood (1996, 1998) recognised that there are a number of descriptive and prescriptive design methodologies developed for general engineering design problems. These methodologies were however argued to be more applicable to problems that required an original design solution. Consequently, they proposed a systematic methodology focussed on the process steps required to represent and understand an existing product. The methodology involves three distinct phases: reverse engineering, modelling and analysis, and redesign.

This methodology will be used as a guide in this research. A framework for this research is illustrated in figure 1.6.1.

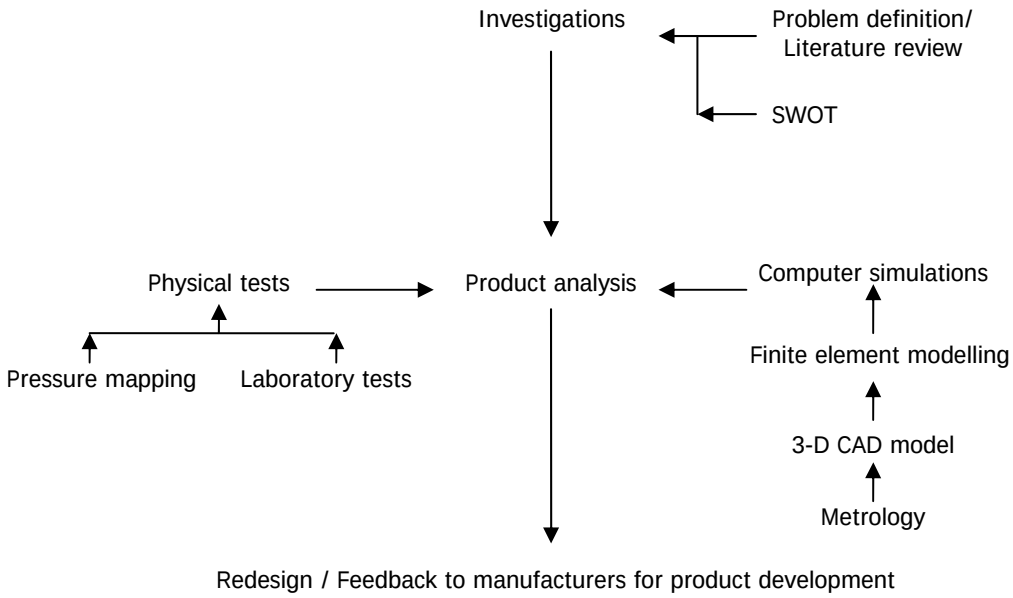

Figure 1.6.1 Research framework

1.7 STRUCTURE OF THE THESIS

Chapter 1 integrates the saddletree and the socio-economic impact of the horse industry on some world economies. An illustration of the evolution of the saddletree over centuries is presented, followed by the motivation for this research. In addition, it identifies the English jumping saddletree as the type of saddletree to be studied in this research, and the aim and objectives of the research are summarised. Following this, a framework to guide the research is described.

Chapter 2 reviews some publications relating to saddletrees and saddles. Some publications relating to the movement of the equine thoracolumbar spine, and, some intellectual properties dating back to the early 19th century are also reviewed.

Chapter 3 presents the process of developing the numerical models from a physical sample. Point-to-point data obtained from a jumping saddletree were input into a

CAD tool to create the geometry which was further used to develop the numerical models. Simplified models and hand calculations to validate the results of the solver are also presented.

Chapter 4 presents the development of static numerical models of an English jumping saddletree. The load and boundary conditions were defined in a manner identical to a cantilever beam thereby providing an opportunity to simulate bending in the models. The effect of the steel reinforcements on the stiffness of the wood-only product was quantified.

Chapter 5 presents further studies on bending in the saddletree. The saddletree is loaded with a rider's seating profile while being supported on the lower surface at the front and rear. The bending deflection under this loading condition is presented. The effects of the steel reinforcements and laminate stacking sequence are investigated and quantified.

Chapter 6 presents the development of transient dynamic numerical models of the pommel section of the English jumping saddletree. The pommel is modelled assuming impact with a rigid body. The effects of the steel reinforcements and impact velocity are presented.

Chapter 7 presents physical experiments on English jumping saddletree specimens conducted in the laboratory and experimental pressure mat measurements.

Chapter 8 presents the application of the CES material selector in exploring

potential candidate materials to replace the current materials applied in constructing the saddletree. This is followed by a proposed design concept.

Chapter 9 presents the findings of the research followed by proposed future work.

It was apparent from the onset that there was a lack of good data and analysis, and publications in the development of saddletrees. It is hoped that this work conducted by the author will help lay the foundations for future research and development in this area.

CHAPTER TWO

LITERATURE REVIEW

2.1 DESIGN

Historians and archaeologists in particular, and conservators have in the past published a number of works on the evolution of the English saddle and saddletree spanning over centuries. These include the works of Gilmour (2004) and Waterer (1975). They have associated the evolution of the designs to the changing roles that the horse was used for by man. While most of the publications have described the transition from one saddle and saddletree to another, there are only a few publications recounting a detailed development of the English jumping saddletree. Intellectual property rights, in form of patents seem to be the most informative source of published literature on this product. Patents are a good source of historical scientific and technical literature (Walker, 1995). A review of these patents will provide an insight into the design intent of their innovators.

The manufacturing processes involved in making saddletrees differ from those involved in making the complete saddle (Hayes, 2008). The saddler is often not the tree-maker. Edwards (1990) claims that saddletree-makers are ignorant of the requirements of the product they make, particularly with regard to the loading conditions that the product will be subjected to. The English saddletree is manufactured with resin bonded beech or birch plywood laminates (BS 6635:2003), or from materials of synthetic origin (BS 7875:1996) (see figure 2.1.1).

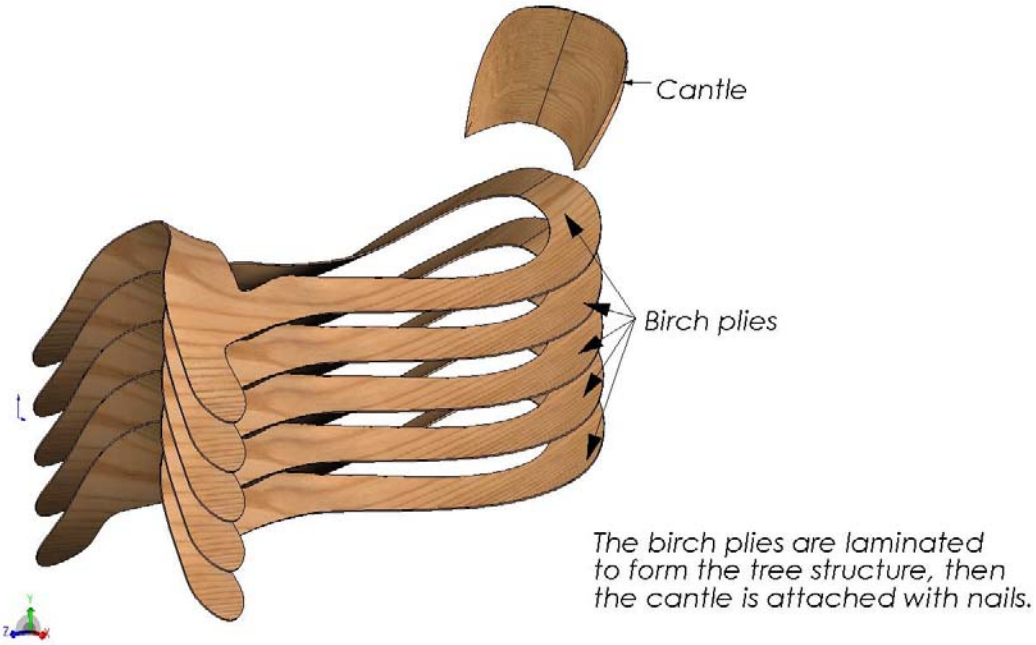

Figure 2.1.1 Laminating the birch plies that make up the tree structure

Metallic parts including the gullet plate, head or cap plate, cantle iron, bar plates, and spring steel are then attached (see figure 2.1.2).

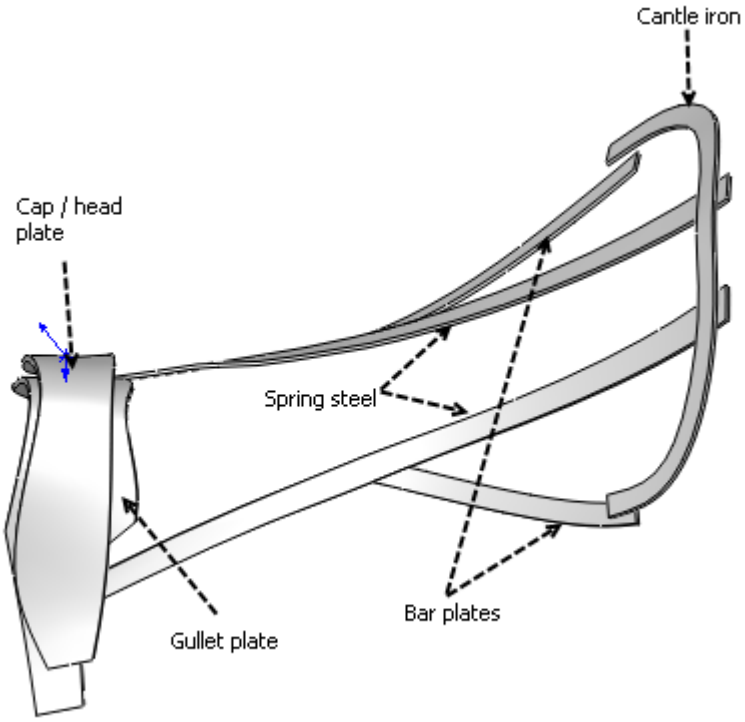

Figure 2.1.2 The steel reinforcements

Saddlers and tree-makers have offered various reasons for the need to strengthen the saddletree with the metal reinforcements. Bates (1976), Beebee and Beebee (1908), Butler (1967), Butler (1909), Davis (1898), Edwards (1990), Lappan (1904), White and Lightfoot (1975), Bayliss (1958), and, Wright and Leckie (1906) all reported strengthening the saddletree with the metal reinforcements. An arched structure of great strength is formed by riveting the gullet plate on the underside of the pommel to the cap plate on the topside of the pommel (Bates, 1976; Beebee and Beebee, 1908; Butler, 1967; Butler, 1909; Davis, 1898; Lappan, 1904; White and Lightfoot, 1975; Bayliss, 1958; Wright and Wedge, 1922; Wright and Leckie, 1906). Liswaniso (2001) suggested that the arched shape protects the horse's spine from the rider's pressure. Side rails connect the front arched shape structure (the pommel) to the rear (cantle). The cantle is also reinforced with the cantle iron while the bar plates reinforce the side rails. Davis (1898) further expressed an opinion that saddle trees which are usually constructed from several pieces of wood, shaped and joined together by various methods, are weak at their joints and become distorted particularly due to the impact of sudden shocks. These shocks, which they are exposed to in usage such as in jumping, cause them to break. To restore a failed saddletree, the complete saddle will have to be disassembled (Hayes, 2008). Hardwick (1936) feared that wooden saddletrees were liable to break; particularly when a horse wearing a saddle falls or rolls (Bates, 1976; White and Lightfoot, 1975). In addition, Butler (1967) argued that the greatest loads are applied by a rider onto the stirrups, which are connected onto the saddlebow (pommel or head) and the side rails. With a view to protecting the saddlebow from spreading under such loads, he noted that it had been customary to apply a metal strengthening plate to the underside of the saddlebow and then rivet the stirrup bars through the saddlebow

onto the gullet plate. The pair of steel plates, which are referred to as, springs or sprung steel are assumed to provide resilience to the seat thereby increasing comfort both to the rider and the horse (Edwards, 1990).

2.2 HORSEBACK MOVEMENTS

Free body diagrams (FBD) have been used to study the loading of the horseback. Van Weeren (2009) reviewed the evolution of the FBD from the Roman era. Galen (AD 129 – 200) was cited to have described the back of quadrupeds with an architectural analogy – a vaulted roof sustained by four pillars. This was followed by the bridge concept analogy (Van Weeren, 2009; Jeffcott, 1979) (see figure 2.2.1 a – c). Van Weeren (2009), Jeffcott (1979), Weaver and Jeffcott (2003), and, Evans, et. al. (1995) credited the popularity of the "bow and string" concept to Slijper (1946) (see figure 2.2.2). The bow represents the thoracolumbar vertebral column (Van Weeren, 2009; Jeffcott, 1979; Weaver and Jeffcott, 2003; Evans, et. al., 1995), the pelvis and their muscles (Jeffcott, 1979); while the string, which tensions the bow is formed by the sternum, abdominal muscles and linea alba.

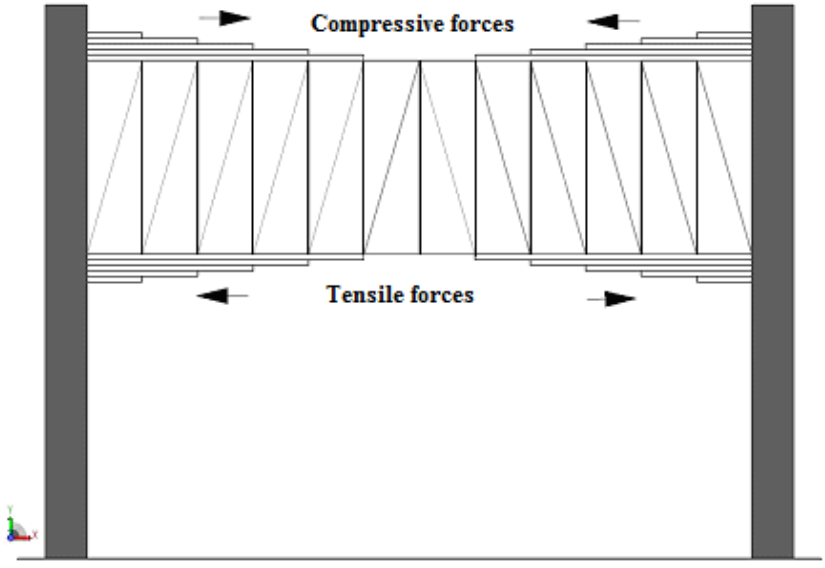

Figure 2.2.1a Bridge concept
(Redrawn from Van Wereen, 2009)

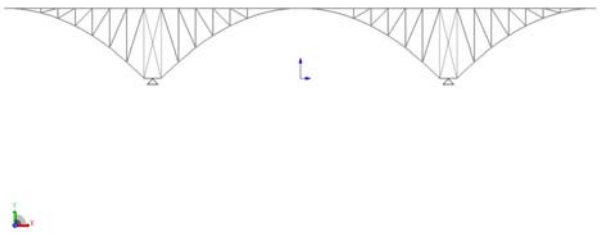

Figure 2.2.1b Parabolic cantilever bridge
(Redrawn from Van Wereen, 2009)

Figure 2.2.1c Inverted parabolic cantilever bridge
(Redrawn from Van Wereen, 2009)

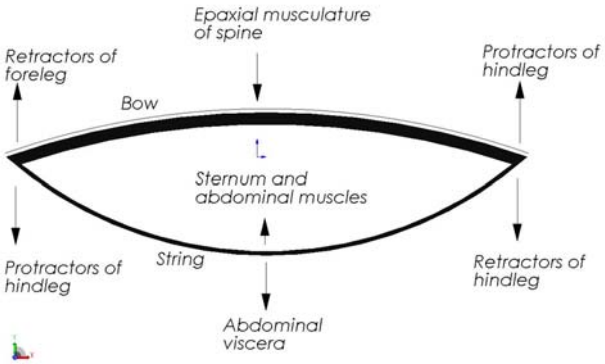

Figure 2.2.2 String and bow concept
(Redrawn Jeffcott, 1979; Van Wereen, 2009)

Horseback movements have been the focus of various studies including those by Denoix and Audigie (2001), Jeffcott (1979), Jeffcott and Dalin (1980), Weaver and Jeffcott (2003), Evans, et al. (1995), Townsend, et al. (1983), Licka and Peham

(1998), Audigie, et al. (1999), Faber, et al. (2001), Licka, et al. (2001), and, Peham and Schobesberger (2006). Jeffcott and Dalin (1980) investigated the rigidity of the horse's vertebral. A set of five thoracolumbar spines, simply supported, (see figure 2.2.3) with a 10kg weight applied at the midpoint, were tested for dorsoventral, lateral, and rotatory movements.

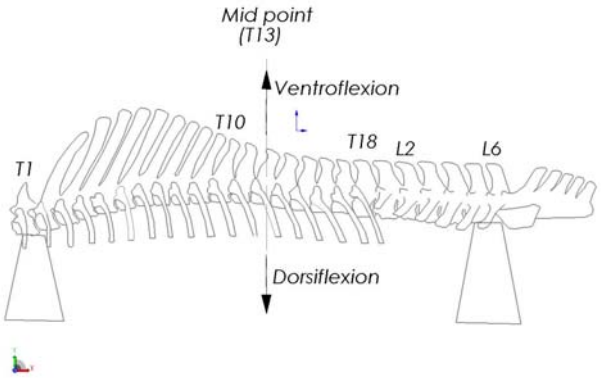

Figure 2.2.3 Supporting the loaded thoracolumbar spine at T1 and L6 (Redrawn Jeffcott and Dalin 1980)

Between T10 and L2, measured displacements were 31.0 mm and 22.1 mm for ventroflexion and dorsiflexion respectively. These movements notwithstanding, the specimens were concluded to be relatively inflexible or rigid. In a separate set up to investigate lateral movements, it was concluded that lateral bending began from T13 onwards. In a related study, Townsend, et al. (1983) pinned down the sacrum in a manner analogous to a cantilever beam and measured dorsoventral flexion and extension, and lateral bending of the thoracolumbar spine. They observed that the least dorsoventral displacement occurred between T2 and T6. Axial rotation and rotational mobility were most prominent between T9 and T14, and, contrary to Jeffcott and Dalin (1980), they observed that lateral bending was most pronounced between T11 and T12. Faber, et al. (2001) observed the most prominent lateral

bending at T10 during canter. At trot, Licka, et al. (2001) observed highest dorsoventral displacement and highest lateral movement at T16 and T5 respectively.

The following three major movements take place in the equine thoracolumbar spine :

- flexion (ventral bending) and extension (dorsal bending) movements (Licka and Peham, 1998; Audigie, et al., 1999; Townsend, et al., 1983; Licka, et al., 2001; Faber, et al., 2001; Jeffcott and Dalin, 1980; Johnston, et al., 2004);
- lateral bending (Townsend, et al., 1983; Licka, et al., 2001; Faber, et al., 2001; Jeffcott and Dalin, 1980; Johnston, et al., 2004); and,
- axial rotation (Townsend, et al., 1983; Faber, et al., 2001; Johnston, et al., 2004).

In addition, Peham and Schobesberger (2006) investigated the stiffness of the equine back and estimated the lateral flexion and ventral extension as 6100 N/m and 650 N/m respectively. Schlacher, et al. (2004) investigated the stiffness of the thoracolumbar spine and deduced the mean stiffness of dorsoventral movement as 2093 ± 611 N/m, mean stiffness of dorsoventral movement at 30^0 as 2182 ± 459 N/m, and, mean stiffness of laterolateral excursion as 1454 ± 156 N/m. These stiffness values are yet to be compared with the stiffness of the saddletree in any publication. In a related study, Oleson, et al. (2005) quantified the stiffness of the human forefoot and compared it with the bending stiffness of running shoes. For most of the reported bending range, they observed that the forefoot stiffness was much larger than the bending stiffness of the shoes. They concluded that the combined stiffness of the foot and the shoe was dominated by that of the foot.

2.3 SADDLERY AND HORSEBACK INTERACTION

Horse riding is accomplished by the interaction between a horse's back and the saddle (Liswaniso, 2001); and, the interaction between the horse and the rider (Jeffcott, et al., 1999). Peham, et al. (2004) observed that there is a significant coupling between the horse and rider through the saddle, which is yet to be fully understood. Von Peinen, et al. (2009) described the saddle as the most important link between the rider and the horse. The use of a non-fitting saddle disturbed the communication between horse and rider thereby influencing the motion variability of the equine gait and the free movement of the horseback (Fruehwirth, et al., 2004; Peham, et al., 2004).

De Cocq, et al. (2008) suggested that coupled with a saddle's relative rigidity and shape, changes in rider position may have affected the pattern of force transmission to the horse's back. The horseback is influenced by the weight of the saddle and rider (De Cocq, et al., 2004, 2006), particularly at the withers (Fruehwirth, et al., 2004). In order to accommodate the back movement of the horse (Denoix and Audigie, 2001), it is desirable for the saddletree to flex (Swain, 2002). The width of the saddletree has been observed to influence pressure distribution beneath the saddle (Meschan, et al., 2006).

Jeffcott (1975) observed that many horseback pain complaints by horse owners were related to horseback riding. He observed in some horses, that the dorsal spines primarily underneath the saddle area were susceptible to back pain and that they performed poorly at trot or at fast exercise. Jeffcott and Dalin (1980) also considered the spine's functional anatomy in relation to the horse's ability to perform at speed

and to jump. Severe tissue pains could be aggravated by pressure from a saddle and a rider (De Cocq, et al., 2004). Discussing the criteria of back pain in the horse, Jeffcott (1979) cited a condition referred to as "cold-back"; there is stiffness and dipping of the spine as a rider seats on a saddle. It was however, unclear if this condition was painful, or resulting from previous back pain, or a disposition of the horse.

In addition to the load of the saddle and rider, Peham and Schobesberger (2004) concluded that ridden horses were exposed to load effects of other forms of dynamic influences; particularly when galloping and jumping (Jeffcott and Dalin, 1980). Simulating a beam that was modelled to represent the horseback, Peham and Schobesberger (2004) observed that an increase in localised stiffness along two-thirds of the beam had more impact than the effects of the load of a rider.

2.4 SADDLE FITTING

Saddle fitting has been been discussed in various publications including Liswaniso (2001), Harman (1995), Pavia and Posnikoff (2005), Billington (2006), Humphries (1998), Harman, et al. (2004), Peham, et al. (2004), Fruehwirth, et al. (2004), Meschan, et al. (2006), and, Jeffcott, et al. (1999). Though poor saddle fit has been related to back pain and poor performance in the horse, objective evaluation of saddles (Mescahn, et al., 2006) and scientific correlations between poorly fitting saddles and clinical problems are lacking (Jeffcott, et al., 1999).

2.5 PRESSURE MAPPING

The development of pressure mapping tools has enhanced the assessment of pressure

distribution at support interfaces (Eitzen, 2004; Tam, et al., 2003; Stinson, et al., 2003). The measurement of saddle pressure distribution is becoming an important procedure in equine research (Liswaniso, 2001). The technology enhances the objective measurements of saddle fit (Jeffcott, et al., 1999) and, makes it easier to identify localised areas of possibly harmful pressure concentrations (Peham and Schobesberger, 2004).

2.5.1 Validity, accuracy, and repeatability

The accuracy and repeatability of pressure mapping tools have been studied. Jeffcott, et al. (1999) employed a force-sensing array (FSA) for static and dynamic pressure measurements between the saddle and the horse. A hand-made wooden saddle horse and 10 normal horses were used in the study. While a linear relationship was recorded between the load on the saddle and the total static pressure measured by the FSA, there was a variation in the dynamic measurements. This was attributed to the complexity of establishing a control sample in the dynamic studies. Also using an FSA system, De Cocq, et al. (2006) corroborated the high correlation coefficient between total pressure and mass of the rider as observed by Jeffcott, et al. (1999).

Jeffcott, et al. (1999) further observed that though pressure contour maps are informative and visually attractive, they were not an objective evaluation of the pressure loading on a horse's back. On the contrary, Stinson, et al. (2003) observed that there was anecdotal evidence suggesting that system operators use the visual pressure maps rather than the numerical values to rank and compare the interfaces they are investigating. The results of the FSA system were considered as repeatable and reliable in ranking over time.

De Cocq, et al. (2008) tested the validity and repeatability of the Pliance system and compared the results with results obtained by De Cocq, et al. (2006) using the FSA system. A high correlation coefficient was recorded between measured force and load on the saddle with the Pliance system. The sensitivity of the sensors was observed to vary with time, and the FSA system would require more frequent calibration than the Pliance system. The Pliance system was concluded to be a valid and reliable system for saddle interface measurements. Sensors saturation, spatial sensitivity, and rounding off of centre of pressure (COP) are the main limitations of the FSA pressure mapping system (Lacoste, et al., 2006).

Bressel and Cronin (2005) further assessed the validity of the FSA system limiting validation procedures to static measurements, which did not replicate seat pressures during pedalling. A correlation coefficient of 0.97 was reported in the study and was comparable to 0.98 obtained by Jeffcott, et al. (1999). Similar to the Stinson, et al. (2003) study, peak pressures displayed lower coefficients and were less stable than mean pressures. The validity of the FSA system in this study was observed to be excellent.

Hostens, et al. (2001) demonstrated the repeatability of the Xsensor ™ system in their study; it was observed to produce repeatable results in static pressure measurements.

In comparison with a Fuji Film Prescale system, a Tekscan I-Scan was observed to have a smaller profile, the capability to produce real time data, and, the ability to evaluate a wider range of loads with great accuracy (Bachus, et al., 2006). Wilson, et

al. (2006) used a Tekscan I-Scan system to measure facet joint loads. The repeatability of facet load measurements in cadaver lumbar spines was determined. It was observed that linear calibration produced more repeatable and more accurate results than those obtained from a two-point calibration. The I-Scan system was found to be consistent in varying loads and loading types. Drewniak, et al. (2007) and Wilson, et al. (2006) observed that sensor selection was crucial in obtaining contact area measurement accuracy in Tekscan systems.

2.5.2 Display properties

Data obtained with a Tekscan pressure measurement system may be displayed as force, box area, contact area, box pressure, contact pressure, peak force, peak box pressure, peak contact pressure, and raw data. The preference of one property over the other has been discussed (Stinson, et al., 2003; Bressel and Cronin, 2005; Jeffcott, et al., 1999; De Cocq, et al., 2008; Meschan, et al., 2006; Eitzen, 2004; Carcone and Keir, 2007).

Whereas, Stinson, et al. (2003) and, Bressel and Cronin (2005) expressed their opinion that average pressure was a more stable measure than peak pressures, Carcone and Keir (2007) suggested that contact area and peak pressure might have been more useful measures in their study.

Eitzen (2004) observed that there were no significant changes in the average and peak measurements over the measurement period, hence, a preference for a frequency analysis.

De Cocq, et al. (2008) cited that the summation of pressure in De Cocq, et al. (2006) had overestimated the force by a factor of 2.1, hence preferred the summation of forces. Jeffcott, et al. (1999) had also evaluated the summation of the measured pressures.

Meschan, et al. (2006) attempted to justify the use of overall total force. The calculation of both the maximum overall force (MOF) and the centre of pressure (Fruehwirth, et al., 2004) have also been reported.

2.5.3 Pressure mapping and finite element analysis

As demonstrated by Ragan, et al. (2002), seat-interface pressure data can be used as load and boundary conditions in developing a finite element model to investigate the pressure or load on an object. In addition, pressure maps obtained from pressure mats have been used to validate computer simulated finite elements results (Carfagni, et al., 2007). A value of 19 Kpa was recorded for maximum pressure predicted by the finite element analysis while a value of 18 Kpa was recorded for maximum pressure obtained from the pressure mapping.

2.6 MATERIAL PROPERTIES OF WOOD

2.6.1 Elastic constants

Wood is an anisotropic material due to its fibrous structure (Mackerle, 2005; Bretos, et al., 1999; Muller, et al., 2003; Tabiei and Wu, 2000; Silva, et al., 2006; Schmidt and Kaliske, 2009). In numerical analysis, solid woods have been modelled based on the assumption that they are orthotropic (Mackerle, 2005; Ribeiro, et al., 2009; Bretos, et al., 1999; Lam, et al., 2004; Serrano, 2001; Tabiei and Wu, 2000; U. S.

Department of Transportation Federal Highway Administration (FHWA), 2007). Laminated woods have also been modelled based on the same assumption (Lang and Fodor, 2002; Brezovic, et al., 2003; Moses and Prion, 2004; Piao, et al., 2005).

The mechanical properties of wood are unique and independent in three mutually perpendicular axes – longitudinal (L), radial (R), and tangential (T) to the grain (Ribeiro, et al., 2009; Forest Products Laboratory (FPL), 1999) (see figure 2.6.1).

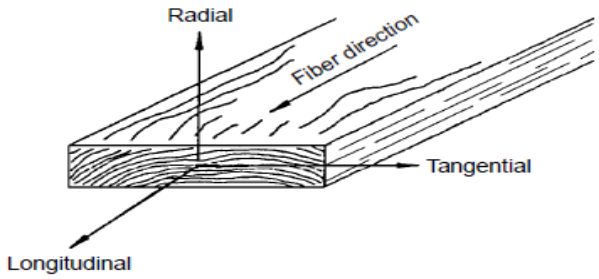

Figure 2.6.1 The three principal axes of wood
(Source: FPL, 1999)

Sub-indices 1, 2, and 3 have also been used to represent the X, Y, and Z-axes respectively (Bretos, et al., 1999). Nine independent constants are required to describe the elastic behaviour of wood (Ribeiro, et al., 2009; Bretos, et al., 1999; Serrano, 2001; Astley, et al., 1997; Qiao, et al., 1998; FHWA, 2007). They include the following:

- Three 3 elastic modulus (E_L, E_R, E_T) or (E_{11}, E_{22}, E_{33})
- Three shear modulus (G_{LR}, G_{LT}, G_{RT}) or (G_{12}, G_{31}, G_{23});
- Three Poisson's ratios (υ_{LR}, υ_{LT}, υ_{RT}) or (υ_{21}, υ_{31}, υ_{32})

Three additional Poisson's ratio constants (υ_{RL}, υ_{TL}, υ_{TR}), therefore summing up to 12 elastic constants, have also been used to formulate the material model (Lang and

Fodor, 2002; FPL, 1999).

Due to the complex structure of wood and the variations in test specimens, the mechanical properties have been averaged (Garratt, 1931; FPL, 1999). The mechanical properties of yellow birch (FPL, 1999) are tabulated in table 2.6.1.

Table 2.6.1 Some elastic constants of Yellow Birch

Modulus of Rupture (MPa)	Modulus of Elasticity (MPa) E_L	10 % + E_L (MPa)
114	13,900	15,290

(Source: FPL, 1999)

Values for the other elastic constants are obtainable with the aid of elastic ratios tabulated in table 2.6.2.

Table 2.6.2 Elastic ratios of Yellow Birch

E_T/E_L	E_R/E_L	G_{LR}/E_L	G_{LT}/E_L	G_{RT}/E_L
0.050	0.078	0.074	0.068	0.017

(Source: FPL, 1999)

Lam, et al. (2004) estimated the elasticity constants values based on $E_T = E_L/1.4$, $E_R = E_L/20$, $G_{LT} = E_L/14$, $G_{LR} = G_{LT}/10$, $G_{RT} = G_{LT}/10$.

The Poisson's ratios have been reported as tabulated in table 2.6.3.

Table 2.6.3 Poisson's ratio for Yellow Birch

υ_{LR}	υ_{LT}	υ_{RT}	υ_{TR}	υ_{RL}	υ_{TL}
0.426	0.451	0.697	0.426	0.043	0.024

(Source: FPL, 1999)

2.6.2 Failure prediction

The earliest failure criteria for wood were acquired empirically (Smith, et al., 2003; MaoHong, 2004). The maximum stress criterion, the maximum strain criterion, and the interactive criteria, which include Tsai-Hill, Tsai-Wu, and Hoffman's criterion seem to be the most popular failure criteria (Groenwold and Haftka, 2006).

Groenwold and Haftka (2006) argued that while the Tsai-Wu criterion was empirical, the maximum stress and maximum strain criteria were based on engineering intuition. They further described the Tsai-Hill criterion as a statement of maximum allowable work. In addition, they argued that unlike maximum stress, maximum strain, and Tsai-Hill criteria, Tsai-Wu criterion lacked physical basis; this notwithstanding, it is frequently used.

Yoshihara, et al (1995) argued that the Hankinson's formula, which does not contain shear strength, was one of the most famous criteria used due to its simplicity. FHWA (2007) however asserted that it was unsuitable for finite element codes.

MaoHong (2004) stated that Hill, Hoffman, Tsai-Wu, and Cowin criteria are often used for wood. Galicki and Czech (2005) considered Hankinson and Kollman, and Ashkenazi criteria. They suggested that the Tsai-Wu and Ashkenazi were the most common criteria used in describing the strength of orthotropic wood. In a review of the Maximum Stress, Tsai-Wu, Hoffman, Norris, Extended Yamada-Sun, Hashin, Modified Hashin, and, Hankinson's criteria, FHWA (2007) considered the Maximum Stress criterion to be the commonly applied limit theory. Moses and Prion (2004) suggested that the maximum stress and maximum strain criteria are the

simplest criteria. Akbulut and Sonmez (2008) also reported the ease in applying the maximum stress criterion, and the reliability of the Tsai-Wu criterion. Considering these two criteria in predicting failure in two different laminate designs, they observed that each criterion compensated for the shortcomings of the other. Hence, they employed the use of both criteria in their investigations.

Smith, et al. (2003) observed that, in comparison with scatter in experimental data, the differences between the failure criteria were relatively small therefore it is impossible to clearly identify the superiority of one criterion over another.

FHWA (2007) formulated a failure model from six strength properties namely:

- X_T Tensile strength parallel to the grain;
- X_C Compressive strength parallel to the grain;
- Y_T Tensile strength perpendicular to the grain;
- Y_C Compressive strength perpendicular to the grain;
- $S_{/\!/}$ Shear strength parallel to the grain;
- $S_{\perp}$ Shear strength perpendicular to the grain.

According to Naik and Murty (1999), the maximum stress failure criterion predicts failure when one or a combination of the following conditions occurs:

$$\begin{aligned} \sigma_L &\geq X_T \quad \text{or} \quad \sigma_L \geq X_C \\ \sigma_T &\geq Y_C \quad \text{or} \quad \sigma_T \geq Y_T \\ \sigma_{LT} &\geq S \end{aligned} \tag{1}$$

The maximum stress failure criterion will not predict failure in any ply of a

composite laminate when the following conditions occur (Omkar, et al., 2008a, b):

$$\begin{array}{ccccc} X_C & > & \sigma_{LL} & < & X_T \\ Y_C & > & \sigma_{TT} & < & Y_T \\ -S & > & \sigma_{LT} & < & +S. \end{array} \quad (2)$$

where σ_{LL}, σ_{TT}, and σ_{LT} are stresses induced in the principal directions.

FPL (1999) and Garratt (1931) reported the strength properties of yellow birch as tabulated in table 2.6.4.

Table 2.6.4 The strength properties of Yellow birch

Compression parallel to grain (MPa)	Compression perpendicular to grain (MPa)	Shear parallel to grain (MPa)	Tension parallel to grain (MPa)	Tension perpendicular to grain (MPa)
56.3[a]	6.7[a]	13[a]	113.784[a]	6.300[a]
23.856[b]	3.103[b]	7.653[b]		3.309[b]

Source: [a] FPL, 1999 and [b] Garratt, 1931

These properties would be used in developing the failure criteria in the non-linear finite element analysis in this research.

2.7 FINITE ELEMENT MODELLING

2.7.1 Introduction to FEM

Though it is impossible to identify the exact starting point of the finite element concept (Clough, 1980), the analytical procedure was first named Finite Element Method by R. W. Clough in his paper at a September, 1960 conference (Bryan, 1999; Clough, 1980). It was originally developed for the analysis of aircraft structures (Rao, 1999). The mathematical foundations are based on earlier developed approximation methods of continuum mechanics including those by Castigliano,

Rayleigh-Ritz method (Adams, 2006; Bryan, 1999; Clough, 1980) and Courant (Adams, 2006; Bryan, 1999).

Most finite element analysis packages are based on the minimum potential energy or the virtual work principles (Gomis-Bellmunt and Campanile, 2010). While the application of the virtual work principle is not restricted to any material behaviour, the application of the minimum potential energy principle is restricted to elastic materials (Madenci and Guven, 2006). For an elastic body, the total potential energy can be defined as (Rao, 2005)

$$\Pi_P = \Pi - W_P \qquad (2.7.1)$$

where,

Π = the strain energy, and

W_P = the work done on the body

The governing equation for static problems derived from the principle of minimum potential energy (Zhang, et al., 2010) is

$$[K]d = f \qquad (2.7.2)$$

where,

K = stiffness matrix,

d = displacement parameters, and

f = applied load.

2.7.2 Mesh generation

One of the most important steps in developing a numerical model is the generation of a mesh (Garimella, 2002; Hammond and Peltier, 1988; Piao, et al., 2005). The accuracy of the analysis and computational time are dependent on the mesh quality

and element density (Piao, et al., 2005; Hammond and Peltier, 1988). The effects of the mesh (element type and size), and some other modelling parameters on computational effort and their consequence on the results of the analysis were investigated by Jaksic and Nilsson (2009). Mesh density was reported to have a strong influence on the deformed models. The accuracy of the analysis was concluded to be relative to the fineness of the mesh. Miller, et al. (2000) compared the finite elements analysis of a non-linear numerical model with 2 varying mesh densities. They observed that the numerical model with intermediate mesh density, which was approximately 30 % of the dense meshed numerical model, was simulated in about 10 % of the analysis time used to simulate the latter. In addition, both models produced identical results.

2.7.3 Element type

Jaksic and Nilsson (2009) were of the opinion that tetrahedral elements ought to be avoided wherever possible because they drastically increased computational time and reduced the accuracy of the results. Brick elements have been used to develop numerical models of wood by Bretos, et al. (1999), Lang and Fodor (2002), Lam, et al. (2004), Moses and Prion (2004), Piao, et al. (2005), Serrano (2001), and, Qiao, et al. (1998). Bretos, et al. (1999) used solid elements to investigate the eigenmodes of wooden bars used in musical instruments. Piao, et al. (2005) used hexahedron elements to model a wood laminated composite pole.

2.7.4 Ply lay-up

The response of sandwich panels and thick laminates to external loading is complicated, and analysis often requires that the response of each layer be taken into

account explicitly (Cho and Averill, 1997). Riahi and Curran (2009) discussed two approaches used to simulate layered materials in computational solid mechanics. They are:

- techniques, which explicitly model the discontinuous nature of the material utilizing interface or contact technology such as the Discrete Element Method (DEM), and the Finite Element Method (FEM);
- the FEM or Finite Difference Method (FDM) equivalent continuum model.

They were of the opinion that discrete techniques were complex and require care in modelling of the interface, but provide a more accurate description of discontinuous materials. In layerwise theory, each ply can be discretized into several three-dimensional elements (Setoodeh, et al., 2009).

2.7.5 Convergence

Finite element analysis is an approximation method (Dutta and Talukdar, 2004, Basciftci, et al., 2004) and theoretically, finite element modelling tends to a limit when the mesh is refined (Lin, et al., 2009). To determine an appropriate mesh density, a convergence study was conducted (Pokharel and Mahendran, 2002; Macloed, 2005; Chang and Yang, 2009; Yonezu, et al., 2009; Theofanous, et al., 2009; Lee and Chang, 2009; Mohsenimanesh, et al., 2009; Phatak, et al., 2009; Nguyen, et al., 2009).

Theofanous, et al. (2009) based their convergence study on elastic eigenvalue buckling analyses. Lee and Chang (2009) used two different element sizes in their convergence study. Her and Liang (2004) used three types of mesh with solid

elements to conduct a convergence test. They presented contact force - time plots. Macloed (2005) used five mesh sizes and plotted three convergence diagrams –

- tip deflection versus degrees of freedom,
- percentage difference for the horizontal stress at the top of the cantilever at the support end versus degrees of freedom,
- percentage difference for the horizontal stress at the top of the cantilever midway between the ends versus degrees of freedom.

The rate of convergence depends on the type of element used, and the number of elements in the mesh (MacLoed, 2005). Mohsenimanesh, et al. (2009) used a series of progressively finer meshes. They compared the predicted maximum and minimum values of contact pressure for each mesh till the changes in the results were less than 5 %. Mesh refinement by Phatak, et al. (2009) resulted in changes less than 1 % in strain predictions.

2.7.6 Finite element analysis – parametric studies

Fam and Son (2008), and Son and Fam (2008) conducted parametric studies on cantilever fibre reinforced polymer (FRP) poles. They investigated various parametric combinations of the outer diameter to thickness (D / t) ratio, and, ply orientation. In addition, Fam and Son (2008) also investigated and compared the effects of a point load and wind pressure in the form of uniformly distributed loads on the models.

Davalos and Qiao (1999) proposed a computational approach for the analysis and optimal design of pultruded FRP shapes under bending. In one of the examples reported, they presented a cantilever box beam that was subject to tip-shear force.

The tip displacement and ply stresses were evaluated in relation to ply angle. In addition, they conducted parametric studies for the optimal design of material architecture for pultruded FRP I-beams.

Serrano (2001) investigated the influence of various geometry, material properties, and loading conditions on the pullout strength of glued-in rods. The parameters varied include: cross-sectional dimensions, rod diameter, length of solid wood, glued-in length, and loading – (pull-compression vs. pull-pull).

2.7.7 Explicit and implicit dynamic transient analysis

Many finite element programs offer both implicit and explicit methods for solving dynamic transient simulations (MSC.Software, 2008). The implicit algorithm depends on the elements of solution at time t_{n+1}, while the elements of solution at time t_{n+1} of an explicit algorithm depend on the solution at time t_n only (Noels, 2002). For a current time step, step *n*, a good estimate of the acceleration at the end of step *n*+1, will satisfy the following equation of motion (MSC.Software, 2008):

$$Ma'_{n+1} + Cv'_{n+1} + Kd_{n+1} = F^{ext}_{n+1} \qquad (2.7.3)$$

where,

M = mass matrix of the structure

C = damping matrix of the structure

K = stiffness matrix of the structure

F^{ext}_{n+1} = vector of externally applied loads at step $n + 1$

a'_{n+1} = estimate of acceleration at step $n + 1$

v'_{n+1} = estimate of velocity at step $n + 1$

$= \quad v_n + (1-\gamma)a_n\Delta t + \gamma a'_{n+1}\Delta t$

d_{n+1} = estimate of displacement at step $n + 1$

$= \quad d_n + v_n\Delta t + ((1-2\beta)a_n\Delta t^2/2 + \beta a'_{n+1}\Delta t^2$

$$M^* a'_{n+1} = F^{residual}_{n+1} \tag{2.7.4}$$

the accelerations are obtained by inverting the M^* matrix:

$$a'_{n+1} = M^{*-1} F^{residual}_{n+1} \tag{2.7.5}$$

where,

M = mass matrix of the structure

$F^{residual}_{n+1}$ = vector of residual loads at step $n + 1$

a'_{n+1} = estimate of acceleration at step $n + 1$

The equation of motion for the explicit methods (MSC.Software, 2008) is:

$$Ma_n + Cv_n + Kd_n = F^{ext}_n \tag{2.7.6}$$

$$Ma_n = F^{ext}_n - F^{\text{int}}_n \tag{2.7.7}$$

$$a_n = M^{-1}F^{residual}_n \tag{2.7.8}$$

where,

F^{ext}_n = vector of externally applied loads

F^{int}_n = vector of internal loads

$F^{\text{int}} = Cv_n + Kd_n$

M = mass matrix

Unlike explicit methods that do not require iterative solutions for each increment, implicit codes require iterative solutions for each time step (Noels, 2004). However,

regardless of the size of its time step, implicit codes can be made unconditionally stable (MSC.Software, 2008). The explicit method is conditionally stable (Sun, et al., 2000) and to remain stable, it requires a time step that must subdivide the shortest natural period in the mesh; the requiring a time increment less than a critical value of the smallest transition times for a dilation wave to cross any element in the mesh (MSC.Software, 2008; Sun, et al., 2000). Explicit time steps are normally 100 to 1000 times smaller than those used in implicit codes and since they are determined by the smallest element, very small elements are to be avoided (MSC.Software, 2008).

The two methods have been compared. Yang, et al. (1995) found both methods to be suitable for their sheet-forming application. They further suggested that the explicit method may be more effective for complex cases with more refined meshes. Sun, et al. (2000) compared both methods for fast and slow contact applications. They observed that for fast contact applications, the explicit method was cheaper than the implicit method. For slow contact applications, they observed that the numerical damping induced in the implicit method removed noise and enhanced the accuracy of the results. MSC.Software, (2010) compared the two methods for a similar application. It was observed that the displacement histories were indistinguishable while the damping in the implicit method prevented oscillations in the velocity history.

2.7.8 Impact analysis – parametric studies

Impactors have also been modelled as rigid bodies in various studies including Lopes, et al. (2009), Johnson, et al. (2001), Naik and Meduri (2001), and, Tu and

Chao (1999). Lopes, et al. (2009) applied a lumped mass and an initial velocity in the vertical direction on to the impactor. Karger, et al. (2007, 2008, 2009) simply modelled the impactor using a point mass.

Studies on the behavior of laminated composite structures subjected to low velocity impact have been reported (Her and Liang, 2004). Some of them have included parametric investigations on the effects of various variables. Krishnamurthy, et al. (2001) studied the impact response of laminated composite shells to a metallic impactor. They considered a few case studies with parametric variations in the velocity of the impactor, the ply orientations, mass and curvature. In addition, Krishnamurthy, et al. (2003) compared the effects of the impactor mass and the impactor velocity and concluded that the impactor velocity had a greater effect on the contact force. They were also of the opinion that ply orientation had a major influence on impact response. In a related parametric study, Tiberkak, et al. (2008) confirmed that the ply stacking sequence had an effect on impact response. They further observed that the impact force and central deflection were proportional to the impact velocity during the loading phase of a simply supported plate, and that an increase in the impactor mass did not lead to an equal increment in the maximum contact force. The contact duration was however observed to increase with an increase in the mass of the impactor.

Her and Liang (2004) studied the influence of shell curvature, clamped or simply supported boundary condition, and impactor velocity on the impact response of the laminated composite structure. The contact force and centre deflections were presented.

Wang, et al. (2006) performed drop-impact analysis on multi-layered printed circuit boards (PCB). A parametric study on the effect of fiber volume fraction, number of copper foil layers and the effect of the material – isotropic and orthotropic on the PCB was reported. They were of the opinion that the study of the displacement amplitude, stress and strain could help predict PCB deflection and warpage, and stress induced failures.

Tu and Chao (1999) performed a series of parametric studies evaluating the effects of laminate thickness, impactor size, mass, and initial velocity on the impact responses.

Bretos, et al. (1999) analysed the bending eigenmodes of wooden bars numerically using finite element modelling. The frequency responses of these bars were recorded.

2.7.9 Results validation

Son and Fam (2008) verified predicted finite element results with experimental results and reported similarities in the load-deflection plots. Lang and Fodor (2002) validated their finite element model by comparing predicted deflections with measured ones. They plotted load – deflection curves with obtained data, and concluded that they could accurately predict stress development and spatial displacements in such joints. Serrano (2001) tabulated the results obtained in varying various parameters. They compared some of the variations with the aid of load displacement plots. Lam, et al. (2004) developed a simple beam finite element model to validate a full-scale physical test model. They plotted load – deflection curves,

and deflection – time curves to compare various cases. Piao, et al. (2005) conducted finite element analysis (FEA) on small-scale and full-scale composite poles; the deflections of both full-size and small-scale members predicted by the FEA were compared with those measured from their experimental study. Davalos and Qiao (1999) conducted 3-point and 4-point bending tests on beams using their proposed computational approach and compared the maximum deflections and strains with experimental results.

2.8 REVERSE ENGINEERING

With the aid of data obtained from the disassembly and digitization of a physical model, reverse engineering techniques have been used to develop finite element models (Cheng, et al., 2001, Thacker, et al., 1998). Cheung, et al. (2004) obtained all information including specific dimensional data of a physical product through reverse engineering of a sample. They performed a CT-scan of the sample, imported the splines into Solid-Works CAD software and modelled a 3-dimensional solid geometric model. The geometric model was exported into a finite element analysis software for meshing and analysis. Lin, et al. (2008) employed a validated finite element model developed by the reverse engineering technique to investigate the mechanical interactions of a product varying the material properties, designs, and thicknesses. Similar to Cheung, et al. (2004), they imported point cloud data into a 3D CAD system and exported the geometrical model to a finite element analysis software. Bagci (2009) created CAD models from physical models using a coordinate measuring machine (CMM) to digitize their data.

CHAPTER THREE

PREPARATIONS FOR FINITE ELEMENT ANALYSIS (FEA)

3.1 INTRODUCTION

Inputs defining a finite element model are mostly based on assumptions (Adams, 2006, 2008) such as geometry, material properties, loads and boundary conditions. These inputs could be based on nominals, worst-case scenarios, or average operating conditions (Adams, 2008). Errors, or uncertainties are associated with incorrect assumptions (Adams, 2006) hence, the accuracy of a solution is partly dependent on the assumptions made (Lawry, 2003) and on the awareness of the assumptions by the user (Adams, 2008). Here, the development of a computational geometry replica to an existing Jumping saddletree is presented. Importing data from the computational geometry to MSC.Patran where it is pre-processed into a finite element model is further presented. This forms the basis for the geometric modelling assumptions made in developing the finite element models presented later in this research. Furthermore, the assumptions made in developing the laminate properties of the finite element models which are presented later in this thesis are also presented.

3.2 GEOMETRIC MODELLING

The development of a geometric model identical to the physical model is fundamental in developing its computational model. In many practical cases, geometric shape data and accurate drawings required for the creation of computer-aided-designs (CAD models) (Javidrad and Rahmati, 2009; Sokovic and Kopac, 2006; Zhang, 2003; Yau, 1997) are unavailable. To create a CAD model identical to

the horse riding jumping saddletree, it was necessary to obtain geometric shape data from an existing product.

3.2.1 Reverse Engineering

Reverse engineering techniques can be applied to develop geometric models from similar physical objects (Lin and Kuo, 2009). Though theoretically simple, it involves a variety of tasks (Lin, et al., 1998). Varady, et al. (1997) presented a flowchart to represent a reverse engineering process (see figure 3.2.1).

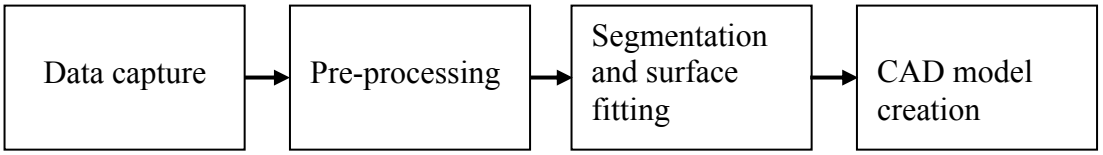

Figure 3.2.1 Phases of reverse engineering
(Redrawn from Varady, et al., 2007)

There are many different ways for acquiring shape data (Bardell, et al., 2003; Tao and Jiyong, 2007; Varady, et al., 1997). They can be obtained either by tactile methods such as Coordinate Measuring Machines (CMM) and robotic arms, or through non-contact methods such as optical scanners and magnetic field measurement machines (Bagci, 2009; Li, et al., 2009; Tao and Jiyong, 2007; Varady, et al., 1997).

For this research, a CMM with a touch-trigger probe was used. CMMs are becoming increasingly important in metrology (Dobosz and Wozniak, 2005; Kweon and Medeiros, 1998). They can be described as Cartesian robots (Bagci, 2009; Bardell, et al., 2003; Kweon and Medeiros, 1998; Yau and Menq, 1995) with a probe that can be used in measuring geometric feature data by continuous probing, scanning, or

points cloud (Bagci, 2009). The components of a CMM system include a 3-axes mechanical set-up, probe head, control unit, and a computer unit (PC) (Bardell, et al., 2003).

The contact probe provides a connection between the work piece and the 3D length measuring system of the CMM (Wozniak and Dobosz, 2003). They are classified as touch-trigger probes, analogue probes (also known as contact scanning probes) (Yague, et al., 2009; Hariharan and Balaji, 2009), and hard probes (Hariharan and Balaji, 2009). Touch-trigger probes are widely used on CMMs (Cauchick-Miguel and King, 1998). A contact probe acquires data by physically touching a work piece, creating and sending a trigger pulse to a computer (Wozniak and Dobosz, 2003), which interprets and records them as specific points in space (Hariharan and Balaji, 2009). The performance of the probe system influences the accuracy of the CMM (Dobosz and Wozniak, 2005; Wozniak and Dobosz, 2003).

Prior to the commencement of measurements, it is necessary to calibrate the probe and set up the coordinate system (Menq and Chen, 1996). The output data of the CMM represent the coordinate values of the centre of the probe in X, Y and Z direction of the touched location on the work piece (Zhang, 2003). An average value of probe pretravel is compensated for during the calibration process (Dobosz and Wozniak, 2005). Artifacts such as gauge-blocks, step-gauges, ball-plates, hole-plates, ball-bars, and ball-cubes can be used to calibrate a probe (Osawa, et al., 2002).

When using a CMM, it may be necessary to measure additional points (Chivate and

Jablokow, 1995). Additional measurement data could be attached to existing data as long as the precise location where they are required in the point data file is recognised (Lin, et al., 1998). The point data may be modified after collection (Chivate and Jablokow, 1995).

In order to acquire sufficient data to represent the saddletree, it was divided into sections. Start and end points were positioned on the edges so as to make it possible to include supplementary data if necessary. Data was obtained by probing the saddletree work piece point-to-point in each section.

Though point-to-point manual probing is demanding (Yau, 1997), less points are measured in comparison with those contained in point-clouds. Most CAD systems are incapable of handling the huge amount of data contained in point-clouds, hence the need for macro programs (Yau, 1997) to pre-process them before exporting the created surfaces to a 3D CAD system for further developments (Budak, et al., 2005; Yau, 1997; Ye, et al., 2008). There is a growing trend in integrating the macro programs with commercial CAD systems as add-ins (Ye, et al., 2008).

CAD models can be created from measured data in two ways, the curve mode and, the surface mode (Zhang, 2003; Bagci, 2009). The point-to-point data acquired by the CMM were output as points having x y z coordinates. They were saved as .txt files and imported directly into SolidWorks CAD/CAM/CAE software. Curves were fitted through the points (see figure 3.2.2) applying the *Insert, Curve*, and, *Curve Through XYZ Points…* command in Solid Works.

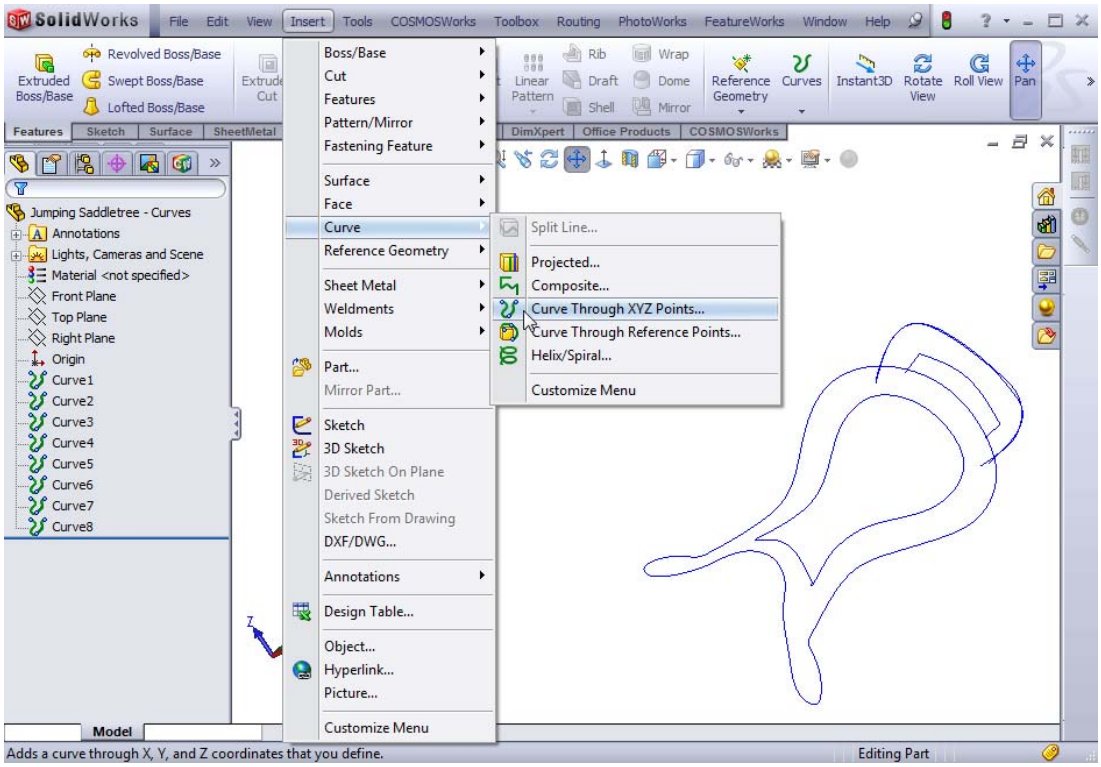

Figure 3.2.2 Curves fitted through imported point data

Curves are important in product modelling (Ye, et al., 2008). They were applied in defining the boundary within which surfaces were created (see figure 3.2.3). The surface function *Insert, Surface*, and, *Fill* was applied.

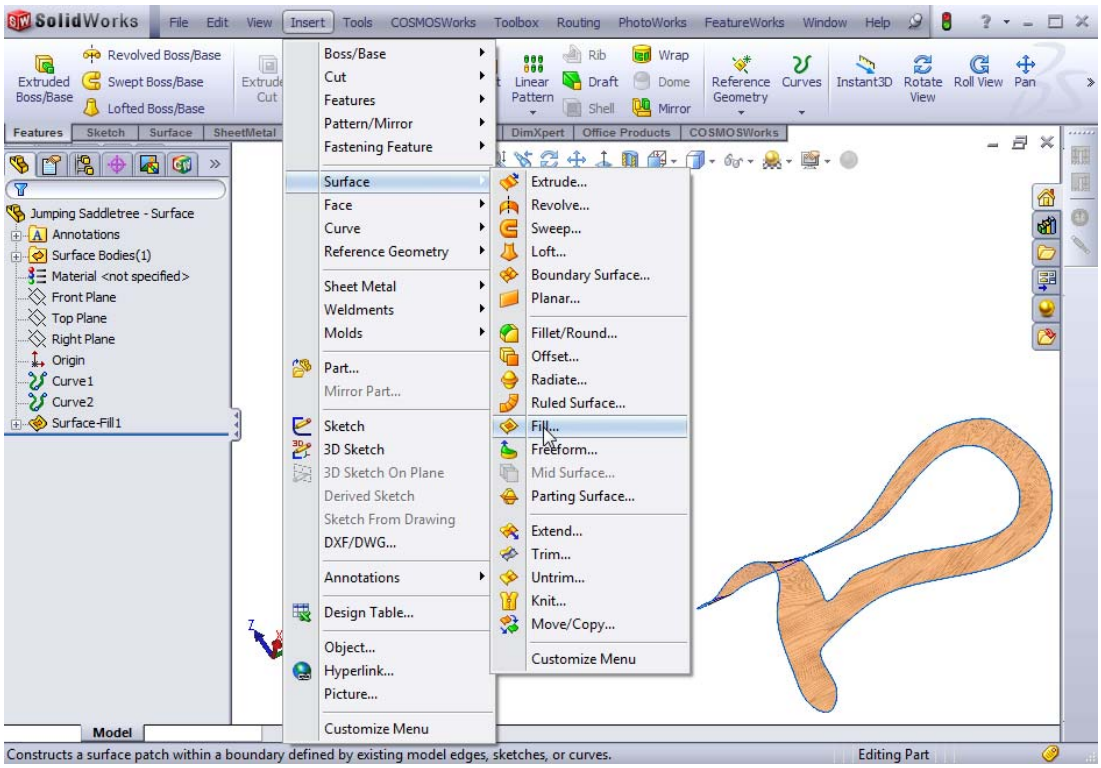

Figure 3.2.3 Surfaces created from Curves

Finally, the all the geometric surfaces are combined together using the Surface function, *Insert, Surface*, and, *Knit* (see figure 3.2.4) to create the required solid models. An option *Try to form solid* is selected.

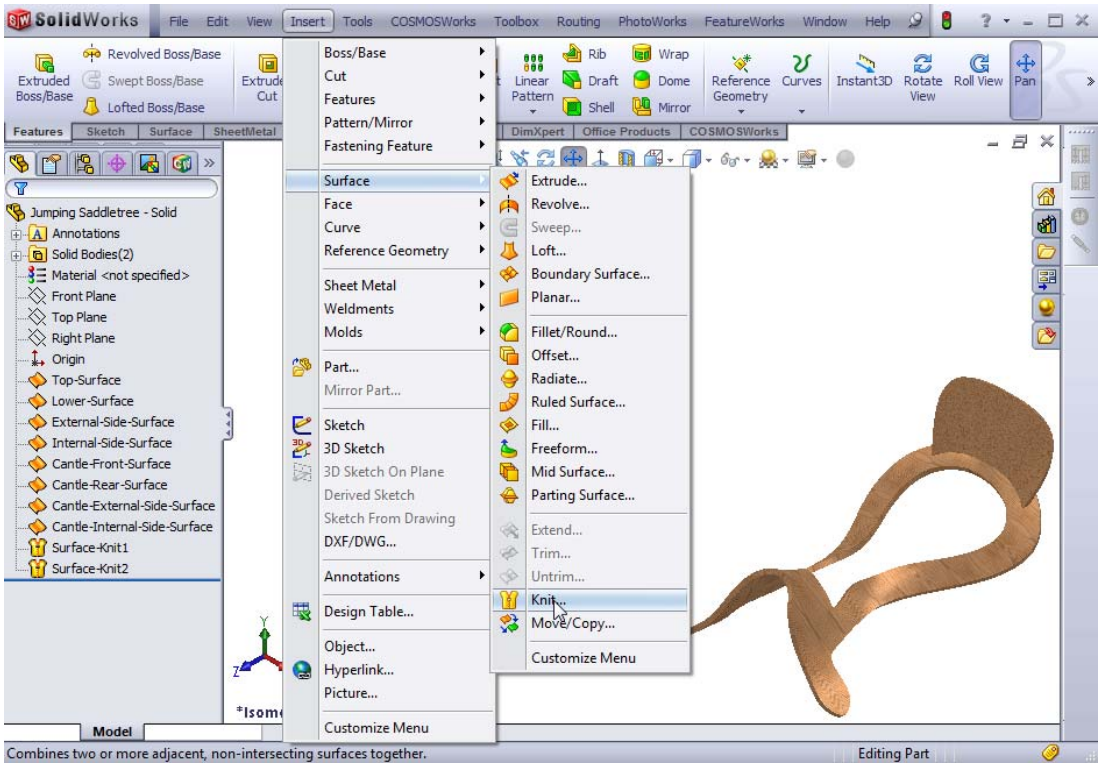

Figure 3.2.4 Solid models created from Surfaces

3.2.2 Data migration from CAD to FEA

In this research, MSC.Patran was applied for pre- and post-processing of the finite element models, while MSC.Marc was applied as the solver (also known as analysis code). MSC.Patran software is employed in creating finite element (FE) models and post-processing results of FE analyses (Leski, 2007; Orifici, et al., 2008). It is one of the most popular FEA tools used in industry (Yang and Reidsema, 2008); it sets the standard for finite element pre- and post-processing (Lakshmininarayana, 2004) and, interfaces with most finite element solvers used in industry (Padhi, et al., 2002; Leski, 2007). MSC.Marc is a nonlinear solver renowned for its contact applications (Lakshmininarayana, 2004; Fan, et al., 2008). A solver checks the input data,

executes it, and generates the output data (Fan, et al., 2008).

There are no automatic adaptation tools capable of creating FE models from design models (Foucault, et al., 2008). CAD models can be imported to CAE systems in standard formats including IGES, STL, ASCII, DXF, and VDA (Sokovic and Kopac, 2006). They could also be imported in parasolid format (Williams, 2000). There is however, a risk of losing model data during the conversion process between different data file formats (Buriol and Scheer, 2008). Translation errors in geometry during data exchange, which may seem insignificant, can cause significant problems (Chong, et al., 2007). A lot of resources are expended in trying to repair these problems (Yang and Han, 2006) by repeating the data exchange or recreating the model (Brunnermeier and Martin, 1999). In addition to the errors in the model, the models may be imported as a group of surfaces rather than as solids.

MSC.Patran has the capabilities of importing ACIS, Parasolid, Catia, Euclid3, Pro/Engineer, Express Neutral, IGES, Neutral, STEP, STL, and VDA. In addition, an existing MSC.Patran database may also be imported.

There is no information about units of measures in MSC.Patran, hence a consistent set of units must be used (Leski, 2007) commencing with the measurements of the imported geometric model. The international system of units, SI has been used in this research.

A geometric model saved in parasolid (x_t) format was imported into MSC.Patran. Some of the bodies created were not triparametric; hence they could not be meshed

using the IsoMesher (see figure 3.2.5). MSC.Patran can mesh solid bodies with the IsoMesh or TetMesh function; while IsoMesh can be used to mesh only congruent triparametric solids with hexahedron (hex) or wedge elements, TetMesh can be used to mesh all solid bodies with tetrahedron (tet) elements. (MSC.Software, 2005). Tet meshes were however, not supported by laminate properties.

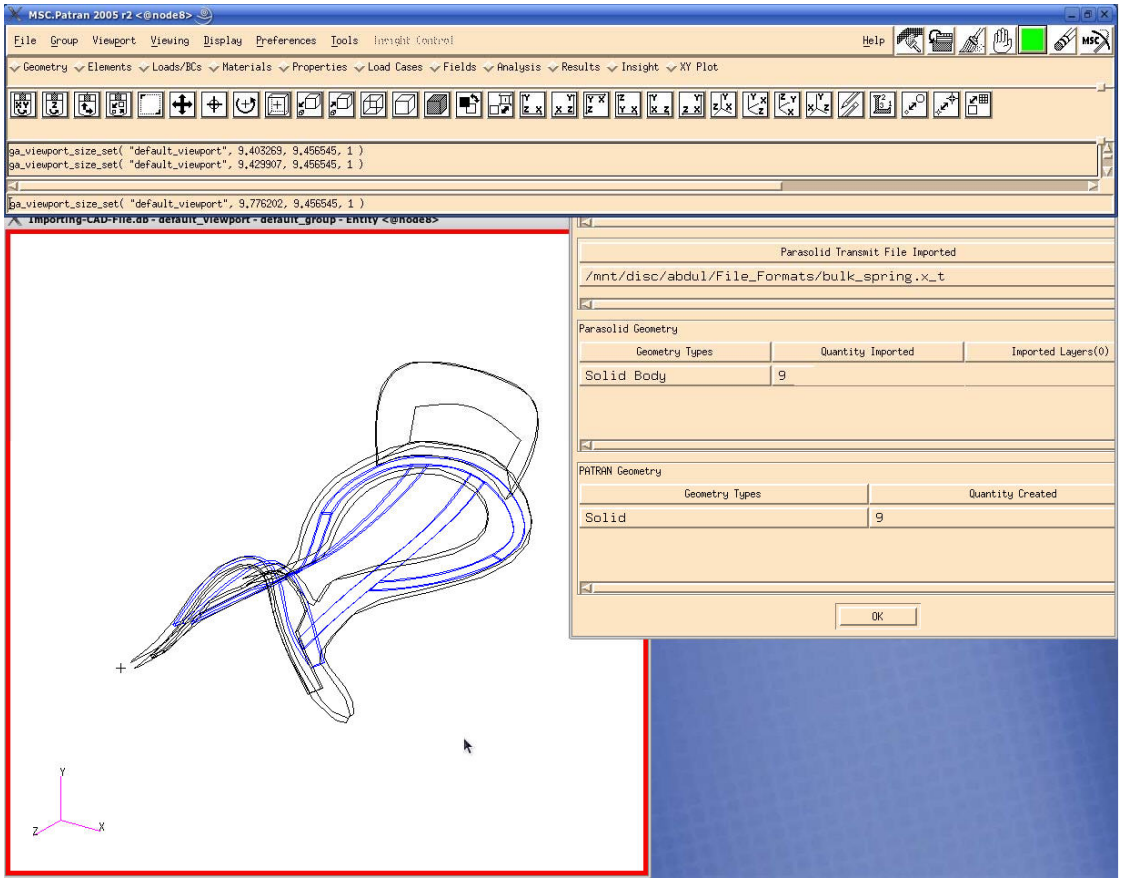

Figure 3.2.5 Blue wireframes represent triparametric solids

The available options for creating hex elements were:

- To remodel the solid bodies that were not triparametric in MSC.Patran; or,
- To create the hex mesh using the following process:
  - create a quadrilateral (quad) mesh using the paver mesher on the top surface of the body;
  - create a set of identical elements by using the *transform, element, translate* function. Set the *Direction Vector* to <0 0 0>;

- project the new nodes of the new set of elements to the other surface using the *modify, node, project* function. The direction is set to *normal;*
- sweep the two sets of elements by using the *Sweep, Element, Loft* function. The number of elements through thickness can be changed using the *Mesh Control* function.

Here, the geometric solid bodies were remodelled in MSC.Patran; the reverse engineered CAD geometry was applied as a guide and constraint. On completion, all the bodies were triparametric and could create hex meshes with the isomesh mesher (see figure 3.2.6).

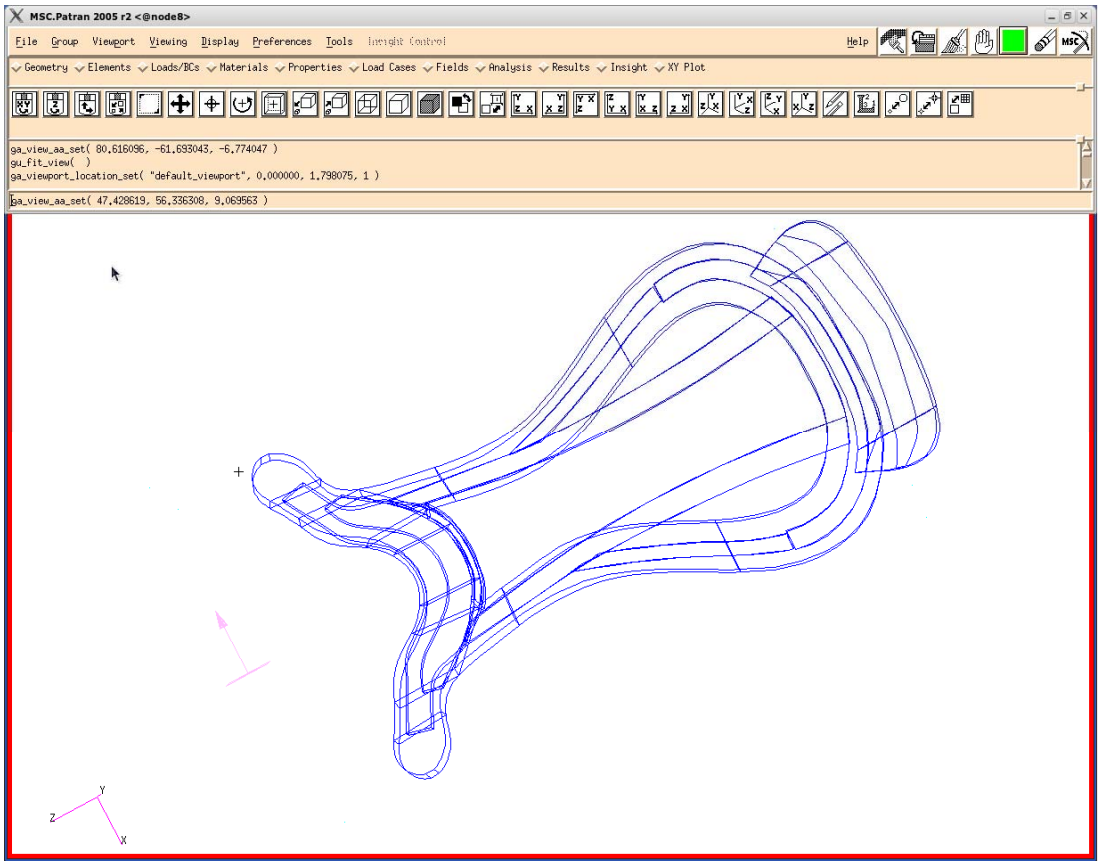

Figure 3.2.6 Recreated triparametric solid bodies

3.3 LAMINATE MODELLING

There are a few commercially available third party codes which can be applied in

modelling laminates. MSC.Laminate Modeler, an MSC.Patran module for aiding the design, analysis, and manufacture of laminated composite structures (MSC.Software, 2008a) is one of them. Without this add-on tool, laminates could be modelled in accordance with some existing structural theories. Reddy (2004) described the approaches used in analysing composite plates in the past. They include the following:

- equivalent single-layer theories (2D) (ESL)
    i. classical laminated plate theory;
    ii. shear deformation laminated plate theories.
- three-dimensional elasticity theory (3D)
    i. traditional 3-D elasticity formulations;
    ii. layerwise theories
- multiple model methods (2-D and 3-D).

Laminates can be modelled in MSC.Patran in the following ways:

- creating a surface or solid geometry and defining its material and element properties as laminates. In the material menu, the *Create, Composite, Laminate* function is selected. In the element properties menu, the *Create*, *3D* or *2D*, *Laminated Composite* (option for *3D*) or *Laminate* (option for *2D*) function is selected. The material name, orientation system, and orientation angle are defined. In the 3D option, the *thickness direction* in respect to the solid body faces is defined.
- creating a surface or solid geometry and defining them as contacting bodies. The material and element properties, orientation system and orientation angles are defined as required by the user.

If the constitutive materials of the laminate are isotropic, the default coordinate system of the software is adequate in defining the orientation system of the element properties in the laminate lay-up, and the analysis coordinate frame. However, if the laminates are made up of orthotropic materials, the coordinates defining the orientation system of the element properties, the ply orientation, and the analysis coordinate frame must be defined.

A laminate orientation code is applied to describe laminates. It is based largely on a code reported to have been included in the 3rd edition of the Advanced Composites Design Guide by the Air Force Structural Dynamics Laboratory (Adams, et al., 2002; U. S. Department of Defence (DoD), 1999). Some features of the code, as described by DoD (1999), and Adams, et al. (2002) include:

- the plies are listed in sequence from the top lamina to the bottom lamina, and enclosed in square brackets to indicate the beginning and the end of the code;
- the orientation of each lamina (or fibre direction) is denoted by a number representing its angle in degrees, and separated by a slash from the next angle.

In addition to the orientation code, there are terms used to describe laminates, which provide an indication of the type of coupling in the plies (Hopkins, 2005) (see table 3.3.1).

Table 3.3.1 Descriptions of Laminates

Term	Description	Example
Asymmetric	Plies not distributed symmetrically about mid-thickness	0/45/60/0
Symmetric	Plies symmetrically distributed about laminate mid-thickness	0/-30/-30/0

Balanced	For every +θ ply there is a -θ ply	30/-30/30/-30
Cross-Ply	Laminate of pairs of 0 degree and 90 degree plies	0/90
Angle Ply	Laminate with plies of equal angle but opposite sign θ	30/-30
Symmetric Cross-Ply	Laminate of 0/90 plies symmetrically distributed about laminate mid-thickness	0/90/90/0
Symmetric Angle Ply	Laminate with the plies of equal angle, θ, symmetrically distributed about the laminate mid-thickness	-30/30/30/-30
Asymmetric Angle Ply	Laminate with the plies of opposite sign for angle, θ, asymmetrically distributed about the laminate mid-thickness	-30/30/-30/30

Source: Hopkins, 2005.

3.3.1 Finite elements for modelling laminates

MSC.Marc contains a broad element library (MSC.Software, 2004; 2007; 2008b); some are structurally classed as *Continuum Composite Elements.* Two brick types, element type 149 and 150 are considered here:

- element type 149 – an 8-node isoparametric composite brick (see figure 3.3.1) which can be used to create hex 8 and wedge 6 elements;
- element type 150 – a 20-node isoparametric composite brick (see figure 3.3.2) which can be used to create hex 20 and wedge 15 elements.

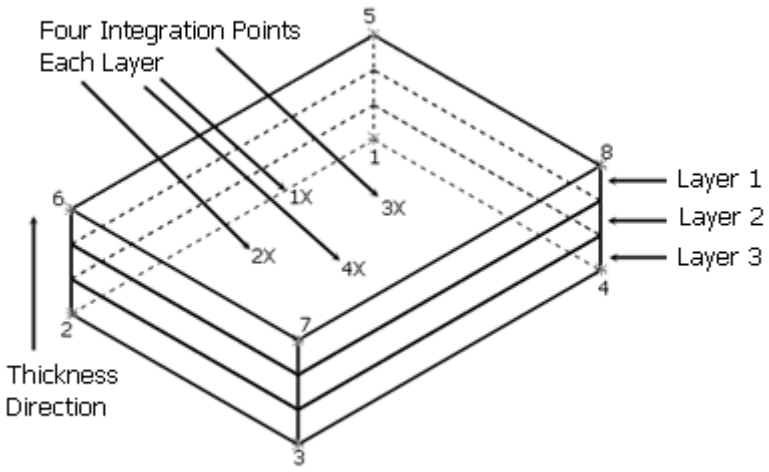

Figure 3.3.1 Elm type 149, 8-node 3-D Composite Element
(Source: MSC Software, 2004; 2007; 2008b)

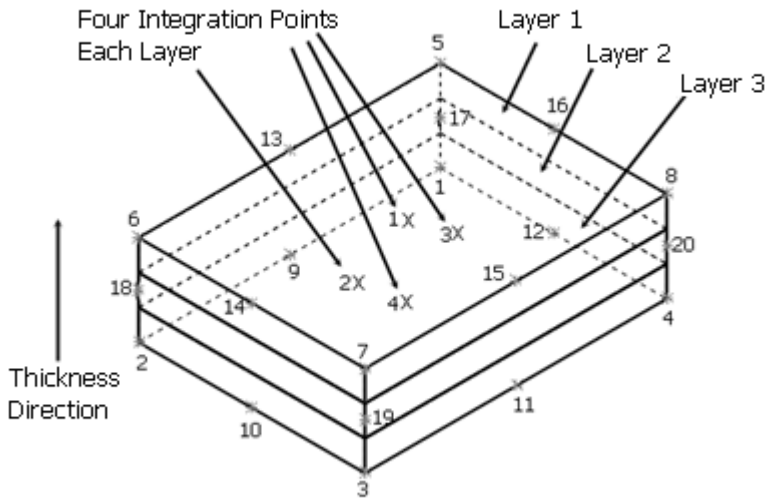

Figure 3.3.2 Elm type 150, 20-node 3-D Composite Element
(Source: MSC Software, 2004; 2007; 2008b)

Element formulations that support the assigning of different material properties to layers through their thickness permit a single element to be used to represent a laminated composite stock, thereby appreciably reducing the number of elements required in an analysis, and consequently, its computational expense (Marsden and Irving, 2002). In addition, the layerwise format maintains a 2-D type data structure similar to finite element models of 2-D equivalent single-layer theories therefore, having a reduced input data volume and allowing an efficient formulation of the element stiffness matrices (Reddy, 2004). Layerwise elements are assumed to have the same modelling capability as conventional 3-D finite elements (Reddy, 2004). A minimum of 2 layers and a maximum of 510 layers may be used within each element (MSC.Software, 2004; 2007; 2008b).

Element type 7, which is a three-dimensional eight-node, first-order, isoparametric element (arbitrarily distorted brick), and element type 21 which is a three-dimensional twenty-nodes, isoparametric, arbitrarily distorted cube (MSC.Software,

2004; 2007; 2008b) may be used when the solid geometries are modelled with contact as illustrated in figure 3.4.4.

3.3.2 Example – Layerwise or conventional 3-D elements

Simplified models can be used to explore input data assumptions and qualify data in terms of eventual goals (Adams, 2006). In this section, the modelling assumptions made in developing the laminate models of the saddletree in later chapters are simplified, and validated with hand calculations. Gibson (1994) described a laminated beam subjected to pure bending as the simplest laminated structure. A simple cantilever beam was simulated in a static analysis. The beam was modelled with layerwise elements (elm 149 and 150) and conventional 3-D elements (elm 7 and 21). Since deformation is the primary output of an FE solution, ensuring that deformation is correct is the first step towards a successful simulation (Adams, 2008).

3.3.2.1 Geometry

A solid body representing a single cantilever beam, and a group of 4 solid bodies representing 4 cantilever plies with their adjacent faces in contact, were modelled (see figures 3.3.3 and 3.3.4). The two configurations represent the methods in which laminates can be modelled in MSC.Patran (as earlier reported in section 3.3). While the thickness of the single beam was 0.006 m, individual thickness of the 4 solid bodies was 0.0015 m; the width and length were 0.04 m and 0.15 m respectively. These dimensions were similar to those defined in Chatiri, et al. (2009) and Sun (2006).

3.3.2.2 Load and boundary conditions

The models were assumed to be fixed "encastre" at one end while a load of 10 N (5 N x2) was applied on the opposite end as illustrated in figures 3.3.3 and 3.3.4. "Glue-all" contact was defined between adjacent bodies in figure 3.3.4.

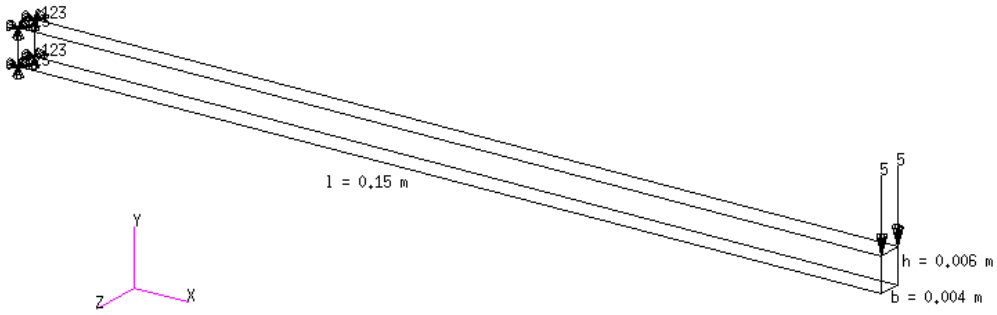

Figure 3.3.3 Solid body geometry representing a cantilever beam

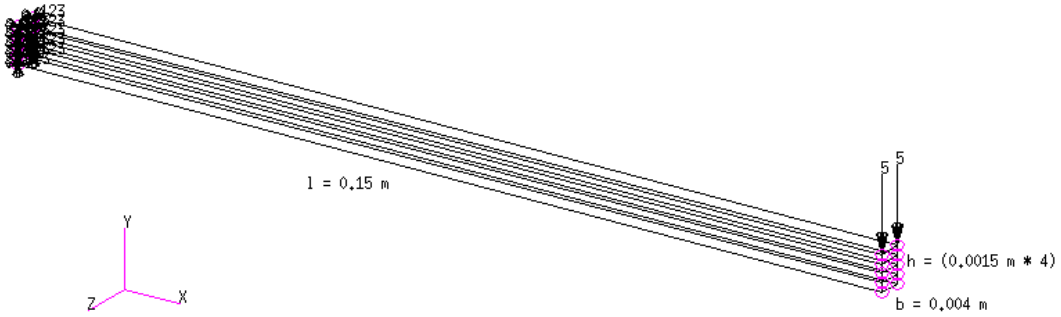

Figure 3.3.4 4 Solid bodies in contact

The pink circles in figure 3.3.4 represent contact between touching bodies.

3.3.2.3 Material properties

The following material properties of birch wood are used to define the geometric models: E_{11} = 1.529E+10, E_{22} = 7.65E+08, E_{33} = 1.19262E+09, ν_{12} = 0.45, ν_{23} = 0.426, ν_{31} = 0.043, G_{12} = 1.039E+09, G_{23} = 2.5993E+08, G_{31} = 1.1314E+09. The geometric model illustrated in figure 3.3.3 was discretized with layerwise

elements, and each layer was defined with the orthotropic properties of birch wood. In view of the complexity in defining material directionality in orthotropic material modelling (Marsden and Irving, 2002) the laminate model was simplified by assuming a lay-up of $[0/0/0/0]_T$. Also, each geometric solid model illustrated in figure 3.3.4 was defined with the orthotropic material of birch wood. The orientations were defined individually.

3.3.2.4 Results

The results of the simulations are presented in table 3.3.2.

Table 3.3.2 Results of simulations of Simplified Models

	Orthotropic			
	Hex 8		Hex 20	
	Laminates Elm type 149	Solid Elm type 7	Laminates Elm type 150	Solid Elm type 21
No of Elements	664	7520	200	4200
No of Nodes	1260	13608	1673	28484
Displacement (mm)	10.10	10.00	10.00	9.97
CPU Time	27.46	229.01	20.74	825.06

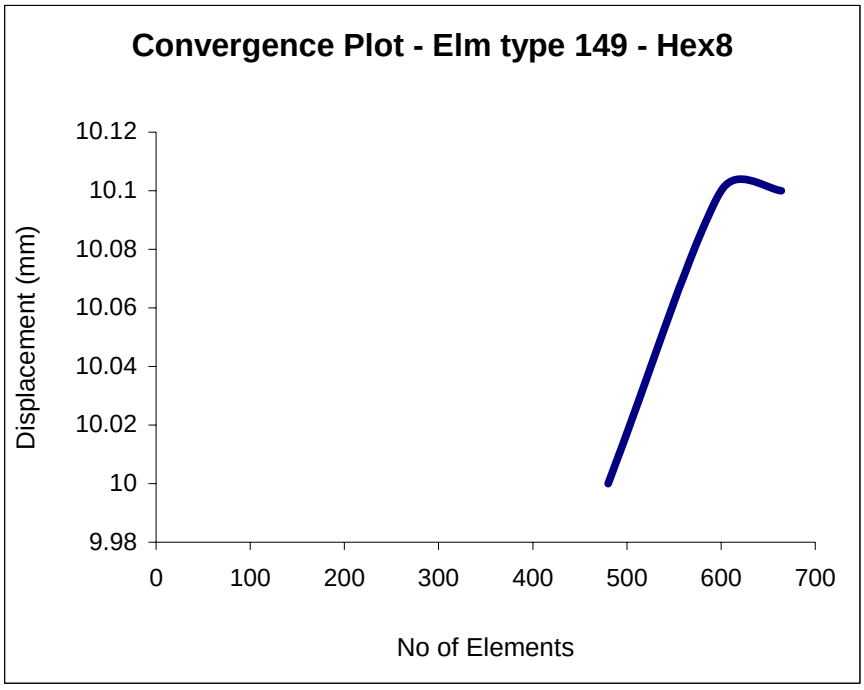

Figure 3.3.5 Convergence plot of FEM with hex 8 mesh, and element type 149

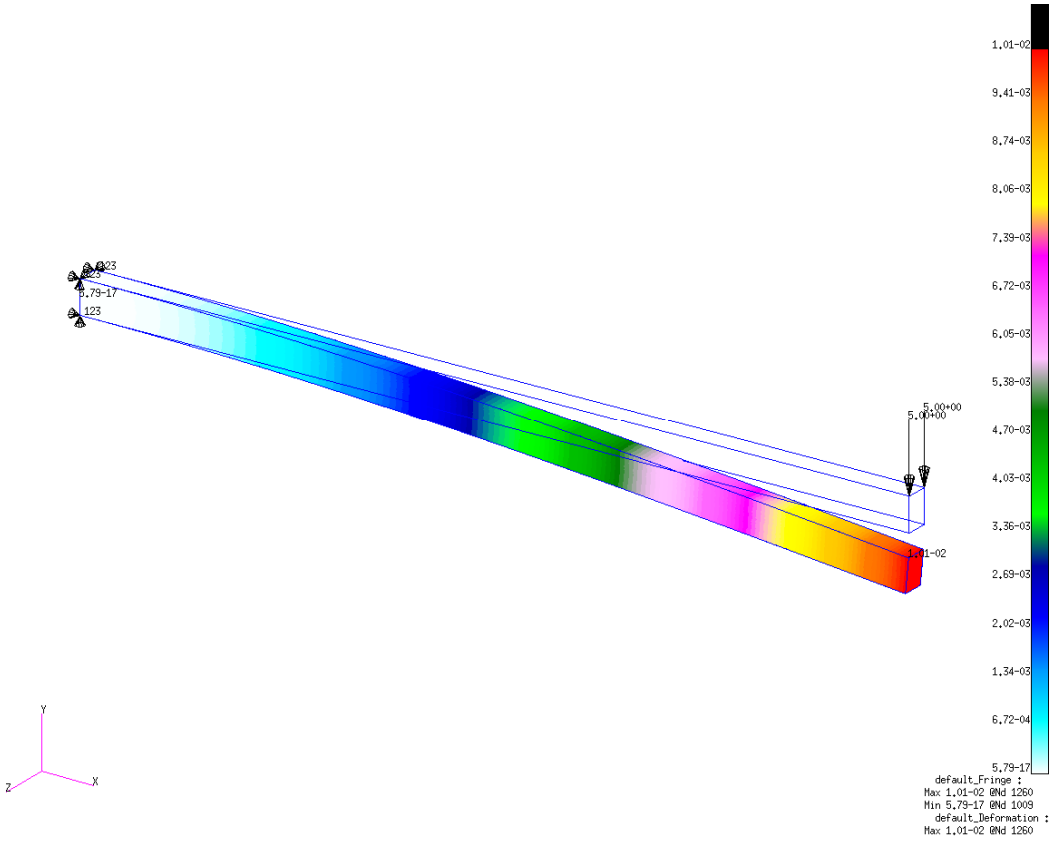

Figure 3.3.6 Deflection of FEM with hex 8 mesh, and element type 149

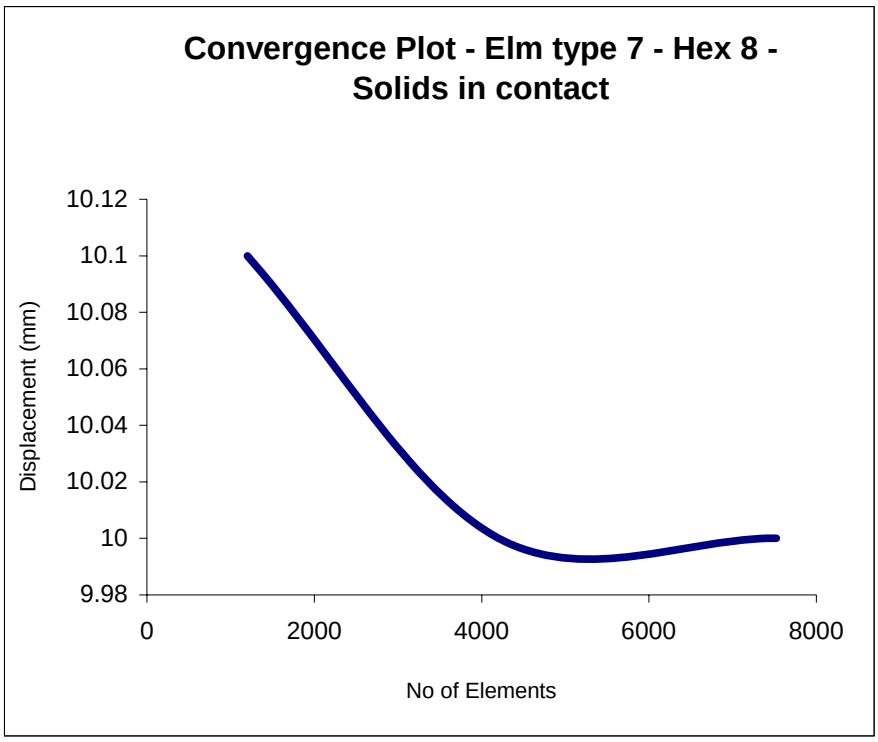

Figure 3.3.7 Convergence plot of FEM with orthotropic material, contact, hex 8 mesh, and element type 7

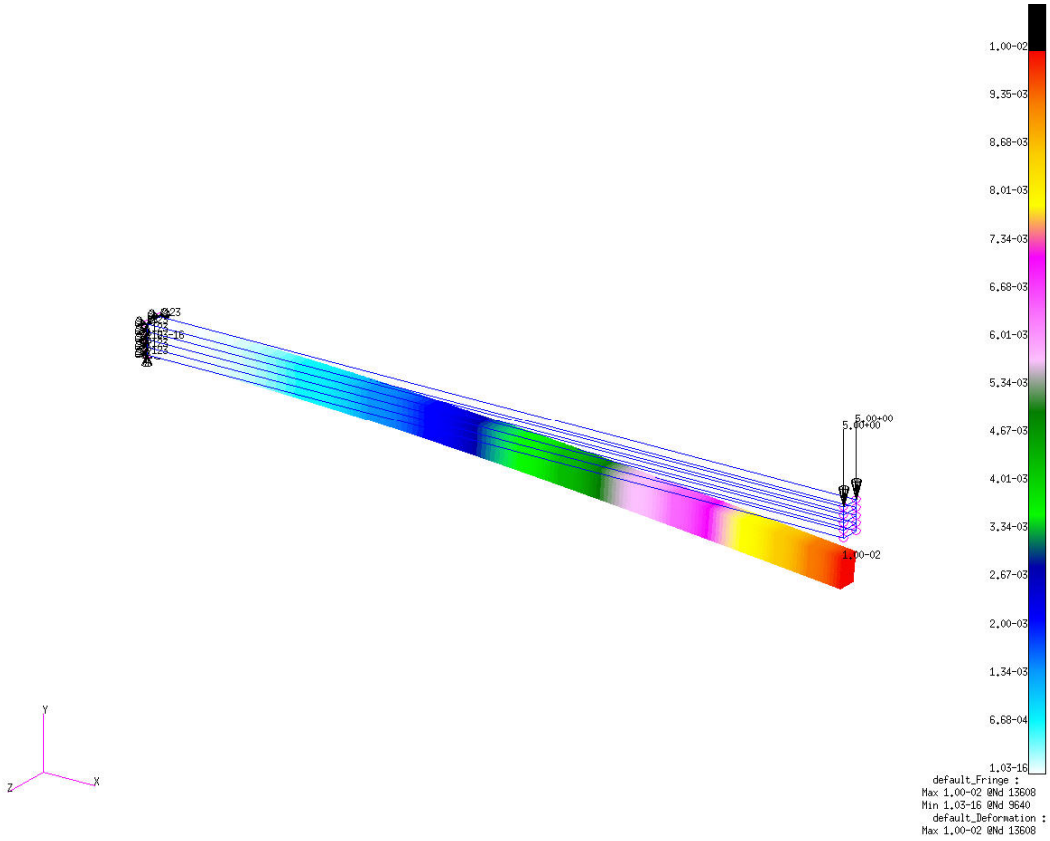

Figure 3.3.8 Deflection of FEM with contact, hex 8 mesh, and element type 7

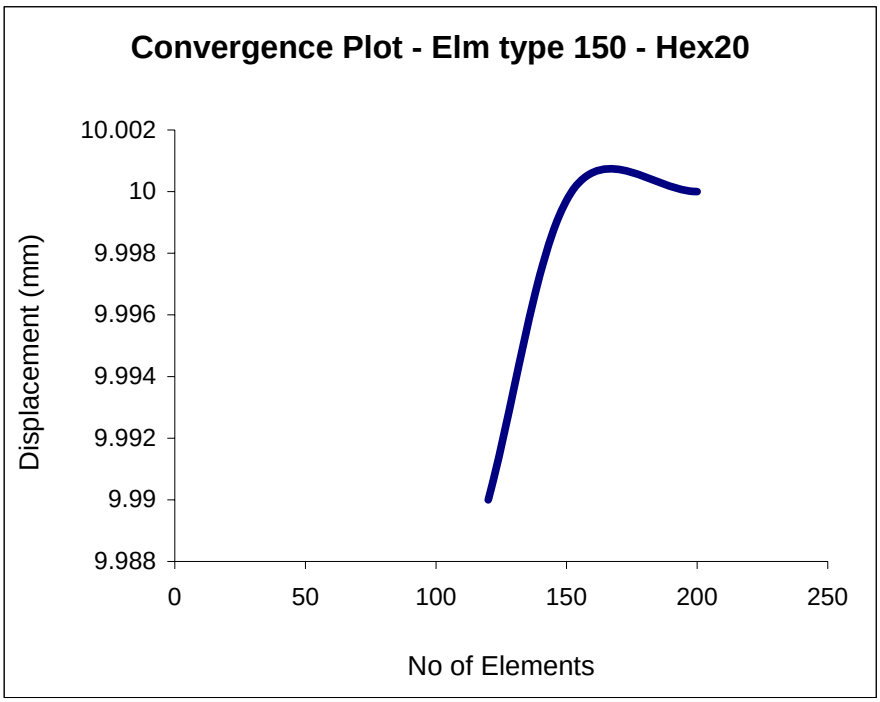

Figure 3.3.9 Convergence plot of FEM with hex 20 mesh, and element type 150

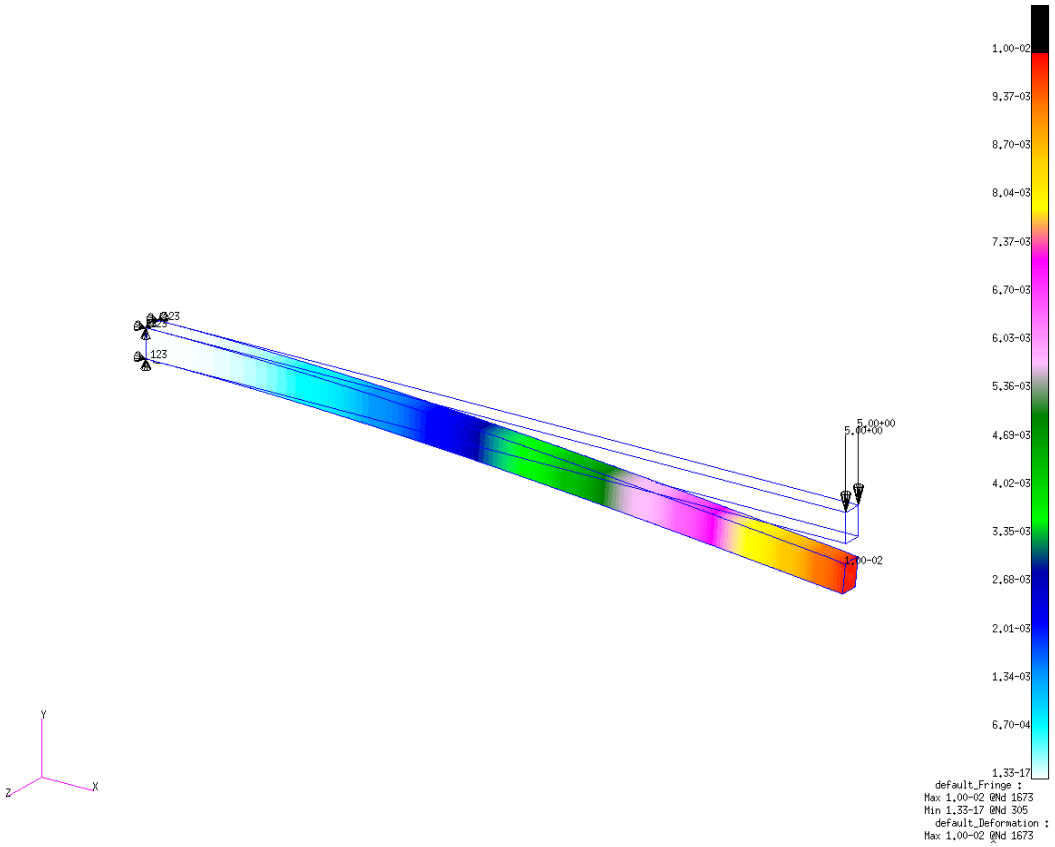

Figure 3.3.10 Deflection of FEM with hex 20 mesh, and element type 150

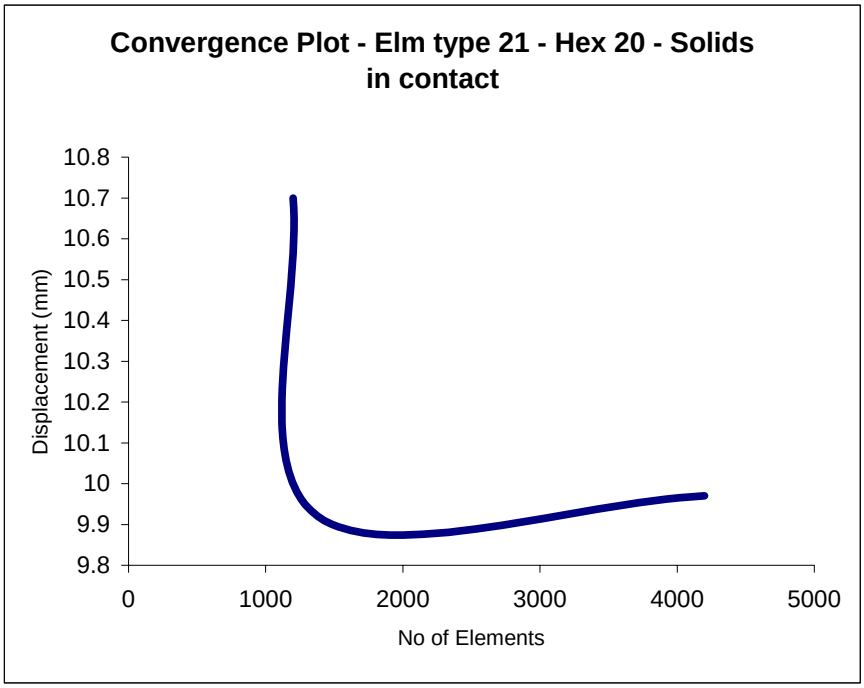

Figure 3.3.11 Convergence plot of FEM with contact, hex 20 mesh, and element type 21

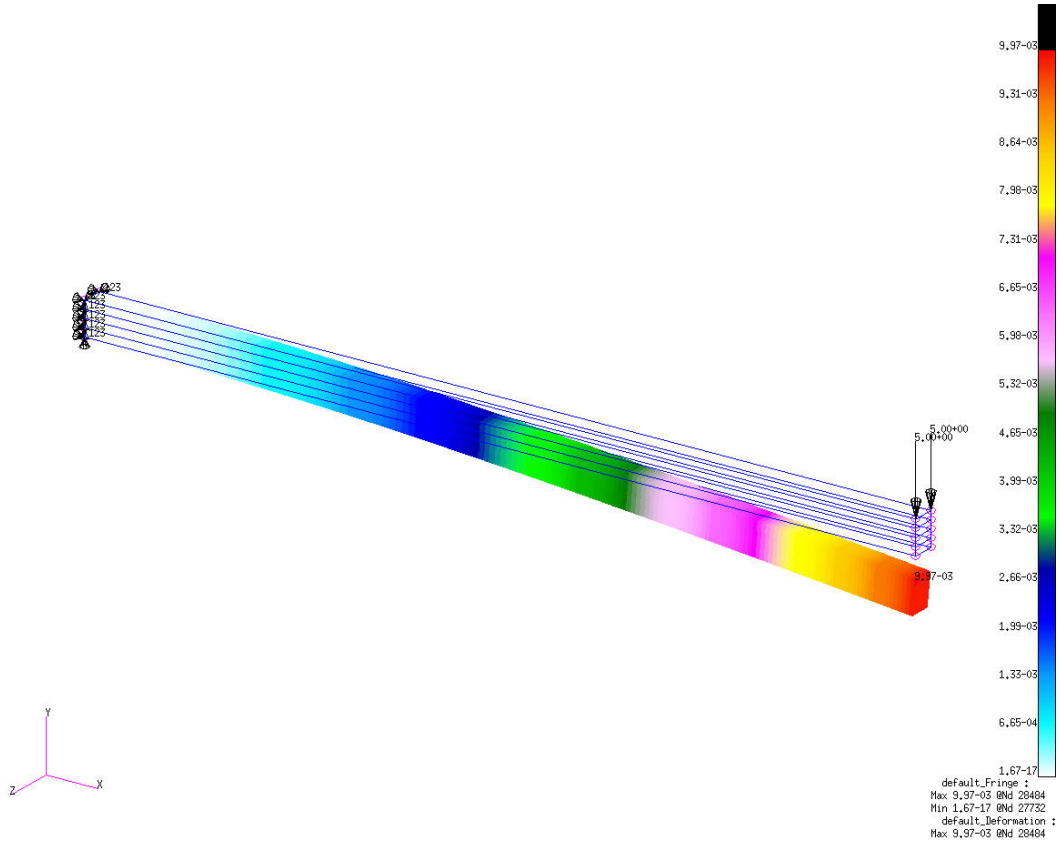

Figure 3.3.12 Deflection of FEM with contact, hex 20 mesh, and element type 21

3.3.2.5 Hand calculations

Hand calculations can be used to quantify expectations of stress and displacement (Adams, 2006). Gibson (1994) developed a theory of laminated beams in pure flexion from the Bernouilli-Euler beam theory. The theory is based on the following assumptions:

- Plane sections normal to the longitudinal axis of the beam remain plane and normal during flexure;
- Both geometric and material properties of the plies are symmetrically arranged about the neutral surface;
- Each ply is linearly elastic with no shear coupling;
- The plies are perfectly bonded together.

The maximum deflection at the tip of a cantilever beam was

$$\delta_{\max} = \frac{PL^3}{3E_f I_{yy}} \tag{3.1}$$

where,

I_{yy} is the moment of inertia about the neutral axis

$$I_{yy} = \int z^2 dA = \frac{bh^3}{12} \tag{3.2}$$

E_f is the effective flexural modulus of the beam (same as the Young's Modulus of beam material for a homogeneous, isotropic beam)

$$E_f = \frac{8}{h^3} \sum_{j=1}^{N/2} (E_x)_j \left(Z_j^3 - Z_{j-1}^3\right) \tag{3.3}$$

Z is the distance from the neutral surface

j is the number of ply

N is the total number of plies.

Given,

L = 0.15 m, b = 0.004 m, h = 0.006 m, N = 4, $Z_0 = 0$, $Z_1 = 0.0015$ m, $Z_2 = 0.003$ m, P = 10 N, and, $(E_x)_j$ = 1.53E+10 Pa, maximum tip deflection was calculated to be 10.21 mm.

Berenberg (1989) derived an equivalent bending stiffness *E*I* for composite beams under pure bending. In addition to the standard beam theory assumptions, the following assumptions were made:

- The beam is of rectangular cross-section;
- Plies lie in the x - z or 1 - 2 plane;
- The shear coupling terms $(\ )_{16}$ and $(\ )_{26}$ of the matrices [A], [B], and [D] are zero.

$$E^* = D_{11}\frac{12}{h^3} \tag{3.4}$$

Inserting equation 3.4 into the standard beam theory gives

$$\omega_{\max} = \frac{Pl^3}{3D_{11}b} \tag{3.5}$$

D_{11} was obtained from the matrix computed by the pre-processor. The maximum deflection was calculated to be 10.1 mm.

3.3.2.6 Discussion

The maximum deflections obtained in the simulation and the one obtained in the hand calculation are summarised in table 3.4.3.

Table 3.3.3 Results of simulations and hand calculations

	Hex 8		Hex 20		Gibson (1994)	Berenberg and UTS (1989)
	Laminates Elm 149	Solid Elm 7	Laminates Elm 150	Solid Elm 21		
No of Elements	664	7520	200	4200		
No of Nodes	1260	13608	1673	28484		
Displacement (mm)	10.10	10.00	10.00	9.97	10.21	10.10
CPU Time	27.46	229.01	20.74	825.06		

In terms of CPU time, element type 150 was recorded to have performed best. Lower-order elements (types 7 and 149) are however preferable to higher-order elements (types 21 and 150) in a contact analysis (MSC.Software, 2004; 2007; 2008b; Hellen, 2003). In terms of solving, element type 149 provided the best solution in comparison with Berenberg and UTS (1989) and Gibson (1994). In addition, element type 149 provided the best solution in comparison with the hand calculations presented in section 3.3.2.5. The general performance of the simple form, lower-order elements can be improved by using very fine meshes (Hellen,

2003). The number of elements reported in table 3.3.3 indicates that finer meshes of Hex 8 (lower-order) elements are required to obtain a solution in comparison with the meshes of Hex 20 (higher-order) elements. It is also worthy to note the similarity in the convergence plots of the layerwise element types 149 and 150. Likewise the similarity in the convergence plots of the conventional 3-D element types 7 and 21.

3.4 SUMMARY

A process of developing a 3-dimensional CAD model identical to the physical model was presented. A CMM fitted with a touch-trigger probe was applied to obtain shape data from the surfaces of the saddletree. Point-to-point data were imported into SolidWorks CAD software and were used to develop geometries. Further, the process of importing the geometry into MSC.Patran was presented. This was followed by a process of repairing the geometry in MSC.Patran.

A numerical model of a cantilever beam modelled with assumptions identical to those presented later in this thesis was later presented. Hand calculations were applied to validate the numerical solutions. It was illustrated that lower-order elements (type 7 and 149) with finer meshes are sufficient in modelling laminate structures. Simplifying the complexity of a model has helped in developing confidence in the solution methodology and software.

CHAPTER FOUR

SIMULATING BENDING IN THE SADDLETREE

4.1 INTRODUCTION

Contact between the saddle and the horseback, and movements in the horseback have been discussed earlier in chapter 2. Three major movements were identified to occur in the equine thoracolumbar spine. They are as follows: flexion and extension, lateral bending, and axial rotation. Furthermore, a three-point-bending configuration and a pinned sacrum set-up analogous to a cantilever beam were reported to have created flexion and extension, and lateral movements in the thoracolumbar spine. Here, the identified modes of movements particularly flexion and bending, produced by the cantilevered spine influenced the choice of the loads and boundary conditions used to define the finite element models of the saddletree.

The development of static numerical models with loads and boundary conditions defined in a manner similar to the modelling of a cantilever beam is presented. The models were not in contact with any external body hence, the simulations provided an opportunity to investigate the saddletree as a product rather than as a part.

4.2 PARAMETERS INVESTIGATED

With a view to understanding the relationship between some of the component parts of the saddletree and their sensitivity to loading, the following parameters were investigated:

- The effect of the metal reinforcements on the wood-only product:

Earlier in the literature review, some saddletree makers were reported to have included metal reinforcements in order to strengthen the wooden product. Furthermore, during a company visit, the author observed that some saddletree makers excluded the pair of spring steel in their saddletree construction. These conditions were simulated; and the effect of the steel reinforcements with and without the pair of spring steel on the stiffness of the wooden product investigated and quantified.

- The effect of varying the thickness of the saddletree:

The effect of varying the thickness of the wood was also quantified in terms of stiffness. While maintaining a constant thickness of the metal reinforcements, the thickness of the wooden frame of the saddletree was varied between 7.5 mm and 4.5 mm.

- The effect of the material type:

The effect of constructing with solid wood in comparison with laminated wood on the stiffness of the saddletree was also investigated.

4.3 PRE-PROCESSING

Finite element analysis involves three independent processes: pre-processing, numerical analysis (also known as the solution stage), and post-processing (analysis of results) (Wijesinghe, et al., 2005; Pellissetti and Schueller, 2009). Finite element models are developed at the pre-processing stage (Khoei, 2002). Earlier in chapter 3, MSC.Patran was identified as the software employed for pre-processing the FE models in this study. The following assumptions were made in developing the FE models in this part of the study:

4.3.1 Geometric models

The geometry used in creating the finite element models was reverse-engineered from an existing physical model and imported into MSC.Patran. The process was reported earlier in chapter 3. In this study, this geometry was assumed to represent an English jumping saddletree. The saddletree-only structure (as illustrated in figures 4.3.1 and 4.3.4), the reinforced saddletree (as illustrated in figures 4.3.2 and 4.3.5), and, the reinforced saddletree without the pair of spring steel (as illustrated in figures 4.3.3 and 4.3.6) were all derived from the reverse-engineered geometry. The thickness variations were 7.5 mm, 6.0 mm, and 4.5 mm for the solid models while the variations of the laminate models were 5, 4, and 3 plies of 1.5 mm thickness. The lipped gullet plate and the cantle iron were 3 mm thick, while the cap plate was 2 mm thick. In addition, the spring steel and the bar plates were 1.3 mm and 1 mm thick respectively.

The cantle, which is the raised rear part that supports the rider's seat (Keefer, 1996) and prevents the rider from slipping off the back of the saddle (Beatie, 1981) was excluded from the saddletree numerical models. Beatie (1981) considered it to be a safety feature. During the initial experimental tests to determine the upper limits beyond which the saddletree would no longer remain elastic, it was observed that the cantle tended to rotate about its axis thereby affecting the measurement of the saddletree deflection. This varied from cantle to cantle. A closer look revealed that the joints of the cantle and the side rail at the rear were suspected to yield. Variations in the pitch or slope of the cantle (Beatie, 1981) may have also been responsible.

In order to avoid conditions that may not be controllable and/or repeatable, the cantle

was excluded from the models. The bars were therefore assumed to be continuous.

4.3.2 Material properties

The material properties were discussed earlier in chapter 2. All the wood models were defined with orthotropic mechanical properties based on the following assumptions: E11 = 1.529E+10 Pa, E22 = 7.65E+08 Pa, E33 = 1.19262E+09 Pa, $\nu12 = 0.45$, $\nu23 = 0.426$, $\nu31 = 0.043$, G12 = 1.039E+09 Pa, G23 = 2.5993E+08 Pa, and, G31 = 1.1314E+09 Pa (Forest Products Laboratory, 1999). Isotropic material properties were assumed for the mild steel reinforcements based on the following: E = 2.1E+11 Pa and, $\nu = 0.29$. In addition, the laminate total stacking sequence was defined as [0/90/0/90/0] for the 7.5 mm thick models, [0/90/0/90] for the 6.0 mm thick models, and, [0/90/0] for the 4.5 mm thick models. Each lamina was 1.5 mm thick.

4.3.3 Load and boundary conditions

Initial experimental tests demonstrated that the wood-only saddletree samples fixed at the pommel and loaded at the rear remained elastic under a load of 20 kg. Consequently, a point load of 196.20 N was applied on the cantle region of the numerical models while the models were fixed at a section of the pommel (as illustrated in figures 4.3.1, 4.3.2, and 4.3.3). In addition, a uniformly distributed load of 50767.00 Pa was applied on a section of the cantle region while the models were fixed at a section of the pommel (as illustrated in figures 4.3.4, 4.3.5, and 4.3.6). To simplify the models, all the parts joined together with rivets on the physical model were assumed to be glued together using the contact feature. In addition, the constraint imposed by the feature ensured that penetration did not occur between the

contacting models during simulation (MSC.Software, 2004; 2008). The pink circles in figures 4.3.2, 4.3.3, 4.3.5, and 4.3.6 illustrate contact between two bodies.

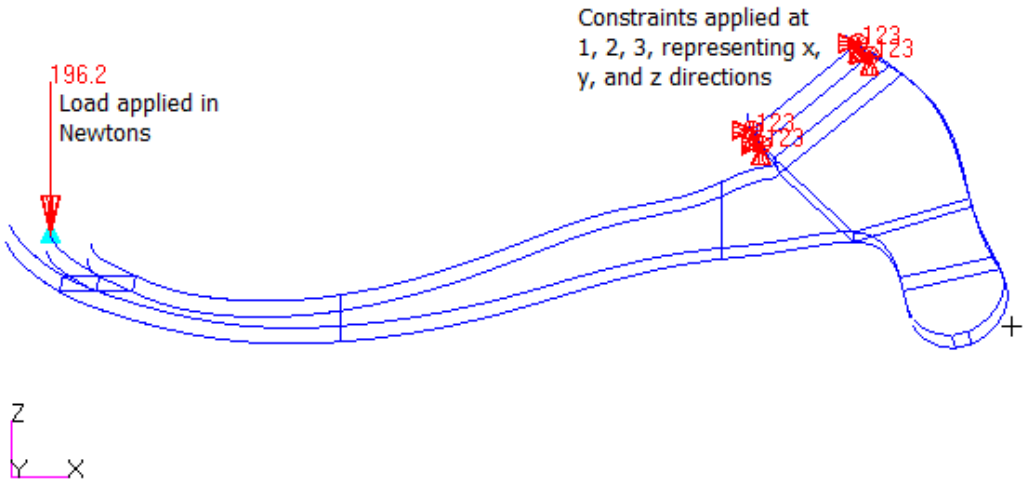

Figure 4.3.1 Saddletree model fixed at the pommel and loaded at the rear with a point-load

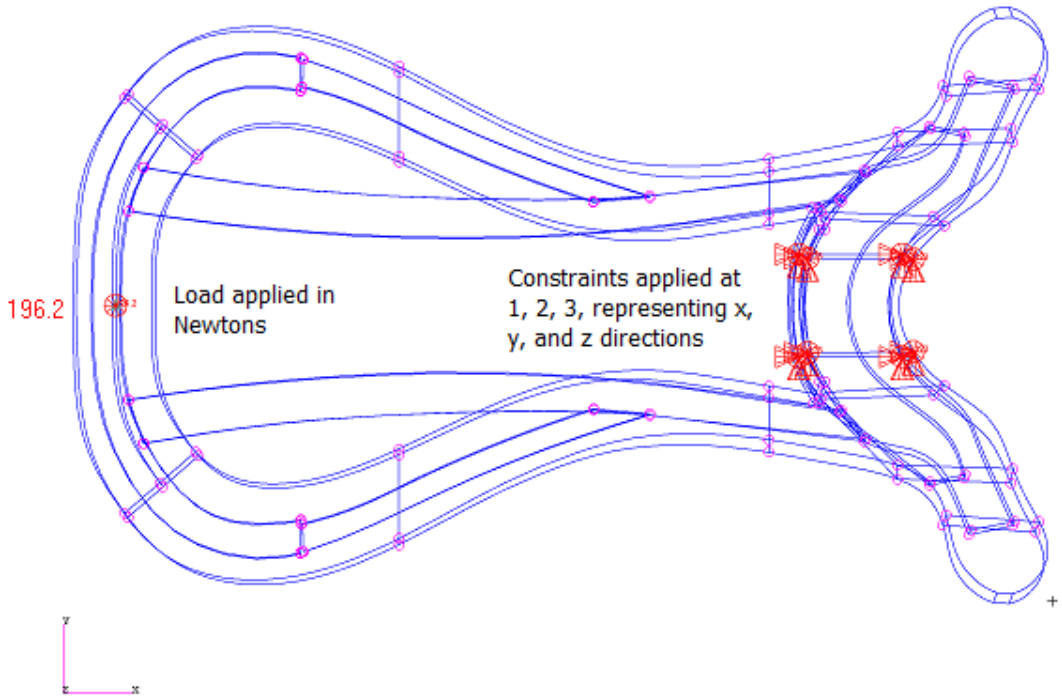

Figure 4.3.2 Reinforced saddletree model fixed at the pommel and loaded at the rear with a point-load

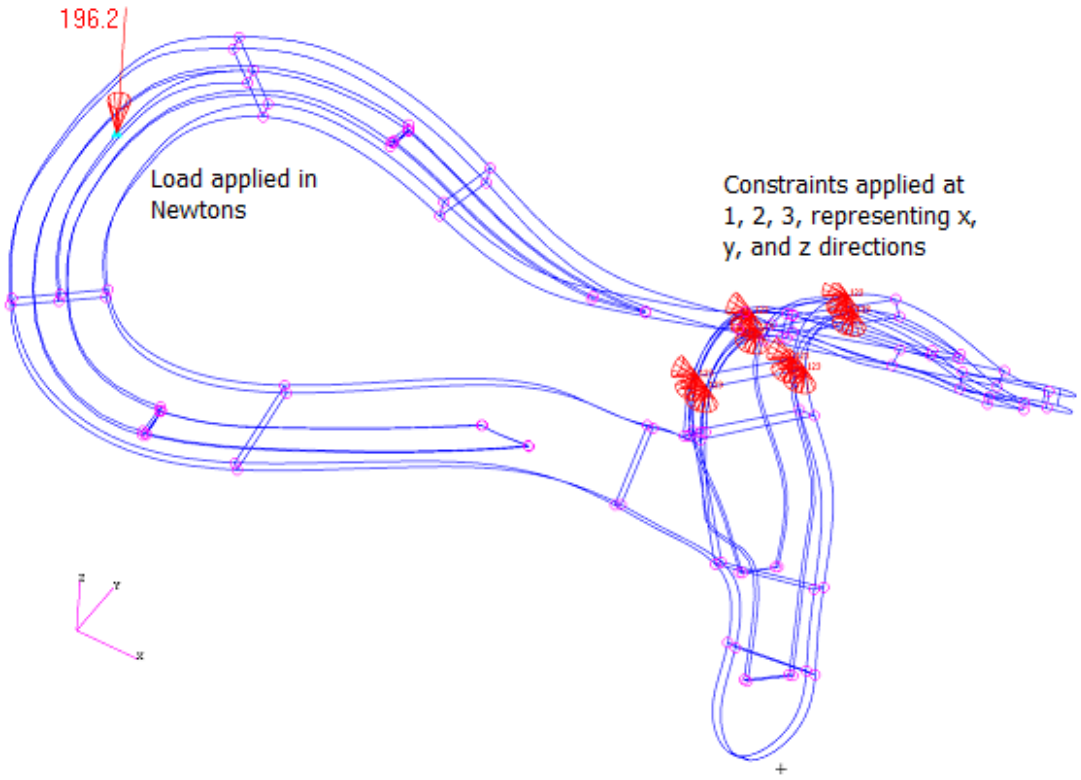

Figure 4.3.3 Reinforced saddletree (excluding the spring steel) model fixed at the pommel and loaded at the rear with a point-load

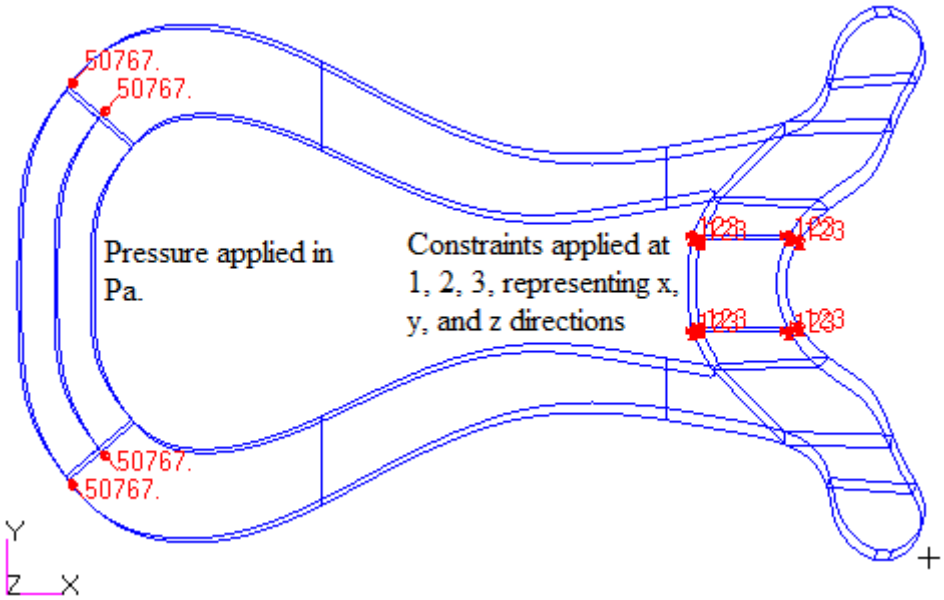

Figure 4.3.4 Saddletree model fixed at the pommel and loaded at the rear with a uniformly distributed load

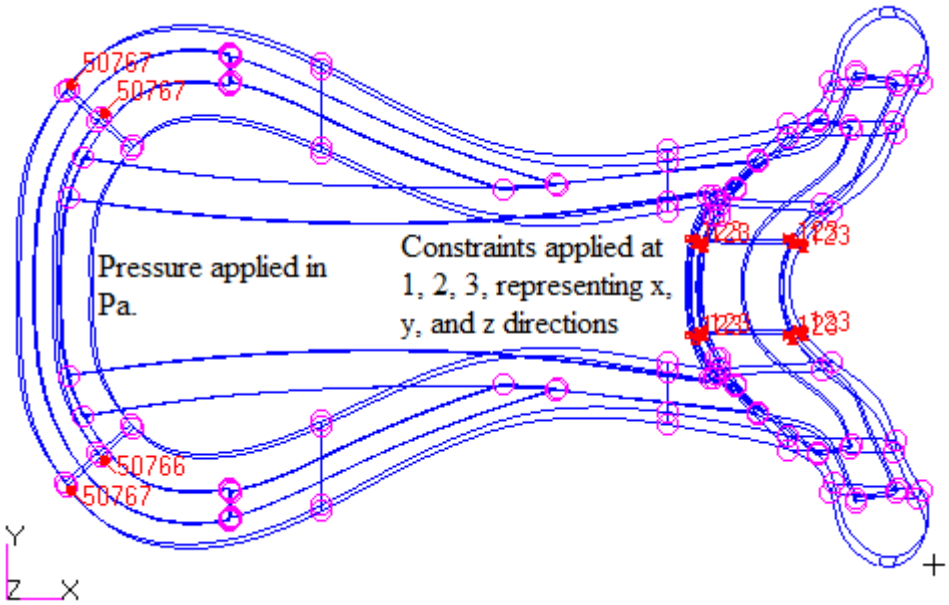

Figure 4.3.5 Reinforced saddletree model fixed at the pommel and loaded at the rear with a uniformly distributed load

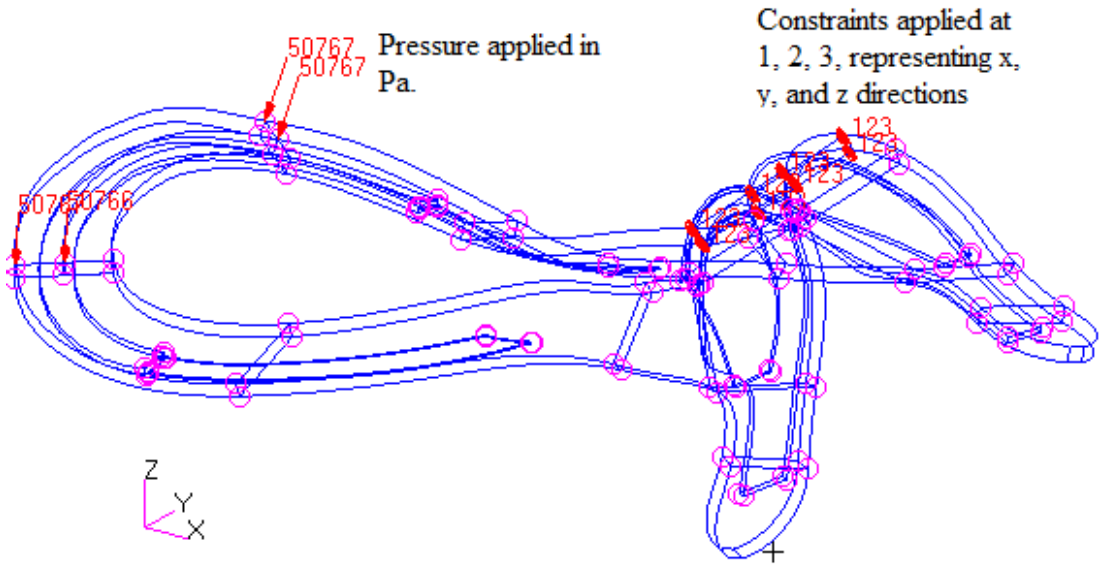

Figure 4.3.6 Reinforced saddletree (excluding the spring steel) model fixed at the pommel and loaded at the rear with a uniformly distributed load

4.3.4 Element and element properties

Conventional 3-D element type 7, an 8-node isoparametric brick was applied to create hex 8 elements for the solid wood models and all the steel reinforcement models while, layerwise element type 149, an 8-node isoparametric composite brick

element was applied to create hex 8 elements for the laminate models. The default elemental coordinate system was selected as a reference for the orientation angles.

4.4 MSC.MARC SOLUTION PARAMETERS

The analysis solver utilises the specifications defined at the pre-processing stage to assemble the element matrices, which are then used in the direct or iterative solution of the systems of equations (Pellissetti and Schueller, 2009). There are three sources of nonlinearities namely: material nonlinearity, boundary nonlinearity, and geometric nonlinearity (Yan and Strenkowski, 2006; Korochkina, et al., 2008; Kong and Wu, 2009).

Linear and nonlinear phenomena can be employed for similar analyses (Bonet and Wood, 1997) however, while a linear case analysis is normally based on the assumptions of small displacements and rotations, and elastic material properties (Karvinen and Pegg, 2006), in a nonlinear case, the magnitude of the deformation is unrestricted (Bonet and Wood, 1997).

The analysis of an elastic model undergoing contact interactions involves constraints on displacements, which are a form of nonlinear mixed boundary conditions wherein both the extent of the actual contact boundary and the contact reaction on this boundary are unknown (Mankame and Ananthasuresh, 2004). Hence, the linearity option was set to nonlinear. The deformable-deformable contact method was applied and, the contact control parameter was set to double-sided. Contact may also cause friction (Xu, et al., 2009) however, in view of the assumption that all contacting bodies were glued together, the friction parameters type option was set to none. The

models that would come into contact during the analysis step were appropriately defined in the contact table (McCarthy, et al., 2005). The loads were treated as incremental, the full Newton-Raphson iterative procedure selected (Spears and Miller-Young, 2006) and, the initial stress stiffness option was set to full.

4.5 POST-PROCESSING

Post-processing is the final step of the FE analysis and it involves the retrieval of derived quantities of interest from the solution vector which corresponds to the vector of the displacements at the nodal degrees of freedom DOF (Pellissetti and Schueller, 2009). Further, it provides visualisation of the computed results of an analysis (Khoei, 2002; Pellissetti and Schueller, 2009; Benzley, et al., 1995). The deformation plots (Pellissetti and Schueller, 2009) are illustrated in the following subsections. The models loaded with a point load and those loaded with a uniformly distributed load are presented in subsections 4.5.1 and 4.5.2 respectively. Figures 4.5.1 to 4.5.24 illustrate the various simulations performed in this chapter. The software deflection measurements are presented in metres.

4.5.1 Point load

4.5.1.1 Saddletree (wood only)

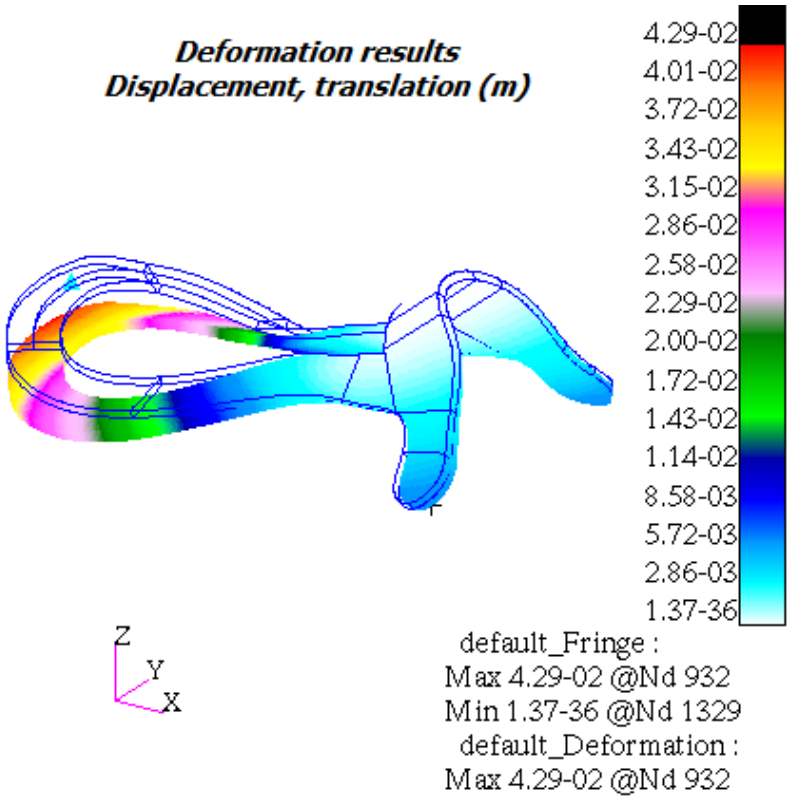

Figure 4.5.1 Saddletree – solid wood material – 7.5 mm thick

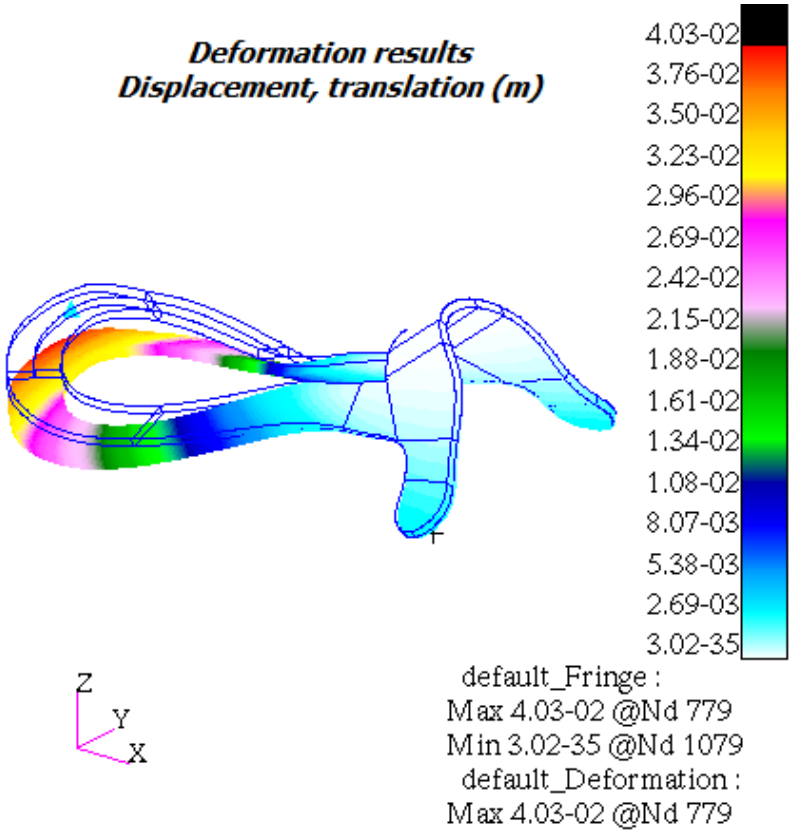

Figure 4.5.2 Saddletree – laminates – 5 plies x 1.5 mm thick

4.5.1.2 Reinforced saddletree

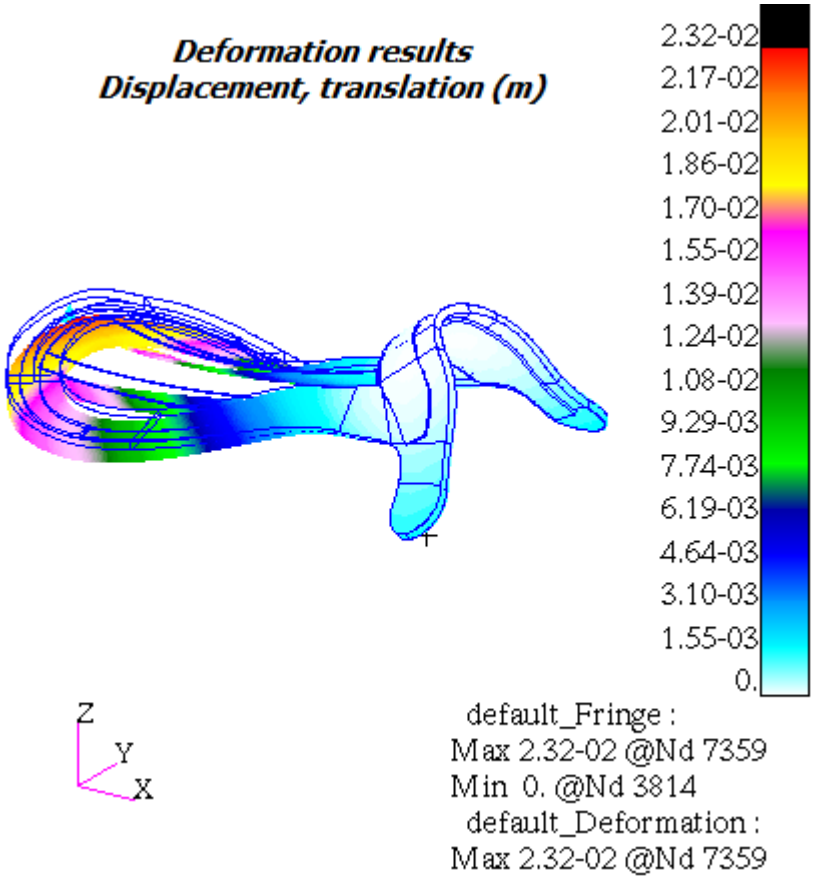

Figure 4.5.3 Reinforced saddletree – solid wood material – 7.5 mm thick

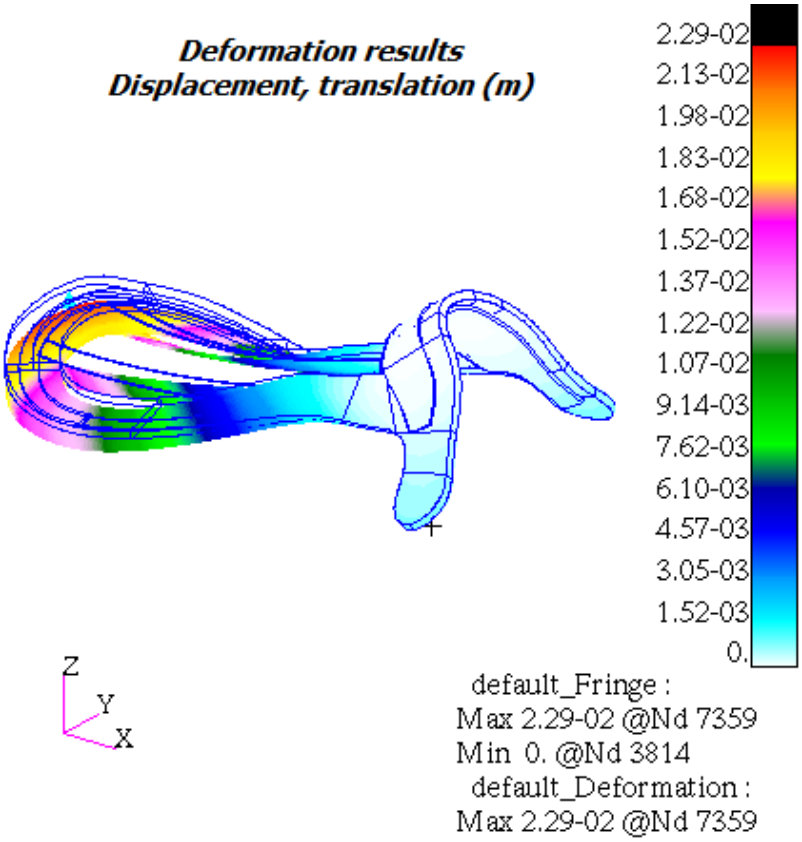

Figure 4.5.4 Reinforced saddletree – laminates – 5 plies x 1.5 mm thick

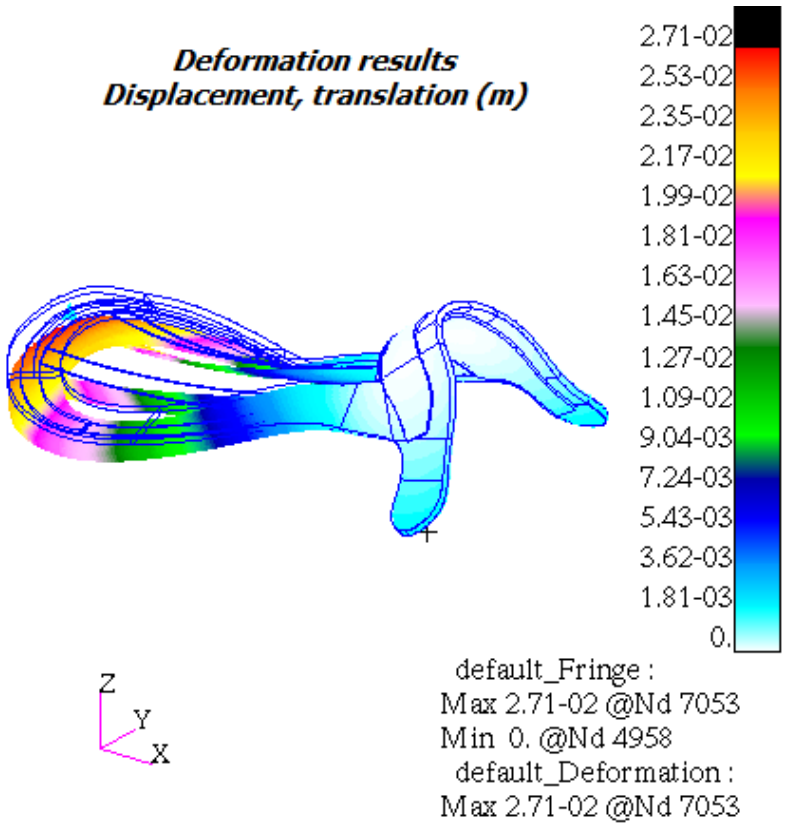

Figure 4.5.5 Reinforced saddletree – solid wood material – 6.0 mm thick

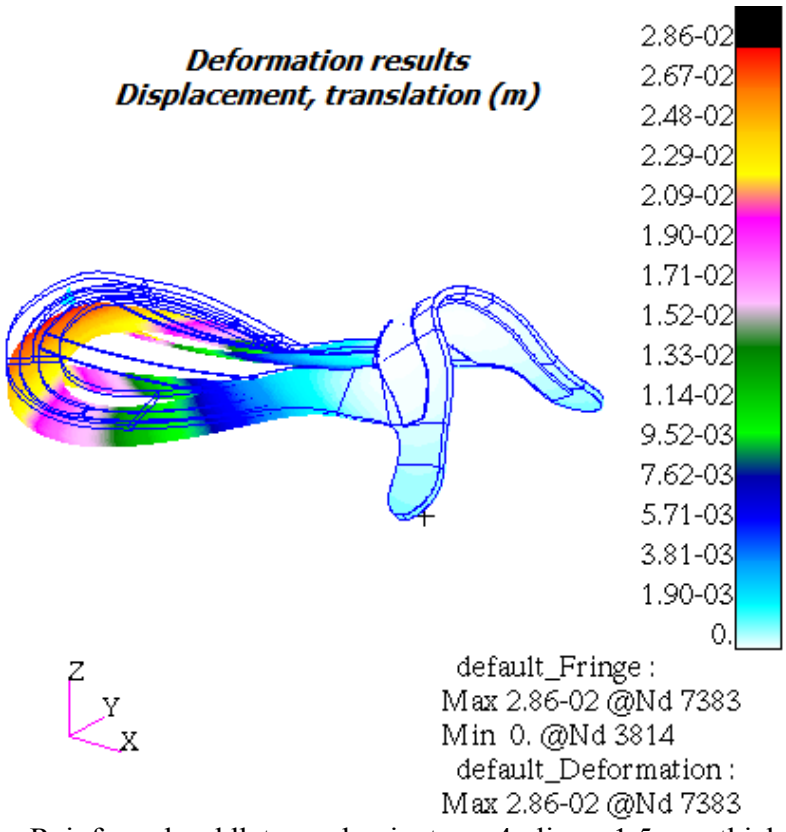

Figure 4.5.6 Reinforced saddletree – laminates – 4 plies x 1.5 mm thick

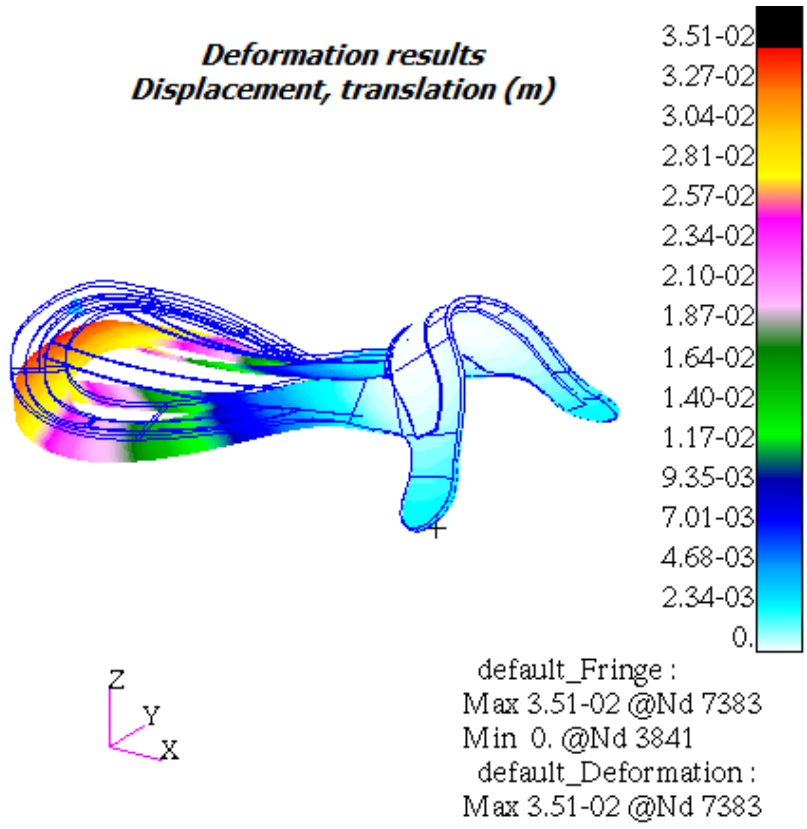

Figure 4.5.7 Reinforced saddletree – solid wood material – 4.5 mm thick

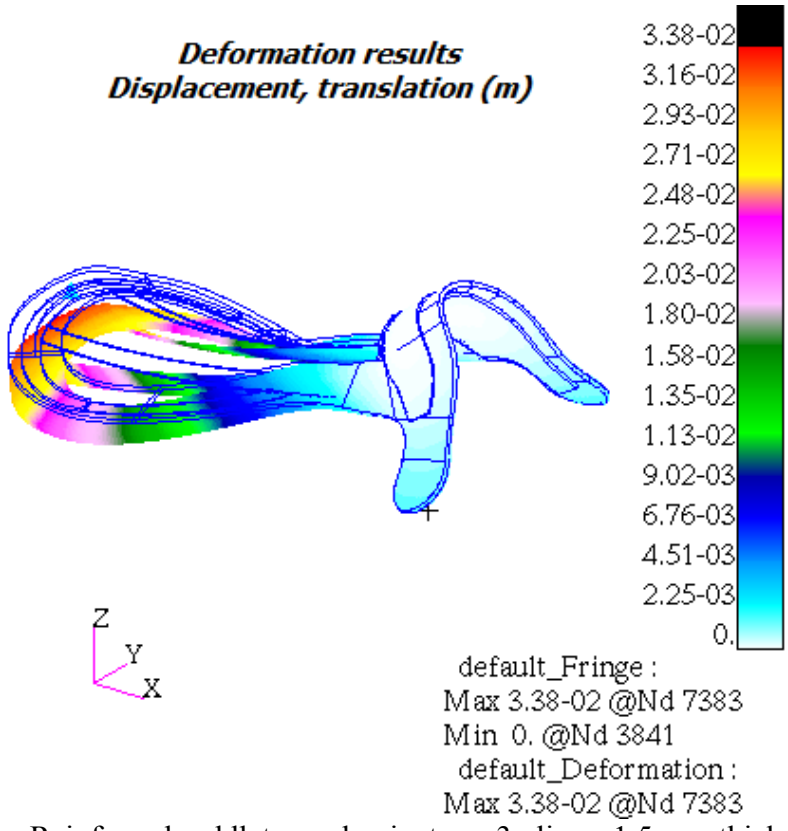

Figure 4.5.8 Reinforced saddletree – laminates – 3 plies x 1.5 mm thick

4.5.1.3 Reinforced saddletree (excluding spring steel)

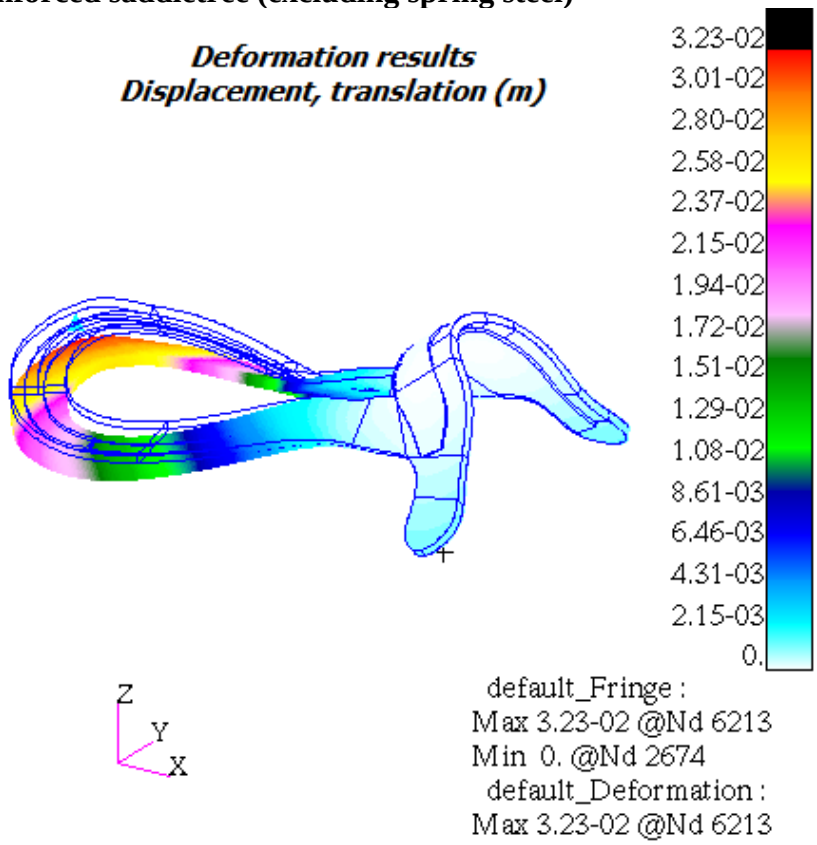

Figure 4.5.9 Reinforced saddletree (without pair of spring steel) – solid wood material – 7.5 mm thick

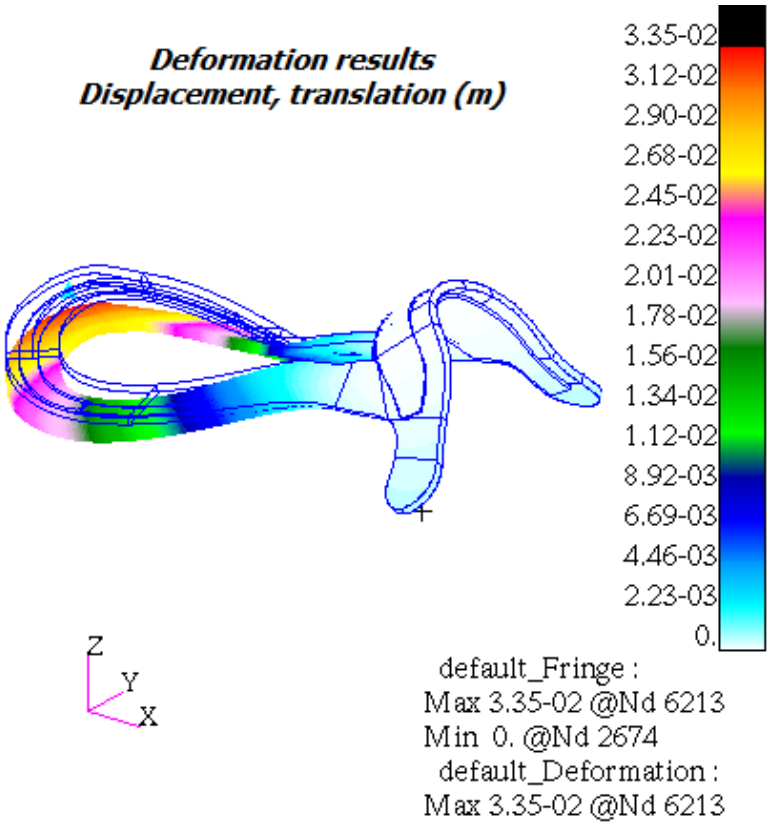

Figure 4.5.10 Reinforced saddletree (without pair of spring steel) – laminates – 5 plies x 1.5 mm thick

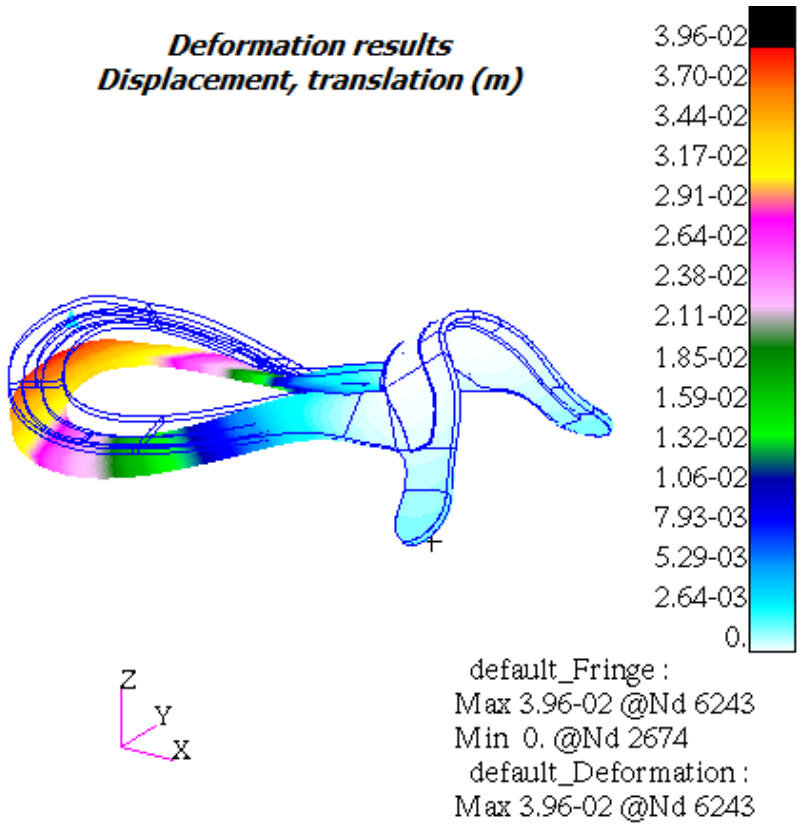

Figure 4.5.11 Reinforced saddletree (without pair of spring steel) – solid wood material – 6.0 mm thick

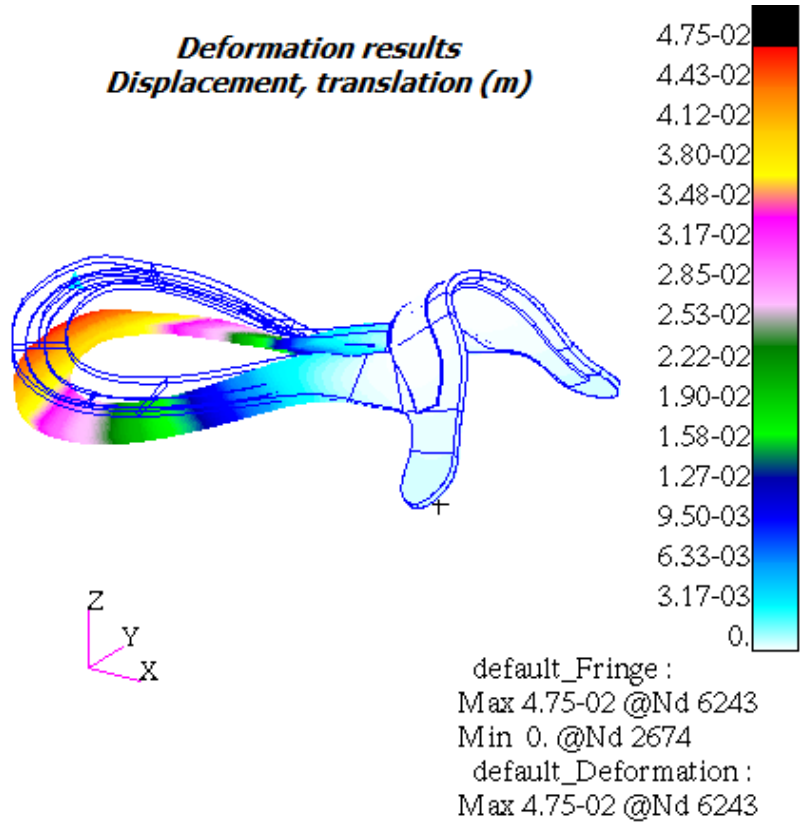

Figure 4.5.12 Reinforced saddletree (without pair of spring steel) – laminates – 4 plies x 1.5 mm thick

4.5.2 Uniformly Distributed Loading (UDL)

4.5.2.1 Saddletree (wood only)

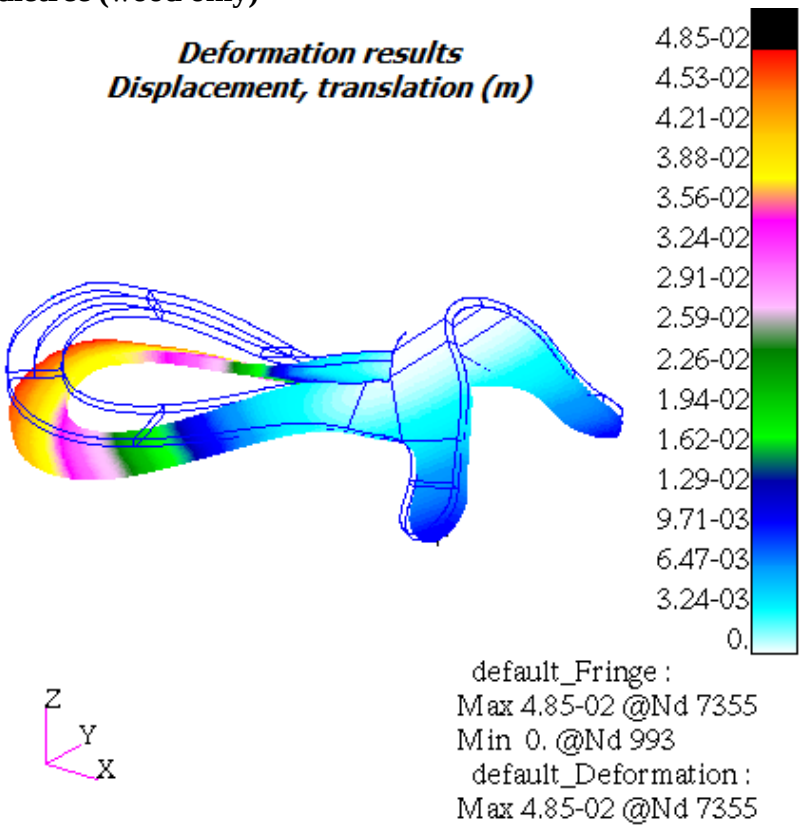

Figure 4.5.13 Saddletree – solid wood material – 7.5 mm thick

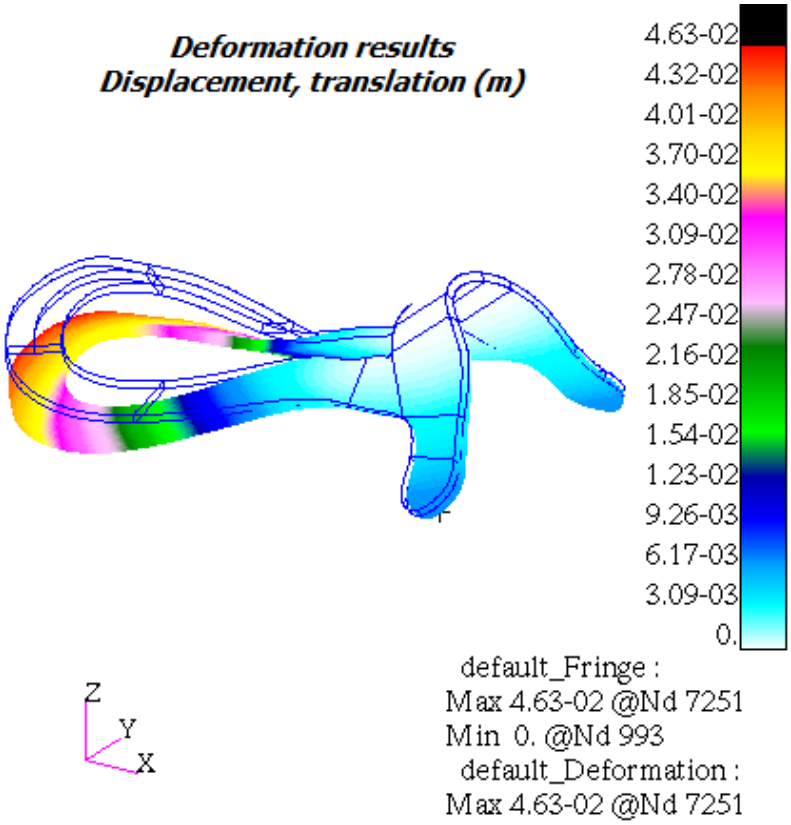

Figure 4.5.14 Saddletree – laminates – 5 plies x 1.5 mm thick

4.5.2.2 Reinforced saddletree

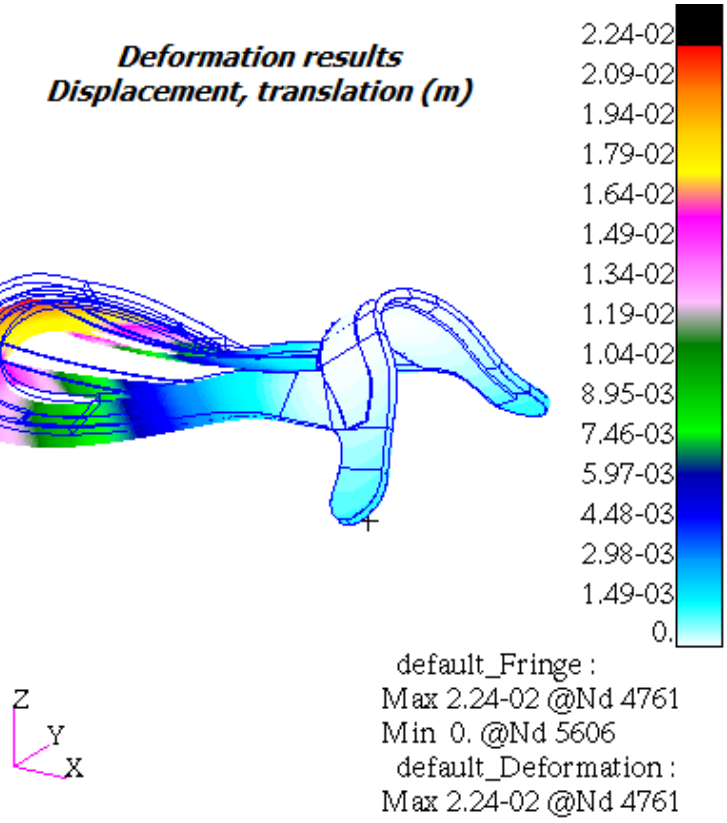

Figure 4.5.15 Reinforced saddletree – solid wood material – 7.5 mm thick

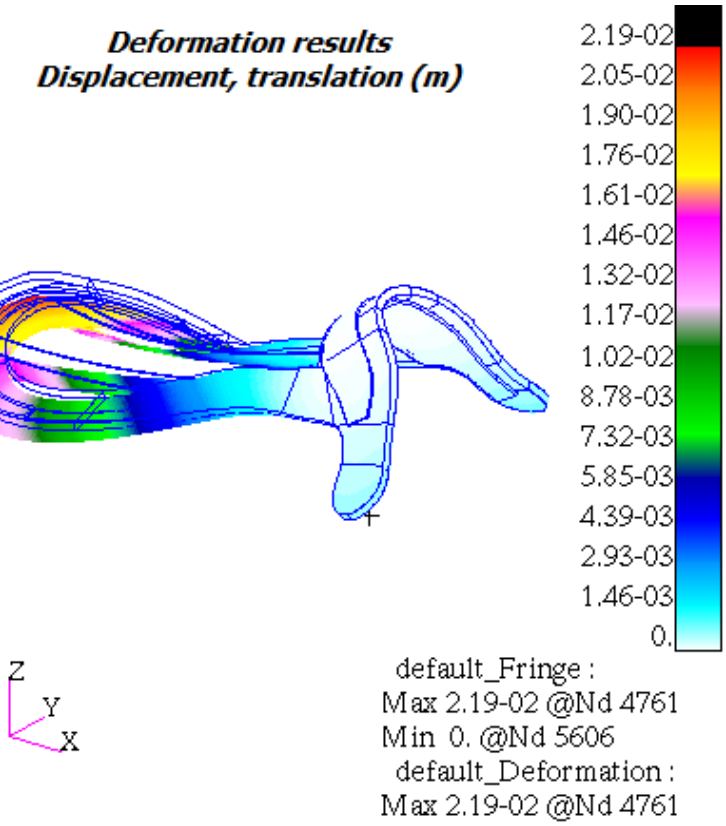

Figure 4.5.16 Reinforced saddletree – laminates – 5 plies x 1.5 mm thick

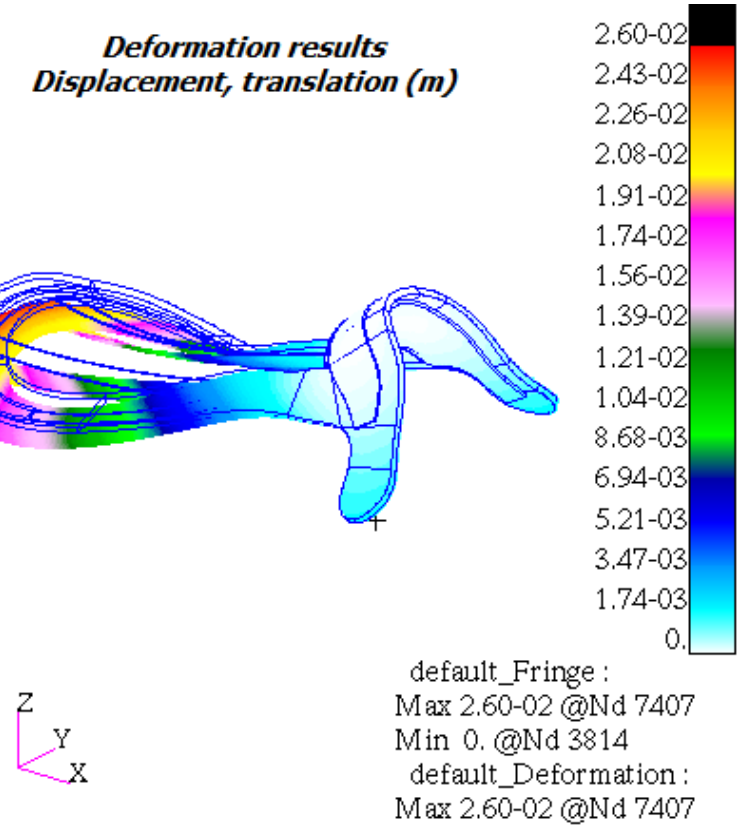

Figure 4.5.17 Reinforced saddletree – solid wood material – 6.0 mm thick

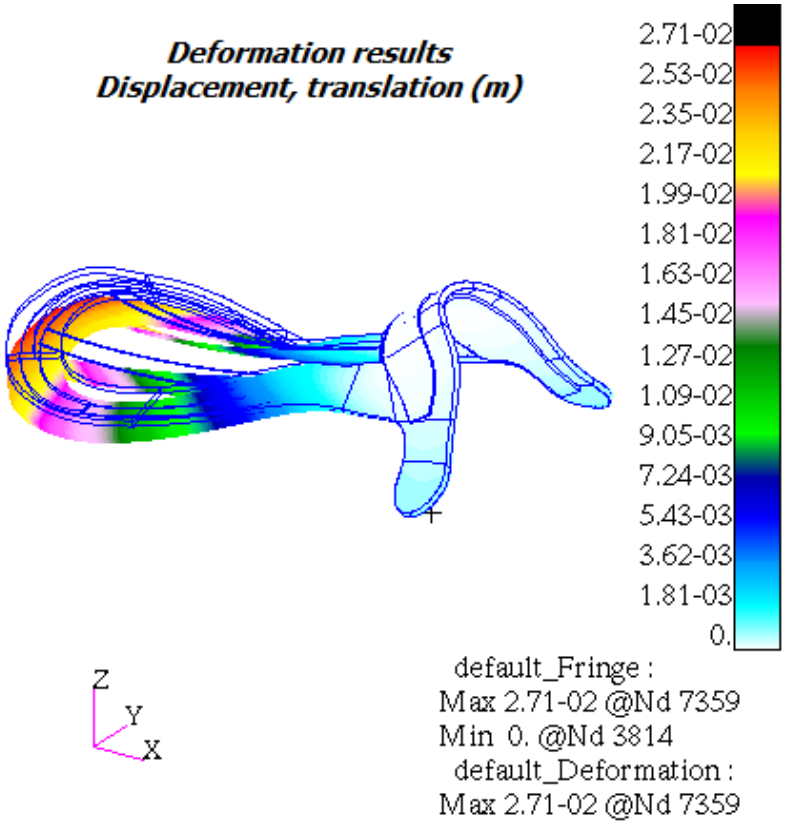

Figure 4.5.18 Reinforced saddletree – laminates – 4 plies x 1.5 mm thick

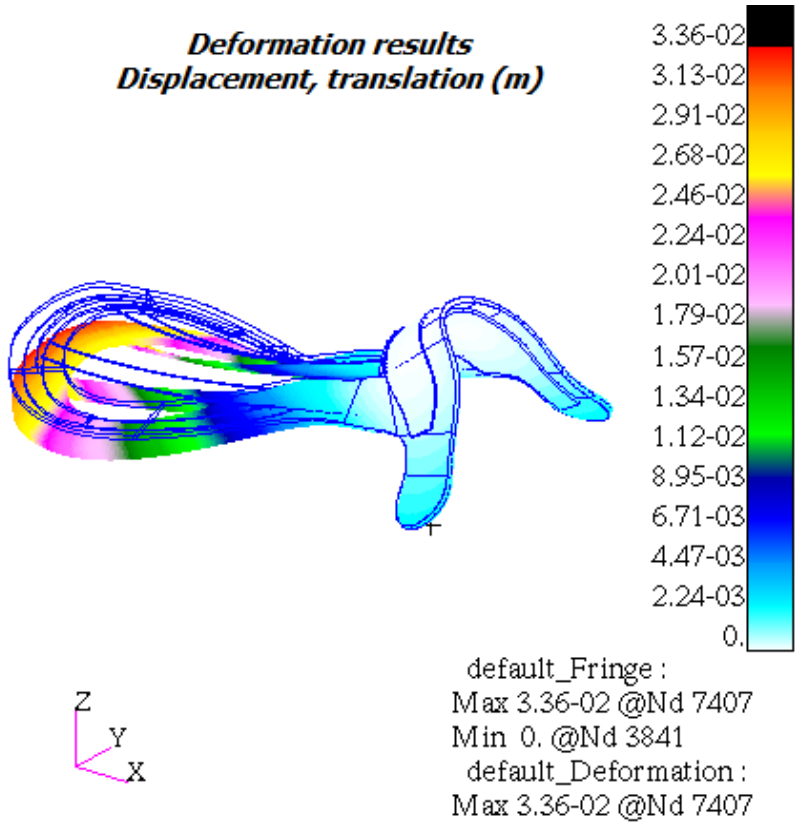

Figure 4.5.19 Reinforced saddletree – solid wood material – 4.5 mm thick

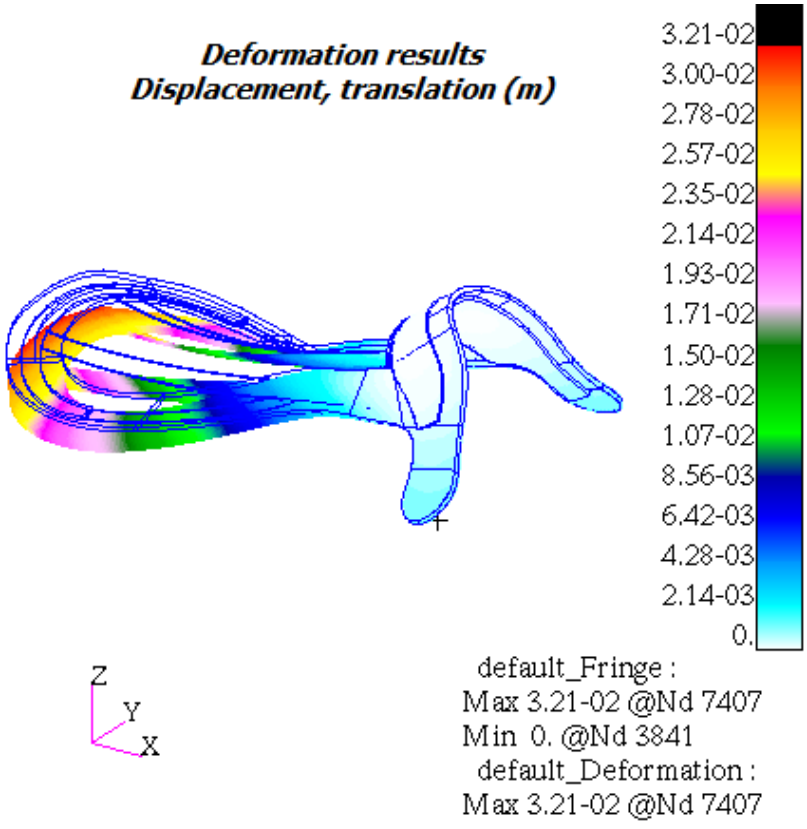

Figure 4.5.20 Reinforced saddletree – laminates – 3 plies x 1.5 mm thick

4.5.2.3 Reinforced saddletree (excluding spring steel)

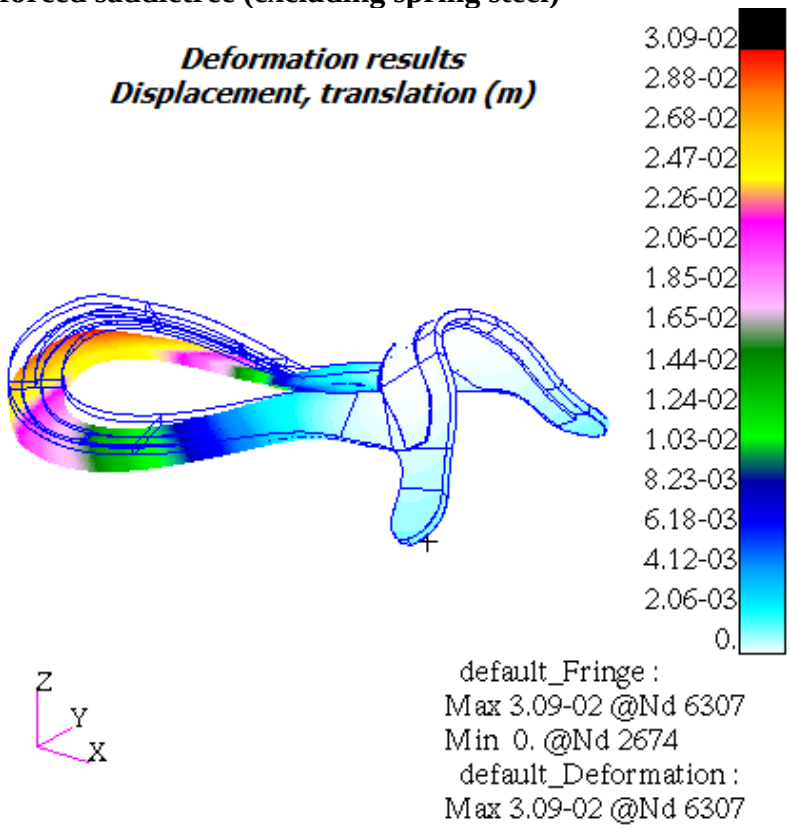

Figure 4.5.21 Reinforced saddletree (without pair of spring steel) – solid wood material – 7.5 mm thick

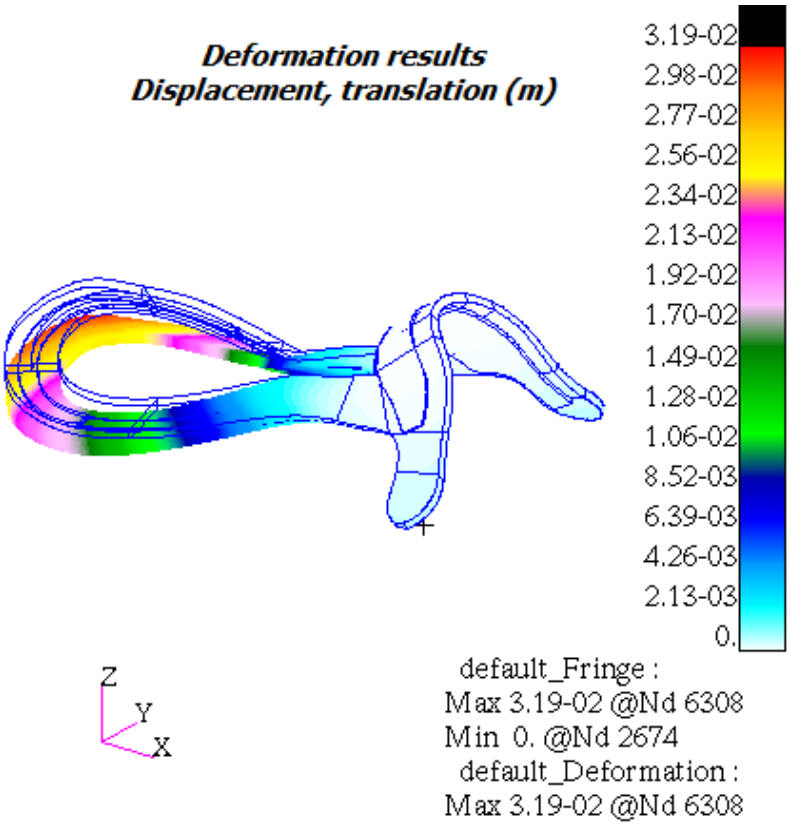

Figure 4.5.22 Reinforced saddletree (without pair of spring steel) – laminates – 5 plies x 1.5 mm thick

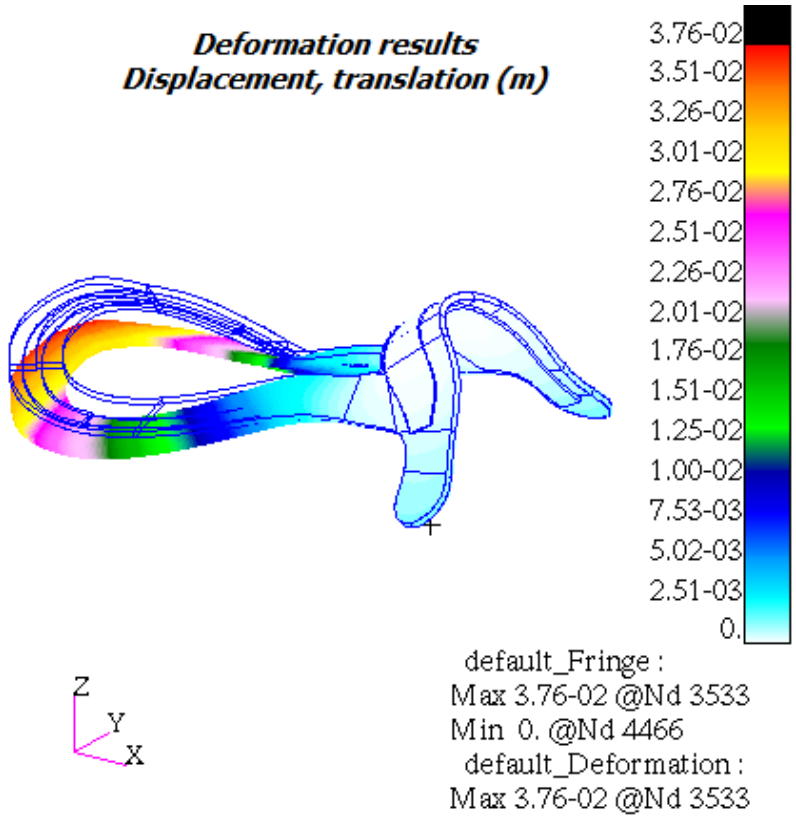

Figure 4.5.23 Reinforced saddletree (without pair of spring steel) – solid wood material – 6.0 mm thick

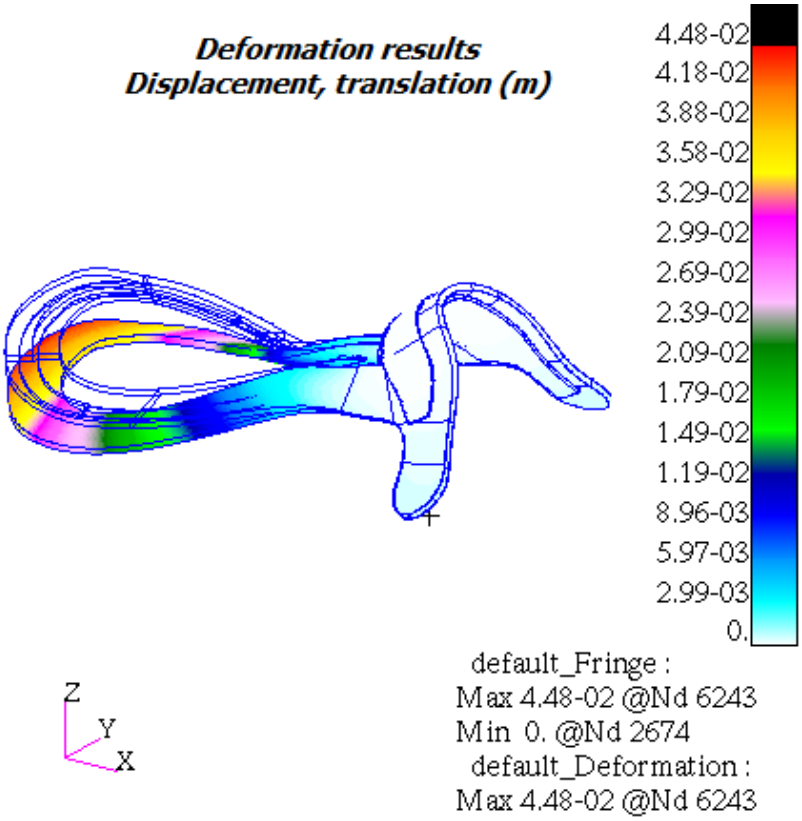

Figure 4.5.24 Reinforced saddletree (without pair of spring steel) – laminates – 4 plies x 1.5 mm thick

4.6 DISCUSSION OF RESULTS

In this chapter, the response to bending of the saddletree without any steel reinforcement plates, with steel reinforcement plates, and with steel reinforcement plates with the exception of the pair of spring steel has been presented. Stiffness is the most significant mechanical property in most structural problems (Clough, 1980), though there are instances where it needs to be managed (Eugene, 1999). It is simply described as a relationship between the deformation of a body and a known load (Butler, et al., 2003). The stiffnesses of the models were considered as a function of material, geometric shape and form, and the ability to resist deformation (Stewart, et al., 2009), and were determined as a measurement of the slope of the load-displacement curves (Eager, et al., 2001; Hodges, et al., 2005; Khashaba, et al., 2006; Stanton and Kawchuk, 2009; Stewart, et al., 2009; Snodgrass, et al., 2008; Yang, et al., 1997). The load-displacement curve is illustrated in figure 4.6.1. The deflections and stiffnesses of the models are summarised in tables 4.6.1 and 4.6.2.

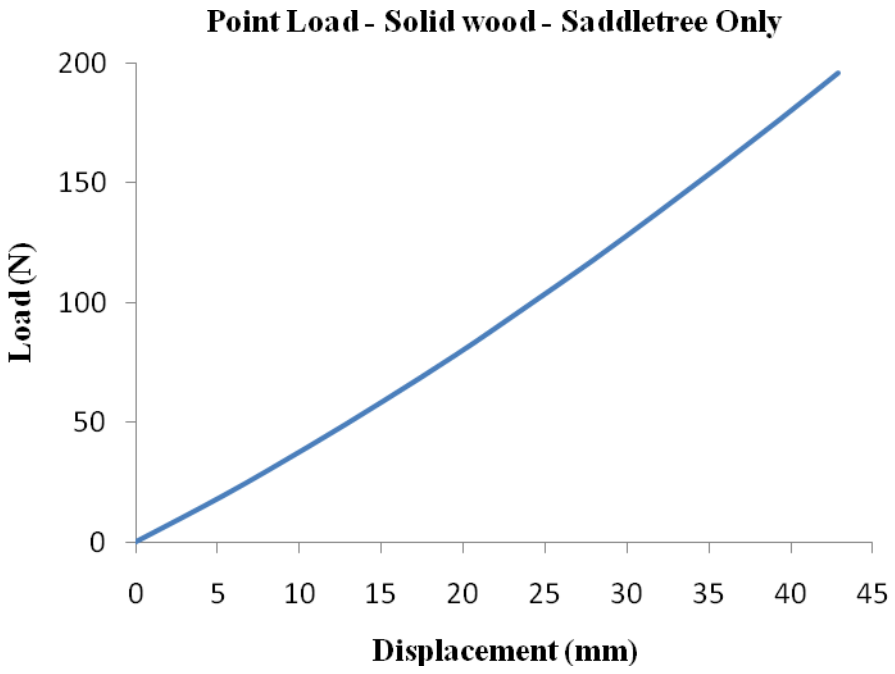

Figure 4.6.1 Load – displacement curve of a numerical model

Table 4.6.1 Deflections and stiffnesses of the saddletree under point load

Point load					
		Solid wood		Laminated wood	
	Wood thickness (mm)	Deflection (mm)	Stiffness (N/mm)	Deflection (mm)	Stiffness (N/mm)
Saddletree	7.5	42.9	4.37	40.3	4.68
Reinforced saddletree	7.5	23.2	8.12	22.9	8.26
	6.0	27.1	6.97	28.6	6.55
	4.5	35.1	5.31	33.8	5.48
Reinforced saddletree (no spring steel)	7.5	32.3	5.8	33.5	5.63
	6.0	39.6	4.71	47.5	3.92

Table 4.6.2 Deflections and stiffnesses of the saddletree under UDL

Uniformly distributed load (UDL)					
		Solid wood		Laminated wood	
	Wood thickness (mm)	Deflection (mm)	Stiffness (N/mm)	Deflection (mm)	Stiffness (N/mm)
Saddletree	7.5	48.5	3.63	46.3	3.87
Reinforced saddletree	7.5	22.4	8.41	21.9	8.58
	6.0	26.0	7.19	27.1	6.86
	4.5	33.6	5.52	32.1	5.73
Reinforced saddletree (no spring steel)	7.5	30.9	6.03	31.9	5.85
	6.0	37.6	4.90	44.8	4.09

4.6.1 The effect of the steel reinforcement on the wood only product

The stiffnesses of the saddletree models are presented in figure 4.6.2. They are classed according to their mode of loading and material type. The model variants are: the wood-only saddletree, the reinforced saddletree, and the reinforced saddletree without the pair of spring steel. The thickness of the saddletree in all the models was 7.5 mm. In the point loading class, the steel reinforcement plates with and without the pair of spring steel increased the stiffness of the solid wood saddletree by 85.81 % and 32.72 % respectively. The stiffness of the laminated wood variant was increased by 76.50 % and 20.30 % respectively.

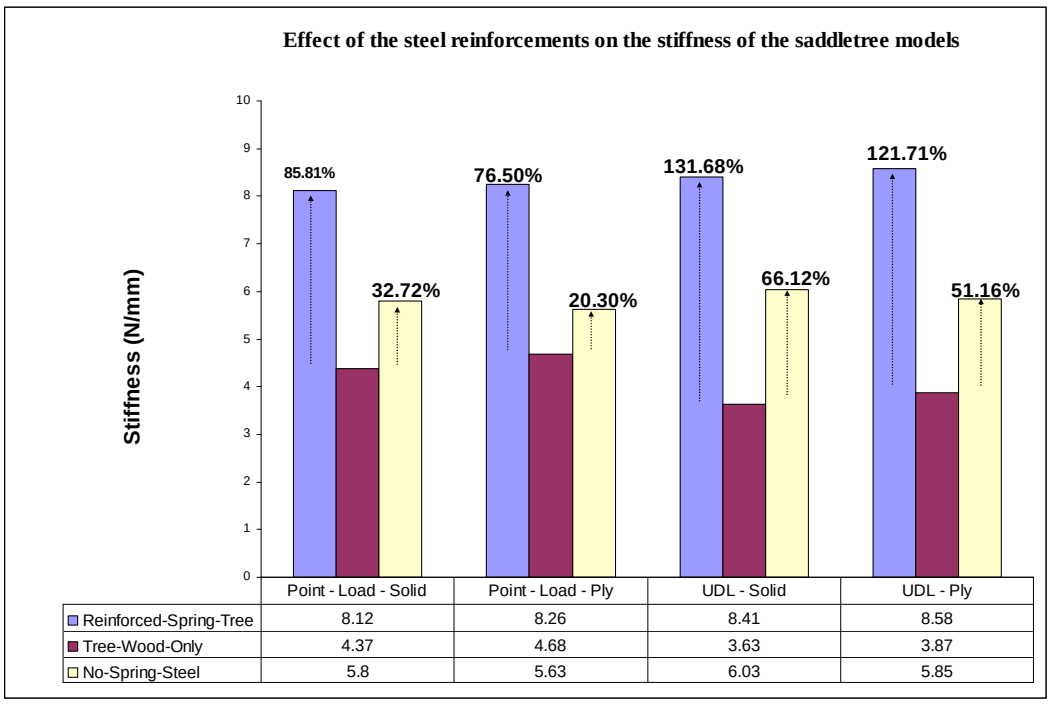

Figure 4.6.2 The effect of the steel reinforcements on the stiffness of the saddletree models (7.5 mm thickness)

In the UDL class, the steel reinforcement plates with and without the pair of spring steel increased the stiffness of the solid wood saddletree by 131.68 % and 66.12 % respectively, while the stiffness of the laminated wood saddletree was increased by 121.71 % and 51.16 % respectively.

4.6.2 The effect of excluding the pair of spring steel

In figure 4.6.2, it can be observed that the exclusion of the pair of spring steel had an effect on the stiffnesses of the 7.5 mm thick reinforced saddletree models. Figure 4.6.3 illustrates a more detailed comparison between the stiffnesses of the reinforced saddletree and the reinforced saddletree models without the pair of spring steel. The comparisons are confined to the 7.5 mm and 6.0 mm thick models. The stiffnesses of the 4.5 mm thick saddletree models in the no spring steel class are excluded from the analysis. It was observed that their principal stresses exceeded the maximum stresses defined for the wood materials. In the point loading class, the

stiffness of the no spring steel reinforced saddletree modelled with 7.5 mm solid wood was 28.57 % less than the stiffness of the reinforced saddletree with the pair of spring steel. Its laminated wood variant was 31.84 % less than the stiffness of the reinforced saddletree with the pair of spring steel. In addition, the 6.0 mm solid wood no spring steel reinforced saddletree was 32.43 % less as stiff as the reinforced saddletree with the pair of spring steel, while its laminated wood variant was 40.15 % less as stiff as the reinforced saddletree with the pair of spring steel.

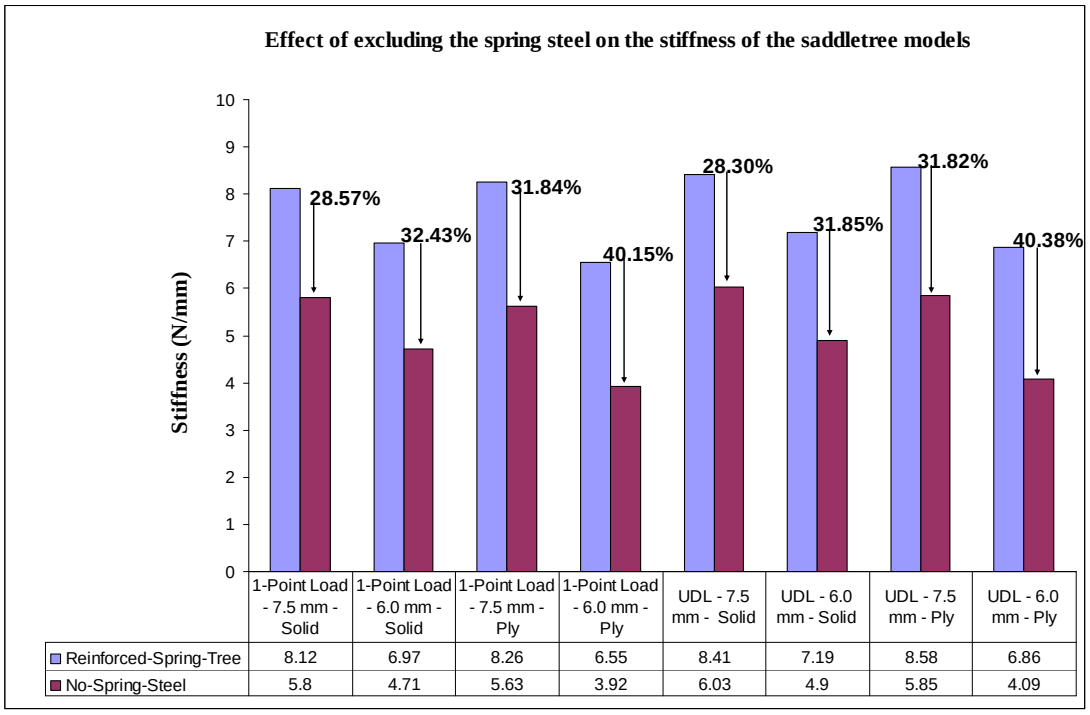

Figure 4.6.3 The effect of excluding the spring steel on the stiffness of the saddletree models

In the UDL class, the stiffness of the no spring steel reinforced saddletree modelled with 7.5 mm solid wood was 28.30 % less than the stiffness of the reinforced saddletree with the pair of spring steel while its laminated wood variant was 31.82 % less. Furthermore, the 6.0 mm solid wood no spring steel reinforced saddletree was 31.85% less as stiff as the reinforced saddletree with the pair of spring steel, while its laminated wood variant was 40.38 % less as stiff as the reinforced saddletree with the pair of spring steel.

4.6.3 The effect of varying the saddletree wood thickness

The effect of varying the thickness of the wooden frame of the reinforced saddletree while maintaining the thickness of the metal reinforcements is illustrated in figure 4.6.4. The stiffnesses of the models are presented according to the mode of loading and the material used. The arrangement provided an opportunity to compare the stiffnesses of the models at 7.5 mm, 6.0 mm, and 4.5 mm thickness. The stiffnesses of the 4.5 mm thick models in the no spring steel category are not included.

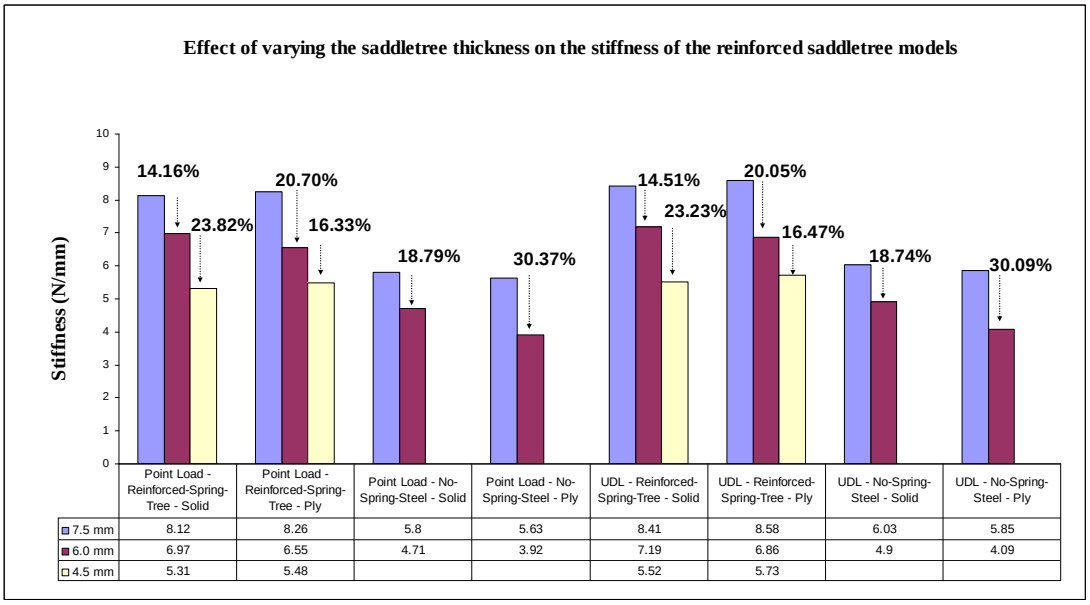

	Point Load - Reinforced-Spring-Tree - Solid	Point Load - Reinforced-Spring-Tree - Ply	Point Load - No-Spring-Steel - Solid	Point Load - No-Spring-Steel - Ply	UDL - Reinforced-Spring-Tree - Solid	UDL - Reinforced-Spring-Tree - Ply	UDL - No-Spring-Steel - Solid	UDL - No-Spring-Steel - Ply
7.5 mm	8.12	8.26	5.8	5.63	8.41	8.58	6.03	5.85
6.0 mm	6.97	6.55	4.71	3.92	7.19	6.86	4.9	4.09
4.5 mm	5.31	5.48			5.52	5.73		

Figure 4.6.4 The effect of varying the wood thickness on the stiffness of the saddletree models

Reduction in the thickness of the solid wood reinforced saddletree under a point load from 7.5 mm to 6.0 mm resulted in a 14.16 % reduction in the stiffness of the 7.5 mm thick model. A further reduction from 6.0 mm to 4.5 mm resulted in a reduction of 23.82 % of the stiffness of the 6.0 mm thick reinforced saddletree model. The reduction in thickness of the laminated wood variant from 7.5 mm to 6.0 mm resulted in the reduction of the stiffness of the 7.5 mm thick model by 20.70 %, while the reduction from 6.0 mm to 4.5 mm resulted in a 16.33 % reduction in the stiffness of the 6.0 mm thick reinforced saddletree model.

The reduction of the thickness of the solid wood reinforced saddletree modelled without the spring steel from 7.5 mm to 6.0 mm resulted in the reduction of the stiffness of the 7.5 mm thick model by 18.79 %. The reduction of the 7.5 mm thick laminated wood variant to 6.0 mm resulted in the reduction of the stiffness of the 7.5 mm saddletree model by 30.37 %.

There was a similarity in the effect of varying the thickness in the point load class in comparison with the effect of varying the thickness in the uniformly distributed load class. Decreasing the thickness of the solid wood reinforced saddletree from 7.5 mm to 6.0 mm under a UDL resulted in a 14.51 % reduction in the stiffness of the 7.5 mm thick model. A further reduction from 6.0 mm to 4.5 mm resulted in a reduction of 23.23 % in the stiffness of the 6.0 mm thick reinforced saddletree model.

Varying the thickness of the laminated wood option from 7.5 mm to 6.0 mm resulted in the reduction of the stiffness of the 7.5 mm thick model by 20.05 %, while the reduction from 6.0 mm to 4.5 mm resulted in a 16.47 % reduction in the stiffness of the 6.0 mm thick reinforced saddletree model.

The reduction of the thickness of the solid wood saddletree modelled without the spring steel from 7.5 mm to 6.0 mm resulted in the reduction of the stiffness of the 7.5 mm thick model by 18.74 %. Similarly, the reduction of the 7.5 mm thick laminated wood variant to 6.0 mm resulted in the reduction of the stiffness of the 7.5 mm saddletree model by 30.09 %.

4.6.4 The effect of loading the cantle region of the saddletree on the pommel

Sequel to loading the saddletree at the cantle region, it was observed that the pommel deflected laterally (as illustrated in figure 4.6.5). The measured deflection of each pommel is tabulated in tables 4.6.3 and 4.6.4.

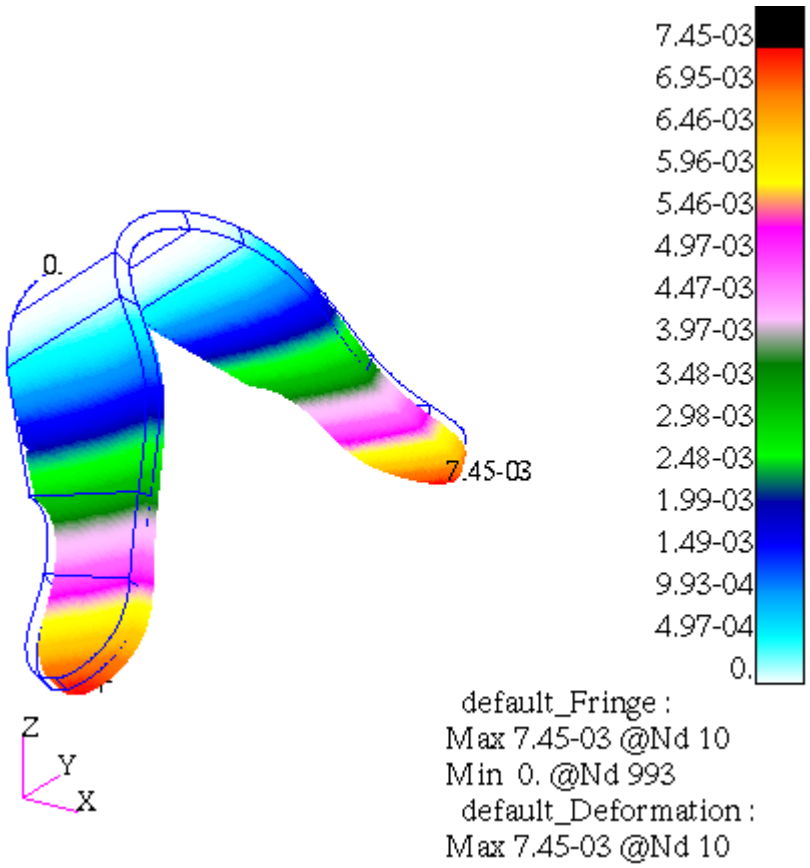

Figure 4.6.5 Lateral deflection observed at the pommel when the saddletree was loaded at the cantle region.

Table 4.6.3 Deflections at the pommel of saddletree models under point load

Point load			
		Solid wood	Laminated wood
	Wood thickness (mm)	Deflection (mm)	Deflection (mm)
Saddletree	7.5	6.68	3.12
Reinforced saddletree	7.5	1.62	1.11
	6.0	2.02	1.39
	4.5	2.71	1.90
Reinforced saddletree (no spring steel)	7.5	1.68	1.17
	6.0	2.03	1.42

Table 4.6.4 Deflections at the pommel of saddletree models under UDL

Point load			
		Solid wood	Laminated wood
	Wood thickness (mm)	Deflection (mm)	Deflection (mm)
Saddletree	7.5	10.8	7.45
Reinforced saddletree	7.5	1.48	1.05
	6.0	1.82	1.25
	4.5	2.40	1.69
Reinforced saddletree (no spring steel)	7.5	1.51	1.05
	6.0	1.80	1.23

4.7 SUMMARY

A scientific approach was applied to develop numerical models of an English jumping saddletree and investigate their sensitivity to load, material, and geometric variations. The models were developed to represent the product without any dependencies, and the static loading and boundary condition assumptions were defined with reference to experimental tests performed on the thoracolumbar spine as cited in the literature review.

The effects of the steel reinforcement plates with and without the pair of spring steel on the stiffness of the saddletree were investigated and quantified. The pair of spring steel was observed to have a more prominent effect on the stiffness of the saddletree models than on the deflections observed at the pommel models. In addition, the effects of constructing with either solid or laminated wood, and, the effects of varying the wood thickness on stiffness were presented. Hitherto, no research or data on the stiffness of the saddletree had been published.

The stiffness solutions are invaluable in benchmarking any further developments or

product evolution. They may be included in a product design specification (PDS). This presents an opportunity to replace ambiguous and informal statements (Bailetti and Litva, 1995) such as considerable weight, acceptable strength characteristics, and strengthened by (White and Lightfoot, 1976) which were presented in earlier patents with a quantifiable parameter. While quantified specifications offer apparent targets in product evolution (Otto and Wood, 1998; 1996), ambiguous or apparently missing information in a product specification results in overdesigned components (Karlsson, et al., 1998). In a review of 1000 firms, Baxter (1995) reported that products that are well defined in the design specification were 3.3 times more likely to succeed than those without it.

CHAPTER FIVE

SIMULATING BENDING IN THE SADDLETREE II

5.1 INTRODUCTION

The interaction between saddlery and horseback was discussed earlier in chapter 2.3 of this thesis. Through the saddle, the saddletree has an interface with the rider and the horseback at its top and bottom surfaces respectively. The interaction between the rider, saddlery, and horse is complex with each component exhibiting individual properties (Witte, et al., 2009). The dorsal processes of the withers are predominantly susceptible to loading (Clayton, et al., 2010), and though there has been a significant interest in evaluating the loads transmitted from the rider to the horse through saddlery (Holmes and Jeffcott, 2010), the important coupling is yet to be fully understood (Peham, et al., 2004). An improved knowledge of the mechanical properties of the components of the system is essential as many orthopaedic symptoms are noticeable in the horse (Witte, et al., 2009).

Schlacher, et al. (2004) determined a mean dorsoventral stiffness of 2093 ± 611 N/m for 14 thoracolumbar spines of horses and, Jeffcott and Dalin (1980) reported a movement of 53.1 mm in the dorso-ventral directions of the equine back. Ekh and Schon (2008) established that an increased stiffness mismatch between contacting bodies in a parametric study resulted in irregular load distribution. In a related study, Oleson, et al. (2005) compared forefoot stiffness in running shoes and the bending stiffness of the running shoe. In another simulation, Hall, et al. (2009) attributed the resulting stress concentration on a thin body as an effect of the stiffness mismatch

between the body and a thicker (and stiffer) contacting body. Here, the author suggests that an evaluation of the stiffness of the saddletree when in contact with a riders load and supported by contacting a surface identical to a horseback, will provide an opportunity to determine if there is a stiffness mismatch with respect to the stiffness of the horseback.

Further, the numerical model for laminated wood provided an opportunity to evaluate the effects of various stacking sequences on the stiffness of the saddletree. Structural properties of laminated composites have been reported to be dependant on their laminate stacking sequence (Department of Defence and the Federal Aviation Administration, 1999; Gurdal, et al., 1999). The stacking of laminates is often limited to combinations of 0^0, 90^0 and $\pm45^0$ in practise (Lopes, et al., 2009; Herencia, et al., 2008; Adali and Verijenko, 2001) due to available manufacturing techniques (Herencia, et al., 2008). Uncommonly, ply angles of 15^0 increments between 0^0 and 90^0 may be used (Adali and Verijenko, 2001).

In creating the stacking sequences, four groups of laminates are created according to the percentage of the 0^0 and 90^0 orientation. The classifications are:

- 20 % of 90^0 and 80 % of 0^0;
- 40 % of 90^0 and 60 % of 0^0;
- 60 % of 90^0 and 40 % of 0^0;
- 80 % of 90^0 and 20 % of 0^0.

Five sequences were modelled using 20 % of 90^0 and 80 % of 0^0 orientations, ten sequences using 40 % of 90^0 and 60 % of 0^0 orientations, ten sequences using 60 % of 90^0 and 40 % of 0^0 orientations, and five sequences using 80 % of 90^0 and 20 %

of 0^0 orientations. They are presented in table 5.1.1.

Table 5.1.1 Laminate stacking sequences

20 % of 90^0 and 80 % of 0^0	40 % of 90^0 and 60 % of 0^0	60 % of 90^0 and 40 % of 0^0	80 % of 90^0 and 20 % of 0^0
$[90/0/0/0/0]_T$	$[90/90/0/0/0]_T$	$[90/90/90/0/0]_T$	$[90/90/90/90/0]_T$
$[0/90/0/0/0]_T$	$[90/0/90/0/0]_T$	$[90/90/0/90/0]_T$	$[90/90/90/0/90]_T$
$[0/0/90/0/0]_T$	$[90/0/0/90/0]_T$	$[90/90/0/0/90]_T$	$[90/90/0/90/90]_T$
$[0/0/0/90/0]_T$	$[90/0/0/0/90]_T$	$[90/0/90/90/0]_T$	$[90/0/90/90/90]_T$
$[0/0/0/0/90]_T$	$[0/90/90/0/0]_T$	$[90/0/90/0/90]_T$	$[0/90/90/90/90]_T$
	$[0/90/0/0/90]_T$	$[90/0/0/90/90]_T$	
	$[0/0/90/90/0]_T$	$[0/90/90/90/0]_T$	
	$[0/0/90/0/90]_T$	$[0/90/90/0/90]_T$	
	$[0/0/0/90/90]_T$	$[0/90/0/90/90]_T$	
		$[0/0/90/90/90]_T$	

BS 7875:1996 and BS 7875:2009 specified a method for testing saddletrees made from synthetic materials for deflection. The test involves positioning a saddletree fitted with stirrup bars as it would be assembled in a saddle and placing it on a steel former of 152 mm diameter, gradually applying a maximum load of 9400N at the stirrup bars, and measuring deflection in millimeters at a predetermined midpoint at the pommel after a time duration of 305 s.

BS 7875:1996 and BS 7875:2009 based the load on a generated downwards force of 2000 lb (907.19 kg) applied to the stirrup bars. Arguably, loading the saddletree at the stirrups is analogous to loading it with a standing rider. The horseback is influenced by riding techniques (De Cocq, et al., 2010) and loads on it have been observed to be greater in sitting trot than in rising trot (De Cocq, et al., 2010; Peham, et al., 2010).

BS 6635:2003 did not specify any method for testing saddletrees made from wood for deflection. Hence, the test process described in BS 7875:1996 and BS 7875:2009 was used as a guide in developing the static numerical models.

5.2 PARAMETERS INVESTIGATED

The deflection of the saddletree was of interest in determining its stiffness relative to the defined boundary conditions. The stiffness of the saddletree reinforced with steel reinforcement plates was also of interest in evaluating the effects of the steel reinforcement plates on the saddletree stiffness. Furthermore, the effect of the laminate stacking sequence on the saddletree stiffness was of interest in exploring alternative lay-ups to the current practice. It is only through a scientific approach to developing this understanding that new and improved designs can be suggested.

5.3 DETERMINING THE METHOD OF LOADING

In order to develop numerical models with realistic load and boundary conditions, a pressure mat was used to define the contact areas of a rider on a bare horseback, and a loaded saddletree on a horseback stand. Data was collected with a Tekscan ConforMat^{TM} (illustrated in figure 5.3.1) which is made up of 1024 (32 x 32) thin (1.78 mm) resistive sensors (Kyung and Nussbaum, 2008).

Wu, et al. (1999) used contour maps obtained from a pressure mat to evaluate the effective contact area and contact force distribution between seated human subjects and a seat. Putti, et al. (2008) suggested that amongst eighteen parameters recorded by a pressure mapping tool, the contact area and force-time integral were two of the most relevant six parameters. Kyung and Nussbaum (2008) concluded that the use of the Conformat^{TM} was appropriate in reflecting the distribution of a body load on a seat. Pressure mats have also been used in equine studies (Clayton, et al., 2010). Their use, validity, accuracy, and repeatabilty were discussed earlier in chapter 2.5 of this thesis. In addition, the use of pressure mapping data in defining load and

boundary conditions in developing numerical models was also reported.

Figure 5.3.1 ConforMat sensor and evolution handle

5.3.1 Validation of ConforMat measurments

The accuracy of the sensor was validated by applying 5 x 10 kg laboratory weights on a seat cushion with the Conformat™ placed between the load and the cushion (as illustrated in figure 5.3.2). Lai and Li-Tsang (2009) evaluated the accuracy of a pressure mat with a range of standardized loads. Standard weights were applied to the sensor and the readings recorded. The force distribution and force per unit time graph generated by the ConforMat™ research software (version 5.84) are illustrated in figure 5.3.3. There was a 2.6 % error relative to the standard weight.

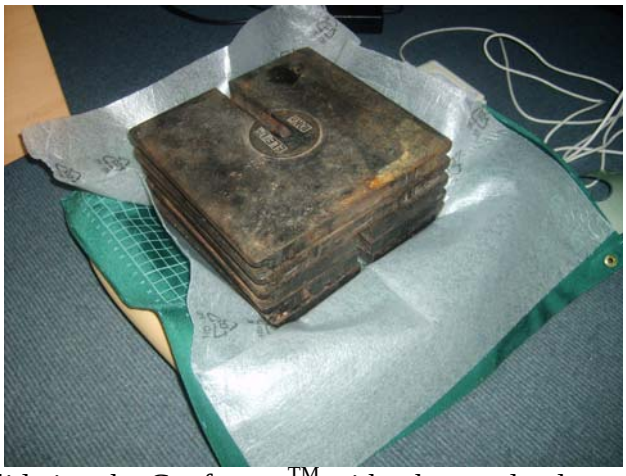

Figure 5.3.2 Validating the Conformat™ with a known load

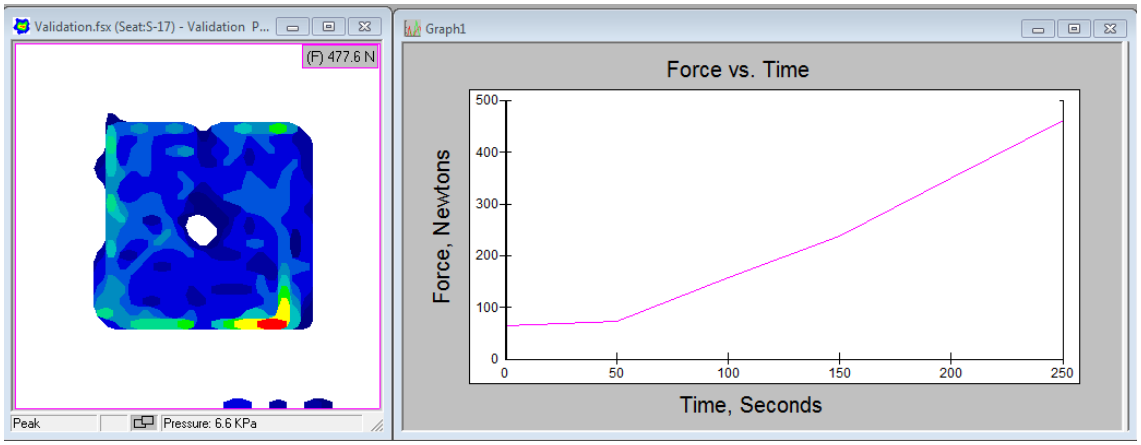

Figure 5.3.3 Force distribution and force time graph of validation

5.3.2 Contour mapping

In this study, the Conformat™ was used to map the effective contact area of a rider sat on a bare horseback (as illustrated in figure 5.3.4). The image file was imported into SolidWorks CAD software and used to develop a sketch geometry which was further projected onto the surface of the saddletree geometry. The projected geometry was further developed into a surface geometry (as illustrated in figure 5.3.5), trimmed adjacent to the edges of the saddletree and exported to MSC.Patran. In the numerical models, the surface geometry was assumed to be a load bearing rigid body.

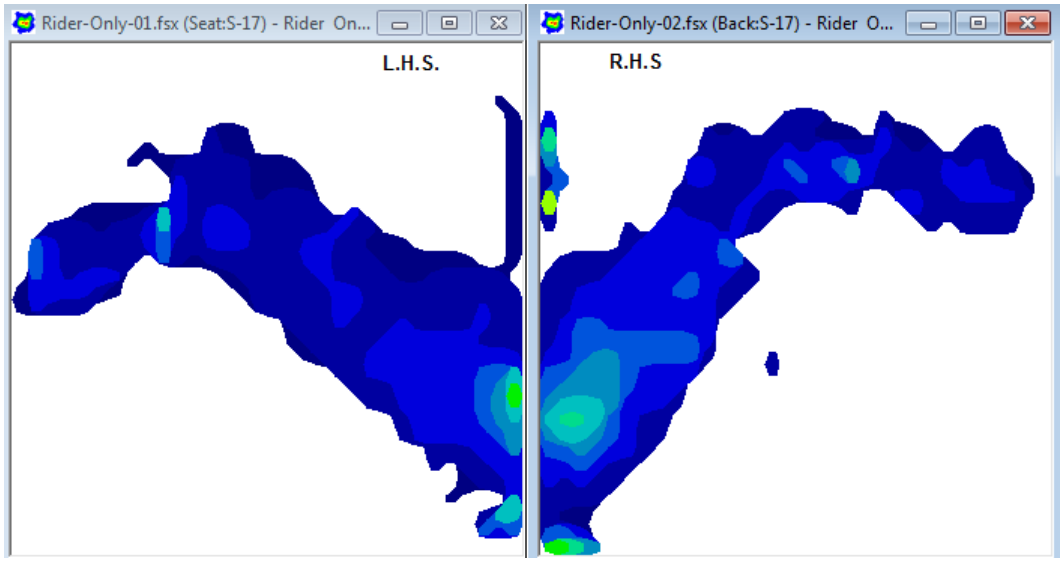

Figure 5.3.4 Contact area of a rider sat on a horseback

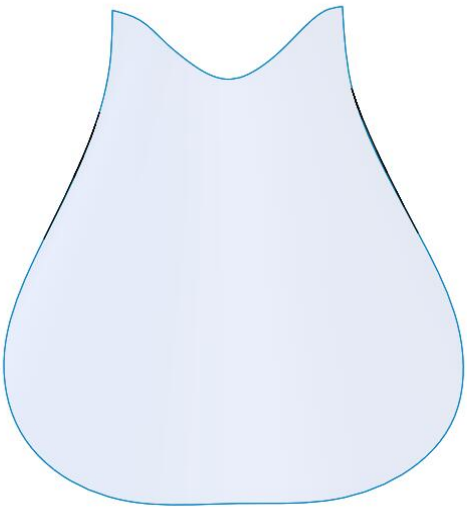

Figure 5.3.5 Surface geometry created from rider – horse contact area

In addition, the Conformat™ was used to determine the area of support which would serve as constraints for the saddletree in the numerical models. It was placed between the saddletree specimen and the horse stand (as illustrated in figure 5.3.6).

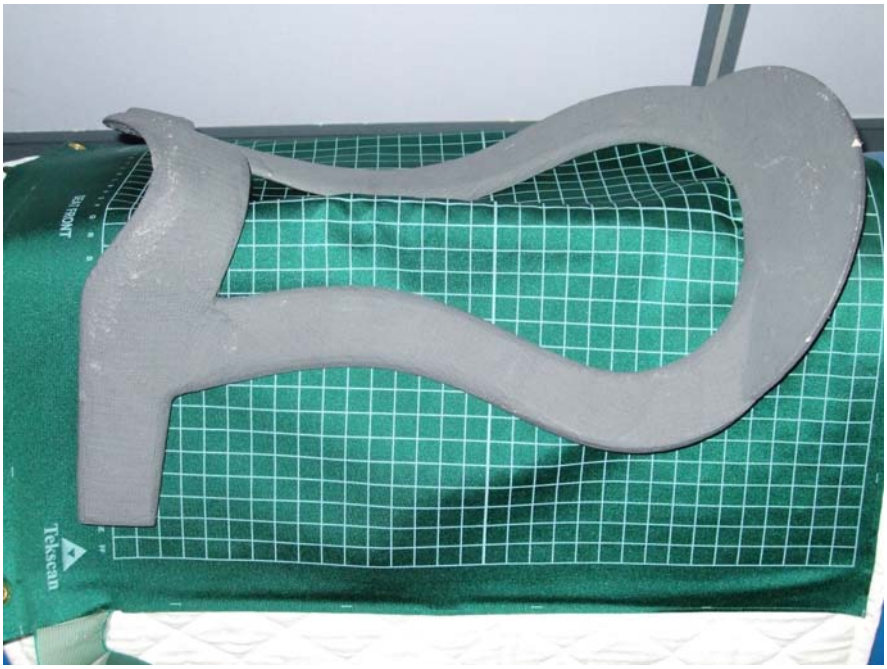

Figure 5.3.6 Saddletree on a plastic saddle stand

A human specimen was sat on the saddletree specimen while it was positioned on a saddle stand thereby creating contact between the saddletree and the saddle stand.

The contour map presented in figure 5.3.7 illustrates that the peak areas of contact which are represented by the red contours are located at the front end under the pommel section and at the rear end under the seat section. It was apparent that there was no contact in some parts of the mid section of the saddletree. Similar to the process used in developing the load application rigid surface, rigid surfaces (as illustrated in figure 5.3.8) were developed from the peak contact contours. They served as constrains for the numerical models

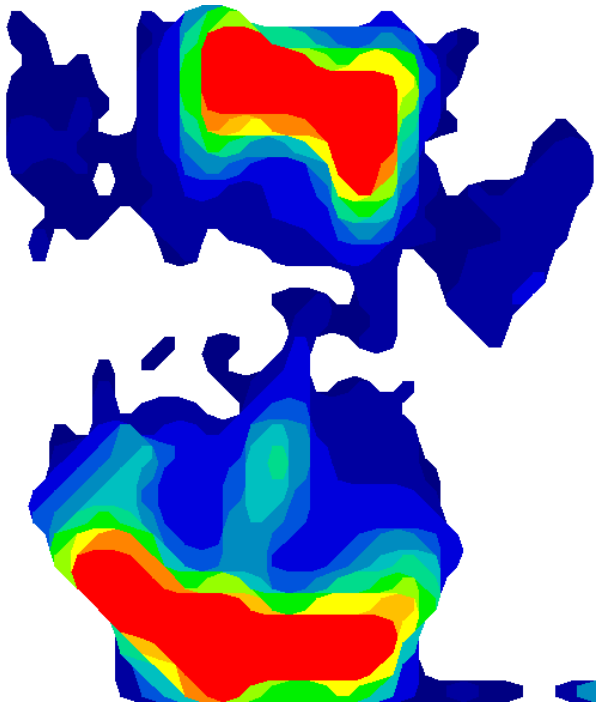

Figure 5.3.7 Contact area of a saddletree on a saddle stand

Figure 5.3.8 Surface geometry created from saddletree – saddle stand contact area

5.4 PRE-PROCESSING

There were some similarities with the pre-processing steps performed to develop the numerical models in chapter 4. With the exception of the surface geometries created from the contact contour maps, all geometries used in developing the numerical models in this part of the research are identical to the ones used in chapter 4 (as illustrated in figure 5.4.1). The material properties and the laminate stacking sequence, the element type, topology, and properties are also identical to those defined for the static models developed in chapter 4. In view of these similarities, the MSC.Marc solution parameters were also identical.

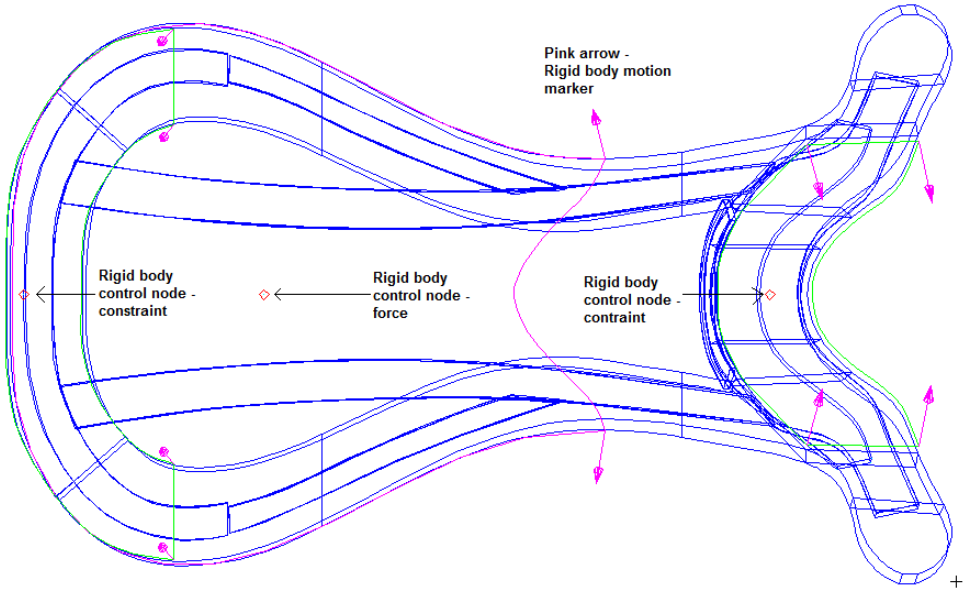

Figure 5.4.1 Illustration of assumptions made in developing the numerical model

The surface geometry used in applying load onto the saddletree and those used in constraining the saddletree were all modelled as rigid contact bodies (as illustrated in figures 5.4.1 and 5.4.2). A node was extracted in the middle of the each surface to control its motion. The motion control for the rigid contact body used in applying the load was set to ***Force/Moment*** and the node extracted from the surface was set as its ***first control node***. The motion control for the rigid contact bodies used in

constraining the saddletree was set to ***Position***, while the ***vector displacement*** was set to x = y = z = 0, and their extracted nodes used as their ***rotation reference points***.

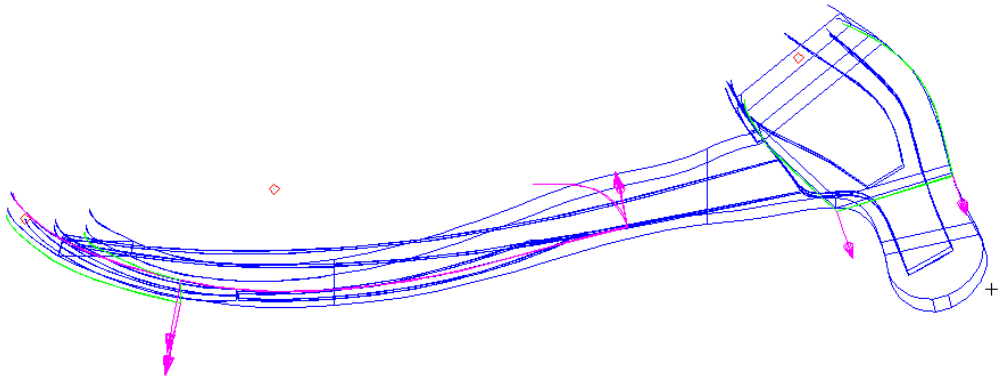

Figure 5.4.2 Magnified control nodes and rigid body motion marker

5.5 POST-PROCESSING

5.5.1 Model deflection

The results of the simulations were post-processed and the deformation (displacement, translation) plots are presented in figures 5.5.1 to 5.5.35. The deflections of the saddletree models without any steel reinforcements, of the reinforced saddletree models, and, of the reinforced saddletree models without a pair of spring steel are presented in figures 5.5.1 to 5.5.6 respectively. Finally, the deflections of the saddletree models developed with varying laminate stacking sequences are presented in figures 5.5.7 to 5.5.35. In order to enhance the visibility of the deflections, the results were magnified by a model scale factor of 0.075, and the geometric models superimposed on the results. The models are presented with maximum displacements measured in metres (m) while the load – displacement graphs are in Newton / millimetre (N/mm).

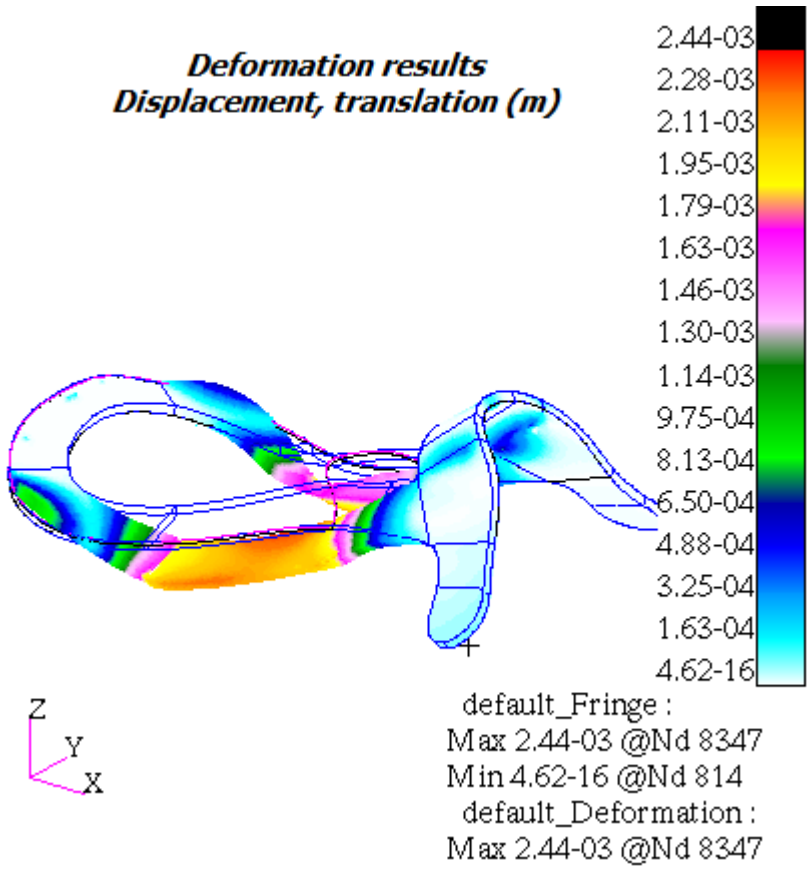

Figure 5.5.1 Solid saddletree

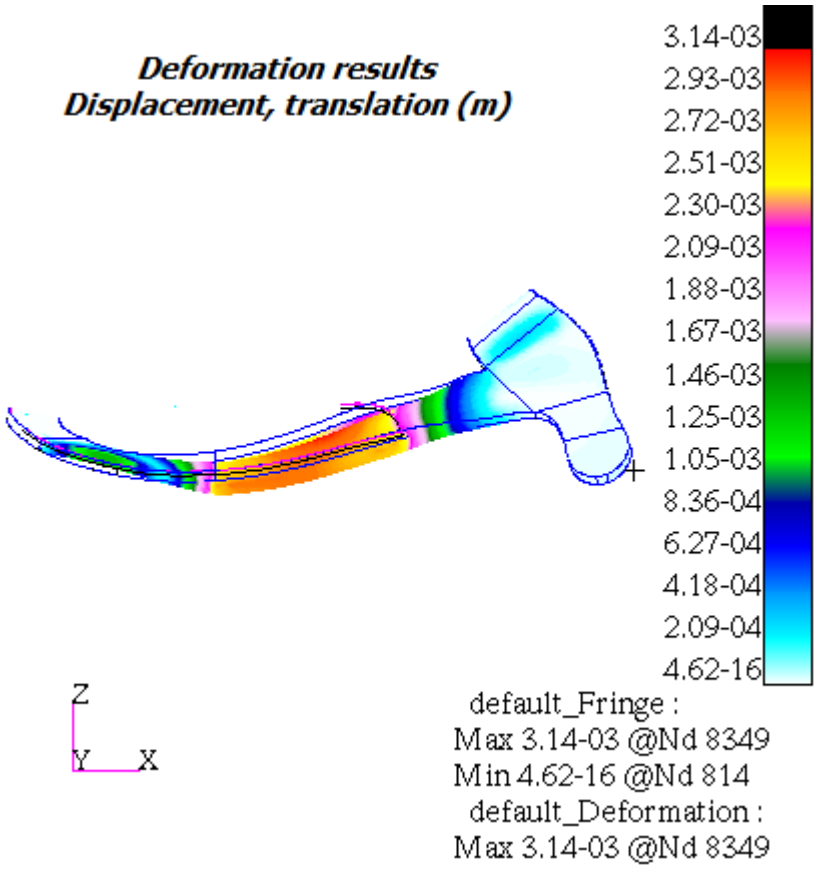

Figure 5.5.2 Laminated saddletree

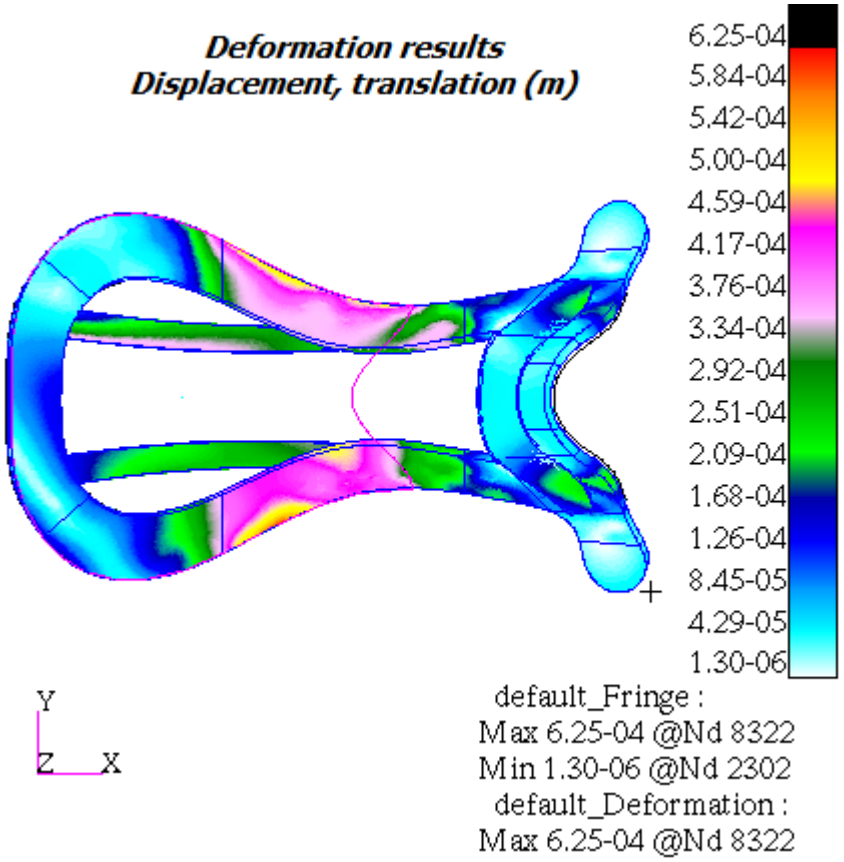

Figure 5.5.3 Reinforced saddletree – Solid

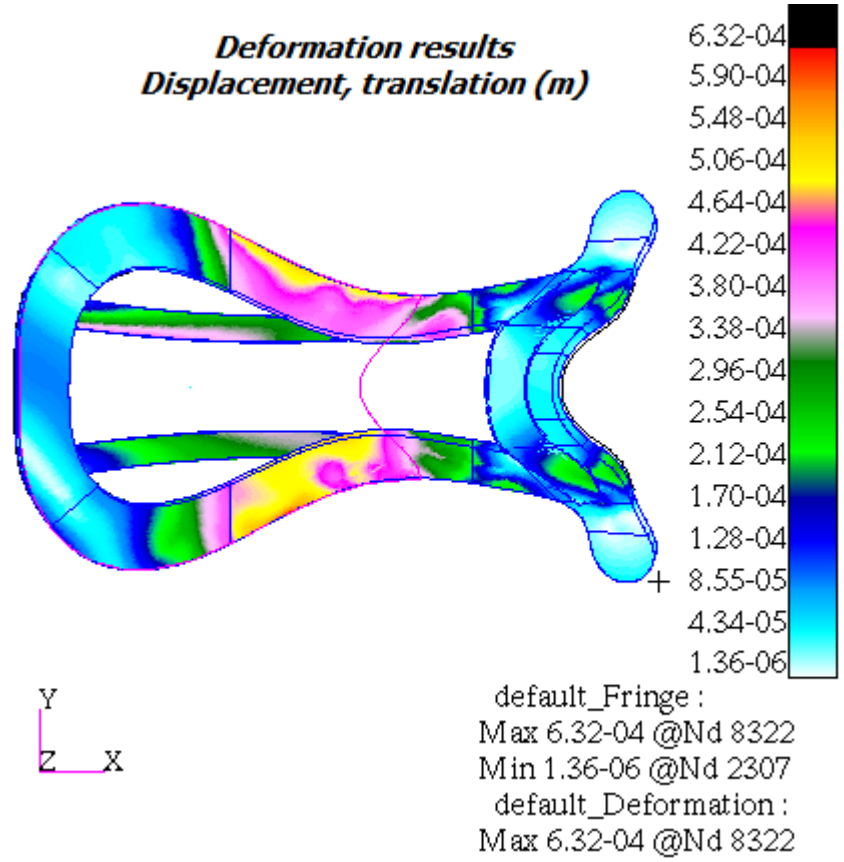

Figure 5.5.4 Reinforced saddletree – Laminates

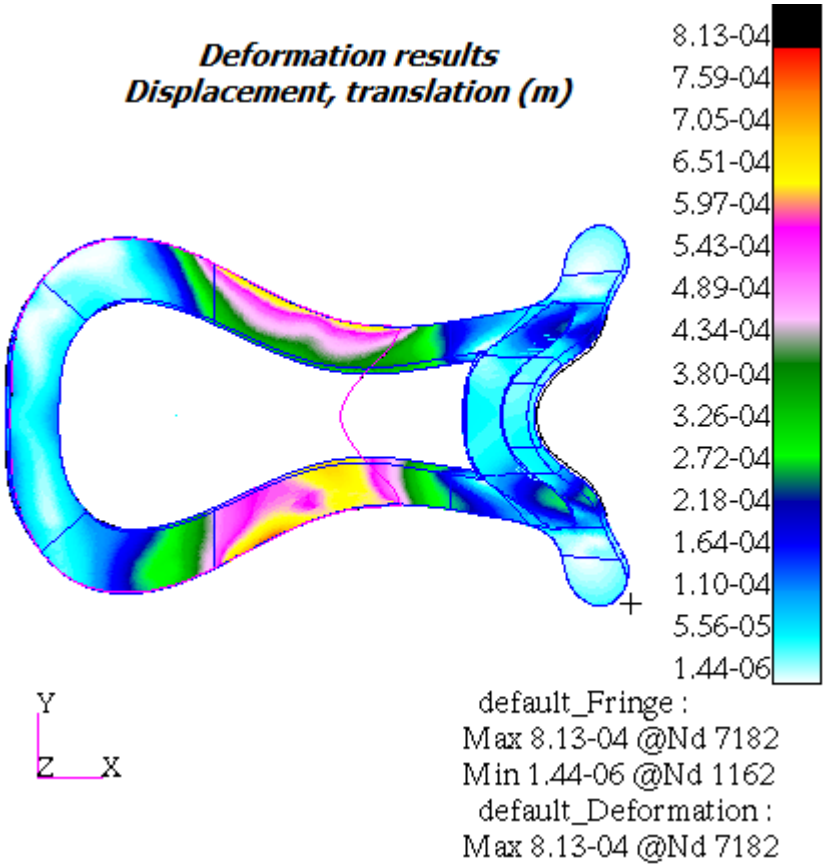

Figure 5.5.5 Reinforced saddletree without spring steel – Solid

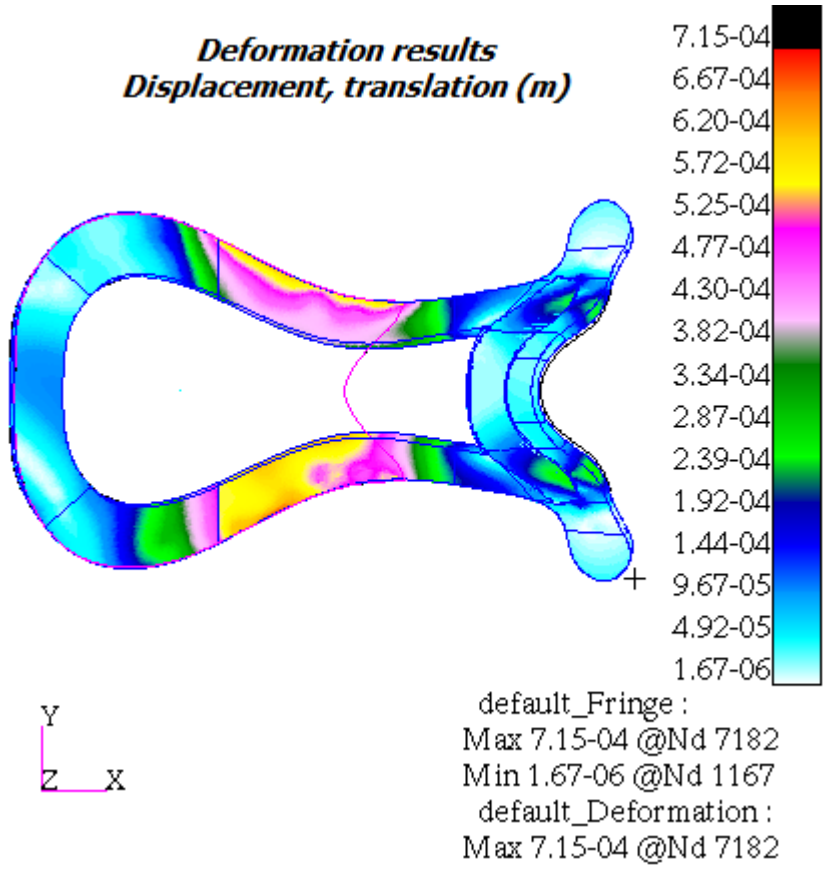

Figure 5.5.6 Reinforced saddletree without spring steel – Laminates

5.5.2 20 % 90 degrees and 80 % 0 degrees stacking sequence

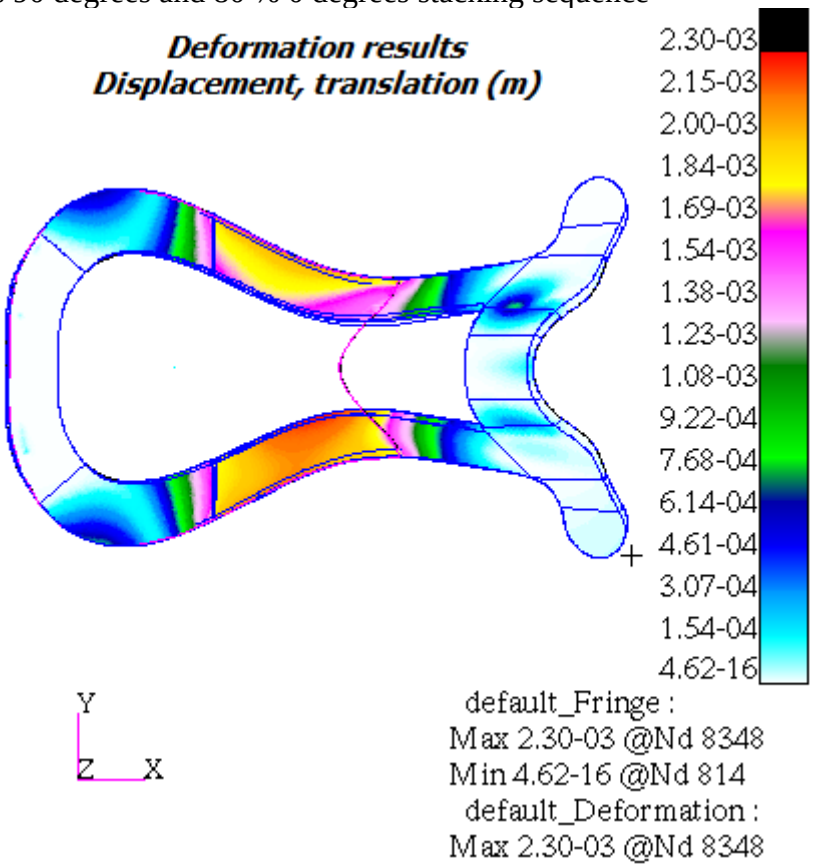

Figure 5.5.7 Laminated saddletree – $[90/0/0/0/0]_T$

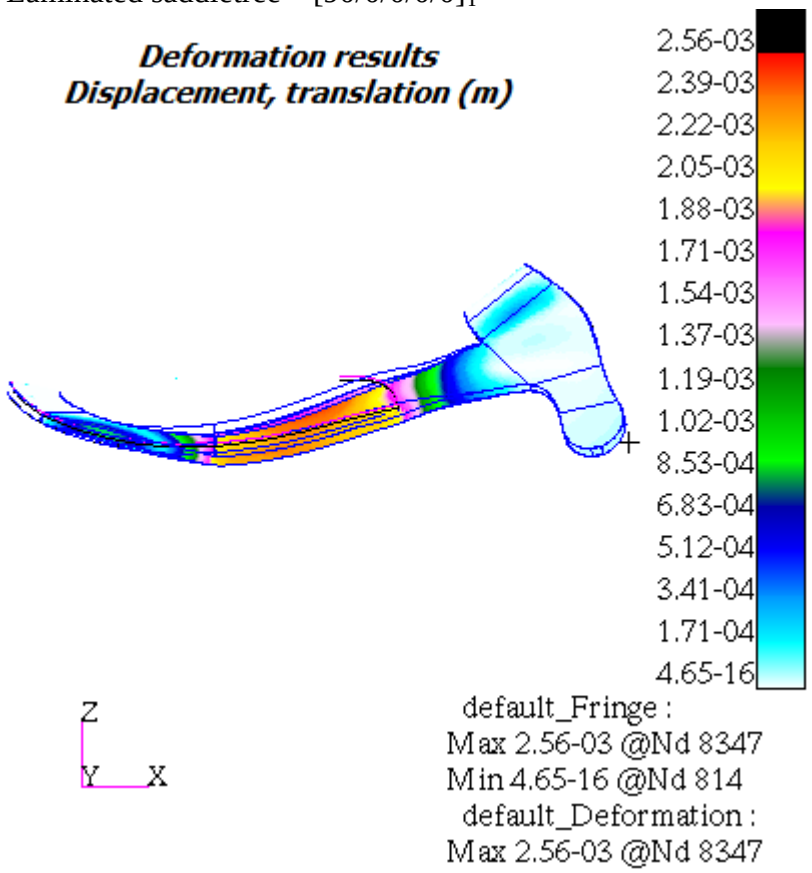

Figure 5.5.8 Laminated saddletree – $[0/90/0/0/0]_T$

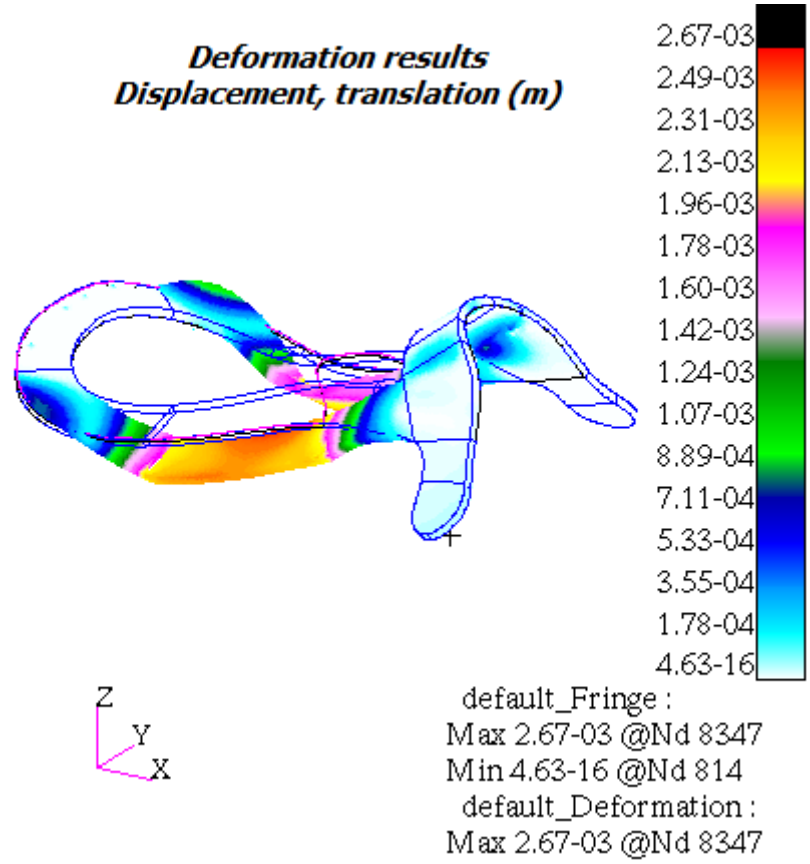

Figure 5.5.9 Laminated saddletree – $[0/0/90/0/0]_T$

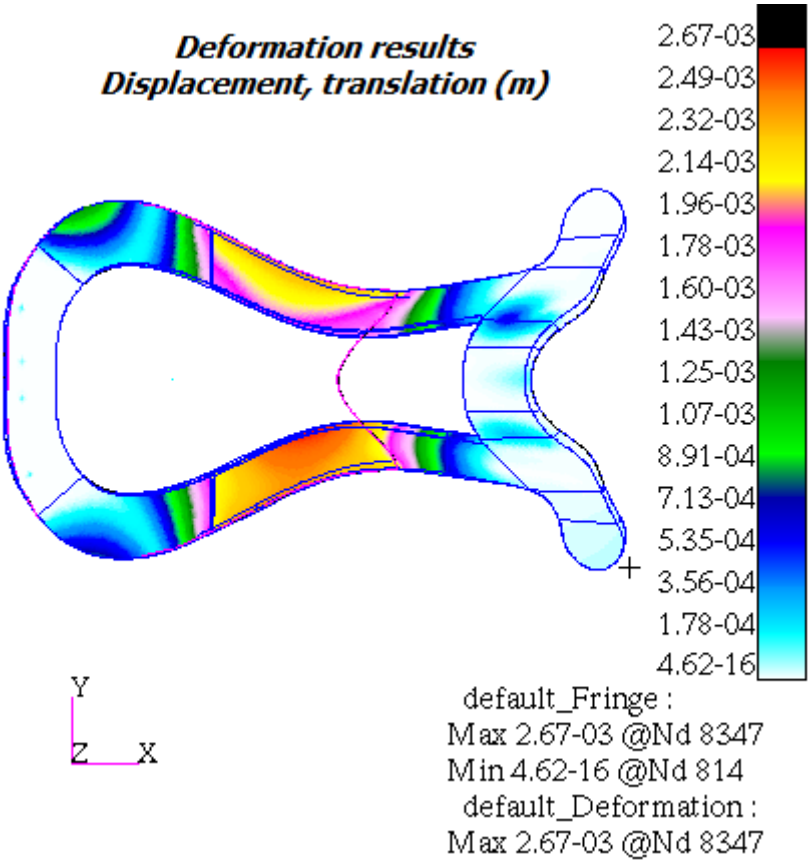

Figure 5.5.10 Laminated saddletree – $[0/0/0/90/0]_T$

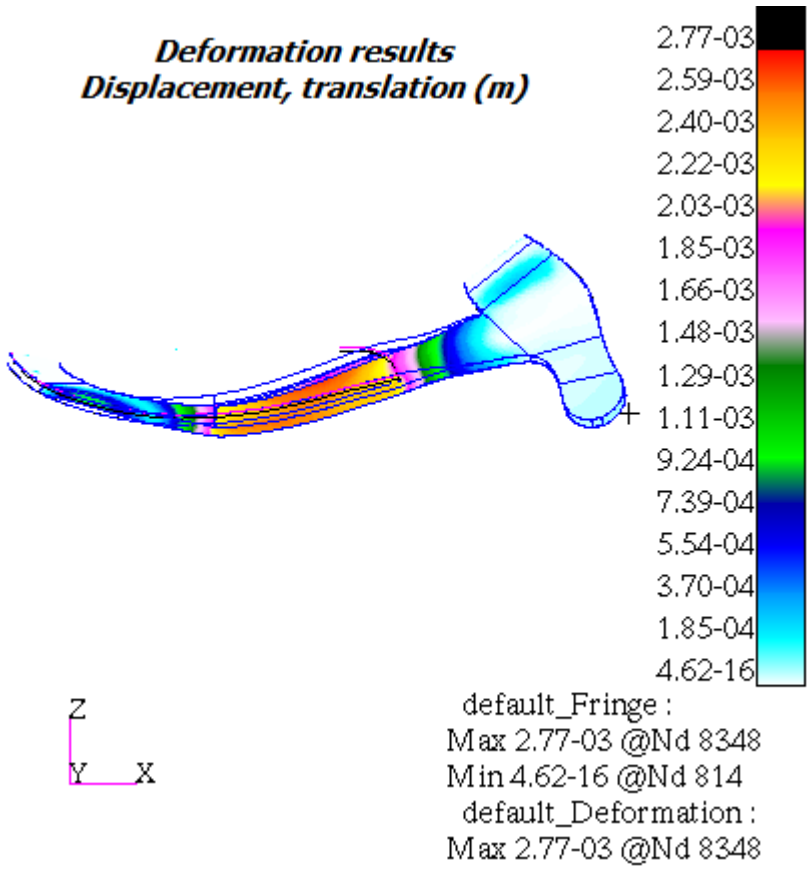

Figure 5.5.11 Laminated saddletree – $[0/0/0/0/90]_T$

5.5.3 40 % 90 degrees and 60 % 0 degrees stacking sequence

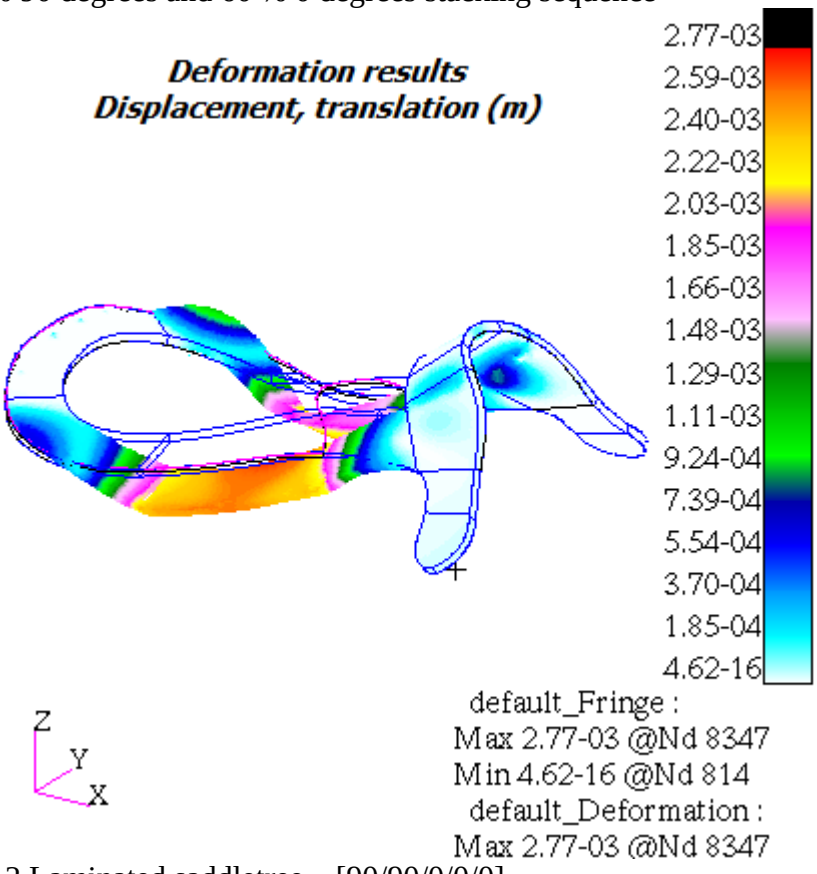

Figure 5.5.12 Laminated saddletree – $[90/90/0/0/0]_T$

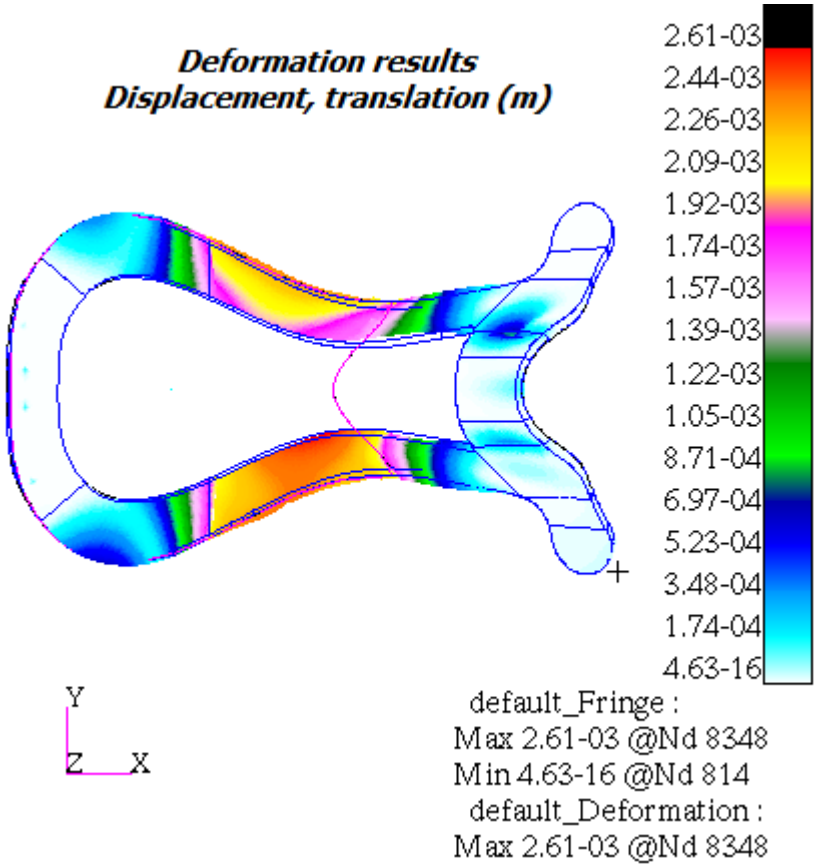

Figure 5.5.13 Laminated saddletree – $[90/0/90/0/0]_T$

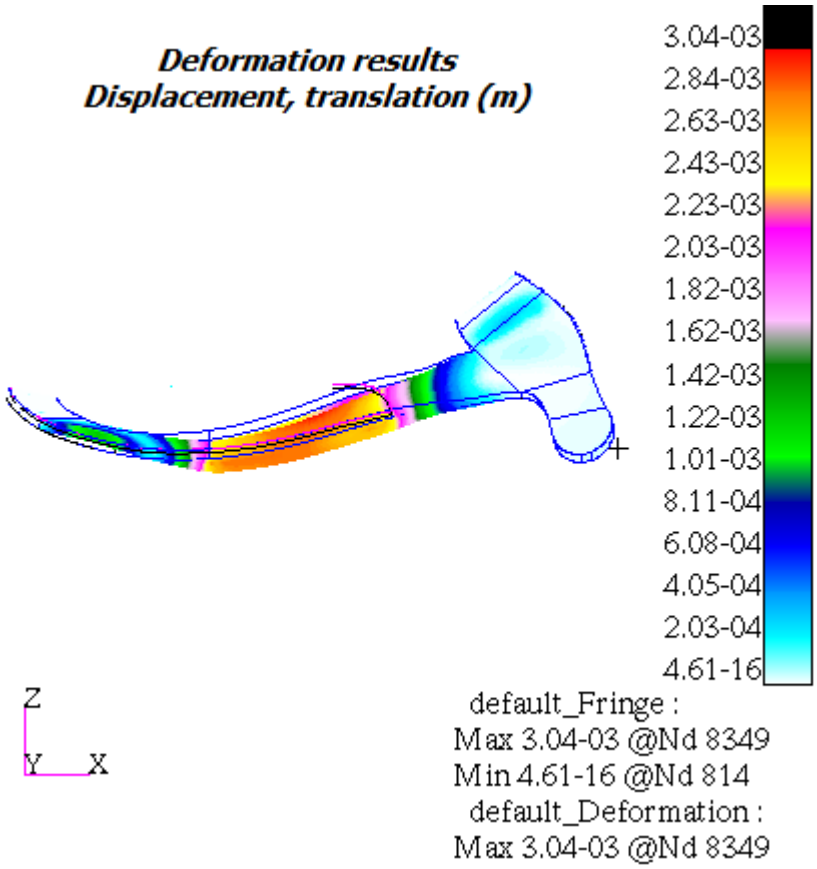

Figure 5.5.14 Laminated saddletree – $[90/0/0/90/0]_T$

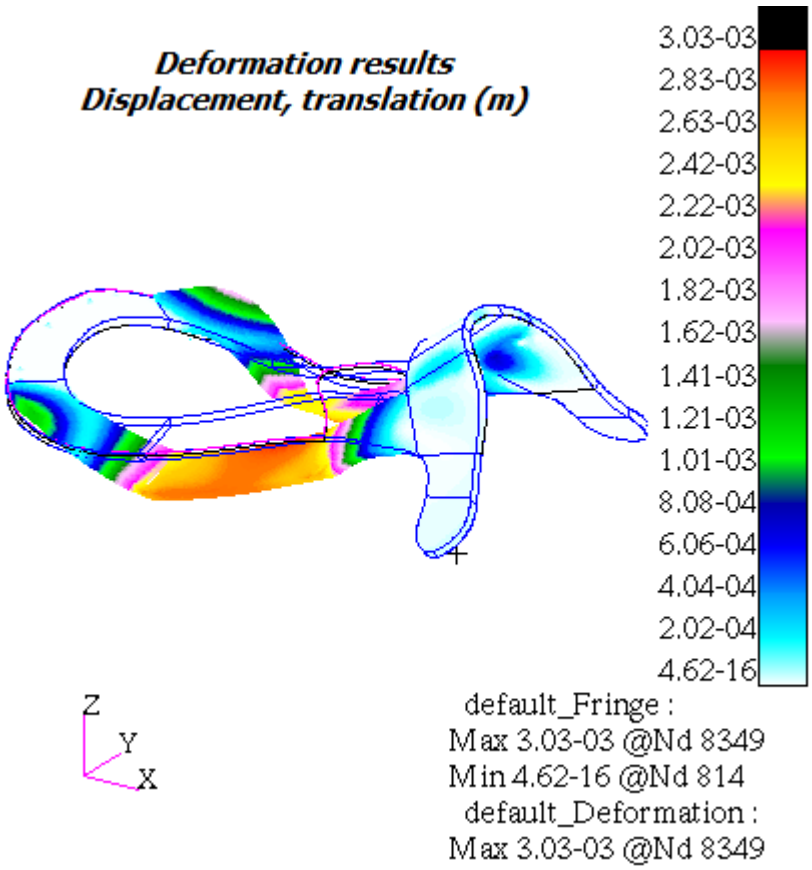

Figure 5.5.15 Laminated saddletree – $[90/0/0/0/90]_T$

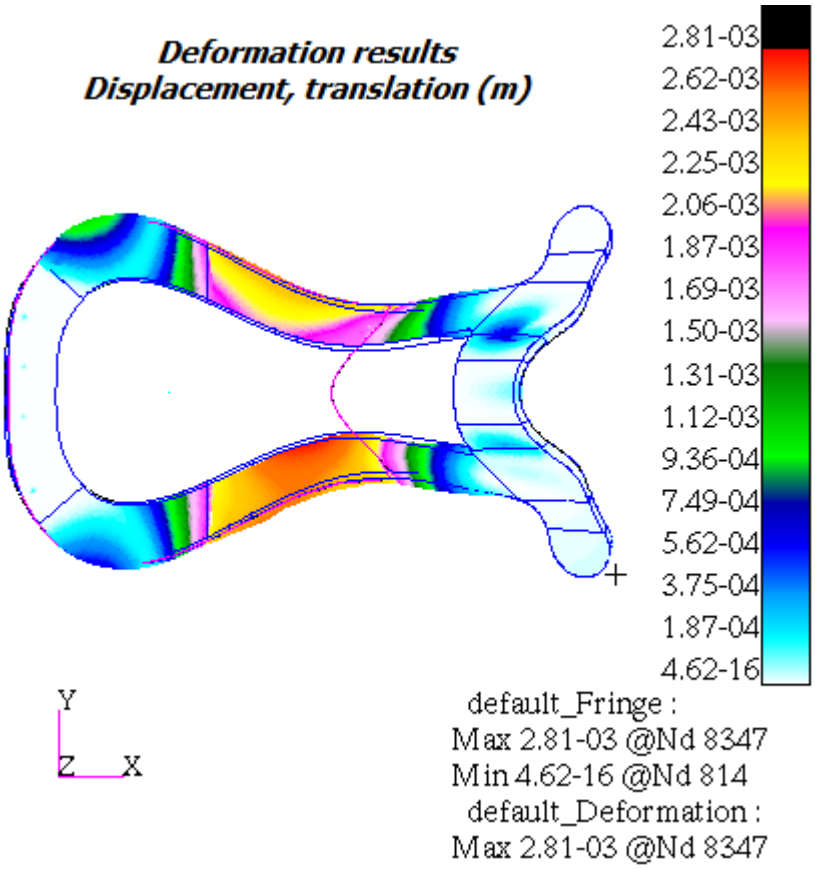

Figure 5.5.16 Laminated saddletree – $[0/90/90/0/0]_T$

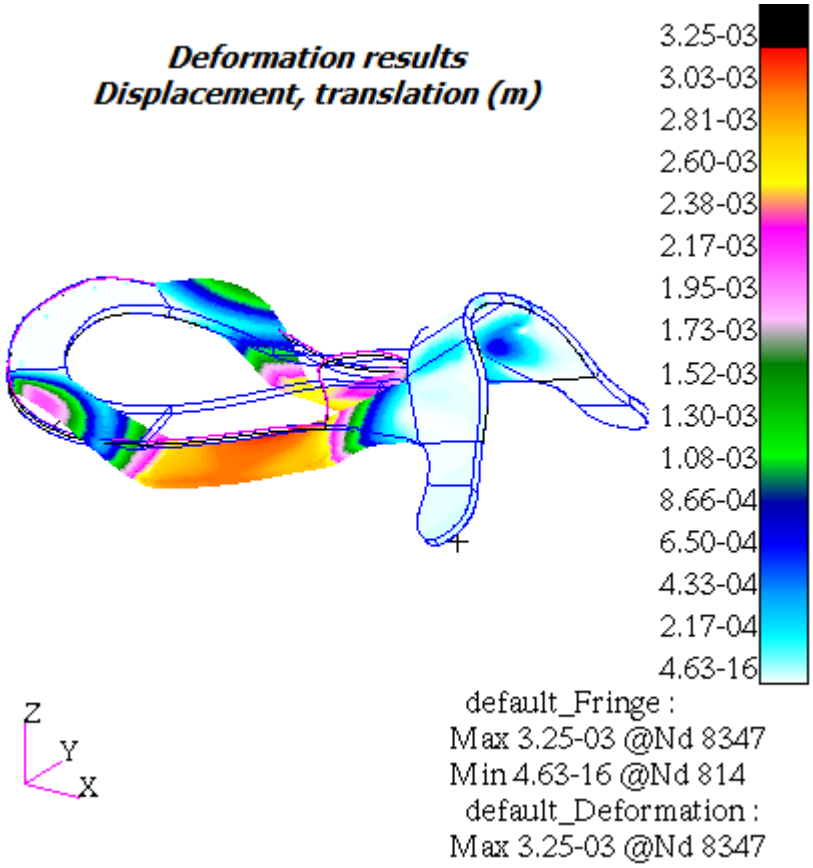

Figure 5.5.17 Laminated saddletree – $[0/90/0/0/90]_T$

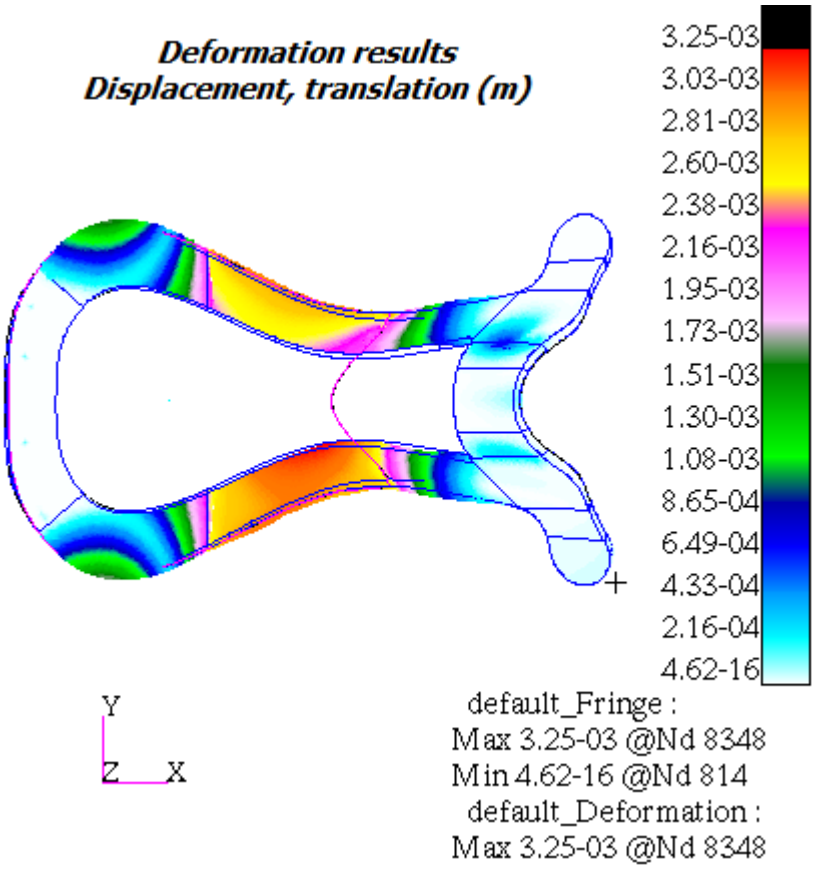

Figure 5.5.18 Laminated saddletree – $[0/0/90/90/0]_T$

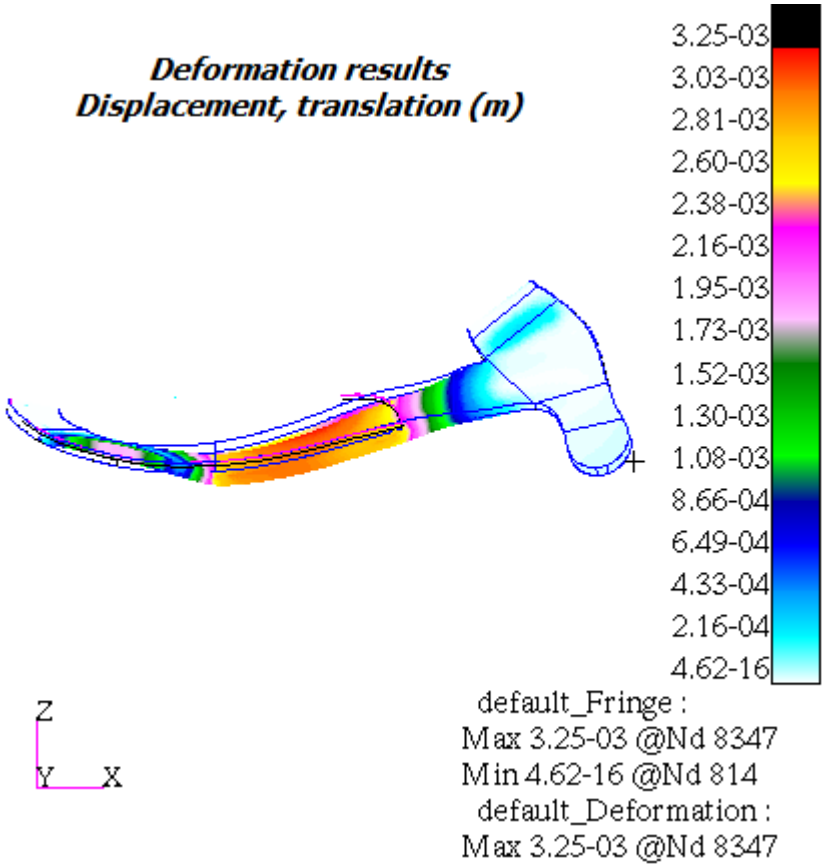

Figure 5.5.19 Laminated saddletree – $[0/0/90/0/90]_T$

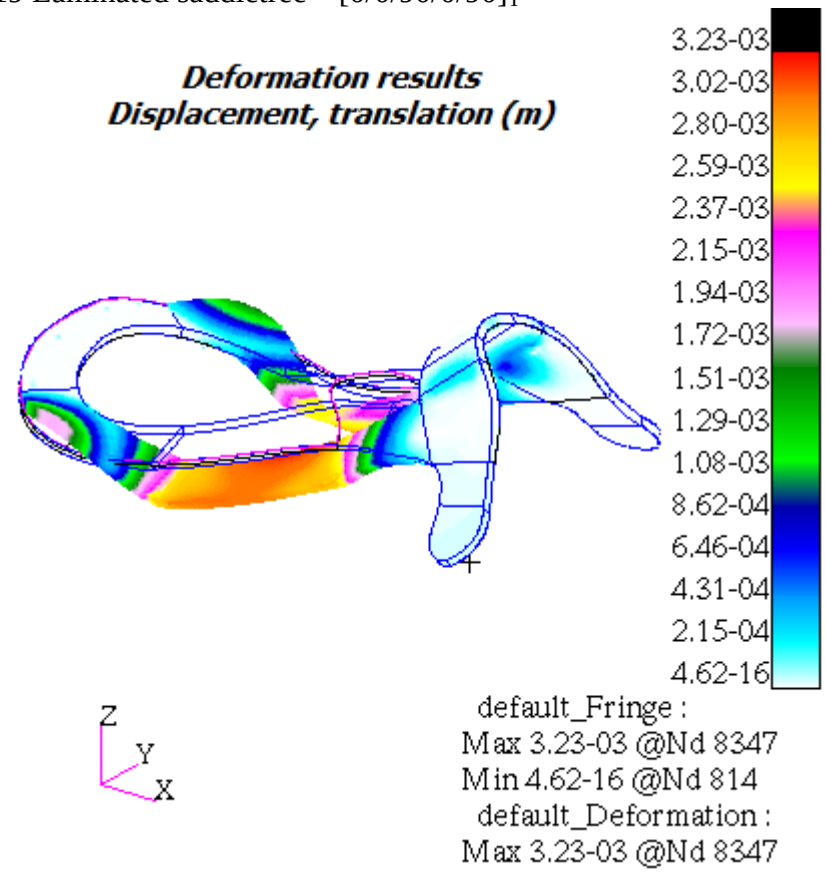

Figure 5.5.20 Laminated saddletree – $[0/0/0/90/90]_T$

5.5.4 60 % 90 degrees and 40 % 0 degrees stacking sequence

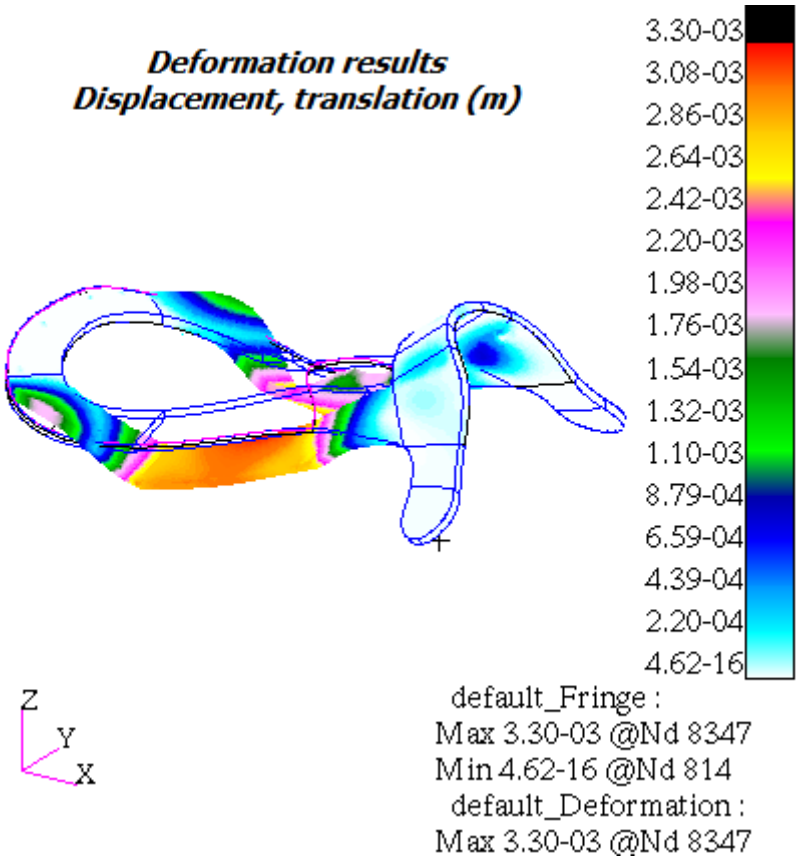

Figure 5.5.21 Laminated saddletree – $[90/90/90/0/0]_T$

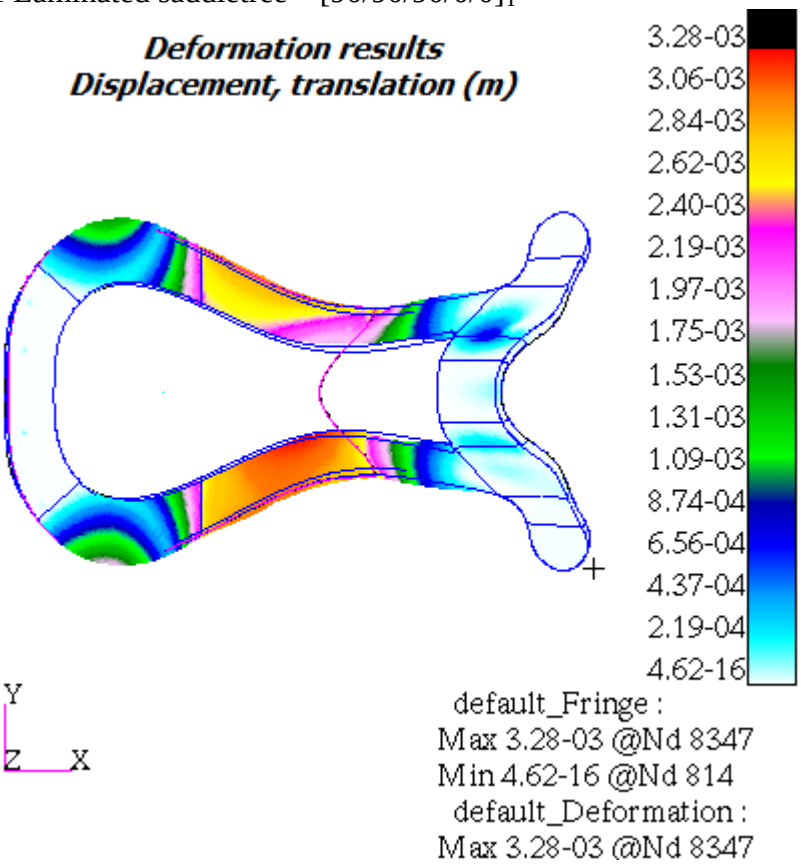

Figure 5.5.22 Laminated saddletree – $[90/90/0/90/0]_T$

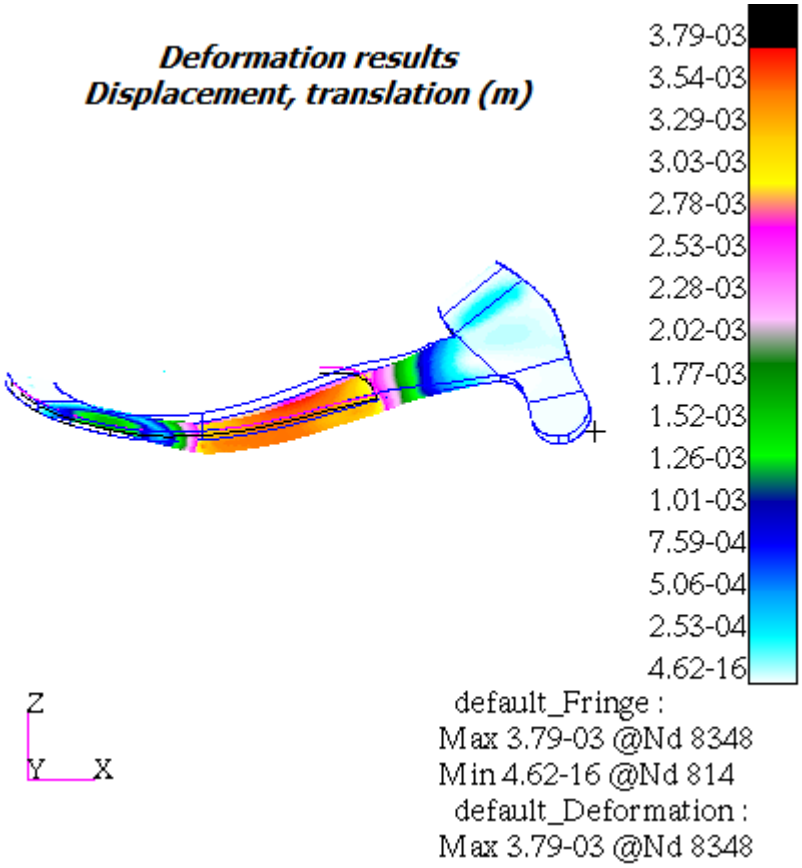

Figure 5.5.23 Laminated saddletree – $[90/90/0/0/90]_T$

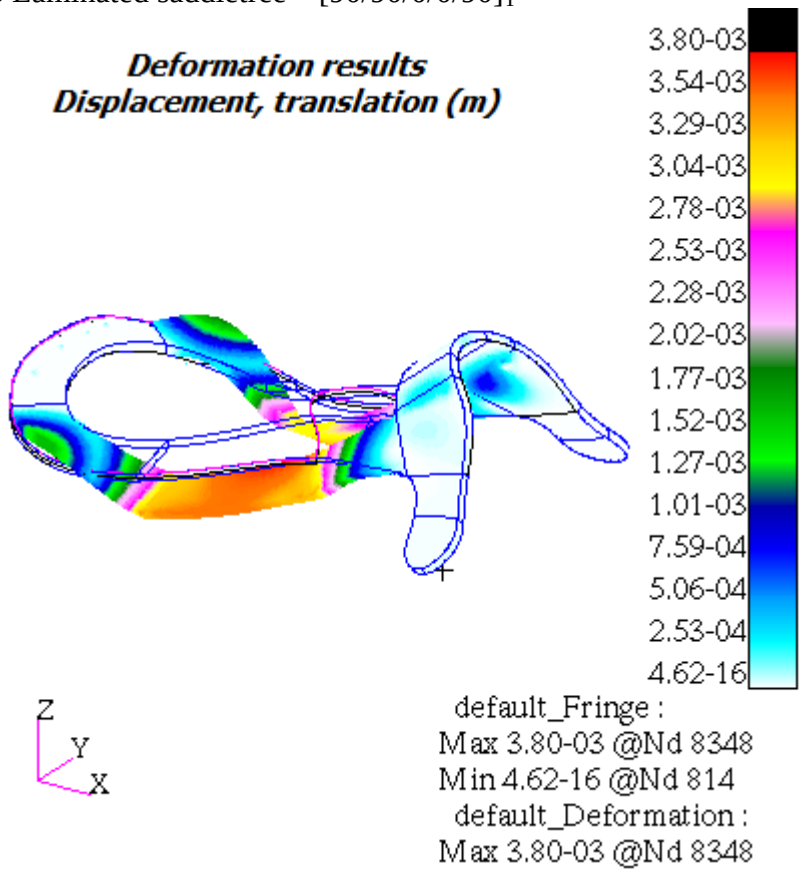

Figure 5.5.24 Laminated saddletree – $[90/0/90/90/0]_T$

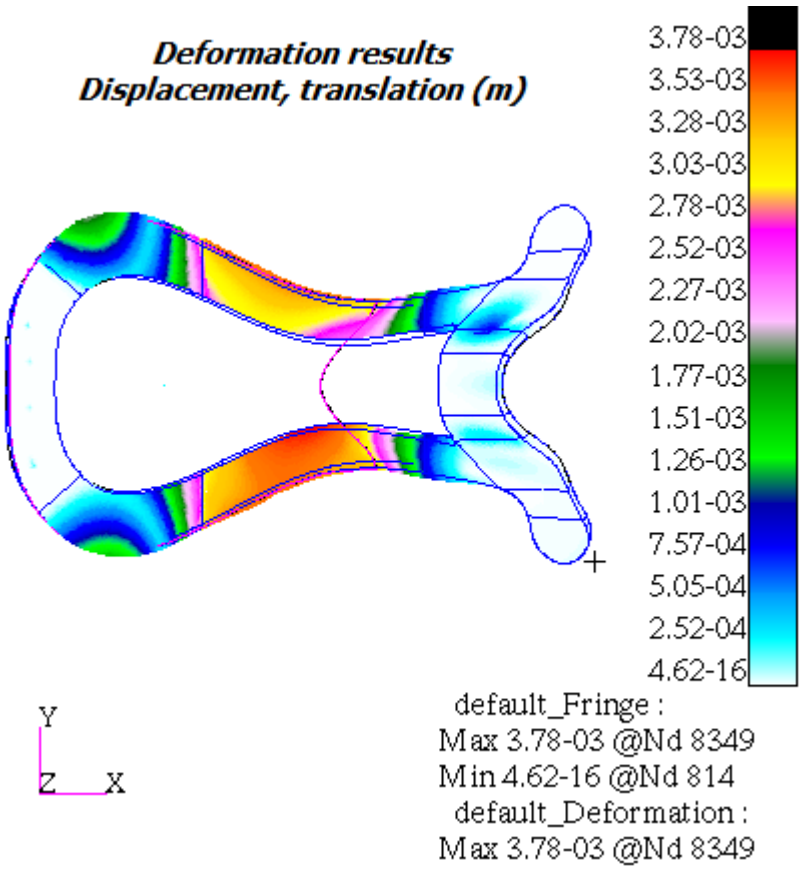

Figure 5.5.25 Laminated saddletree – $[90/0/90/0/90]_T$

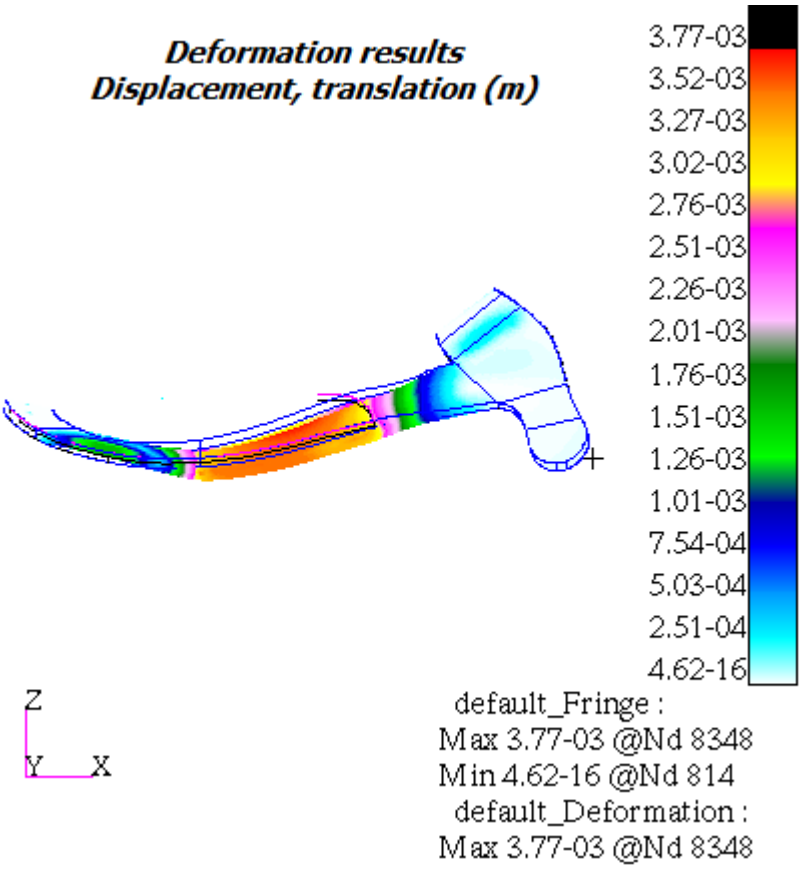

Figure 5.5.26 Laminated saddletree – $[90/0/0/90/90]_T$

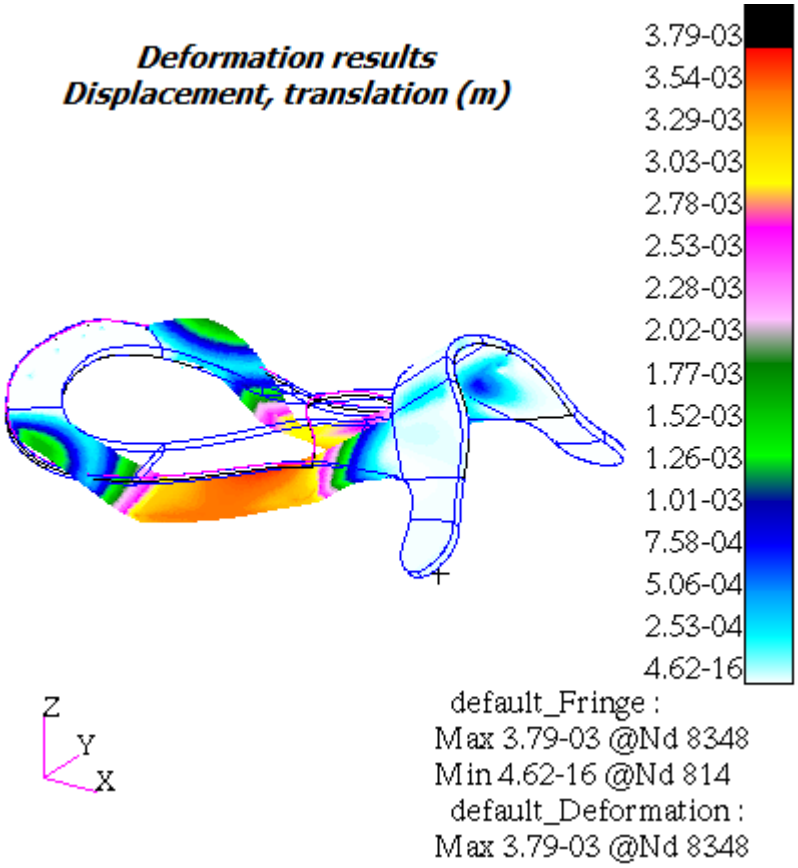

Figure 5.5.27 Laminated saddletree – $[0/90/90/90/0]_T$

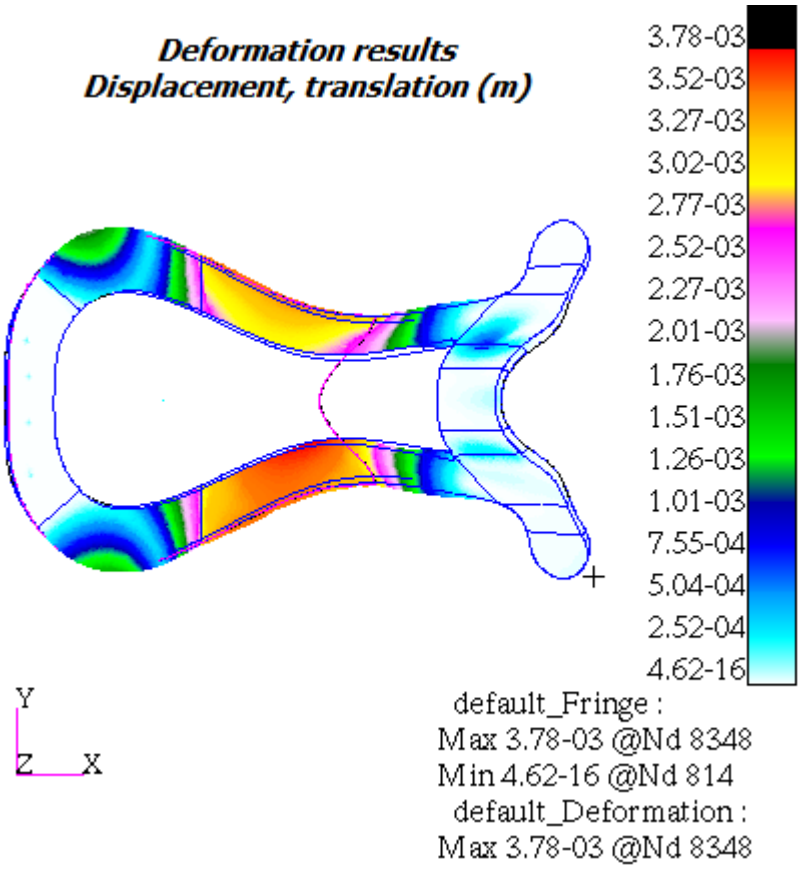

Figure 5.5.28 Laminated saddletree – $[0/90/90/0/90]_T$

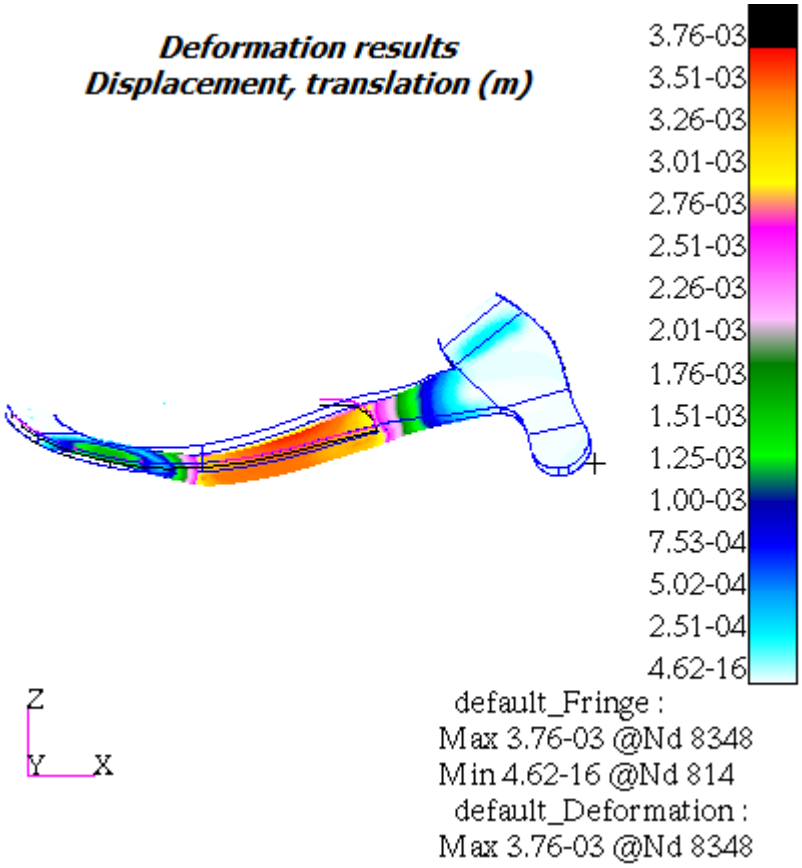

Figure 5.5.29 Laminated saddletree – $[0/90/0/90/90]_T$

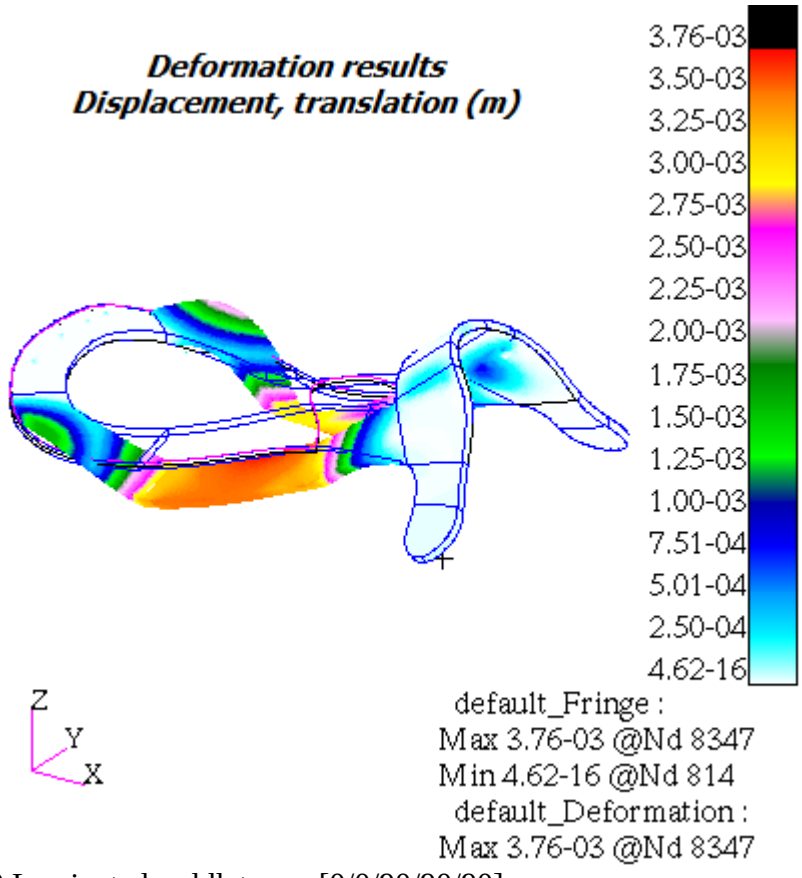

Figure 5.5.30 Laminated saddletree – $[0/0/90/90/90]_T$

5.5.5 80 % 90 degrees and 20 % 0 degrees stacking sequence

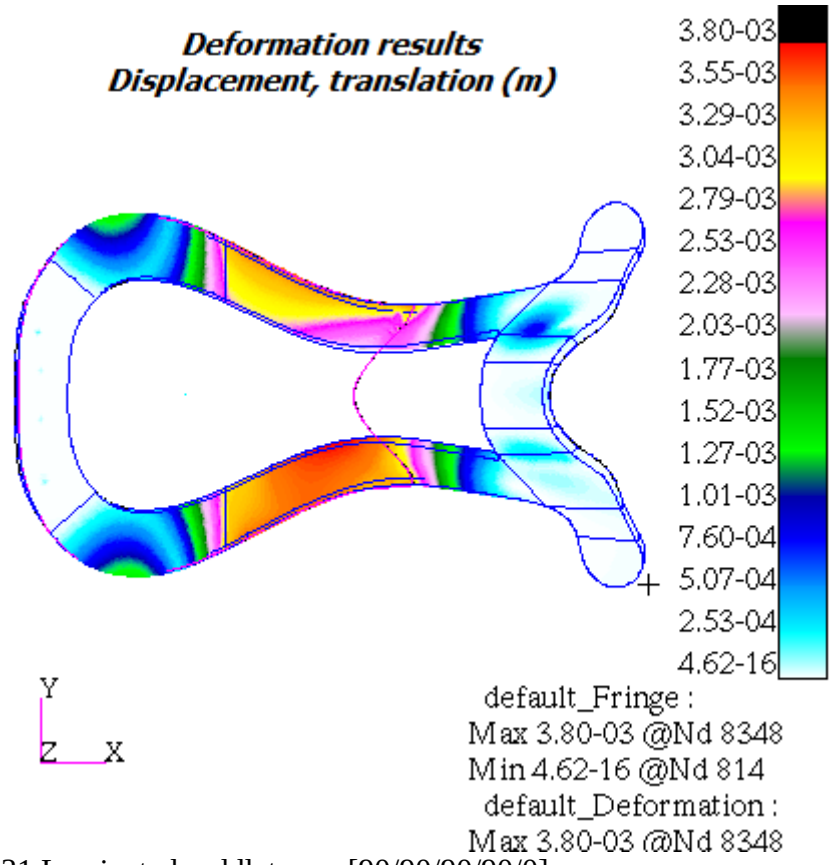

Figure 5.5.31 Laminated saddletree – $[90/90/90/90/0]_T$

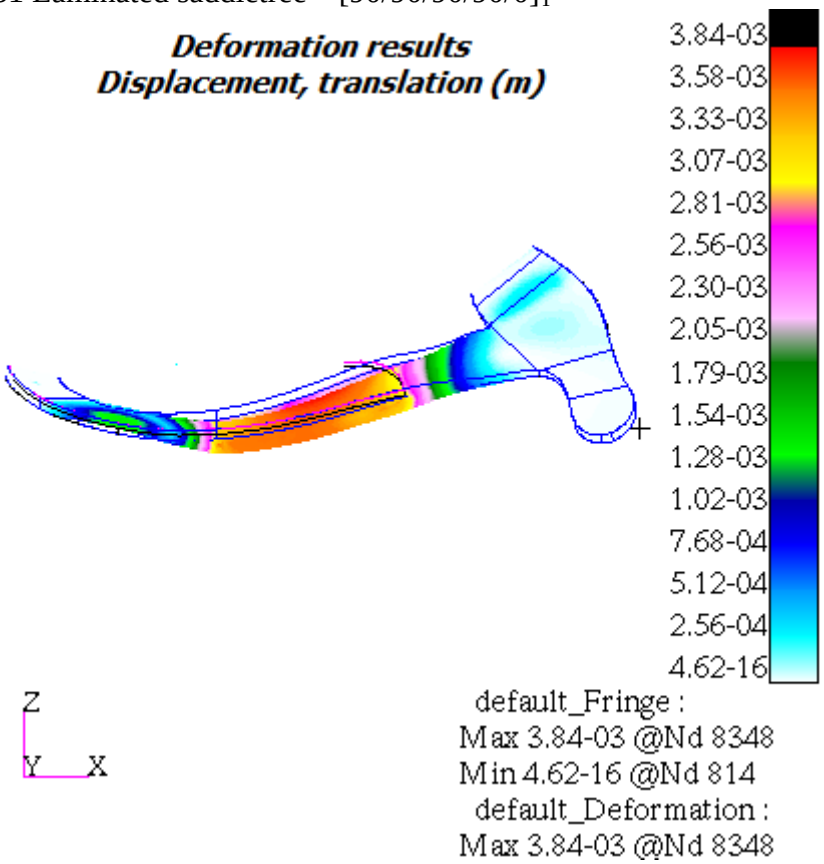

Figure 5.5.32 Laminated saddletree – $[90/90/90/0/90]_T$

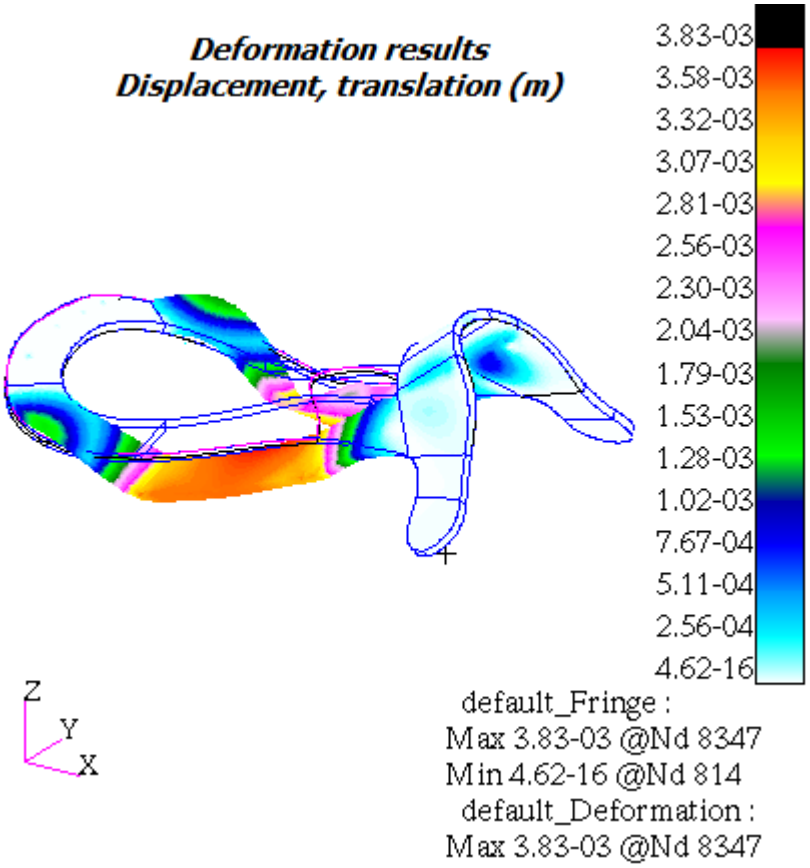

Figure 5.5.33 Laminated saddletree – $[90/90/0/90/90]_T$

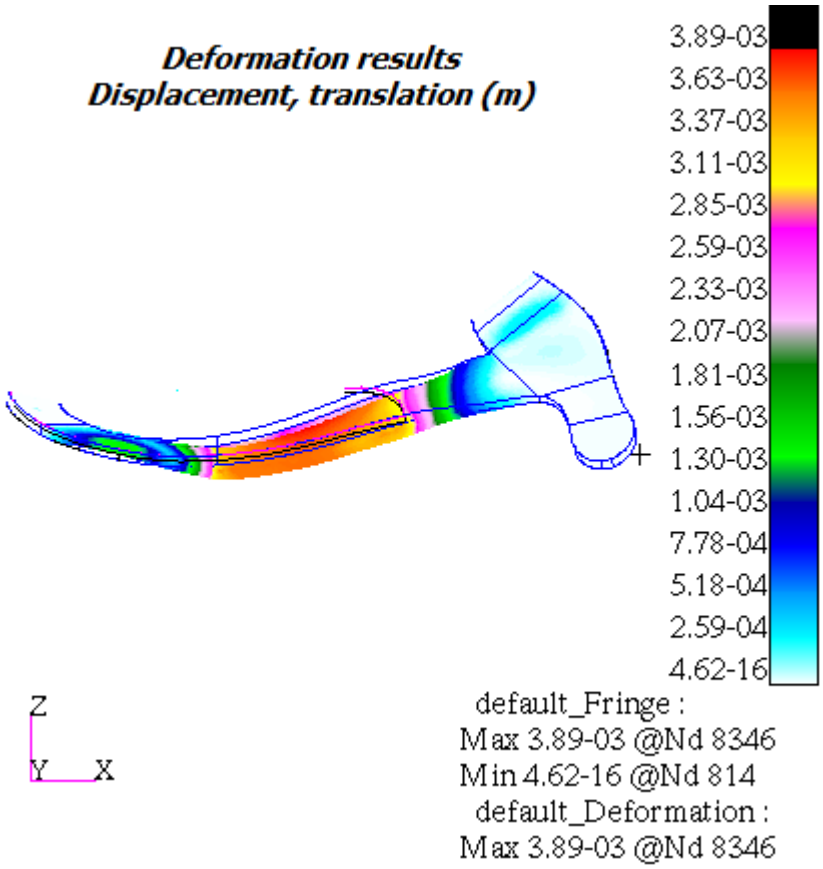

Figure 5.5.34 Laminated saddletree – $[90/0/90/90/90]_T$

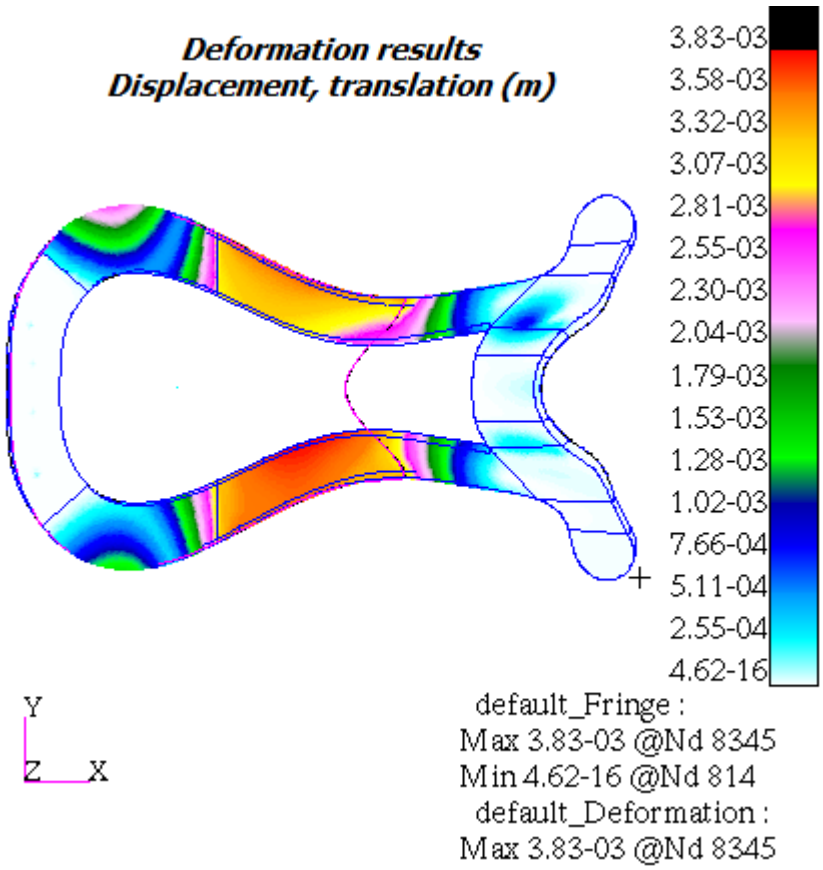

Figure 5.5.35 Laminated saddletree – $[0/90/90/90/90]_T$

5.6 DISCUSSION OF RESULTS

The saddletree has been simulated based on an assumption that it is in contact with three (3) node controlled rigid bodies – one bearing the applied load, and the others acting as fixed constraints. The boundary conditions in this chapter are similar to the set up reported in Jeffcott and Dalin (1980) in investigating the rigidity of the horse's thoracolumbar spine (as illustrated in figure 2.2.3 of section 2.2 of this thesis).

The ability to quantify the stiffness of the saddletree within a user environment is of great significance. Schlacher, et al. (2004) had earlier been reported (in section 2.2 of this thesis) to have deduced a mean stiffness of 2.093 N/mm for the dorsoventral movement of the thoracolumbar spine. The least possible stiffness of the saddletree has been determined here to be 347.02 N/mm. Sports and clinical researchers are

interested in the role of stiffness as it relates to both performance and injury (Butler, et al., 2003). A design analogy can be made with shoes. Stacoff, et al. (1989, 1991) as cited in Morio, et al. (2009) suggested that the stiffer the shoe, the greater its effects on the natural motion of the foot. Morio, et al. (2009) further concluded that foot motions were constrained by the forefoot. In comparison with the mean stiffness of the dorsoventral movement of the thoracolumbar spine reported in the work of Schlacher, et al. (2004), it is evident that a stiffness mismatch occurs between the saddletree and the thoracolumbar spine. This poses a risk of inhibiting the natural movements of the horseback and may be responsible for the overt signs of back pain (Jeffcott, 1975).

5.6.1 The effects of reinforcing the saddletree on the stiffness of the saddletree

In chapter 4, the steel reinforcement plates were observed to have increased the stiffness of the wood-only product. The simulations in this chapter provide further knowledge on the effect of the reinforcement plates on the wood only product under a different loading condition. The stiffness of the saddletree models, which were deduced from the slopes of the load-displacement graphs (similar to figure 4.6.1), and their response to the steel reinforcement plates are presented in figure 5.6.1. They are classed according to their material type and geometry.

While the steel reinforcement plates with and without the pair of spring steel increased the stiffness of the solid wood saddletree by 365.75 % and 260.37 % respectively, they increased the stiffness of the laminated wood saddletree by 447.40% and 386.77 % respectively.

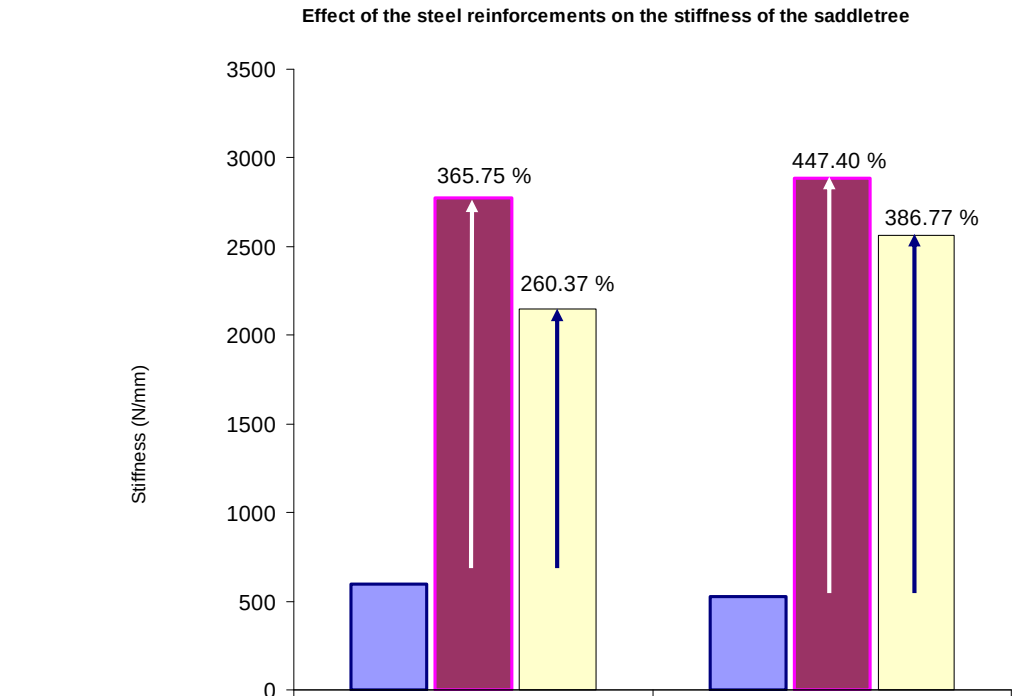

	Solid wood - Stiffness (N/mm)	Laminated wood - Stiffness (N/mm)
Wood Only	596.16	526.62
Reinforced tree	2776.62	2882.73
No sprung steel reinforced tree	2148.39	2563.44

Figure 5.6.1 The effect of the steel reinforcements on the stiffness of the saddletree

5.6.2 The effects of stacking sequence on the stiffness of the saddletree

The stiffnesses of the saddletree modelled with 20 % of 90^0 and 80 % of 0^0, 40 % of 90^0 and 60 % of 0^0, 60 % of 90^0 and 40 % of 0^0, and, 80 % of 90^0 and 20 % of 0^0 are illustrated in figures 5.6.2 to 5.6.5 respectively. There can be several dissimilar bending stiffnesses for a known total laminate thickness even if the properties of the lamina along their on-axis are the same (Gurdal, et al., 1999). The minimum and maximum stiffnesses were $[90/90/0/90/90]_T$ at 347.02 N/mm and $[0/90/0/0/90]_T$ at 824.96 N/mm respectively, while the closest similarities amongst the 30 sequences were $[90/0/0/90/90]_T$, $[0/90/90/0/0]_T$, and $[90/90/0/0/0]_T$ at 533.29 N/mm, 533.31 N/mm, and, 533.61 N/mm. There is a similarity in the variation of the stiffnesses of the 20 % of 90^0 and 80 % of 0^0 and 80 % of 90^0 and 20 % of 0^0. The stiffnesses seem

to converge with the positioning of the 90^0 and 0^0 in the middle of the laminates. Also, their graphs seem to be a mirror image of each other.

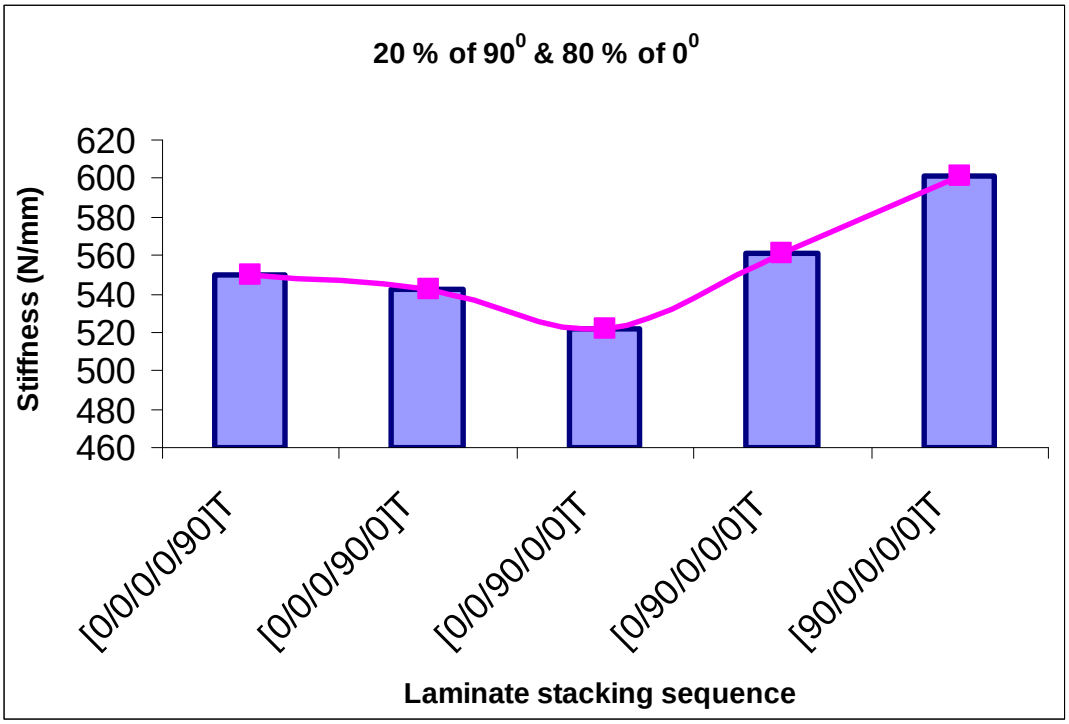

Figure 5.6.2 20 % of 90^0 and 80 % of 0^0

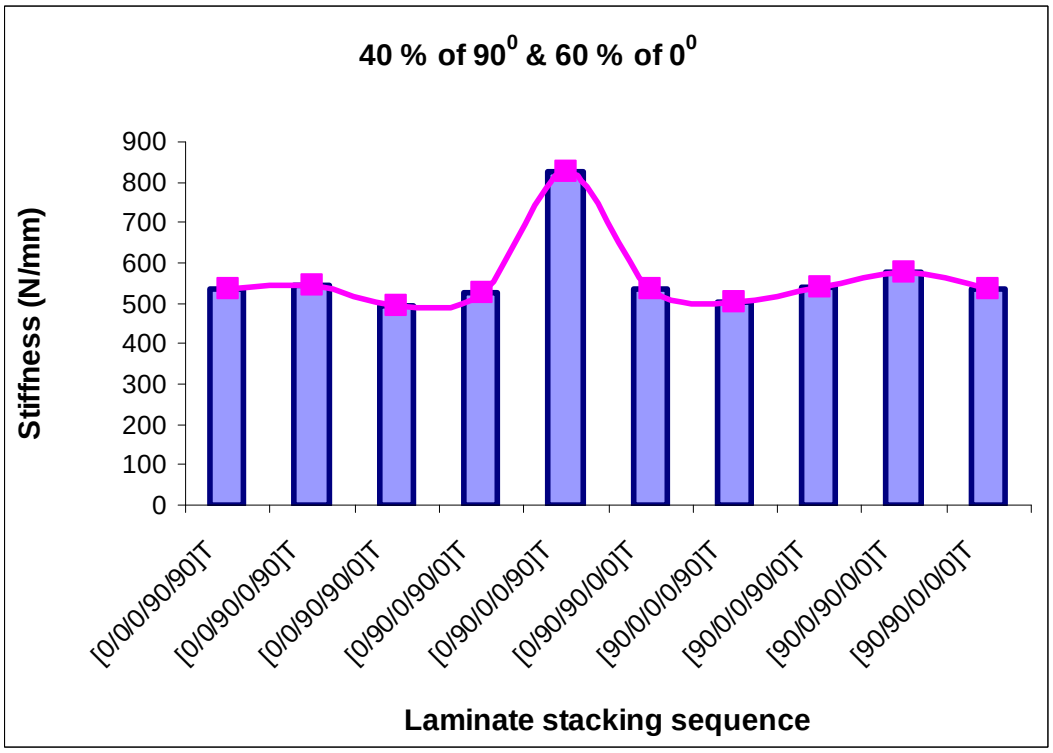

Figure 5.6.3 40 % of 90^0 and 60 % of 0^0

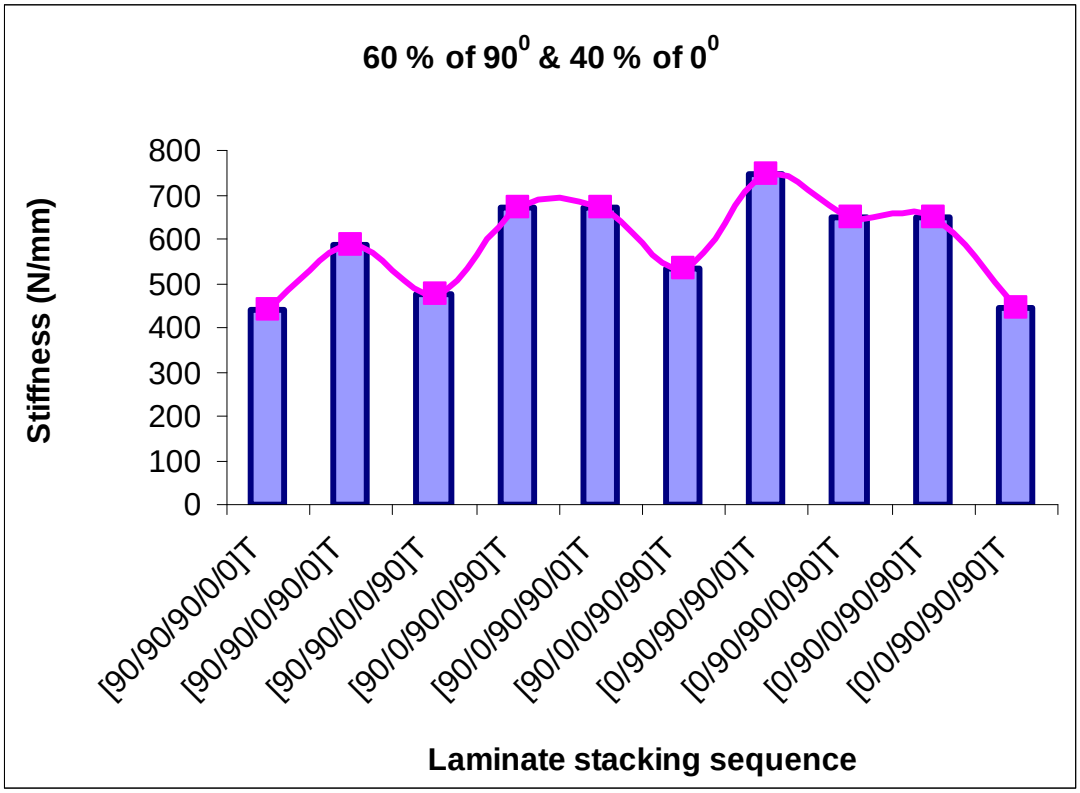

Figure 5.6.4 60 % of 90^0 and 40 % of 0^0

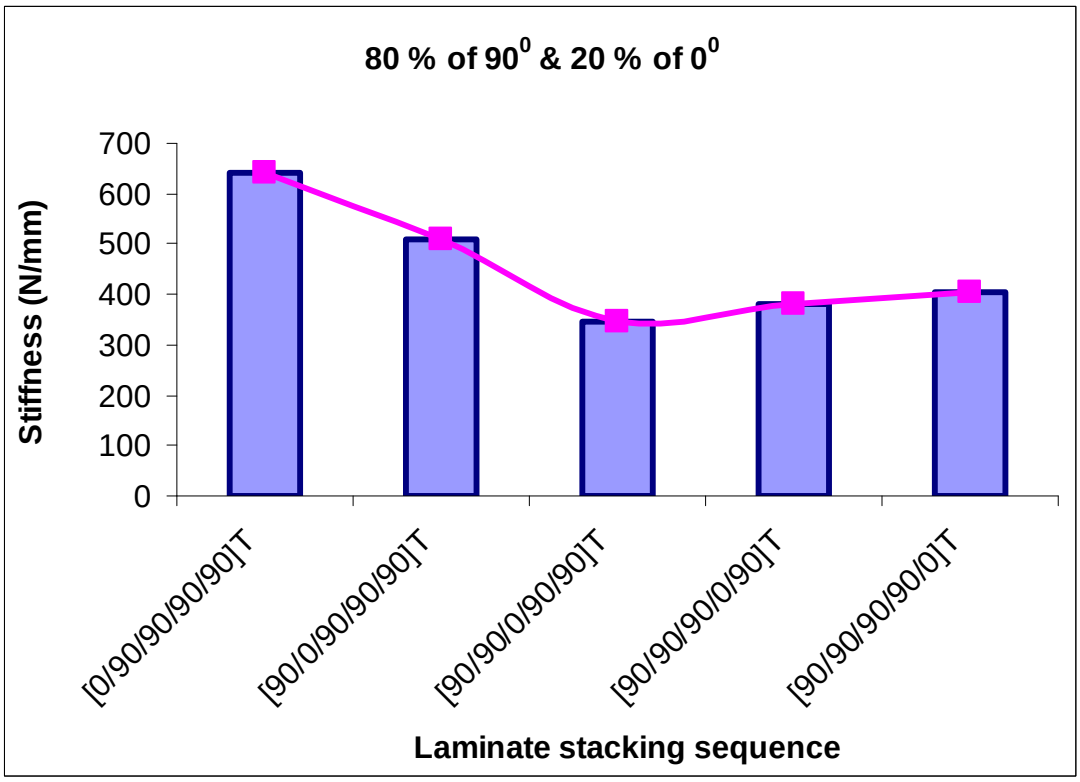

Figure 5.6.5 80 % of 90^0 and 20 % of 0^0

5.7 SUMMARY

The saddletree was modelled simplifying its complex interaction (Witte, et al., 2009) with a rider and a horseback. The steel reinforcements without the pair of spring steel increased the stiffness of the solid wood saddletree by a factor of 3.6 while the stiffness of the laminated wood saddletree was increased by a factor of 4.9. And, the steel reinforcements with the pair of spring steel increased the stiffness of the solid wood saddletree by a factor of 4.7, while the stiffness of the laminated saddletree was increased by a factor of 5.5.

In addition, variations in the laminate stacking sequence between 20 % of 90^0 and 80 % of 0^0, and 80 % of 90^0 and 20 % of 0^0 had a significant effect on the stiffness of the laminated saddletree resulting in stiffnesses ranging between 347.02 N/mm and 824.96 N/mm.

In comparison with the mean stiffness of the dorsoventral movement of the thoracolumbar spine as deduced by Schlacher, et al. (2004), a stiffness mismatch occurs between the saddletree and the thoracolumbar spine.

CHAPTER SIX

IMPACT SIMULATION OF THE SADDLETREE POMMEL

6.1 INTRODUCTION

Numerical models of the English jumping saddletree under static loading conditions have been presented earlier in chapters 4 and 5 of this thesis. The models developed provided an opportunity to investigate the sensitivity of an English jumping saddletree to loading, geometric and, material variations. In addition, the effect of the steel reinforcements on the stiffness of the saddletree was quantified. The numerical models presented in this chapter aim to explore the response of the pommel section of the saddletree to transient dynamic loading.

Saddletrees were reported to break as a result of the impact of sudden shocks experienced during jumping (Davis, 1898) or in the event of a saddled horse rolling or falling over (White and Lightfoot, 1976). BS 7875 (1996) and BS 7875 (2009) specified the method of testing saddletrees made from synthetic materials for impact resistance. The test process involves dropping a mass onto the saddletree, measuring the permanent set and then examining for visible damages.

Unlike BS 7875 (1996) and BS 7875 (2009), BS 6635 (2003) did not specify any method of testing saddletrees made from wood for impact resistance. Hence, the test process described in BS 7875 (1996) and BS 7875 (2009) was used as a guide in developing the dynamic numerical models. The input parameters were however changed to reflect a more realistic situation as presented later in this chapter in the

load and boundary conditions section.

Rather than simulate the complete saddletree, only the pommel section was simulated. The pommel is placed above the withers and, ideally it should be secured in a manner that allows the saddletree to conform to the shape of the withers (Harman, 2009). The pommel is secured on the highest part of the horseback (Jeffcott, 2009) hence there is likelihood that it would be the first point of contact during a fall. In addition, it is the most reinforced section of the saddletree.

6.2 PARAMETERS INVESTIGATED

BS 7875:1996 and BS 7875:2009 specified the measurement of the permanent set after impact. The acceleration, displacement, and velocity histories are presented and are used to evaluate the effects of the cap and gullet plates on the pommel and the effect of the material choice.

6.3 PRE-PROCESSING

The following assumptions were made in developing the FE models in this chapter:

6.3.1 Geometric models

The geometries used in developing the numerical models were obtained from those used in chapter 4; the process used to create them was presented in chapter 3. The geometries include the pommel-only structure (as illustrated in figure 6.3.1) and the reinforced pommel (as illustrated in figure 6.3.2). The lipped gullet plate was 3 mm thick, while the cap plate was 2 mm thick. In addition, a flat rectangular shaped surface geometry was created to represent the contact body.

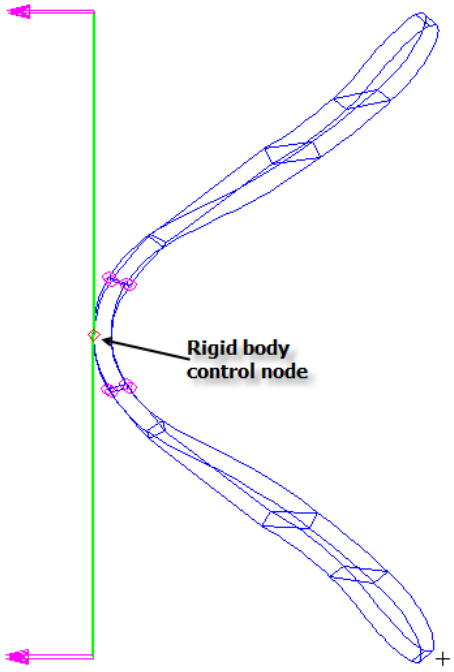

Figure 6.3.1 Pommel-only model in contact with a rigid surface

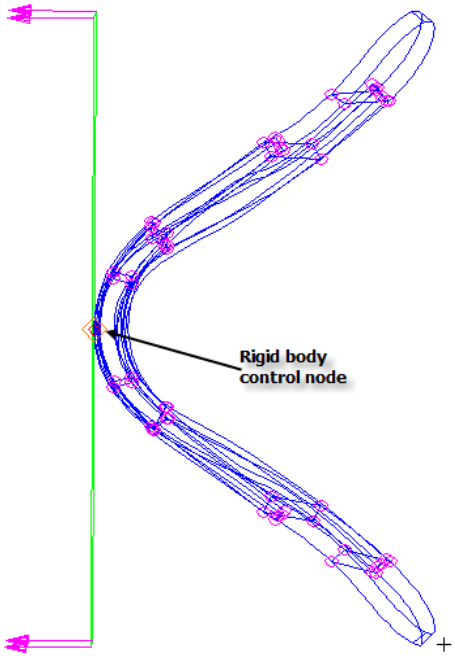

Figure 6.3.2 Reinforced pommel model in contact with a rigid surface

6.3.2 Material properties

The elastic constitutive model used to define the wood material was based on the following assumptions: E11 = 1.529E+10 Pa; E22 = 7.65E+08 Pa; E33 =

1.19262E+09 Pa; ν12 = 0.45; ν23 = 0.426; ν31 = 0.043; G12 = 1.039E+09 Pa; G23 = 2.5993E+08 Pa; and, G31 = 1.1314E+09 Pa (Forest Products Laboratory, 1999). Density ρ, which is particularly important in performing a modal analysis (Bretos et al., 1999), was assumed to be 630 kgm^{-3} (Finnish Forest Industries Federation, 2002). A maximum stress failure criterion was used to define the failure constitutive model for the wood material based on the following assumptions: maximum tensile stress X = 1.1378E+08 Pa, maximum compressive stress X = 5.63E+07 Pa, maximum tensile stress Y = 6.3E+06 Pa, maximum compressive stress Y = 6.7E+06 Pa, and maximum shear stress XY = 1.3E+07 Pa (Forest Products Laboratory, 1999). The material properties of the steel reinforcements were assumed to be: E = 2.1E+11 Pa and, ρ = 7830 kgm^{-3}, ν = 0.29, and yield stress = 2.5E+08 Pa.

The laminate total stacking sequence was defined as $[0/90/0/90/0]_T$ and each lamina was 1.5 mm thick.

6.3.3 Load and boundary conditions

6.3.3.1 Determination of velocity range

The velocity of an impacting body can be calculated considering the principle of conservation of energy by assuming that potential energy is converted to kinetic energy at the point of impact (Wilcox, 2006).

$$mgh = \frac{1}{2}mv^2 \tag{6.1}$$

Assuming there is no change in mass, m, then,

$$v = \sqrt{2gh} \tag{6.2}$$

h was assumed to be the sum of the height of a rider on a horse measured at the

withers and the height of a fence. A rider is about 2 m from the ground when sat on a saddled horse (Balendra, et al., 2007) and the height of the fence may vary between 1.50 m and 2.38 m (Bobbert, et al., 2005). Therefore,

$3.50 \text{ m} < h < 4.38 \text{ m}$ (6.3)

Substituting equation 6.3 into equation 6.2 and solving for v,

$8.29 \text{ ms}^{-1} < v < 9.27 \text{ ms}^{-1}$

Biewener and Taylor (1986) reported the absolute speed of a horse at maximum gallop to be 7.5 ms^{-1}. Hole, et al. (2002) reported the velocity of some horses before jumping as 7.51 ms^{-1}, and, Powers and Harrison (2000) reported the horizontal velocity in the final approach stride preceding a jump as 7.37 ms^{-1}. In addition, BS EN 14572 (2005) specified impact velocities of 4.4 m/s, 6.3 m/s and 7.7 m/s respectively for low energy, and high energy impacts meant for testing high performance helmets for equestrian activities. Furthermore, Foero Rueda, et al. (2009) simulated the impact of equestrian helmets at impact velocities of 4.4ms^{-1}, 5.4ms^{-1}, and 7.7 ms^{-1}. In order to accommodate the variation, the impact velocity was set to 7.0 ms^{-1}, 8.5 ms^{-1}, and 10 ms^{-1}.

6.3.3.2 Determination of the analysis time and time step

Impact occurs over a brief duration (Gilardi and Sharf, 2002), normally within a few microseconds (Hughes, 1992) or milliseconds (Wang et al., 2005). BS 7875:1996 and BS 7875:2009 did not specify the time or time step for impact. Prior to conducting dynamic analysis, MSC.Software (2008; 2000) and Dawson, et al. (1999) carried out a modal analysis to estimate an appropriate time step for the transient dynamic analysis. The deformation of the model at each mode was observed (Liu, et

al., 2009) and the natural frequency of the modal shape that best represents the numerical model identified. MSC.Software (2008; 2000) assumed that modes with frequencies up to that of the selected mode are properly integrated, and applied equation (6.4) to estimate the time step of an impact analysis.

$$\Delta t / T < 1 / 15 \qquad (6.4)$$

The impact time T and the time step Δt were determined to be 3 ms and 1.3 E-04 s respectively.

6.3.3.3 Contact bodies

A combination of input parameters is allowable in finite element analysis (Koc, et al., 2000) hence it was possible to combine deformable and rigid bodies in a simulation. The pommel and the steel plates were defined as deformable contact bodies while a "glue-all" contact condition was defined for the touching faces. The response of the impacted body was not important in this study hence it was adequate to model it as a rigid body. The rigid body position was referenced with a node extracted in its centre (as illustrated in figures 6.3.1 and 6.3.2).

The interaction between the interfaces of the position controlled rigid body and the deformable bodies should facilitate the distribution of load in a manner liable to cause deformations in the deformable body, resulting in an attempt to conform its top surface to the rigid body (Palazotto, et al., 2000). A "glue-all" contact condition was defined for the deformable pommel and the rigid body. Further, the "allow separation" option was selected so as to investigate if the pommel models would bounce after impact.

6.3.4 Element and element properties

All the models were discretized with the isomesh into hex 8 element topology. The solid wood pommel and steel plates were modelled with type 7 elements while the laminate models were modelled with type 149, an 8-node isoparametric composite brick element. Coordinate frame 1 was selected as the reference for the orientation angles.

6.4 MSC.MARC SOLUTION PARAMETERS

The multifrontal sparse solver type was selected and the linearity option was set to nonlinear. Solution type was set to transient dynamic. Nonlinear geometric options were set to allow for large displacements and strains, and the loads were treated as total loads. Load iteration parameters option was set to ***fixed*** while the earlier determined time step size and total time were input in the ***fixed increment parameters*** section. Finally, the implicit dynamic operator ***Single Step Houbolt*** which is recommended for dynamic contact problems due to its high-frequency dissipation that dampens undesired, numerically triggered, high-frequency oscillations (MSC.Software, 2000), was selected.

6.5 POST-PROCESSING

The peak deflections of the models after the first time step at t = 1.30e -04 s, and the final time step at t = 3.00e -03 s are presented in figures 6.5.1 to 6.5.12. The models are classified as solid wood and laminated wood models. MSC.Patran provides various options of post-processing the results of a simulation. The ***Quick plot*** option which offers a combination of a ***fringe*** and a ***deformation*** result was set to displacement translation. Displacement is measured in metres (m).

6.5.1 Solid wood

6.5.1.1 Pommel only

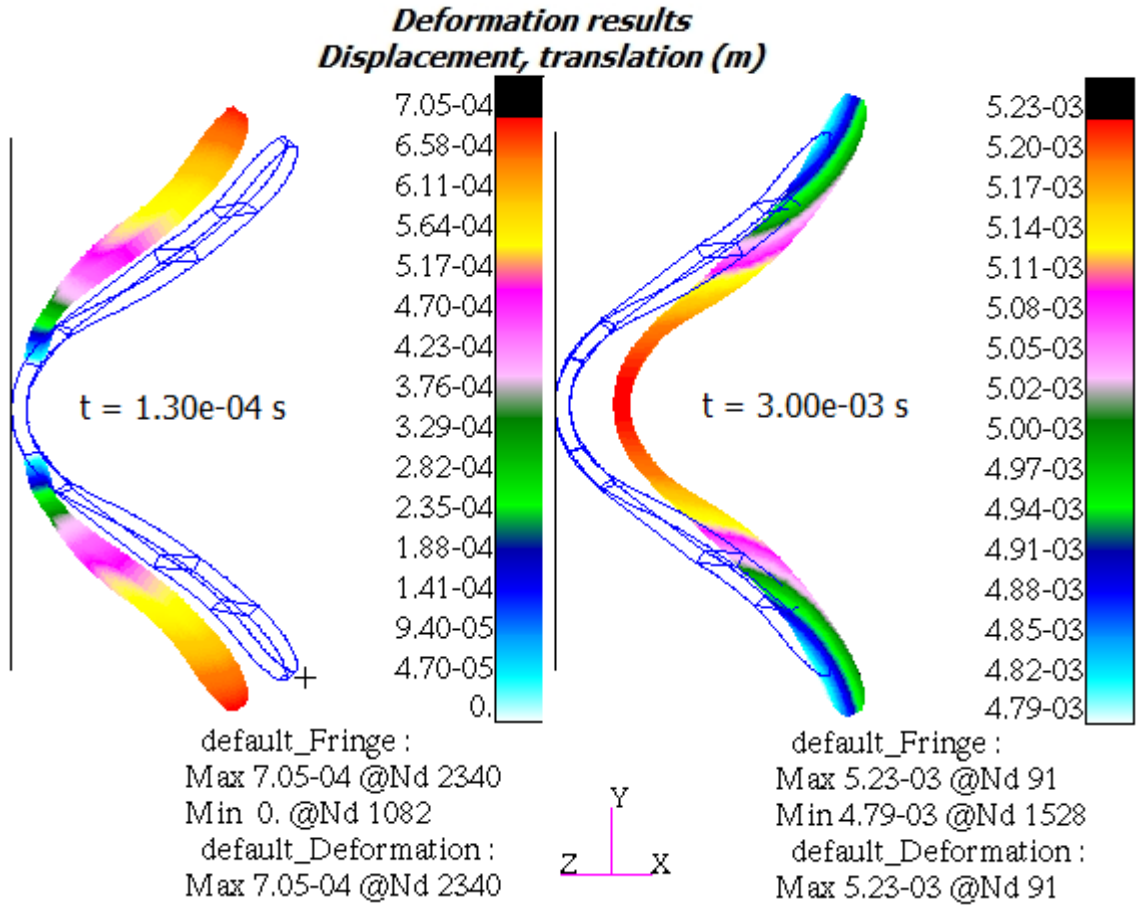

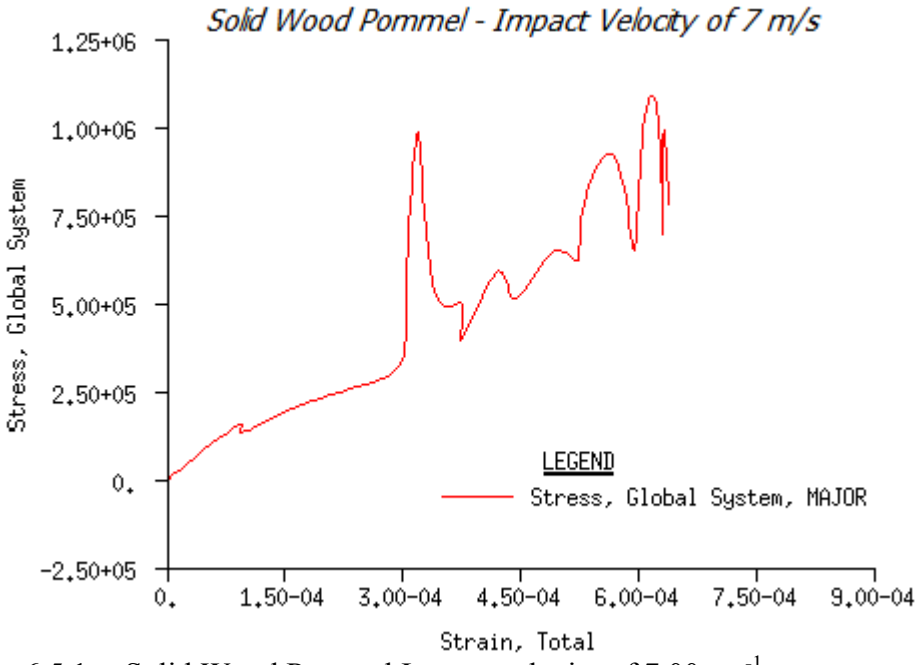

Figure 6.5.1 Solid Wood Pommel Impact velocity of 7.00 ms^{-1}

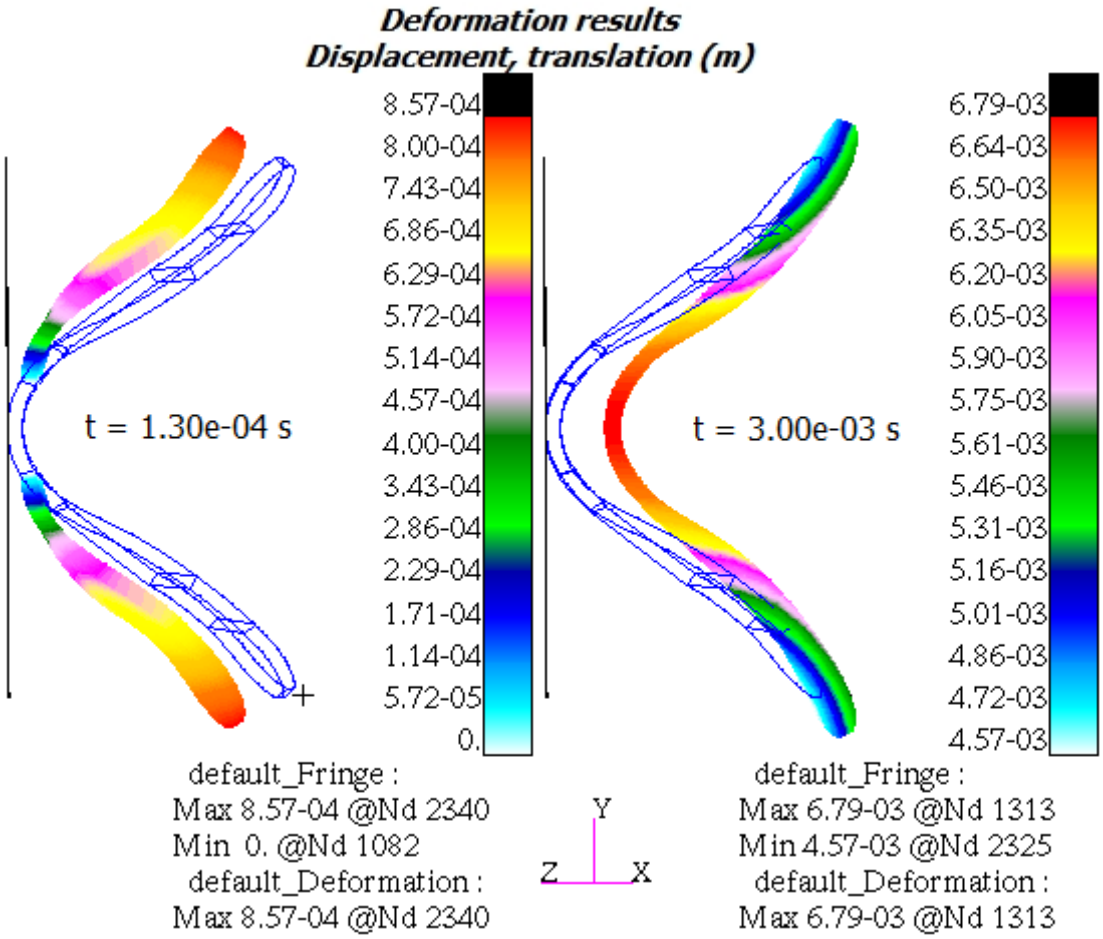

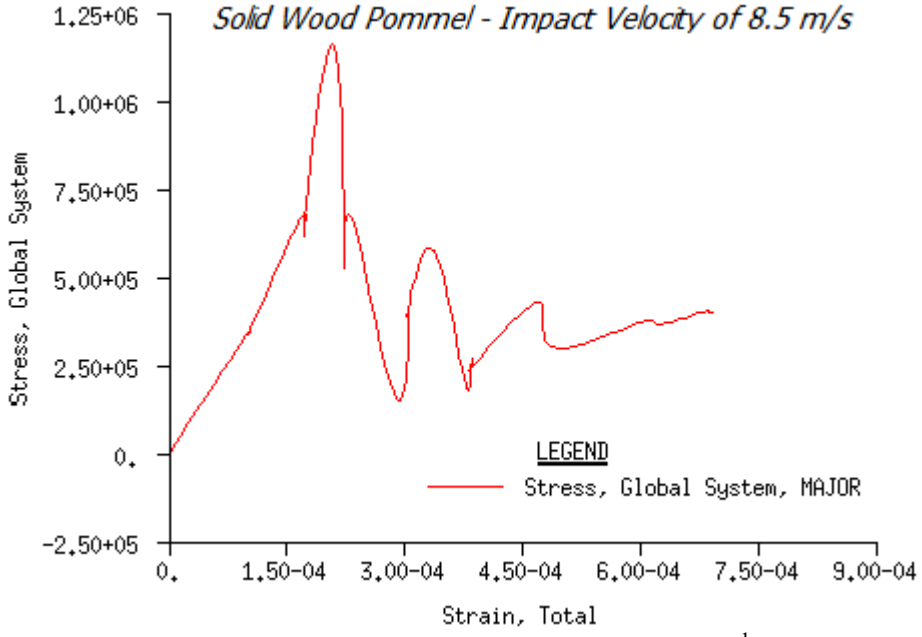

Figure 6.5.2 Solid Wood Pommel Impact velocity of 8.50 ms^{-1}

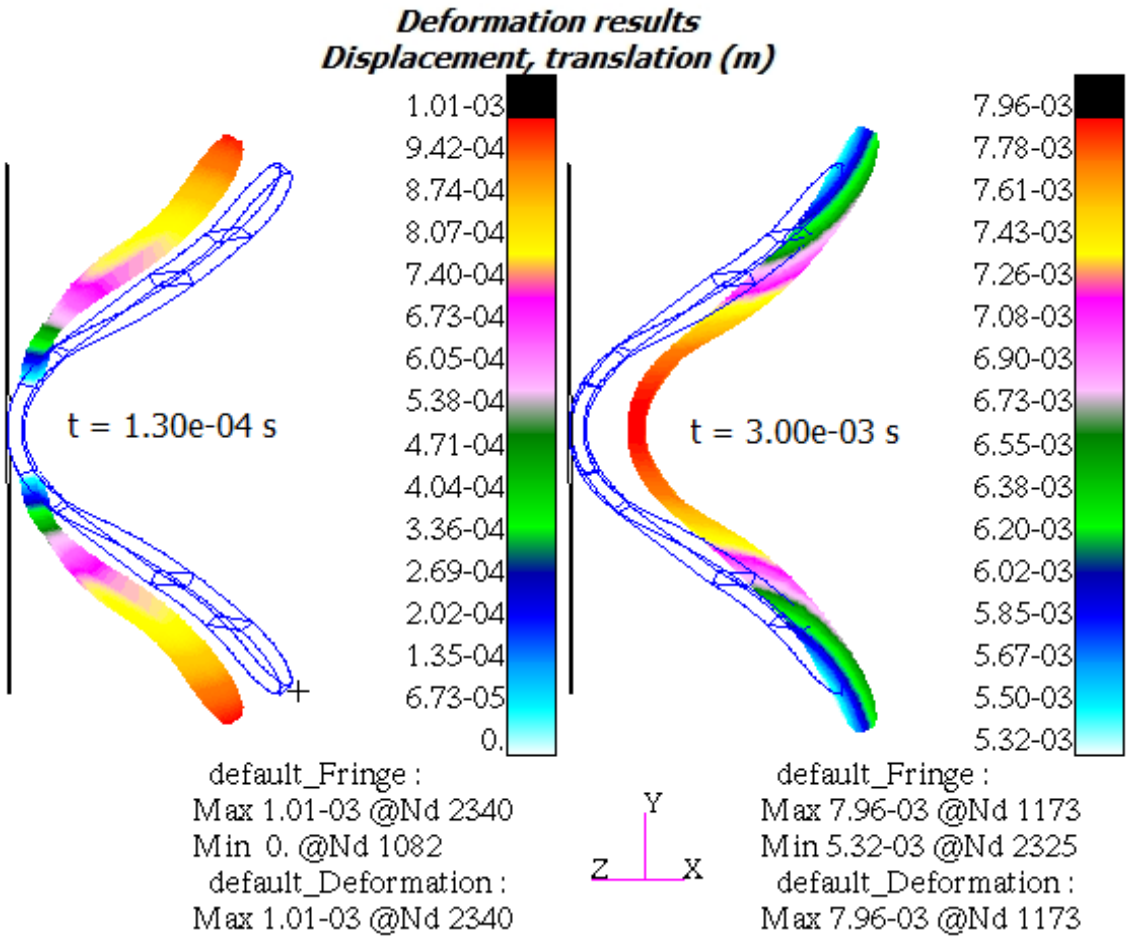

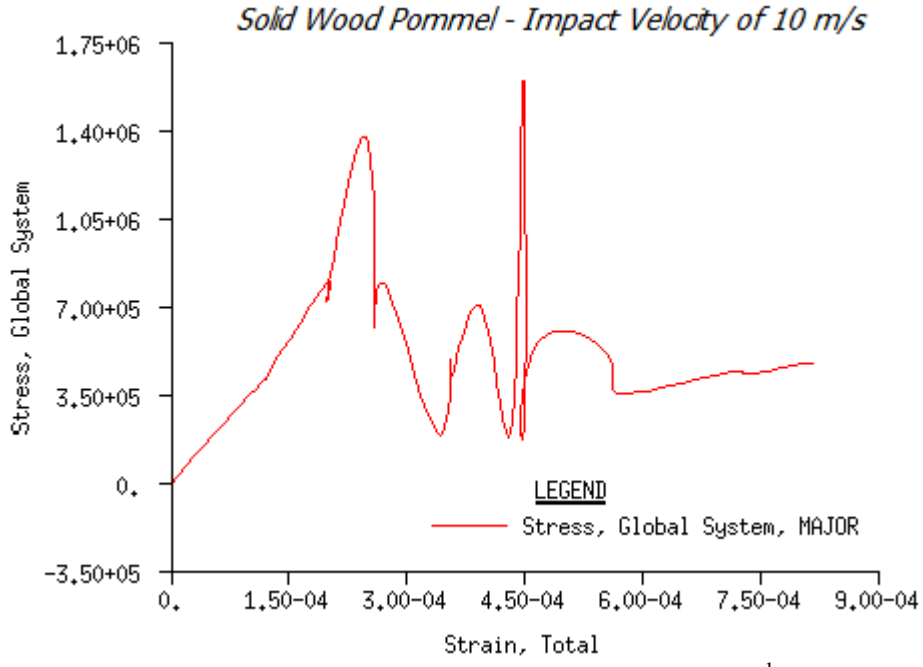

Figure 6.5.3 Solid Wood Pommel Impact velocity of 10.00 ms^{-1}

6.5.1.2 Reinforced pommel

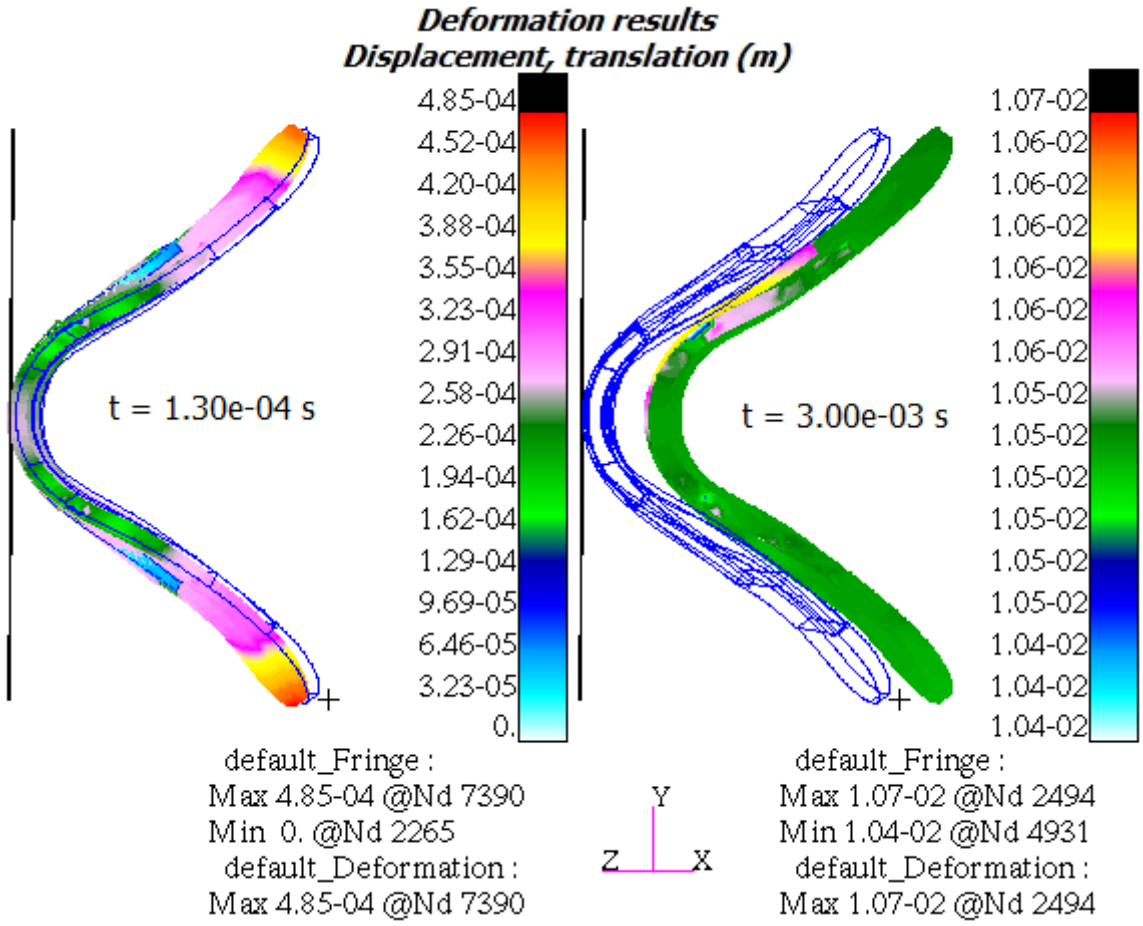

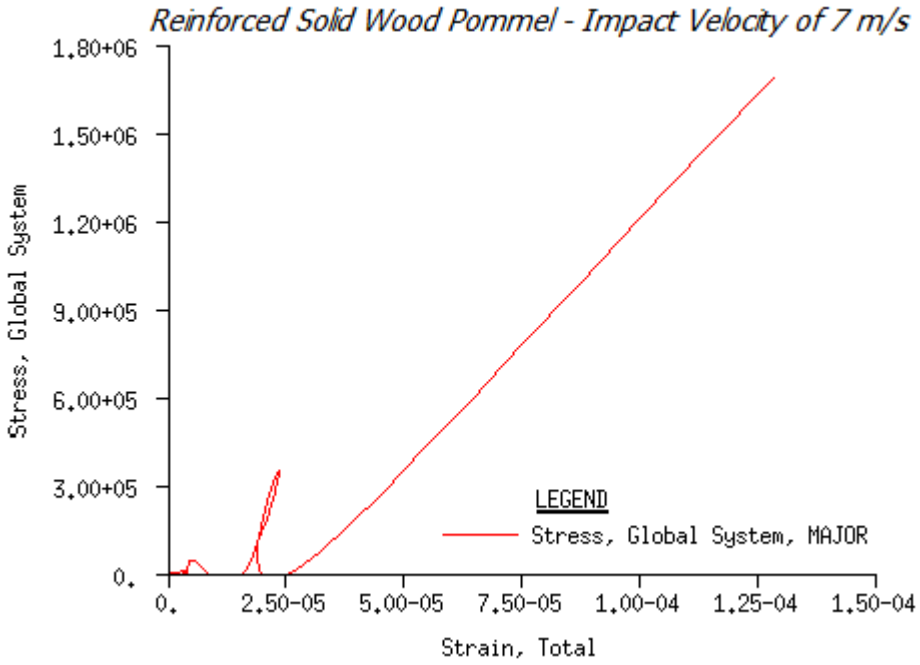

Figure 6.5.4 Reinforced Solid Wood Pommel Impact velocity of 7.00 ms^{-1}

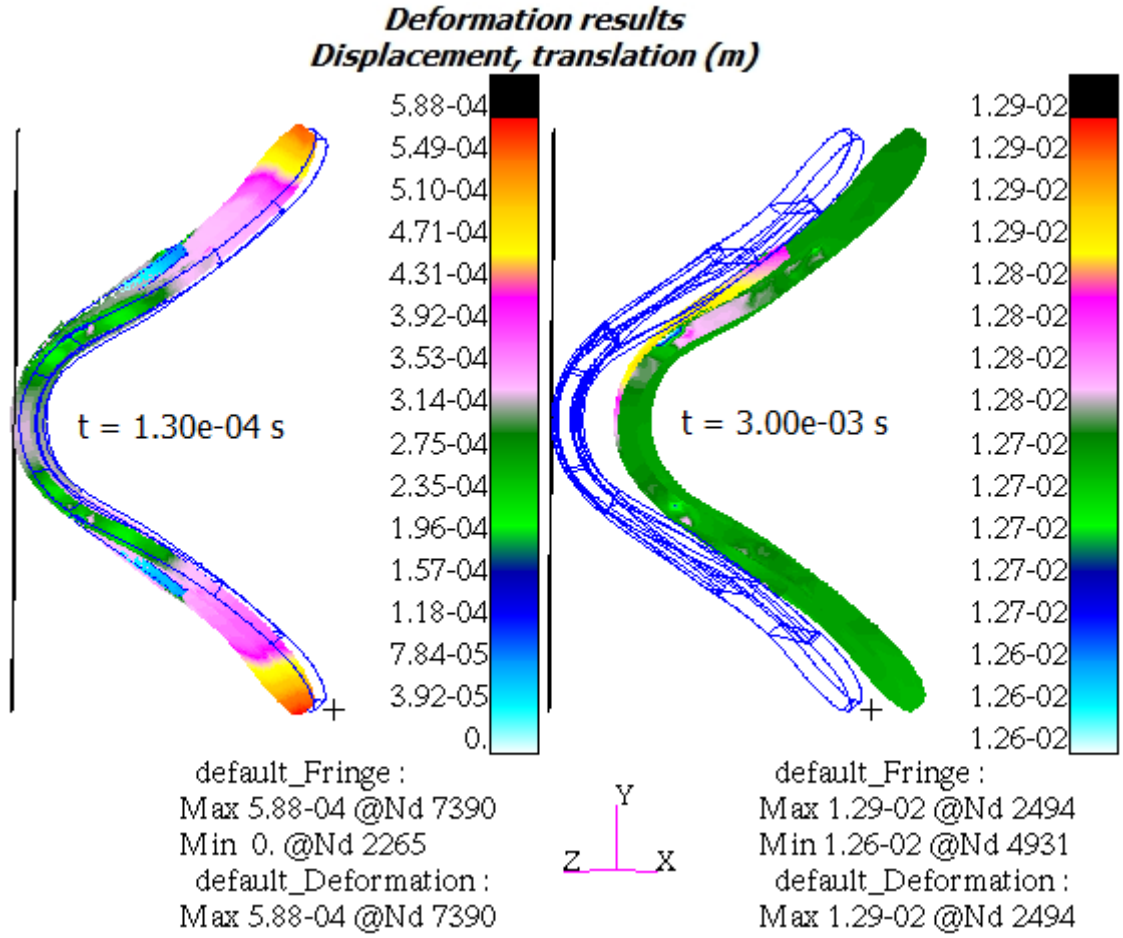

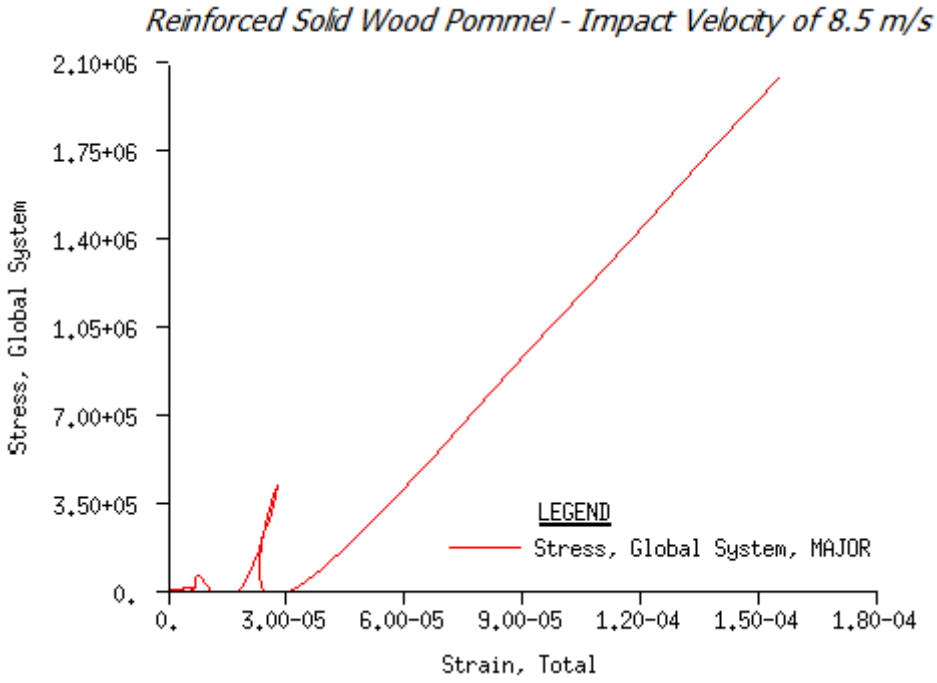

Figure 6.5.5 Reinforced Solid Wood Pommel Impact velocity of 8.50 ms^{-1}

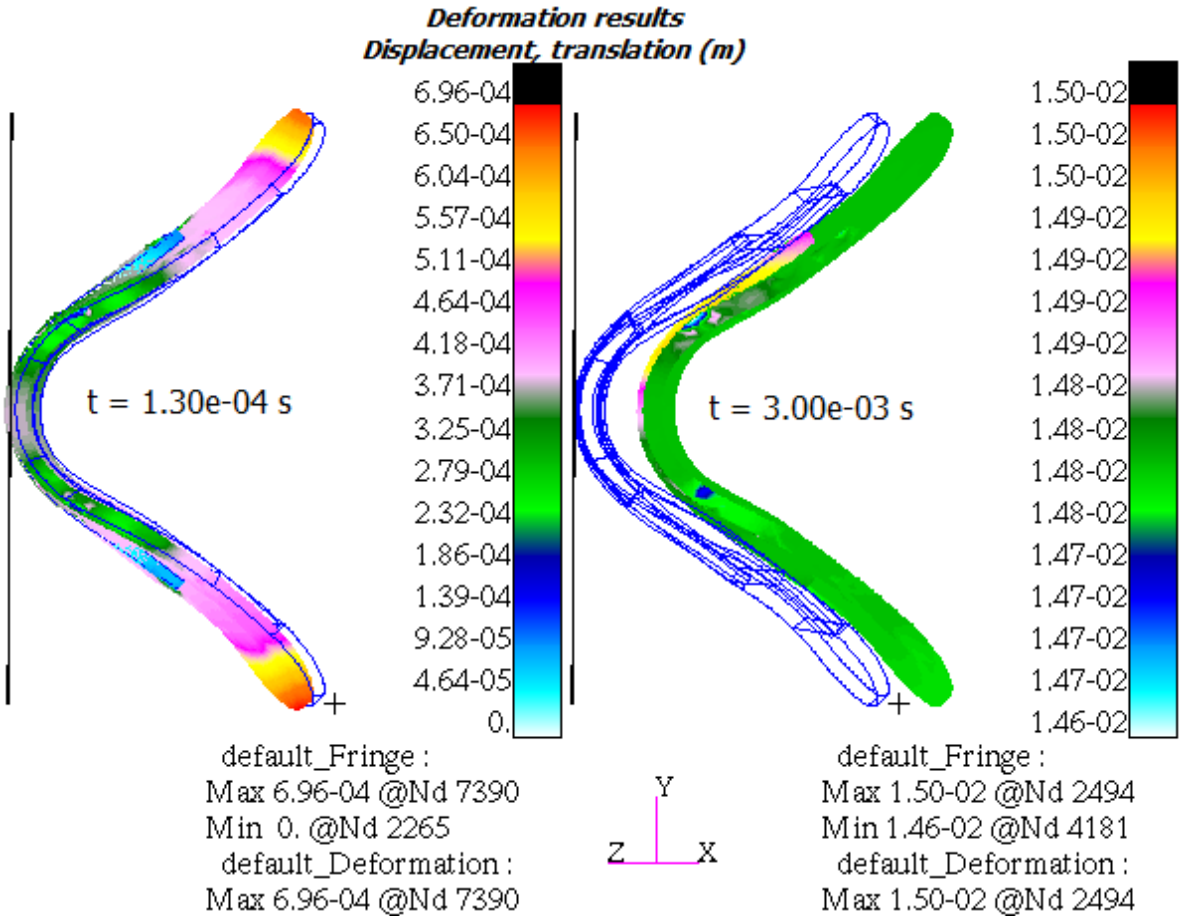

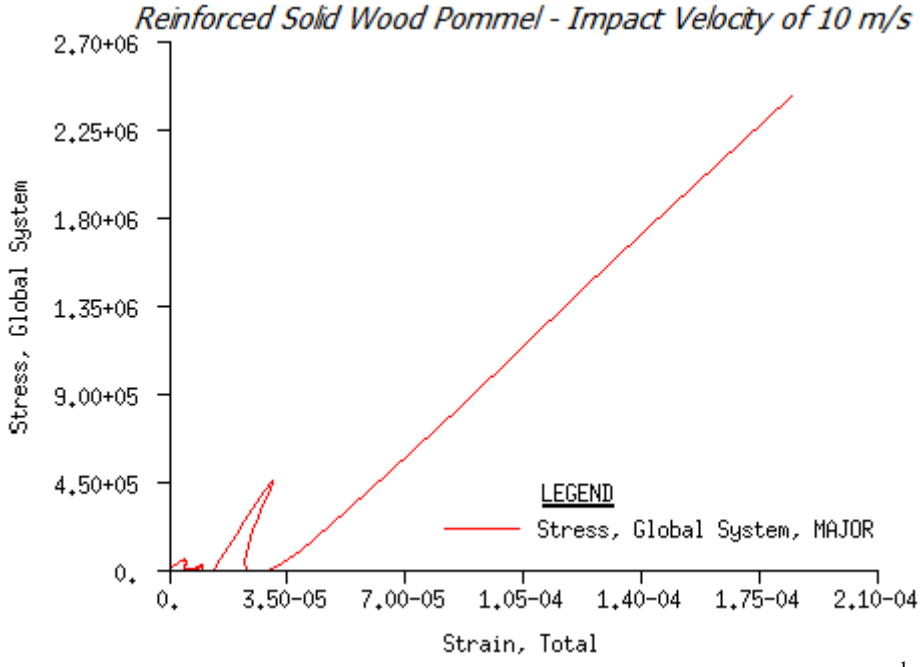

Figure 6.5.6 Reinforced Solid Wood Pommel Impact velocity of 10.00 ms^{-1}

6.5.2 Laminated wood

6.5.2.1 Pommel only

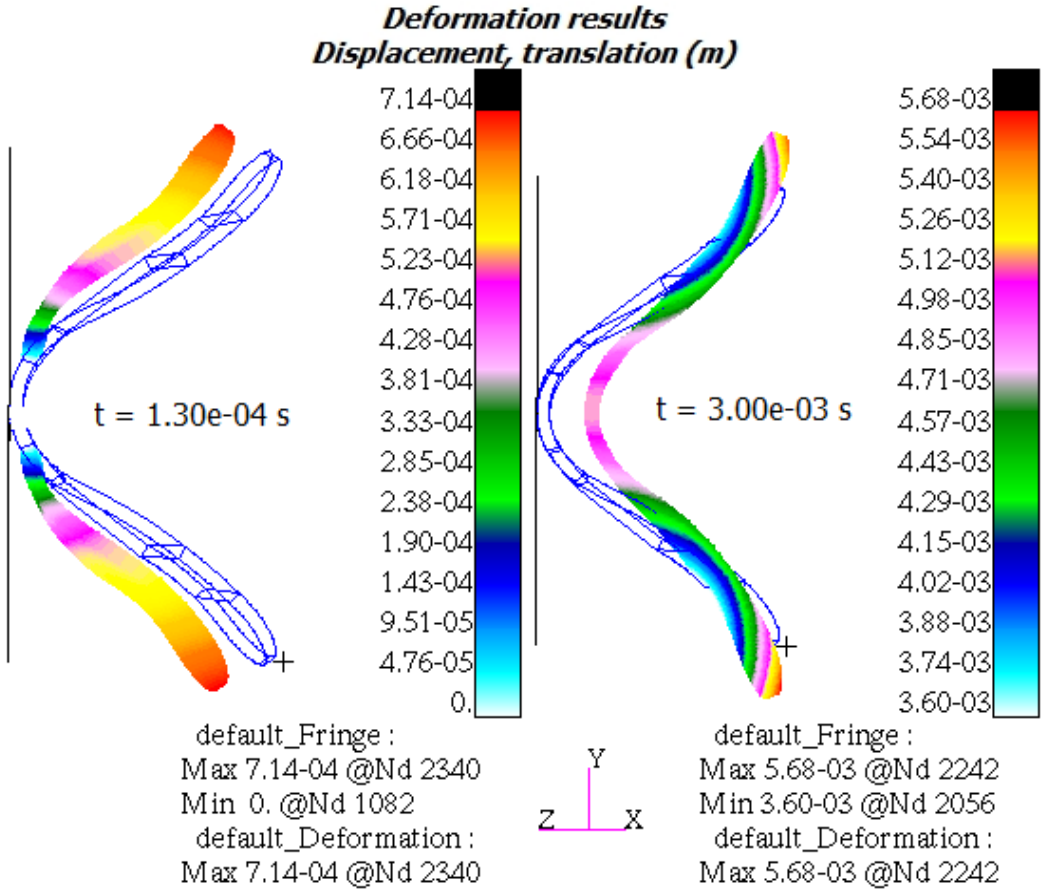

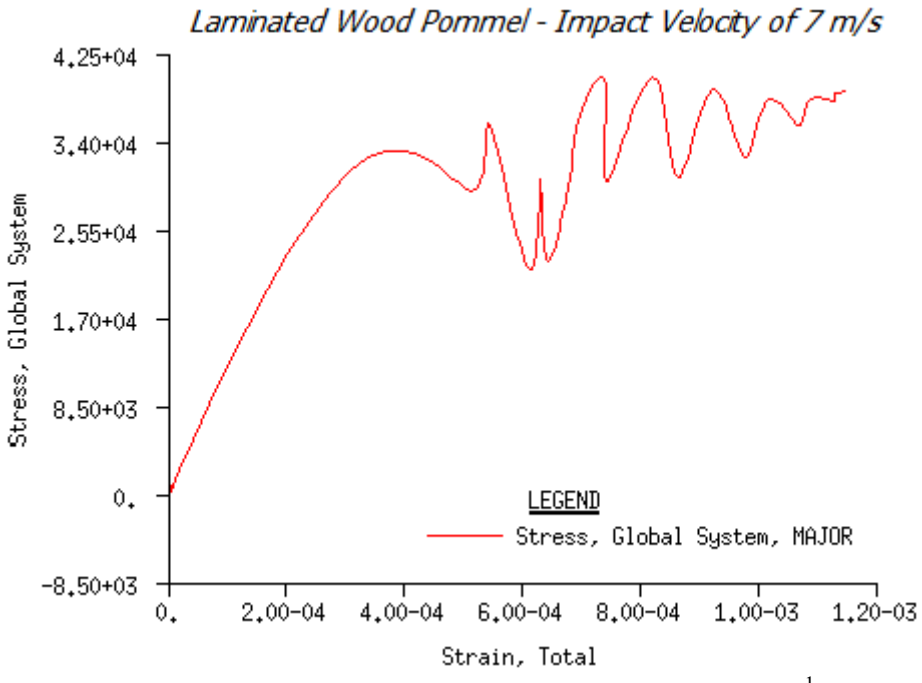

Figure 6.5.7 Laminated Wood Pommel Impact velocity of 7.00 ms^{-1}

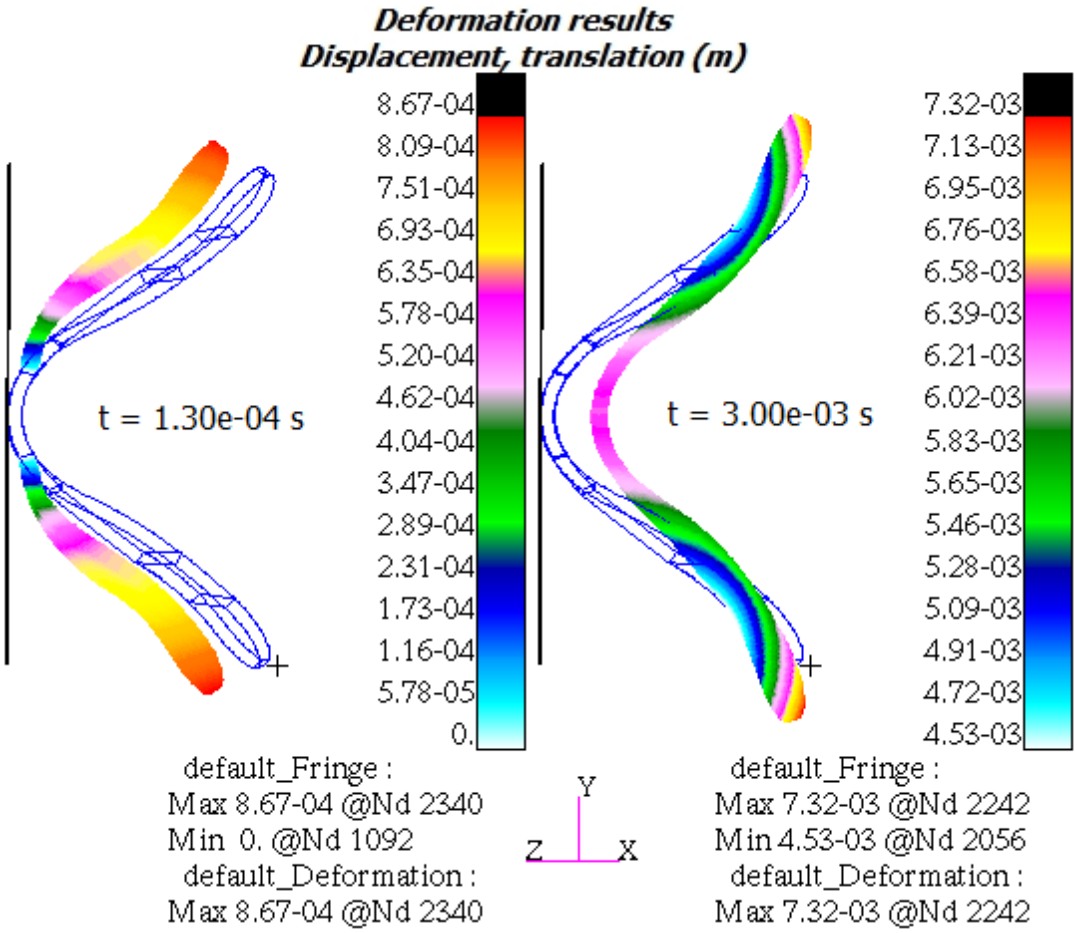

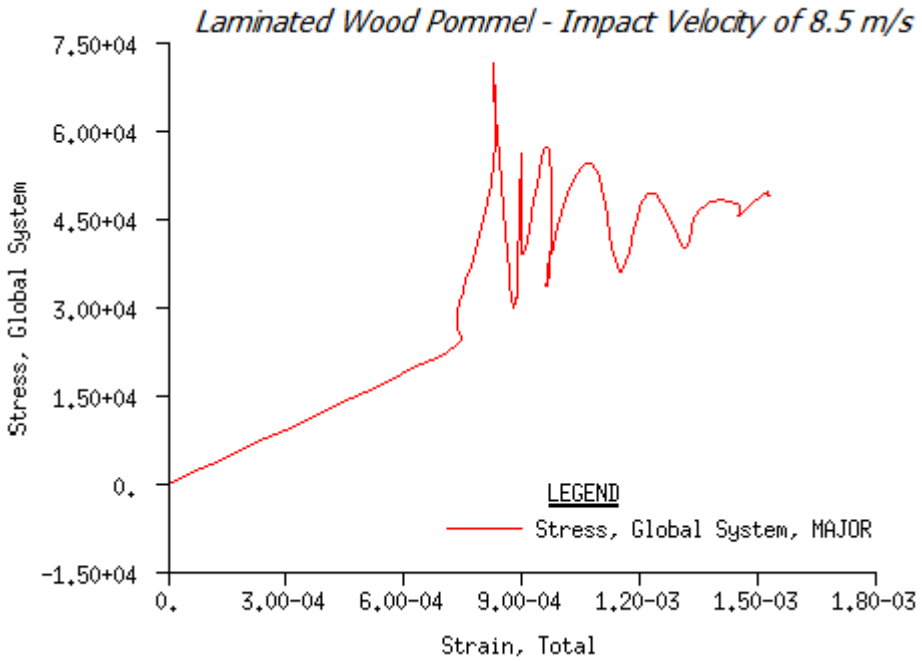

Figure 6.5.8 Laminated Wood Pommel Impact velocity of 8.50 ms^{-1}

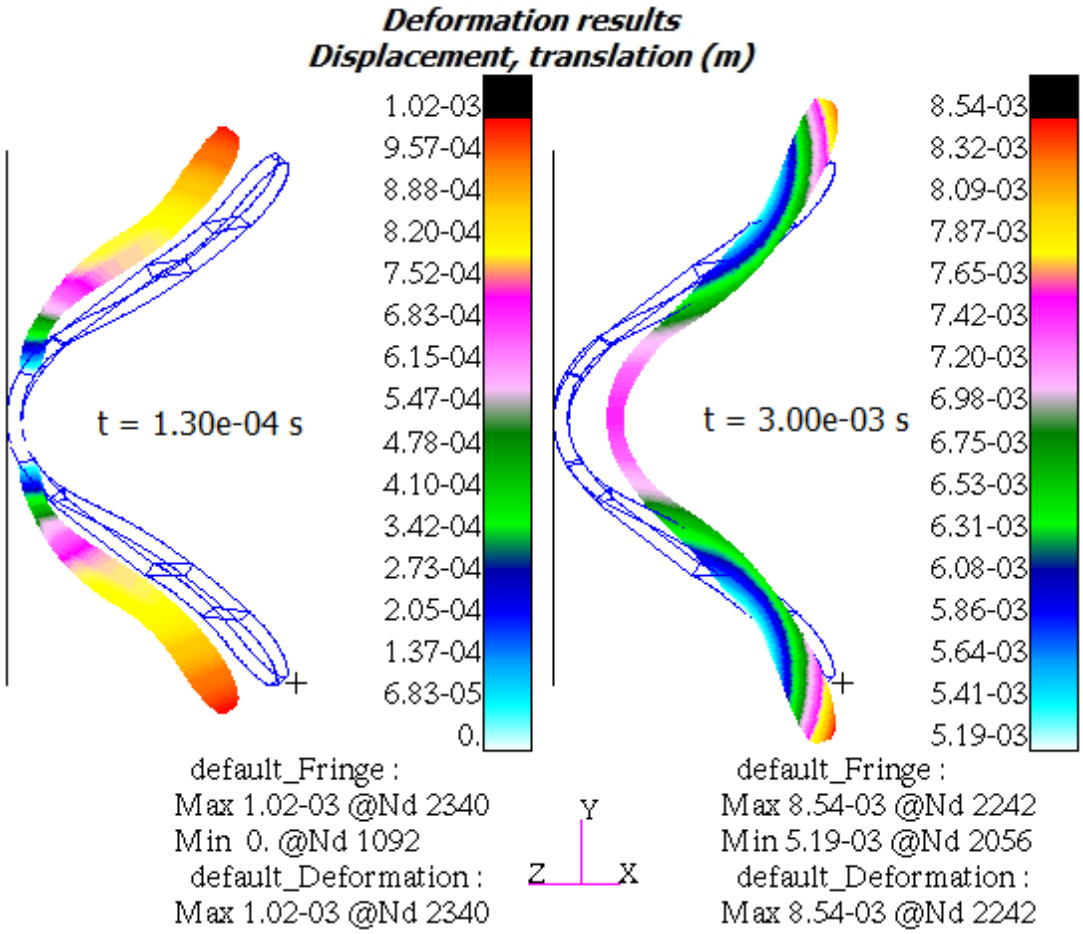

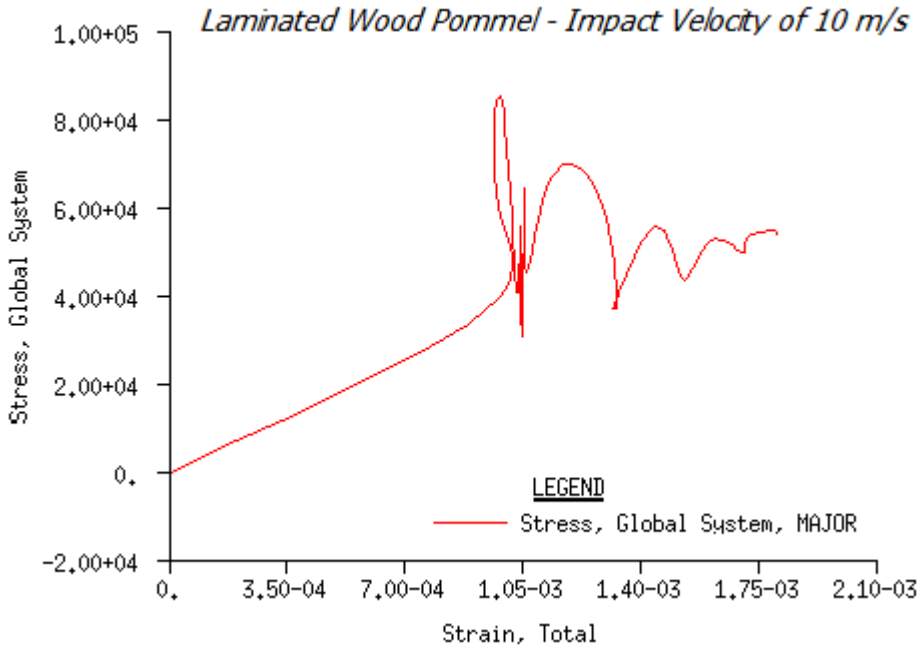

Figure 6.5.9 Laminated Wood Pommel Impact velocity of 10.00 ms^{-1}

6.5.2.2 Reinforced pommel

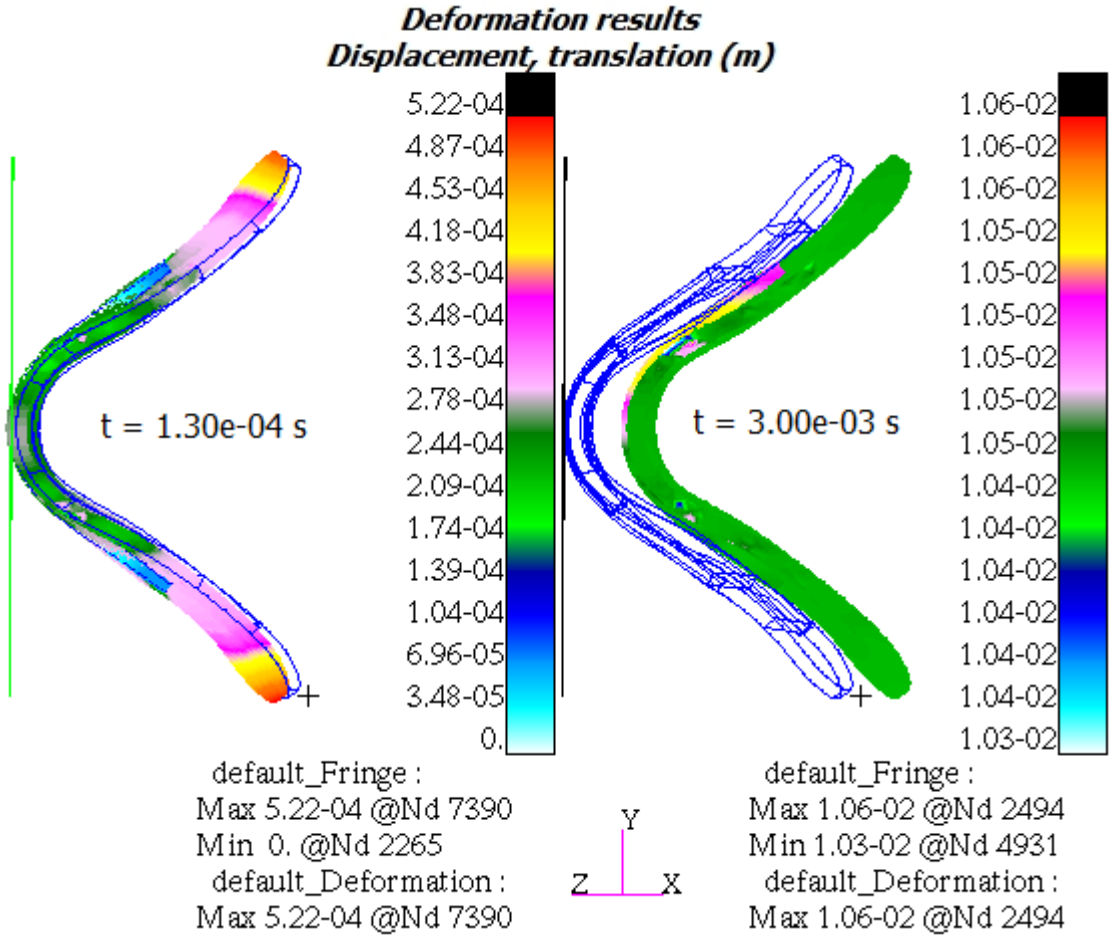

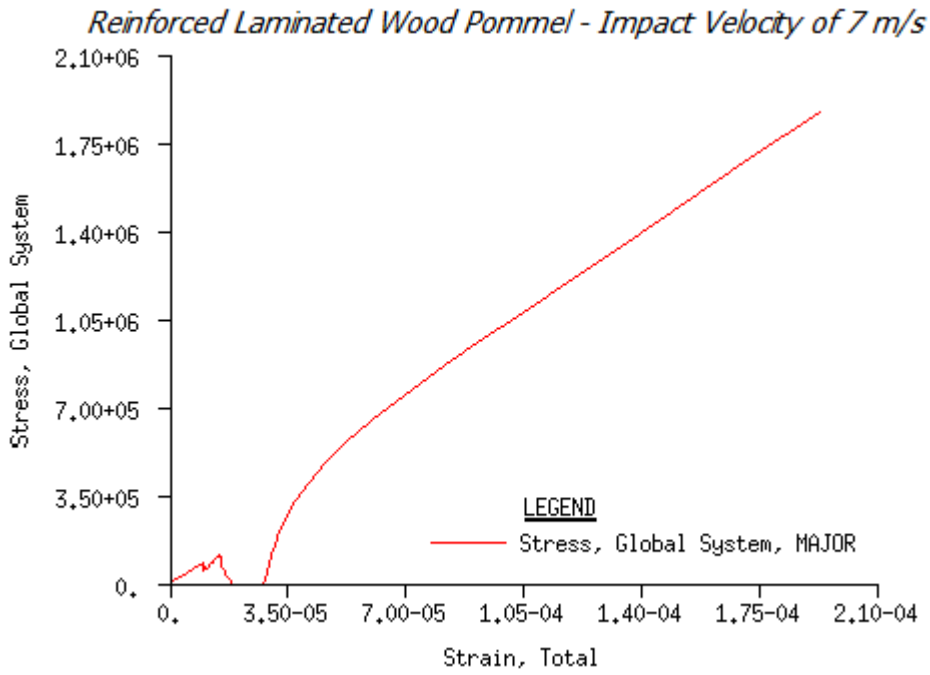

Figure 6.5.10 Reinforced Laminated Wood Pommel Impact velocity of 7.00 ms^{-1}

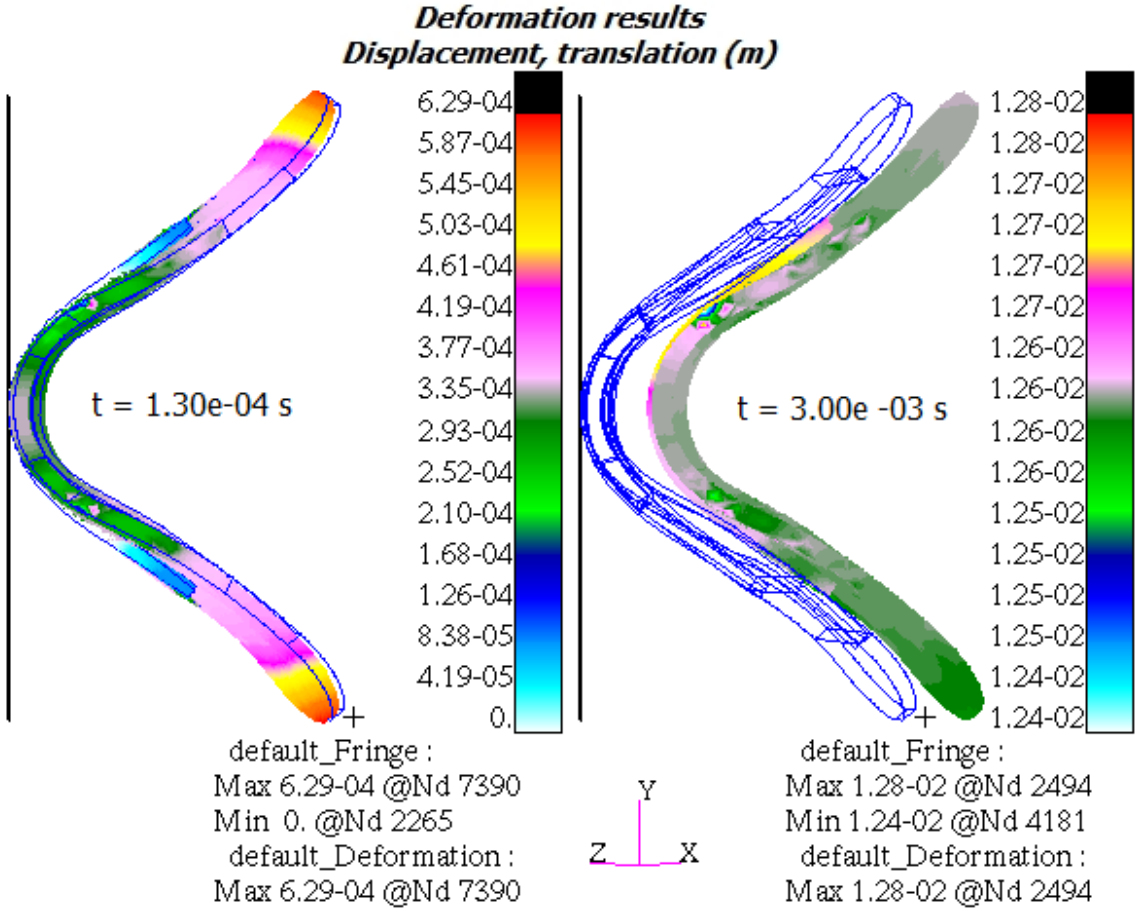

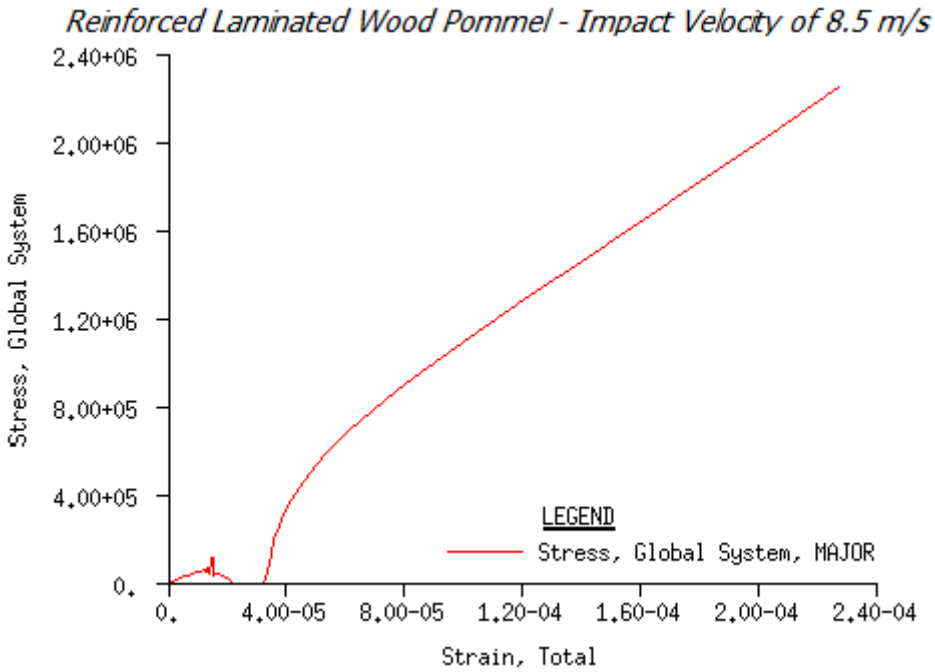

Figure 6.5.11 Reinforced Laminated Wood Pommel Impact velocity of 8.50 ms^{-1}

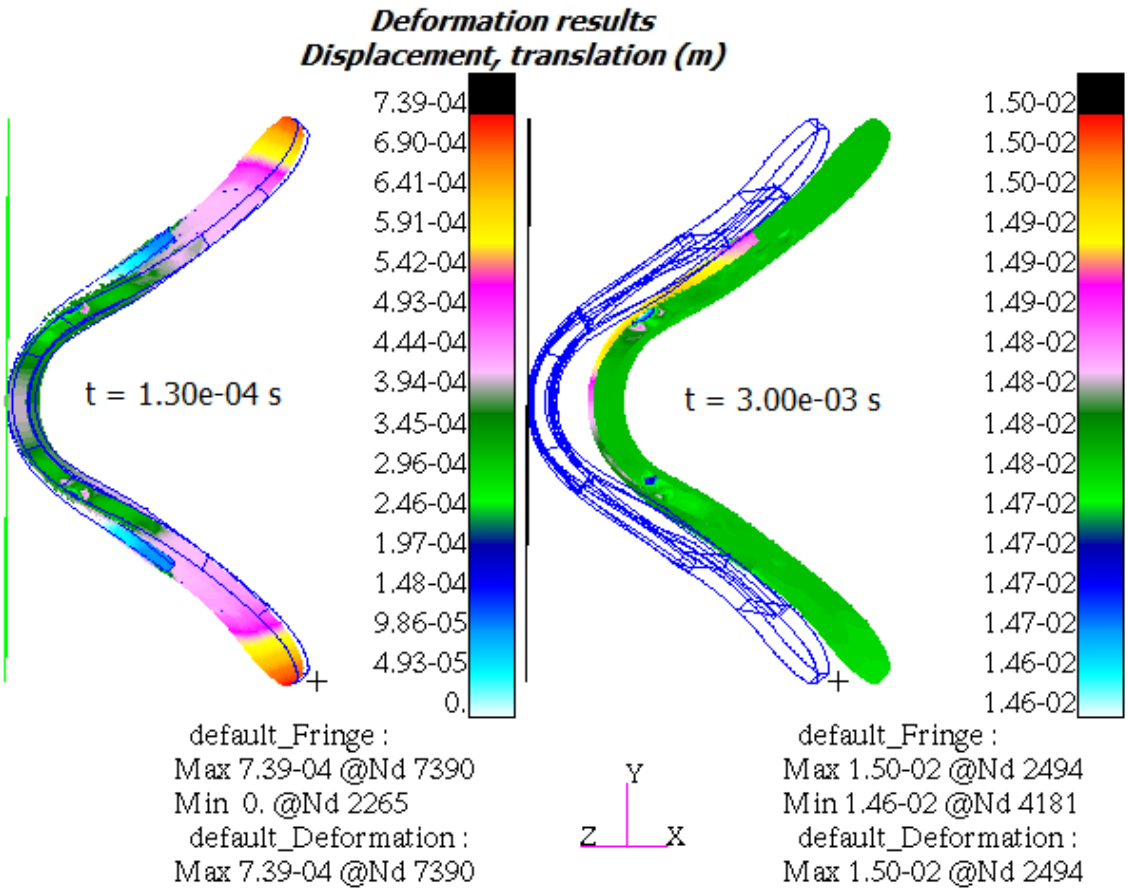

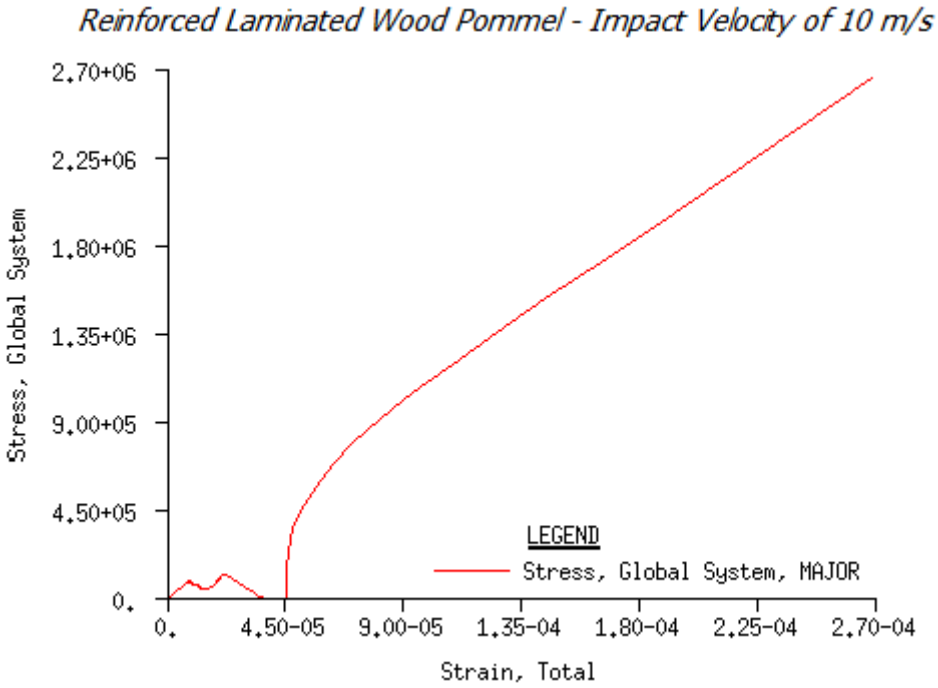

Figure 6.5.12 Reinforced Laminated Wood Pommel Impact velocity of 10.00 ms^{-1}

6.6 DISCUSSION OF RESULTS

In addition to the global deflections of the models during and after impact, a stress-strain curve is presented to illustrate the reaction of the models during impact (as illustrated in figures 6.5.1 to 6.5.12). It was observed that at all impact velocities, all the wood only models exhibited a similar deflection pattern which appeared symmetric relative to the middle of the pommel models, and increased outwards towards its tips (as illustrated in figures 6.5.1 – 3, and 6.5.7 – 9). After impact, all the models bounced off the rigid body. It was observed that in addition to a change in the deflection pattern, none of them returned back to their original shapes. While the maximum deflections in the solid models were observed to occur at the mid-section of the models, maximum deflections in the laminated models were observed to occur at their tips. Despite the variation in the patterns between the solid and laminated models, the deflections were symmetric to the middle of the pommel in all the models.

Deflections of the reinforced pommel models (as illustrated in figures 6.5.4 – 6, and 6.5.10 – 12) at impact also displayed a similar symmetric pattern between the reinforced solid wood models and the reinforced laminated wood models. Similar to the wood only models, at impact, maximum deflections were observed at the tips of the reinforced pommels. Maximum deflections of the solid wood models were a magnitude of approximately 1.45 times greater than those of the reinforced pommel while the maximum deflections of the laminated wood models were a magnitude of approximately 1.38 times greater than those of the reinforced pommel. It was observed that the variation of the impact velocities had no significant influence on the effects of the steel reinforcement plates on the maximum deflections of both the

solid wood and the laminated wood models. Similar to the wood only models, after impact, the steel reinforced pommel models also bounced off the rigid body. It was observed that while the 3 mm thick lipped gullet plate exhibited an identical deflection with the wooden pommel, maximum deflection occurred in the 2 mm thick cap plate.

Acceleration history plots of a node located at the middle of the top surface of the pommel are presented in figures 6.6.1 – 3. They present an insight to the local response of the models to the impact. In addition, they are used to evaluate the effects of the steel reinforcements on the wood only models. The local position of the node is identical in all the pommel models.

6.6.1 Impact velocity of 7 m/s

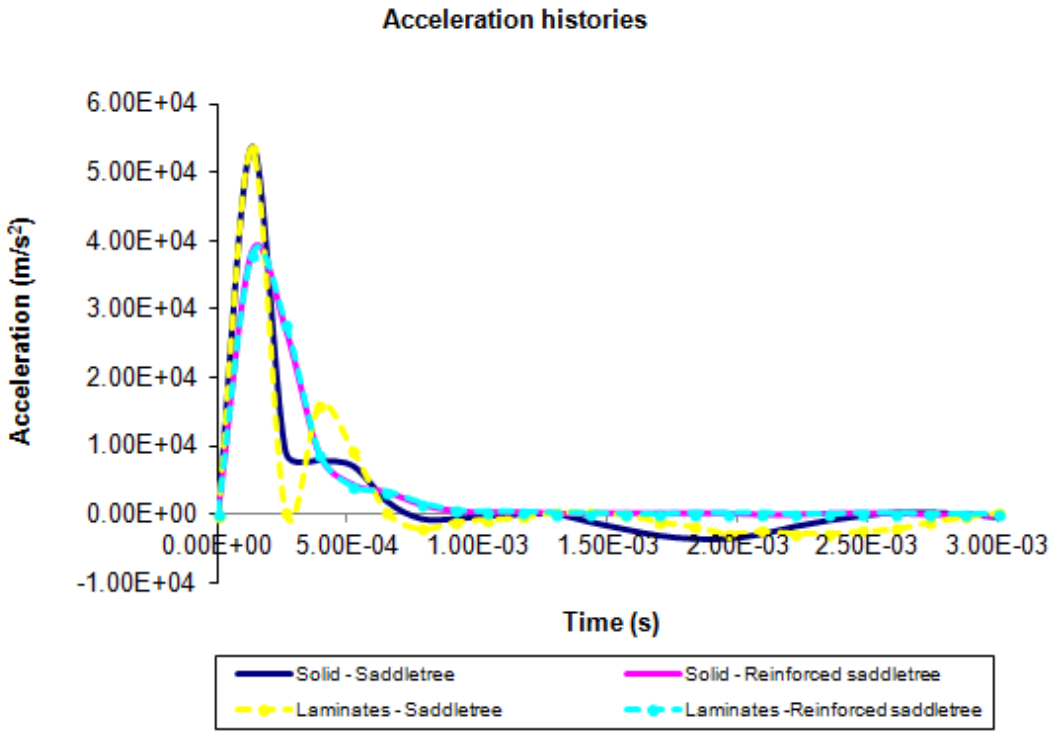

Figure 6.6.1 Acceleration histories of a selected node – 7 m/s impact velocity

6.6.2 Impact velocity of 8.5 m/s

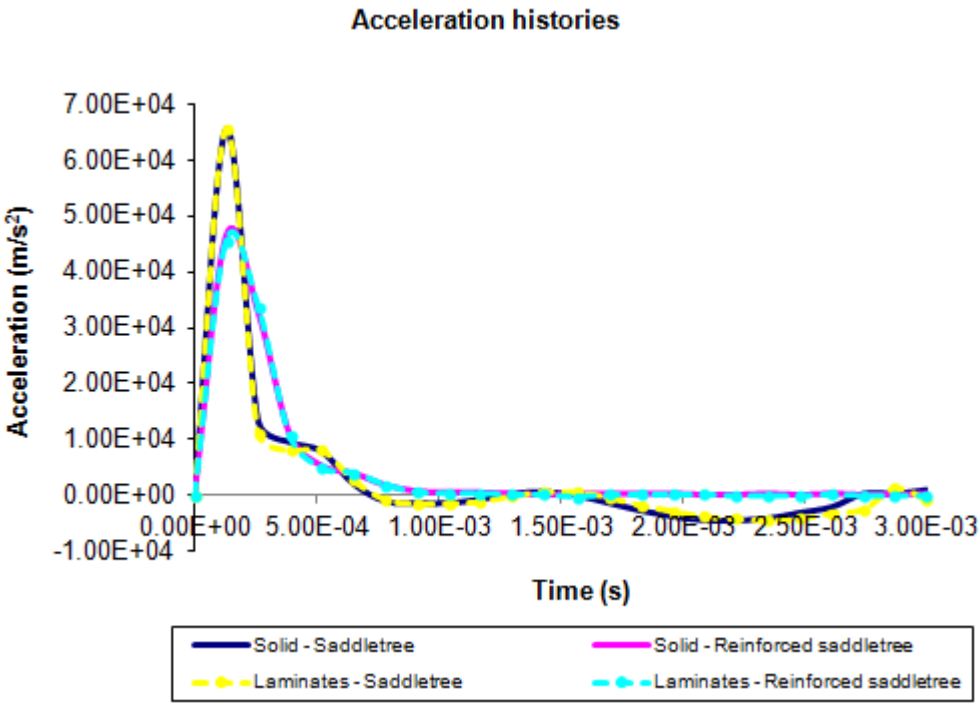

Figure 6.6.2 Acceleration histories of a selected node – 8.5 m/s impact velocity

6.6.3 Impact velocity of 10 m/s

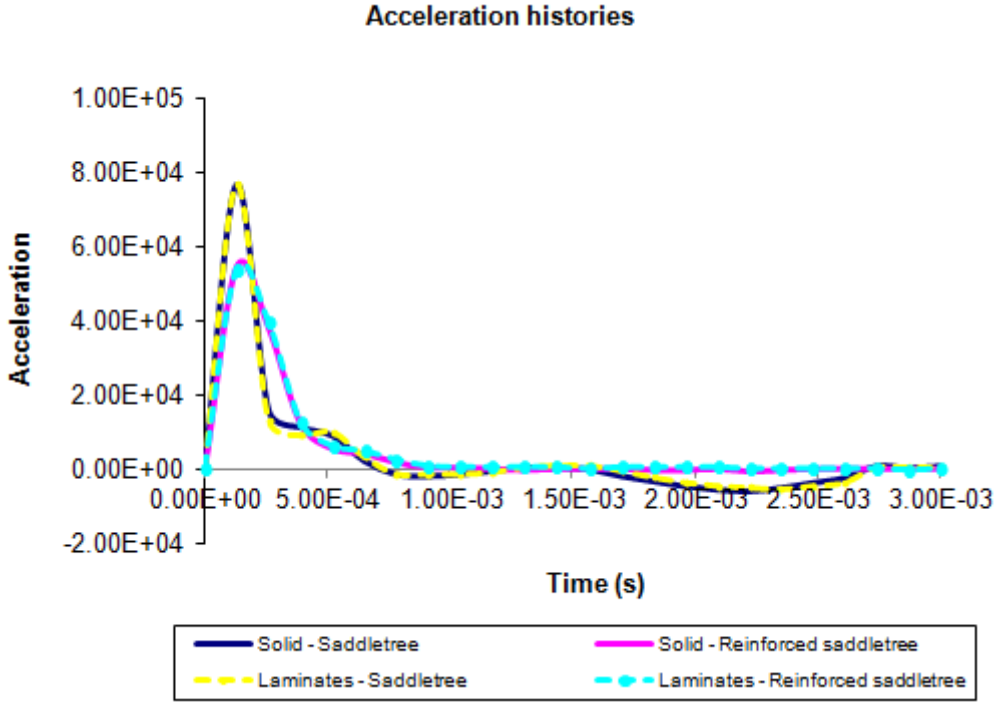

Figure 6.6.3 Acceleration histories of a selected node – 10 m/s impact velocity

Though oscillations were damped out during impact by the single-step Houbolt operator (MSC.Software, 2010), the acceleration histories of the pommel only model illustrate noticeable oscillations after impact. The amplitudes of the oscillations of the laminate model were greater than those of the solid wood model. It was further observed that these oscillations were damped by the steel reinforcement plates in the reinforced pommel models. Similar to the occurrence in the global models, it was also observed that the histories of the reinforced solid wood models were identical to the histories of the reinforced laminated models.

Peak acceleration was attained by all the models at impact. At impact velocities of 7m/s, 8.5m/s, and 10m/s, the steel reinforcement plates reduced the peak acceleration of the solid wood model by 28.62%, 28.75%, and 28.55% respectively. In addition, at impact velocities of 7m/s, 8.5 m/s, and 10 m/s, the steel reinforcement plates reduced the peak acceleration of the laminated model by 29.34%, 30.40%, and 29.88%.

6.7 SUMMARY

Transient dynamic numerical models of the pommel of an English jumping saddletree have been developed in MSC.Patran. The models have been used to evaluate the reaction of the pommel to impact. The time and time step used in the simulations were determined with the aid of a modal analysis, while the velocity range was determined in consideration of the sum of the heights of the withers of a horse at a jump and a jump fence.

Though damage and delamination were not investigated, the effects of the steel

reinforcement plates on the wooden pommel were investigated. In addition to the deformations observed in the reinforced pommels, the damping of the oscillations of the nodal histories suggests that the function of the steel reinforcement plates during impact is best described as a damper.

It was also observed that impact velocity has no appreciable influence on the effect of the reinforced plates on the wood only models. For the global model, varying the impact velocities had no significant influence on the effects of the steel reinforcement plates on the peak displacement of the wood only models. For the selected node, varying the impact velocities had no significant influence on the effects of the steel reinforcement plates on the peak accelerations and velocities of the wood only models.

CHAPTER SEVEN

PHYSICAL EXPERIMENTATION

7.1 INTRODUCTION

Clough (1980) advocated the use of a combined analytical-experimental approach particularly when exploring new grounds with a view to defining and quantifying the parameters which characterize a structural system. Experiments have been reported to be ideal in investigating the behaviour and failure of structures (Hawileh, et al., 2010). Though they are expensive and require adequate resources (Hawileh, et al., 2010; Mao, et al., 2010) such as facilities, space, and manpower (Hawileh, et al., 2010), they are significant in validating the accuracy of the predictions of numerical simulations (Ivanyi and Ivanyi, 2009), and provide unique information (Kramer, et al., 2005).

Earlier in section 3.4 of this thesis, a simplified beam finite element model was presented. The maximum displacements obtained were comparable with the maximum displacement deduced published literature and from hand calculations. Later in chapters 4, 5, and 6, the finite element method which provides a procedure to mathematically model physical phenomena (Khoei, 2002) was applied to develop numerical models and investigate the performance of the saddletree and the pommel under different load and boundary conditions.

7.2 CANTILEVER SADDLETREE

Here, the results presented from the numerical simulations in chapter 4 of this thesis

are validated using controlled physical laboratory experiments. A total of 6 English jumping saddletree specimens made from laminated wood were available for this experiment; 3 specimens (Casciati and Domaneschi, 2007) of each were tested with and without the steel plate reinforcements.

Similar to the geometries used in developing the numerical models, the cantles were removed from the physical saddletree specimens. The specimens were clamped at the pommel while the load was applied at the rear (cantle position) by a Zwick/Roell 1474 materials testing machine (as illustrated in figure 7.2.1). A point load of 196.20N was applied in 10 equal increments, and the vertical displacement travelled by the specimen after each increment was recorded.

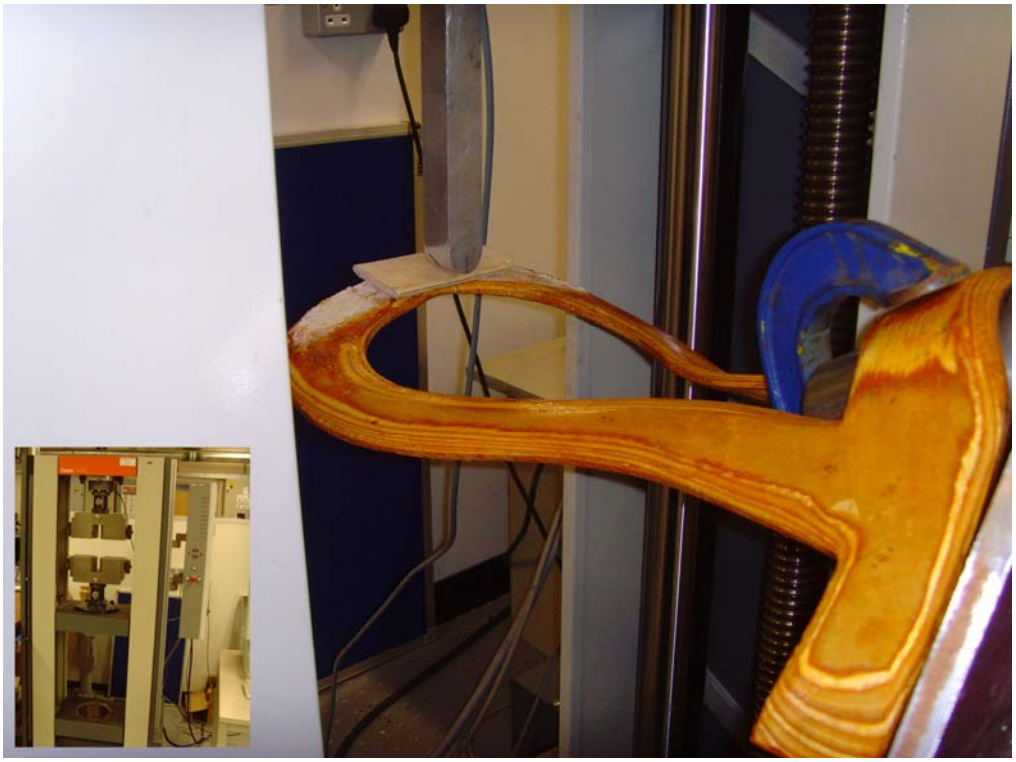

Figure 7.2.1 Cantilevered saddletree specimen

7.2.1 Results

The displacements and stiffnesses of the specimens are presented in tables 7.2.1 and 7.2.2. Similarities in the response distributions (Mehta and Patel, 1996) of each

specimen in comparison with those from numerical modelling are investigated using statistical techniques. The IBM Statistical Package for the Social Sciences (SPSS) Statistics 18 and the GraphPad Prism 5 were both applied in analysing the data.

Table 7.2.1 Displacement and stiffness of the saddletree specimens and the numerical model – saddletree only

	Saddletree_ Specimen_1	Saddletree_ Specimen_2	Saddletree_ Specimen_3	Saddletree_ FEA
Max displacement (mm)	52.8	41.83	40.1	40.3
Stiffness (N/mm)	3.79	4.63	4.85	4.68

Table 7.2.2 Displacement and stiffness of the reinforced saddletree specimens and the numerical model – saddletree with reinforcements

	Reinforced_ Saddletree_ Specimen_1	Reinforced_ Saddletree_ Specimen_2	Reinforced_ Saddletree_ Specimen_3	Reinforced_ Saddletree_ FEA
Max displacement (mm)	28.18	15.83	25.54	22.9
Stiffness (N/mm)	7.38	12.31	7.93	8.26

7.2.2 Discussion of results

A correlation analysis (presented in tables 7.2.3 and 7.2.4) at 0.01 confidence level was applied to evaluate the relationship (Viceconti, 2006) between the experimental data and the data obtained from the numerical models. Though there are a few numerical techniques for pairwise comparison of data (Andersson, et al., 2007), the Pearson correlation is widely used in measuring the strength of the linear relationship between two variables (Lena and Margara, 2010; Son and Baek, 2008). A correlation close to 1 indicates a similarity between two variables while a correlation close to 0 indicates a distinction between the two variables (Lena and Margara, 2010; Son and Baek, 2008).

Table 7.2.3 Correlation between the saddletree specimens and the numerical model

		Saddletree_ Specimen_1	Saddletree_ Specimen_2	Saddletree_ Specimen_3
Saddletree _FEA	Pearson Correlation	0.998	1.000	0.999
	Sig. (2-Valued)	0.000	0.000	0.000
	Sum of squares and cross-products	1727.066	1335.749	1283.058
	Covariance	191.896	148.417	142.562
	N	10	10	10

Table 7.2.4 Correlation between the reinforced saddletree specimens and the numerical model

		Reinforced_ Saddletree_ Specimen_1	Reinforced_ Saddletree_ Specimen_2	Reinforced_ Saddletree_ Specimen_3
Reinforced _Saddletree _FEA	Pearson Correlation	0.991	0.999	0.995
	Sig. (2-Valued)	0.000	0.000	0.000
	Sum of squares and cross-products	475.674	283.193	437.619
	Covariance	52.853	31.466	48.624
	N	10	10	10

7.3 PRESSURE MAPPING

In Chapter 5 of this thesis, a Tekscan ConforMat^{TM} was applied to evaluate and define the contact areas between a rider and a bare horseback, and between a loaded saddletree and a horsestand. The contact mappings were developed into rigid body finite element models and assumed to represent the load bearing surface and the supports for the saddletree models. The deflections of the numerical models were later presented. Due to the inability of the pressure mat to measure deflections between contacting surfaces, it was imperative to consider another measurement property common to both the pressure mat and the numerical models which would be suitable to compare the numerical modelling technique. As discussed earlier in section 2.5.2, data obtained with a pressure measurement system may be displayed in

various formats. In addition, there are no standard methods for measuring or displaying interface pressure measurements (Shelton and Lott, 2003).

7.3.1 Results

A peak contact pressure of 82.7 KPa and an average contact pressure of 15.4 KPa were measured by the pressure mat positioned between the loaded saddletree and the saddle stand (see figures 7.3.1 and 7.3.2).

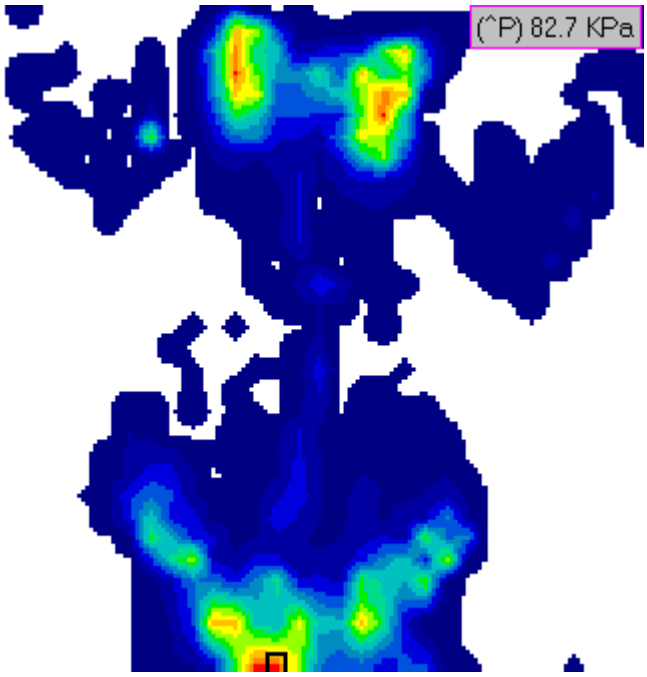

Figure 7.3.1 Peak contact pressure measured by the ConforMat

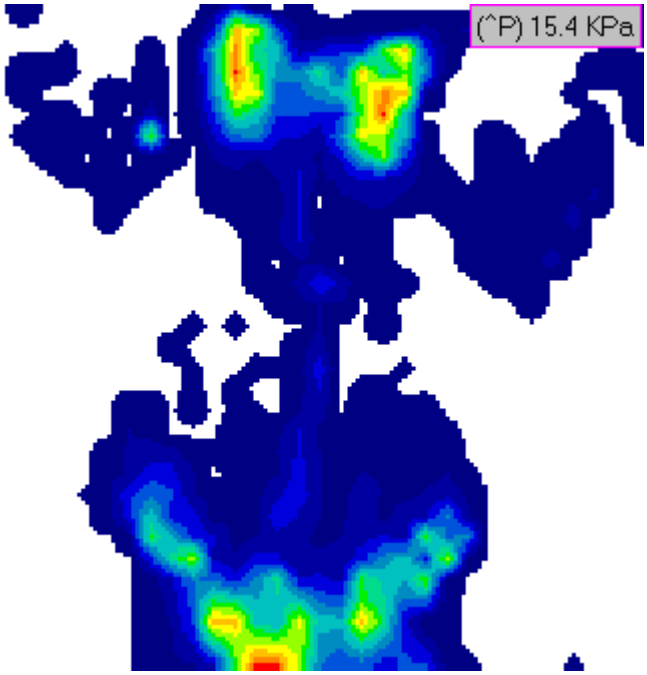

Figure 7.3.2 Average contact pressure measured by the ConforMat

The contact stress between the deformable contacting numerical models and the rigid contacted numerical model is presented in figure 7.3.3. The viewport legend presents a peak value of 96.1 KPa while an average contact stress of 16.94 KPa was deduced.

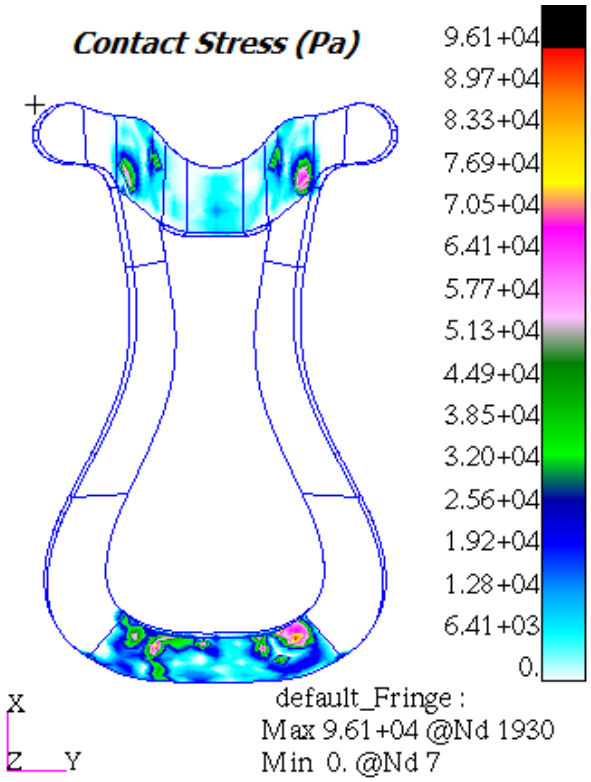

Figure 7.3.3 Contact stress between the deformable and rigid numerical models

7.3.2 Discussion of pressure mat results

It is important to note that the pressure mat can only measure interface parameters hence it was only applied to measure surface parameters. Relative to the measurements of the pressure mat, percentage errors in the solutions of the numerical model were estimated to be 16.2 % and 10.0 % for the peak and the average contact stresses respectively. Considering earlier validation of both tools, the author was confident that the variation in the construction of the saddletrees, and complex contact loading conditions between the saddletree and horsestand were the sources of error. Though the physical model was identical to the geometry of the finite element model, there was a slight variance in the angle of the pommel.

7.4 UNIVERSAL COMPRESSION-FLEXURE TESTS

Dynamic transient simulations of the pommel section of the saddletree were presented in chapter 6 of this thesis. In the absence of an experimental rig adequate for performing a similar impact experiment, the use of standard impact benchmarks and, comparison and validation with benchmarks in the MSC.Software increased confidence in the solutions.

To complement the findings of the numerical models, and to further augment the knowledge on the failure modes of the pommel, the Zwick/Roell 1474 materials testing machine was applied to test the pommel to failure. The specimens were supported in a position (as illustrated in figures 7.4.1 and 7.4.2) identical to the positioning of the numerical models. While the top of the pommel was constrained from axial translations, the tips were allowed to flex. A “Universal compression-flexure test” program available in the Zwick/Roell 1474 materials testing machine

was selected for the experiments. The test speed of the machine was set to 100 mm/min (1.67 e-03 m /s), while the load was applied via the grips and measured by integrated load cells.

Figure 7.4.1 Pommel only

Figure 7.4.2 Reinforced pommel

7.4.1 Results

7 specimens of the pommel and 5 specimens of the reinforced pommel were tested. The results are presented in tables 7.5 and 7.6. The elastic and plastic behaviour of

the specimens can be deduced from the force - displacement relationships (as illustrated in figures 7.4.3 and 7.4.4) recorded during the tests (Khanal et al., 2008).

Table 7.4.5 Pommel results of flexure tests

	Pommel Specimens						
	1	2	3	4	5	6	7
F at Yield (N)	218.86	184.28	127.79	239.91	231.31	189.00	382.34
Fmax (N)	346.23	206.67	127.79	244.35	231.31	213.28	382.34

Table 7.4.6 Reinforced pommel results of flexure tests

	Reinforced Pommel Specimens				
	1	2	3	4	5
F at Yield (N)	1250	2010	880	970	1290
Fmax (N)	5871.00	9138.61	6053.65	5800.76	7413.30

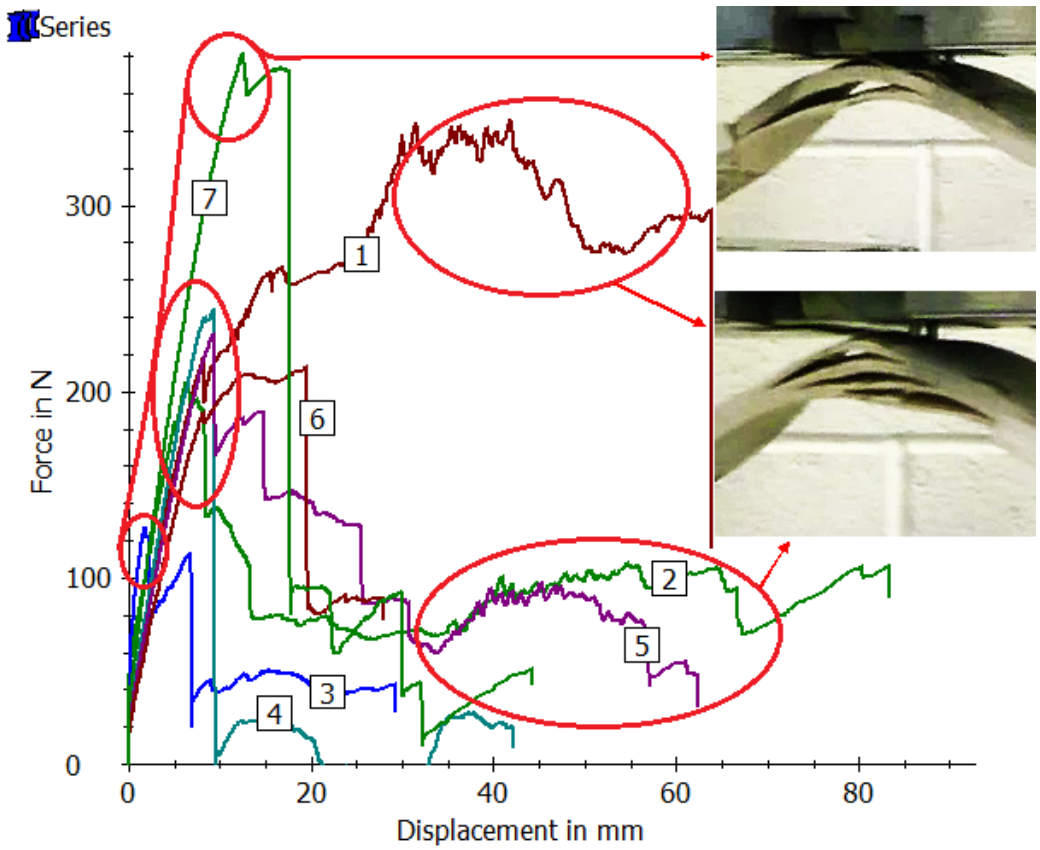

Figure 7.4.3 Load – displacement curve of pommel specimens

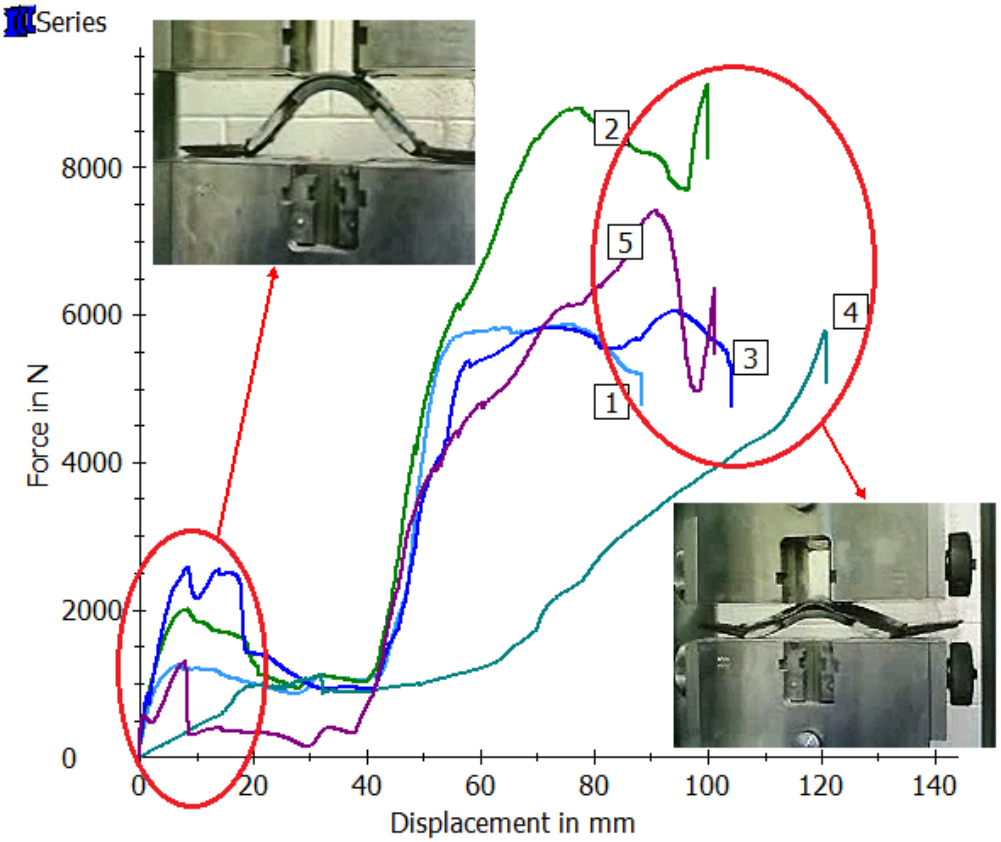

Figure 7.4.4 Load – displacement curve of the reinforced pommel specimens

7.4.2 Discussion of pommel results

7.4.2.1 Plain pommel (no-reinforcements)

Similar to the response of the numerical models presented in chapter 6, the pommel specimens were observed to flex at the tips. The load – deflection curves in addition to the inserted images (see figure 7.4.3) illustrate the failure mechanisms in the specimens. Delamination was observed to be the primary mode of failure in the laminated wood only specimens. A delamination is subject to crack driving forces resulting from a combination of mode I (opening or peeling), mode II (sliding or shear) or mode III (anti-plane shear) (Prasad and Kumar, 2008). It is one of the characteristic failure modes known to occur in laminates (Raju, et al., 2010; De Moura, et al., 2009; Cottone, et al., 2007; Kouchakzadeh and Sekine, 2000) between plies of varying angles or orientations (Olsson, 2003; Kouchakzadeh and Sekine,

2000). The top inset image in figure 7.4.3 illustrates the initiation of the delamination at the interlaminate boundary between the first and second laminates. They may have occurred under bending loads as a result of mismatched bending response between the differently oriented plies (De Moura, et al., 2009).

Multiple delaminations are not uncommon in laminated structures (Rodman, et al., 2008). The spread of the initial delamination may influence the mechanical properties of a laminate (Yoshihara, 2005; Kim et al., 1997; Jain and Mai, 1995). For specimens 3, 5, and 7, the load – displacement curves depict a weakening of the specimens by the initial delamination. The curves further illustrate that successive delaminations occurred at forces less than that which resulted in the initial failure mode. For specimens 1, 2, 4, and 6, successive delamination occurred at forces higher than that which caused the initial failure mode. For some of the specimens, delamination was followed by in-plane failure.

7.4.2.2 Reinforced pommel

Similar to the pommel only specimens, the reinforced pommel specimens were observed to flex at their tips. In addition to the load – deflection curves, the inserted images (see figure 7.4.4) illustrate the failure mechanisms in the specimens. In these specimens, delamination was not observed between the laminates. The results suggest that the steel reinforcement plates provided an effective method of enhancing resistance to delamination.

The lipped gullet plate is constructed to cover the pommel extending towards its tips while the cap plate covers the opposite face and does not normally exceed the

location where the side rails join with the pommel. Initial yield in the specimens was observed to occur at the ends of the cap plate. After the initial yield, the position of support of the specimens change from the tip of the pommel to the tip of the cap plate thereby requiring more load to bend. This resulted in the increase in the applied load after the lower yield was attained.

7.5 SUMMARY

The solutions of the numerical simulations presented in chapter 4 of this thesis were verified using controlled physical laboratory experiments. The geometries used in developing the numerical models were identical to the physical saddletree specimens. There was a good correlation between the results from both sources.

Interface pressures measured by a Tekscan ConforMat^{TM} have been compared with the contact stresses obtained from the numerical models presented in chapter 5. Percentage errors in the solutions of the numerical model relative to the mapped pressure between the saddletree and the horsestand were estimated to be 16.2% and 10.0 % for the peak contact stress and the average contact stress respectively.

Finally, applying a compression-flexure test, it was observed that delamination was the principal failure mode of the pommel. It was further observed that the steel reinforcement plates provided an effective method of enhancing resistance to delamination.

CHAPTER EIGHT

MATERIALS SELECTION & DESIGN CONCEPT DEVELOPMENT

8.1 INTRODUCTION

The significance of materials selection has been well recognized (Maniya and Bhatt, 2010). Innovative designs and the correct selection of materials are employed to facilitate technological advancements, attract consumer's attention, and increase market share (Ashby and Johnson, 2002). Though the choice of a material may be influenced by the design, it is common for the advancement in materials technology to influence new product development or the evolution of an existing one (Ashby, 2005; Ramalhete, et al. 2010). Selecting a suitable material is an important step in a design process (Deng and Edwards, 2007; Edwards and Deng, 2007); and is equally as important as the other stages in the design process (Sapuan, 2001). When design requirements are incompatible with the attributes of known materials, it is not uncommon for designers to consider alternative materials (Sapuan, 2001). Depending on the explicit requirements for an application (Edwards and Deng, 2007), designers and engineers may have to consider numerous selection criteria (Shanian and Savadogo, 2006). There is a wide range of material properties and performance attributes available (Shanian and Savadogo). In addition to having a clear understanding of the functional requirements of the product (Reddy and Gupta, 2010), other requirements such as processing (shaping, joining, and finishing) methods (Edward and Deng, 2007; Ashby, 2005), and, cost (Reddy and Gupta, 2010) may influence the material selection process.

A number of collections of design data for materials choice exist (van Kesteren, 2008). There are over 150,000 materials (Ramalhete, et al. 2010; Fernandez, et al. 2010) to choose from, and about 1,000 various manufacturing processes (Ashby, et al. 2004) stored in handbook references and computer systems (Sapuan, 2001). The computerised systems such as CES, Matweb, and CAMPUS (van Kesteren, 2008) facilitate a rapid retrieval from large computer database (Sapuan, 2001).

8.2 CES MATERIAL SELECTOR

The CES Selector software provides a procedure that establishes a link between material and function (Reddy and Gupta, 2010) that can be combined with the process data (Van Kestean, 2008). The steps involved include – defining the function of the component and the objective(s) sought, defining the constraint(s) it must satisfy, and establishing the free variable(s) the designer may opt for to meet the objective(s) (Ashby, et al., 2004). Each function has an associated material index which measures the suitability of a material for a defined function (Ashby, et al., 2004; Caceres, 2009; Reddy and Gupta, 2010). The material index is generally independent of the details of the design hence it is applicable in an idealized function (Ashby, et al., 2007). The ideas are then mapped on materials and process charts simplifying the survey for potential candidate materials (Ashby, 2005).

8.3 CASE STUDY

Ideally, the saddletree should support the saddle in distributing the load of the rider while protecting the thoracolumbar spine from contact with the rider and the saddletree. It should retain its elasticity under a bending load and should be

compliant with the bending movements of the horseback. In addition, it should support the weight of the rider during shock loads.

8.3.1 Minimizing stiffness

The side rails of the saddletree can be idealized as a simply supported beam (as illustrated in figure 8.3.1).

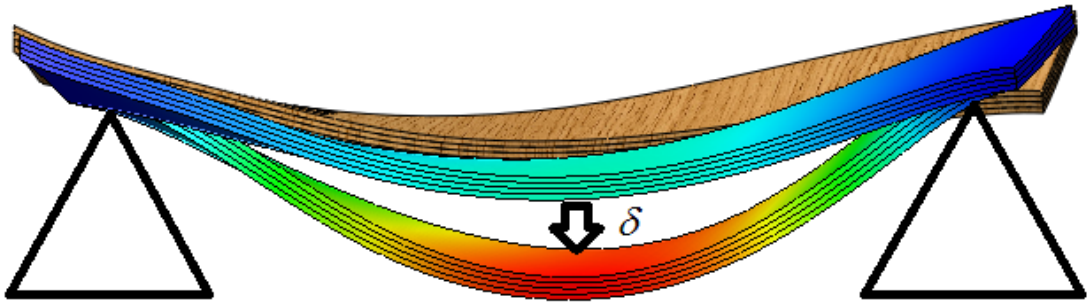

Figure 8.3.1 Flex in a section of the side rail

They connect the front (pommel) and the rear (cantle) sections of the saddletree, and also function as the seat frame for the rider. The objective was to minimize its stiffness thereby enhancing compliance with the horseback subject to the constraint that it remains elastic. The objective has to be converted into one or more performance equations (Fernandez, et al., 2010). The stiffness of the idealised rectangular beam is:

$$\mathrm{K} = \frac{\mathrm{P}}{\delta} = \frac{C\mathrm{EI}}{l^3} \tag{8.1}$$

For designs based on stiffness, a shape factor ϕ_{B}^{e} for beams under elastic bending loads (CES, 2005) is:

$$\phi_{\mathrm{B}}^{e} = \frac{4\pi\mathrm{I}}{\mathrm{A}^2} \tag{8.2}$$

It is a dimensionless property which can be applied in estimating the structural efficiency of a section shape (CES, 2005; Liang, et al., 2005).

$$\mathrm{I} = \frac{\mathrm{A}^2 \phi_{\mathrm{B}}^e}{4\pi} \tag{8.3}$$

Substituting equation 8.3 for I in equation 8.1,

$$\mathrm{K} = \frac{C\mathrm{E}}{l^3} \frac{\mathrm{A}^2 \phi_{\mathrm{B}}^e}{4\pi} = \left(\frac{C\mathrm{E}}{l^3} \right) \left(\frac{l^2 \times b^2 \phi_{\mathrm{B}}^e}{4\pi} \right) \tag{8.4}$$

To remain elastic, the maximum stress must be less than the modulus of rupture σ_{MOR} (equivalent to σ_{yield}). The flexural stress is:

$$\sigma_f = \frac{3\mathrm{P}l}{2bd^2} \tag{8.5}$$

$$b = \frac{3\mathrm{P}l}{\sigma_f 2d^2} \tag{8.6}$$

Substituting equation 8.6 for b in equation 8.4, and grouping the material properties,

$$\mathrm{K} = \left(\frac{9C\mathrm{P}^2 l}{16\pi d^4} \right) \left(\frac{\phi_{\mathrm{B}}^e \mathrm{E}}{\sigma_f^2} \right) \tag{8.7}$$

The stiffness of the design is minimized by choosing materials with high values of

$$M_1 = \left(\frac{\sigma_f^2}{\mathrm{E}\phi_{\mathrm{B}}^e} \right) \tag{8.8}$$

The default axes of the charts are logarithmic hence, logs of equation 8.8 are written as:

$$\log_{10} \sigma_f = \frac{1}{2} \log_{10} \mathrm{E}\phi_{\mathrm{B}}^e + \log_{10} M_1 \tag{8.9}$$

Equation 8.9 is a family of guidelines (as illustrated in figure 8.3.2a) of slope 0.5 on a plot of $\log_{10} \sigma_f$ against $\log_{10} \mathrm{E}\phi_{\mathrm{B}}^e$ corresponding to a value of the material index (Thakker, et al. 2008).

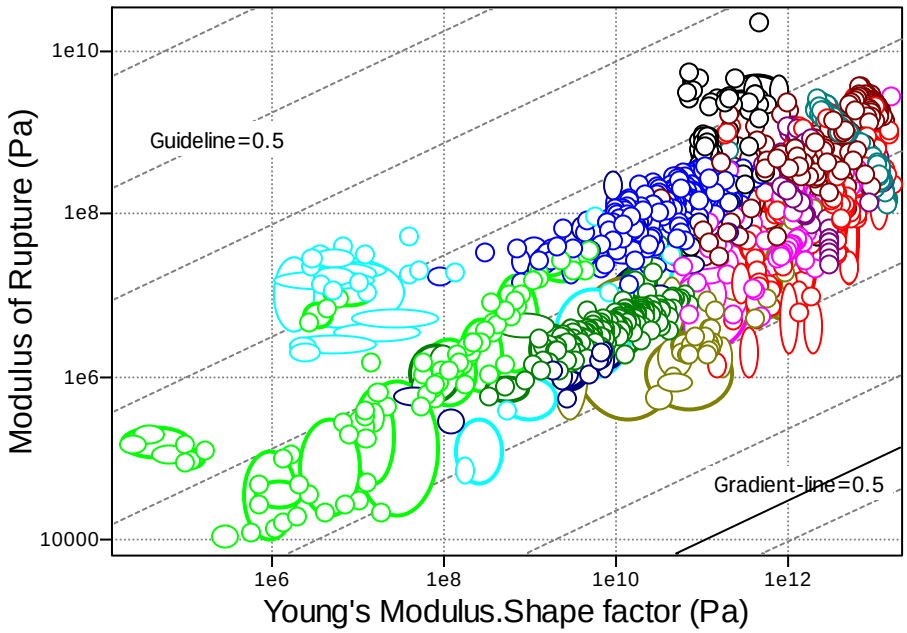

(a)

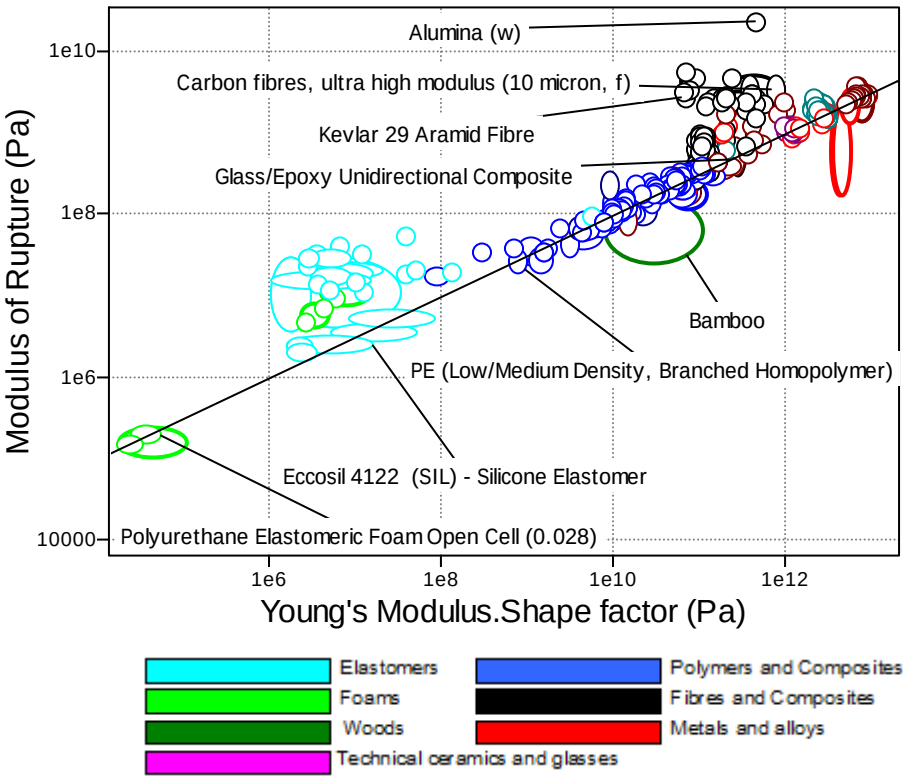

(b)

Figure 8.3.2 (a and b) Flexural stress – Young' Modulus.Shape factor plot

The gradient-line and guide-lines have identical slopes. Raising the gradient-line (as illustrated in figure 8.3.2b) increases the value of the material index and optimises the selection of a material (Ashby, et al., 2004; CES, 2005) suitable for the desired function. The top 50 materials and their M_1 values are presented in table 8.3.1.

Table 8.3.1 Potential candidates for minimized stiffness and their M_1 values

Material	$M_1 = \left(\frac{\sigma_f^2}{\mathrm{E}\phi_{\mathrm{B}}^e} \right)$
Alumina (w)	0.053
Alumina Fibre	0.005
Alumina, Nextel 480 (11 micron, f)	0.01
Alumina, Saphikon sapphire monocrystal (100 micron, f)	0.007
Boron (AVCO 102-200 micron, f)	0.006
Borsic (SiC/B/S 100-150 micron, f)	0.008
Butyl Rubber (BR) - 50% HAF black	2.917
Carbon Fibre	0.007
Carbon fibres, high modulus (5 micron, f)	0.01
Carbon fibres, high strength (5 micron, f)	0.02
Carbon fibres, ultra high modulus (10 micron, f)	0.005
Chlorinated PolyEthylene (CPE)	3.733
Chlorosulphonated Polyethylene (CSM)	0.947
Epichlorohydrin-Ethlene Oxide (CO & ECO)	1.842
Ethylene Propylene Terpolymer (EPDM)	0.947
Ethylene-Propylene (EPM)	8.03
Glass Fibre (High Strength)	0.057
Glass, C grade (10 micron monofilament, f)	0.048
Glass, E grade (0.4-12 micron monofilament, f)	0.043
Glass, S grade (10 micron monofilament, f)	0.053
Kevlar 149 Aramid Fibre	0.015
Kevlar 29 Aramid Fibre	0.039
Kevlar 49 Aramid Fibre	0.02
Natural Rubber (NR), 50% HAF black	4.917
Natural Rubber (NR), unfilled	10
Nickel-chromium-cobalt-molybdenum alloy, Rene 41, wire	0.009
Nitrile Rubber (NBR) Acrylonitrile Butadiene	3.69
PolyUrethane TPlastic Elastomer (PU) (a)	2.753
PolyUrethane TPlastic Elastomer (PU) (b)	8.933
PolyUrethane TPlastic Elastomer (PU) (c)	6.437
PolyUrethane Thermo-Set (PUTS)	1.325
Polyacrylate (ACM)	1.963
Polychloroprene (Neoprene)	8.03
Polyisoprene	8.468
Polyurethane Foam (Microcellular, High Density)	1.229
Polyurethane Foam (Microcellular, Medium Density)	1.655
Polyurethane Microcellular Foam, Closed Cell (0.70)	1.626
Polyvinylchloride (PVC) - 0.003 (Plasticised)	2.212
Polyvinylchloride (PVC) - 0.007 (Plasticised)	1.394
Silica (25-35 micron monofilament, f)	0.082
Silicon Carbide Fibre	0.008
Silicon Carbide, Nicalon NL-200 (15 micron, f)	0.014
Silicon Carbide, Nicalon NL-300 (12 micron, f)	0.015
Silicon Carbide, Nicalon NL-400 (15 micron, f)	0.014
Silicon Carbide, Tyranno M (8.5 micron, f)	0.014
Silicon carbide (p)	0.006
Spectra 1000 Polyethylene Fibre	0.019
Spectra 900 Polyethylene Fibre	0.02
Styrene-Butadiene (SBR)	2.063
Tungsten (f)	0.006

8.3.2 Minimizing mass

A second objective was defined to reduce mass subject to the constraint that it remains elastic.

$$\rho = \left(\frac{m}{v} \right) \tag{8.10}$$

The objective function is to reduce the mass which is written as:

$$m = v\rho = lbh\rho \tag{8.11}$$

To remain elastic, the maximum stress must be less than the modulus of rupture σ_{MOR}. The flexural stress is:

$$\sigma_f = \frac{3\mathrm{P}l}{2bd^2} \tag{8.12}$$

Solving for b and substituting in equation 8.11,

$$m = (lh\rho)\left(\frac{3\mathrm{P}l}{2\sigma_f d^2} \right) \tag{8.13}$$

$$m = \left(\frac{3\mathrm{P}l^2 h}{2d^2} \right)\left(\frac{\rho}{\sigma_f} \right) \tag{8.14}$$

The mass m is minimized by choosing materials with large values of

$$M_2 = \left(\frac{\sigma_f}{\rho} \right) \tag{8.15}$$

$$\log_{10}\sigma_f = \log_{10}\rho + \log_{10} M_2 \tag{8.16}$$

Equation 8.16 is a family of guidelines of slope 1 on a plot of $\log_{10}\sigma_f$ against $\log_{10}\rho$ corresponding to a value of the material index.

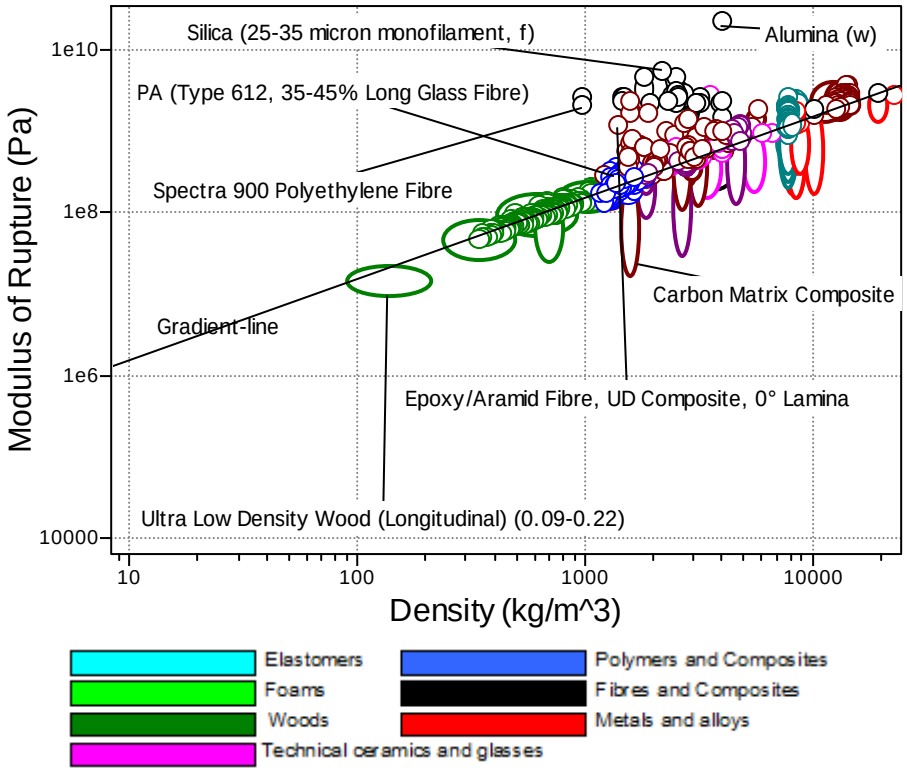

Figure 8.3.3 Flexural stress – density plot

Raising the gradient-line (as illustrated in figure 8.3.3b) increases the value of the material index and reduces the number of potential materials for a design function. The top 50 materials and their M_2 values are presented in table 8.3.2.

Table 8.3.2 Potential candidates for minimized mass and their M_2 values

Material	$M_2 = \left(\frac{\sigma_f}{\rho}\right)$
Al-47%SiC(f), Longitudinal	0.51
Al-50%B(f), Longitudinal	0.48
Al-60%C-M40(HM-C-Fibre), Longitudinal	0.47
Alumina (p)	0.39
Alumina (w)	6.06
Alumina Fibre	0.39
Alumina, Nextel 480 (11 micron, f)	0.75
Alumina, Nextel 610 (12 micron, f)	0.58
Alumina, Saphikon sapphire monocrystal (100 micron, f)	0.61
Aluminium/Boron Composite	0.31
BMI/HS Carbon Fibre, UD Composite, 0° Lamina	1.08
Boron (AVCO 102-200 micron, f)	0.93
Borsic (SiC/B/S 100-150 micron, f)	1.12
Carbon Fibre	1.87
Carbon fibres, high modulus (5 micron, f)	2.03
Carbon fibres, high strength (5 micron, f)	2.55
Carbon fibres, ultra high modulus (10 micron, f)	1.76
Carbon fibres, very high modulus (5 micron, f)	1.22

Diamond	0.8
Epoxy SMC (Carbon Fibre)	0.38
Epoxy/Aramid Fibre, UD Composite, 0° Lamina	0.9
Epoxy/HS Carbon Fibre, UD Composite, 0° Lamina	1.25
Epoxy/HS Carbon Fibre, Woven Fabric Composite, Biaxial Lamina	0.49
Epoxy/HS Carbon Fibre, Woven Fabric Composite, QI Laminate	0.35
Epoxy/S-Glass Fibre, UD Composite, 0° Lamina	0.91
Glass Fibre (High Strength)	1.9
Glass, C grade (10 micron monofilament, f)	1.31
Glass, E grade (0.4-12 micron monofilament, f)	1.31
Glass, S grade (10 micron monofilament, f)	1.89
Glass/Epoxy Unidirectional Composite	0.51
Kevlar 149 Aramid Fibre	1.87
Kevlar 29 Aramid Fibre	1.91
Kevlar 49 Aramid Fibre	1.73
Magnesium/Carbon Fibre Composite	0.33
Mg(+2%Al)-30%Graphite (f), Longitudinal	0.36
Mg(+4%Al)-30%Graphite (f), Longitudinal	0.36
Mg-70%B(f), Longitudinal	0.38
PEEK/IM Carbon Fibre, UD Composite, 0° Lamina	1.55
Polyimide/HS Carbon Fibre, Woven Fabric Composite, Biaxial Lamina	0.51
Silica (25-35 micron monofilament, f)	2.67
Silicon Carbide (140 micron, f)	0.72
Silicon Carbide Fibre	0.95
Silicon Carbide, Nicalon NL-200 (15 micron, f)	1.08
Silicon Carbide, Nicalon NL-300 (12 micron, f)	1.15
Silicon Carbide, Nicalon NL-400 (15 micron, f)	1.07
Silicon Carbide, Tyranno M (8.5 micron, f)	1.2
Silicon Nitride	0.22
Silicon carbide (p)	0.87
Spectra 1000 Polyethylene Fibre	2.84
Spectra 900 Polyethylene Fibre	2.32

8.3.3 Intersection of selection stages in the CES Selector

For a product requiring the optimization of multiple parameters (Reddy and Gupta, 2010), the effect of each optimization may be considered with respect to the other(s) (Shanian and Savadogo, 2009). Though multiple selection stages in a CES project are independent (CES, 2005), they are linked within the software (Aceves, et al., 2008) and can be combined listing their intersection (Ashby, et al., 2004). The top ten potential candidates after combining and intersecting the material indices M_1 and M_2 are presented in table 8.3.3.

Table 8.3.3 Potential candidates after intersecting M_1 and M_2

Material	$M_1 = \left(\frac{\sigma_f^2}{\mathrm{E}\phi_{\mathrm{B}}^e}\right)$	$M_2 = \left(\frac{\sigma_f}{\rho}\right)$
Alumina (w)	0.053	6.061
Carbon Fibre	0.007	1.869
Carbon fibres, high modulus (5 micron, f)	0.01	2.027
Carbon fibres, high strength (5 micron, f)	0.02	2.555
Glass Fibre (High Strength)	0.057	1.895
Glass, C grade (10 micron monofilament, f)	0.048	1.305
Glass, E grade (0.4-12 micron monofilament, f)	0.043	1.311
Glass, S grade (10 micron monofilament, f)	0.053	1.888
Kevlar 29 Aramid Fibre	0.039	1.91
Silica (25-35 micron monofilament, f)	0.082	2.668

The process can be described as a trade-off between attributes resulting in candidate materials with better average performance indices (Shanian and Savadogo, 2009). The material indices M_1 and M_2 of beech and birch woods which are the material currently used are presented in table 8.3.4.

Table 8.3.4 Material indices M_1 and M_2 of birch and beech woods

Material	$M_1 = \left(\frac{\sigma_f^2}{\mathrm{E}\phi_{\mathrm{B}}^e}\right)$	$M_2 = \left(\frac{\sigma_f}{\rho}\right)$
Birch	0.001	0.14 – 0.19
Beech	0.001 – 0.002	0.1 4

8.3.4 Maximizing elastic stored energy

To support the weight of the rider particularly during shock loadings, the use of springs which could store and release elastic energy (Al-Qureshi, 2001; Ashby and Jones, 2005; Childs, 2004; Mahdi, et al., 2006; Nohut and Schneider, 2009) was considered. A pair of springs similar to leaf springs is attached to the saddletree. The objective function of the material selection was to maximize the elastic energy stored without failing. The elastic potential energy (or strain energy) (McLester and Pierre, 2008) is

$$\cup_e = \frac{1}{2}\left(kx^2\right) \tag{8.17}$$

where k is the spring constant and x is the spring extension.

The spring constant

$$k = \frac{\mathrm{AE}}{l} \tag{8.18}$$

Substituting k in equation 8.18 in equation 8.17,

$$\bigcup_e = \frac{1}{2}\left(\frac{\mathrm{AE}}{l}\right)x^2 \tag{8.19}$$

The elastic strain per unit volume (CES, 2005; Qian and Zhao, 2002; Matejicek, et al., 2004; Nohut and Schneider, 2009) is

$$\bigcup_e = \frac{1}{2}\left(\frac{\mathrm{AE}}{\mathrm{A}l^2}\right)\Delta l^2 \tag{8.20}$$

$$\bigcup_e = \frac{1}{2}\left(\frac{\sigma^2}{\mathrm{E}}\right) \tag{8.21}$$

The material must exhibit high strength against applied load (Nohut and Schneider, 2009; Qui and Ren, 2006) and to remain elastic, the maximum stress must be less than maximum flexural stress σ_f .

$$\bigcup_e = \frac{1}{2}\left(\frac{\sigma_f^2}{\mathrm{E}}\right) \tag{8.22}$$

The material index for the best material for springs is

$$\mathrm{M}_3 = \left(\frac{\sigma_f^2}{\mathrm{E}}\right) \tag{8.23}$$

$$\log_{10}\sigma_f = \frac{1}{2}\log_{10}\mathrm{E} + \log_{10} M_3 \tag{8.24}$$

Equation 8.24 is a family of guidelines of slope 0.5 on a plot of $\log_{10}\sigma_f$ against $\log_{10}\mathrm{E}$ corresponding to a value of the material index.

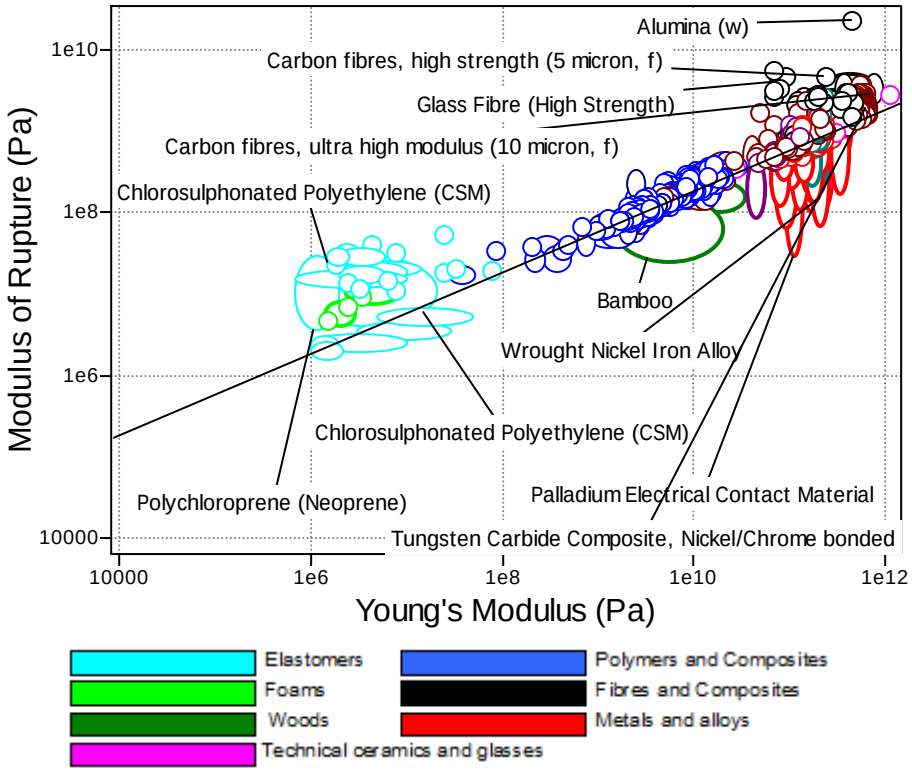

Figure 8.3.4 Flexural stress – Young' Modulus plot

The top 50 materials and their M_3 values are presented in table 8.3.5.

Table 8.3.5 Potential candidates for maximized stored elastic energy and their M_3 values

Material	$M_3 = \left(\frac{\sigma_f^2}{E}\right)$
Alumina (w)	0.053
Butyl Rubber (BR) - 50% HAF black	4.375
Carbon Fibre	0.007
Carbon fibres, high modulus (5 micron, f)	0.01
Carbon fibres, high strength (5 micron, f)	0.02
Carbon fibres, ultra high modulus (10 micron, f)	0.005
Chlorinated PolyEthylene (CPE)	5.6
Chlorosulphonated Polyethylene (CSM)	1.515
Epichlorohydrin-Ethlene Oxide (CO & ECO)	2.763
Epoxy/HS Carbon Fibre, UD Composite, 0° Lamina	0.014
Epoxy/S-Glass Fibre, UD Composite, 0° Lamina	0.036
Ethylene Propylene Terpolymer (EPDM)	1.515
Ethylene-Propylene (EPM)	12.04
Glass Fibre (High Strength)	0.057
Glass, C grade (10 micron monofilament, f)	0.048
Glass, E grade (0.4-12 micron monofilament, f)	0.043
Glass, S grade (10 micron monofilament, f)	0.053
Kevlar 149 Aramid Fibre	0.015
Kevlar 29 Aramid Fibre	0.039
Kevlar 49 Aramid Fibre	0.02
Molybdenum high speed steel, AISI M47	0.011

Molybdenum high speed tool steel, AISI M42	0.011
Molybdenum high speed tool steel, AISI M43	0.011
Molybdenum high speed tool steel, AISI M44	0.011
Molybdenum high speed tool steels, AISI M41	0.011
Natural Rubber (NR), 50% HAF black	7.375
Natural Rubber (NR), unfilled	15
Nitrile Rubber (NBR) Acrylonitrile Butadiene	5.534
PEEK/IM Carbon Fibre, UD Composite, 0° Lamina	0.016
PI (Thermoset)	0.1
PolyUrethane TPlastic Elastomer (PU) (a)	4.129
PolyUrethane TPlastic Elastomer (PU) (b)	13.4
PolyUrethane TPlastic Elastomer (PU) (c)	9.655
PolyUrethane Thermo-Set (PUTS)	2.12
Polyacrylate (ACM)	2.944
Polychloroprene (Neoprene)	12.04
Polyisoprene	12.7
Polyurethane Foam (Microcellular, High Density)	2.088
Polyurethane Foam (Microcellular, Medium Density)	2.814
Polyvinylchloride (PVC) - 0.003 (Plasticised)	3.538
Polyvinylchloride (PVC) - 0.007 (Plasticised)	2.231
Silica (25-35 micron monofilament, f)	0.082
Silicon Carbide Fibre	0.008
Silicon Carbide, Nicalon NL-200 (15 micron, f)	0.014
Silicon Carbide, Nicalon NL-300 (12 micron, f)	0.015
Silicon Carbide, Nicalon NL-400 (15 micron, f)	0.014
Silicon Carbide, Tyranno M (8.5 micron, f)	0.014
Spectra 1000 Polyethylene Fibre	0.019
Spectra 900 Polyethylene Fibre	0.02
Styrene-Butadiene (SBR)	3.3

8.4 DISCUSSION OF MATERIALS SELECTION FOR SADDLETREE

8.4.1 Minimizing stiffness

While most structures benefit from the enhancement of their stiffnesses (Eugene, 1999), there are many important cases where stiffness reduction is beneficial, resulting in improved performance (Eugene, 1999; Butler, et al., 2003). The stiffness of the saddletree has been evaluated and presented earlier in this thesis. A stiffness mismatch was recognized between the saddletree and the thoracolumbar spine; presenting a risk of the saddlery obstructing the natural movement of the horseback, resulting in diminished performance, and health and welfare problems.

A design analogy can be made with shoes; they are primarily designed to protect the foot from injuries (Wolf, et al., 2008; Cheng and Perng, 1999), similar to the

saddletree providing protection for the thoracolumbar spine. Shoes are subordinate to the feet (Cheng and Perng, 1999) and precise conformity of the feet and shoes is a requirement for performance in some applications (Van der Putten and Snijders, 2001). Children's shoes have also been reported to flex in compliance with their feet (Walther, et al., 2008). Likewise, the saddletree should be compliant with the movements of the horseback. Material index M_1 was derived to explore potential candidate materials suitable to satisfy significant design requirements (Edwards and Deng, 2007) for the saddletree - reduced stiffness subject to the constraint that it does not yield to bending loads.

From a total of 3573 possible material candidates, 50 material candidates with the highest values of M_1 were presented in table 8.3.1. Based on the material index, elastomers were most suitable for the objective function. Generally, elastomers are capable of withstanding large strains (Amin, et al., 2002; Doyle, et al., 2009; Edwards, 1998; Fatt and Ouyang, 2007; Fatt and Ouyang, 2008; Mars and Fatemi, 2002) without permanent deformations making them ideal for many applications (Mars and Fatemi, 2002). They are used extensively in the footwear industry due to their outstanding toughness, resilience, and flexibility (Allen, et al., 2005; Van der Putten, and Snijders, 2001). Polyurethane TPlastic Elastomers are applied in making midsoles of running shoes (Heidenfelder, et al., 2006), soles and heels for sports shoes and football boots (CES, 2005; Edwards, 1998), polyisoprene is applied in making shoes (CES, 2005), styrene-butadiene is applied in shoe soles and heels (Edwards, 1998; Tsai and Powers, 2009), chlorinated polyethylene is applied in making shoe soles (CES, 2005). Other polymers not included in the CES database such as ethylene vinyl acetate (EVA) and DoPont's Elvax range (Allen, et al., 2005)

are also applied in making midsoles.

8.4.2 Minimizing mass

For the 2nd objective function, material index M_2 was derived to explore potential candidate materials suitable to satisfy significant design requirements (Edwards and Deng, 2007) for the saddletree - reduced mass subject to the constraint that it does not yield to bending loads. From a total of 3573 possible candidate materials, 50 material candidates with the highest value of M_2 were presented in table 8.3.2. Based on the objective function, fibres performed best with alumina whiskers exhibiting the highest material index value followed by spectra polyethylene fibres, silica, carbon fibres, Kevlar fibres, and glass fibres. Their high strength and stiffness, and low density (Zi, et al., 2008) properties have made them attractive for use in various engineering applications in the aerospace, automotive, and civil engineering industries (Ochola, et al., 2004). They have also been applied in the evolution of sports equipment. In most sports, changes in equipment such as applying composites to manufacture pole vaults and tennis rackets have resulted in changes in performance however some sports are less sensitive to these changes (Davis, 2007). Composite materials can be applied as single fibres, yarn, or woven mat (CES, 2005).

Recently, carbon fibre which is more expensive (Aceves, et al., 2008; Fuchs, et al., 2008; Mahdi, et al., 2006; Varvani-Farahani, et al., 2007; Zi, et al., 2008) and stiffer (Chiu, et al., 2007; Colomb, et al., 2008; Fuchs, et al., 2008) than glass fibre has been introduced in the manufacture of saddlery. Barnsby (n. d.) introduced carbon fibre saddletrees in the XTREEM event and show jumping saddles. Quantum

redesigned the saddle replacing the saddletree with a carbon fibre fin referred to as the chassis (Baker, 2009; Quantum, n.d.). Unfortunately, there are no reviewed publications on their research and development hence, the difficulty in understanding or critiquing the philosophy of their works. Based on available information on Barnsby's website, weight savings seems to have been the primary goal of their development. They wanted to introduce material technology applied in Formula 1 racing cars (Barnsby, n.d.). Based on available information on Quantum's website and Baker (2009), Quantum's objectives were to improve pressure distribution on the horse's back and reduce the overall weight of the saddle. They wanted a stiff and light weight product; their approach applied technology based on developing car components and consumer products (Baker, 2009). There was no indication that either of them quantified the stiffness of the saddletree before and after the development. Neither were the effects of their developments on the pressure distribution of existing products quantified.

8.4.3 Combining objective functions of stiffness and mass

The top 10 potential candidate materials resulting from the combination and intersection of M_1 and M_2 were presented in table 8.3.3. In comparison with the material indices of birch and beech wood presented in table 8.3.4, it is evident that the trade-off performed in the intersection was a compromise resulting in the choice of potential material candidates that satisfy the performance objective of minimizing mass at the expense of the performance objective of minimizing stiffness. To evaluate the trade-off, the material indices are compared with those of birch and beech wood and are presented in table 8.4.1.

Table 8.4.1 Comparison of M_1 and M_2 values of potential candidates with birch and beech wood

Material	M_1	M_2
Alumina (w)	26.5 – 37.88	31.9 – 43.3
Carbon Fibre	3.5 – 5.01	9.84 – 13.35
Carbon fibres, high modulus (5 micron, f)	4.87 – 7	10.7 – 14.48
Carbon fibres, high strength (5 micron, f)	9.89 – 14.13	13.4 – 18.25
Glass Fibre (High Strength)	28.5 – 40.7	9.98 – 13.54
Glass, C grade (10 micron monofilament, f)	23.9 – 34.14	6.87 – 9.32
Glass, E grade (0.4-12 micron monofilament, f)	21.5 – 30.71	6.9 – 9.36
Glass, S grade (10 micron monofilament, f)	26.3 – 37.51	9.93 – 13.48
Kevlar 29 Aramid Fibre	19.4 – 27.67	10.1 – 13.64
Silica (25-35 micron monofilament, f)	41.2 – 58.9	14 – 19.06
Polyisoprene	4234.23 – 6048.91	0.18 – 0.13
Polyurethane TPlastic Elastomers	1376.34 – 6380.95	0.15 – 0.25
styrene-butadiene	1031.25 – 1473.21	0.15 – 0.11
chlorinated polyethylene	1866.67 – 2666.67	0.087 – 0.064

The M_1 benefit of the elastomers over birch and beech wood far outweighs that of the composites over birch and beech wood while the M_2 benefit of the composites outweighs the benefit of the elastomers.

Based on knowledge gained earlier during this research, the author is convinced that this is a situation where stiffness reduction in the product design is highly sought after. A saddletree design is constrained, not by choice but by nature, to an optimal range of stiffness (Eugene, 1999) of the horseback. Weight savings achieved by replacing traditional materials with light-weight materials have been widely reported to enhance product performance across several industries, including but not limited to aerospace and transportation applications (Ning, et al., 2009), automotive applications (Fuchs, et al., 2008; Miller, et al., 2000), defence systems (Ubeyli, et al., 2007), and, marine applications (Ning, et al., 2009; Osnes and McGeorge, 2009). It

is imperative to emphasize that the increase in the utilization of composite materials is greatest in applications where their superior specific strength and specific stiffness characteristics (Ning, et al., 2007, 2009) are required. Like weight savings, stiffness has been related to both performance and injury (Butler et al., 2003). Stiffness reduction for some products results in improved performance due to changing load and deformation distribution patterns, and, reduction in stress concentration between contacting surfaces (Eugene, 1999). Undoubtedly, the application of materials that flex better than birch and beech laminates will result in optimized saddletrees that will guarantee minimal interference and disturbance of the natural movement of the horse (Hausberger, et al., 2008) thereby improving performance and reducing the risks of saddlery related injuries. A choice of a composite will only improve the flex obtained using birch or beech wood by between 4 and 59 times while a choice of an elastomer will improve the flex obtained using birch or beech wood by between 1031 and 6049 times. A choice of composite over elastomer based on weight savings will represent only a minute improvement over the existing saddletree structure compared to the envisaged improvement as a result of applying an elastomer, more so when an elastomer could be combined with innovative weight saving designs.

Furthermore, through innovative designs for footwear applications, elastomers have been applied to provide a close contact feel between the feet and the contacting surface (Van der Putten and Snijders, 2001; Wallden, 2010); this knowledge can be applied in the design of the saddletrees to enhance close contact required for effective communication between the rider and the horse.

8.4.4 Maximizing elastic stored energy

The influence of the pair of spring steel on the stiffness of the saddletree has been reported earlier in chapters 4 and 5 of this thesis. Applying the performance criteria defined for the objective function, elastomers exhibited the highest material index M_3 value (see Table 8.3.5). Though they are reported to have a high loss factor (CES, 2005; Burgess, 1998), rubber springs have been used in a wide range of engineering applications (Luo and Wu, 2006). The novel works of Dr. Alex Moulton have been widely reported; his rubber springs were extensively used in Moulton bicycles and the Rover Mini (Hadland, 2009; Roy, 2004). Recently, Quantum (n.d.) applied rubber suspension bumpers to the rear of their saddle seats.

The material index M_3 values indicate that elastomers performed better than metals, which are traditionally applied in making springs (Chiu, et al., 2007); composites, which have also been applied in making vehicle leaf springs (Al-Qureshi, 2001; Mahdi, et al., 2006; Varvani-Farahani, et al., 2007) and, ceramics, which have a low loss factor but undergo brittle failure (Nohut and Schneider, 2009).

Furthermore, elastomers or rubber based materials have often been suitable in mitigating the effects of spontaneous or impact loads due to their low modulus, large extensibility, and high damping characteristics (Fatt and Ouyang, 2007; 2008). Dampers and shock absorbers have been applied for the purpose of saving energy stored and enhancing the performance of springs (Chiu, et al., 2007).

8.5 DESIGN CONCEPT DEVELOPMENT

Based on the author's experience with some locally based saddlers and saddletree

makers, he is of the opinion that in view of the conservatism of the industry professionals, rather than introducing a radical innovation process or idea, an incremental or continuous innovation process (Veryzer, 1998) may be more acceptable. Hence, there is an opportunity to explore new concepts while retaining some traditional methods.

In the concept presented in figures 8.5.1 to 8.5.3, the traditional wooden frame saddletree is replaced with an elastomer saddletree situated above a pair of memory foams. Elastomer spring / dampers are placed between the glass fibre frame and the saddletree. The glass fibre frame doubles as a spring and a seat platform for the rider. Traditional seat foam is placed on the glass fibre frame and finally, a traditional covering in form of leather or synthetic leather is draped over the structure.

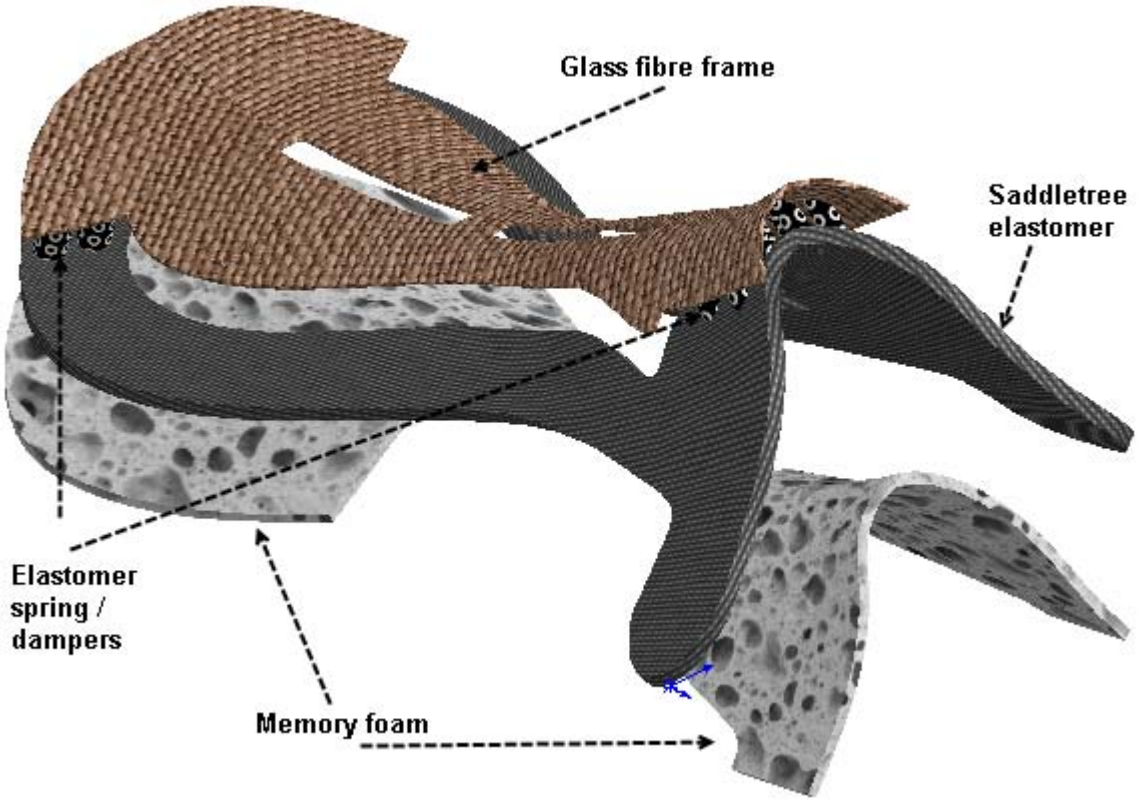

Figure 8.5.1 Isometric view orientation of the concept

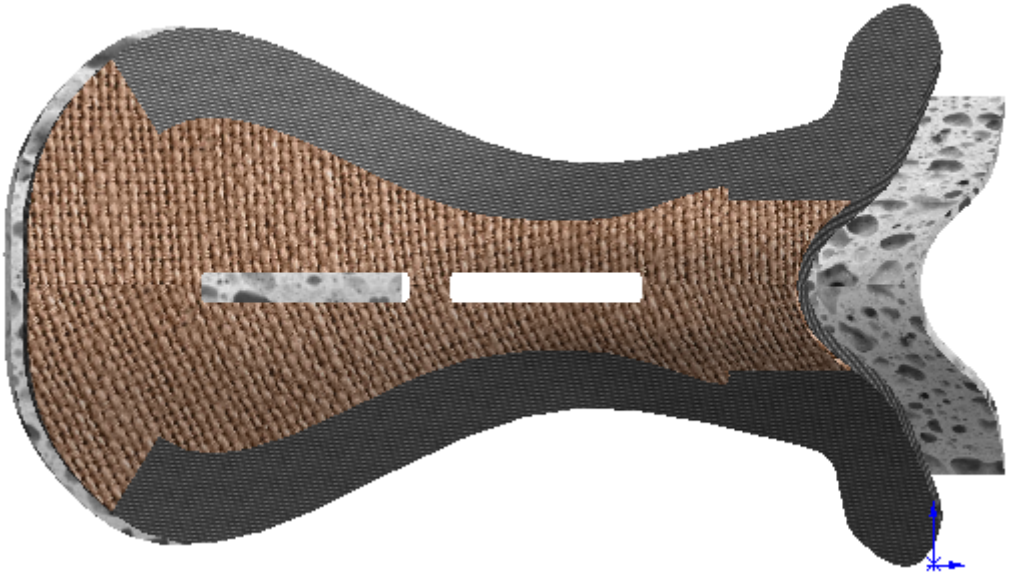

Figure 8.5.2 Top view of the concept

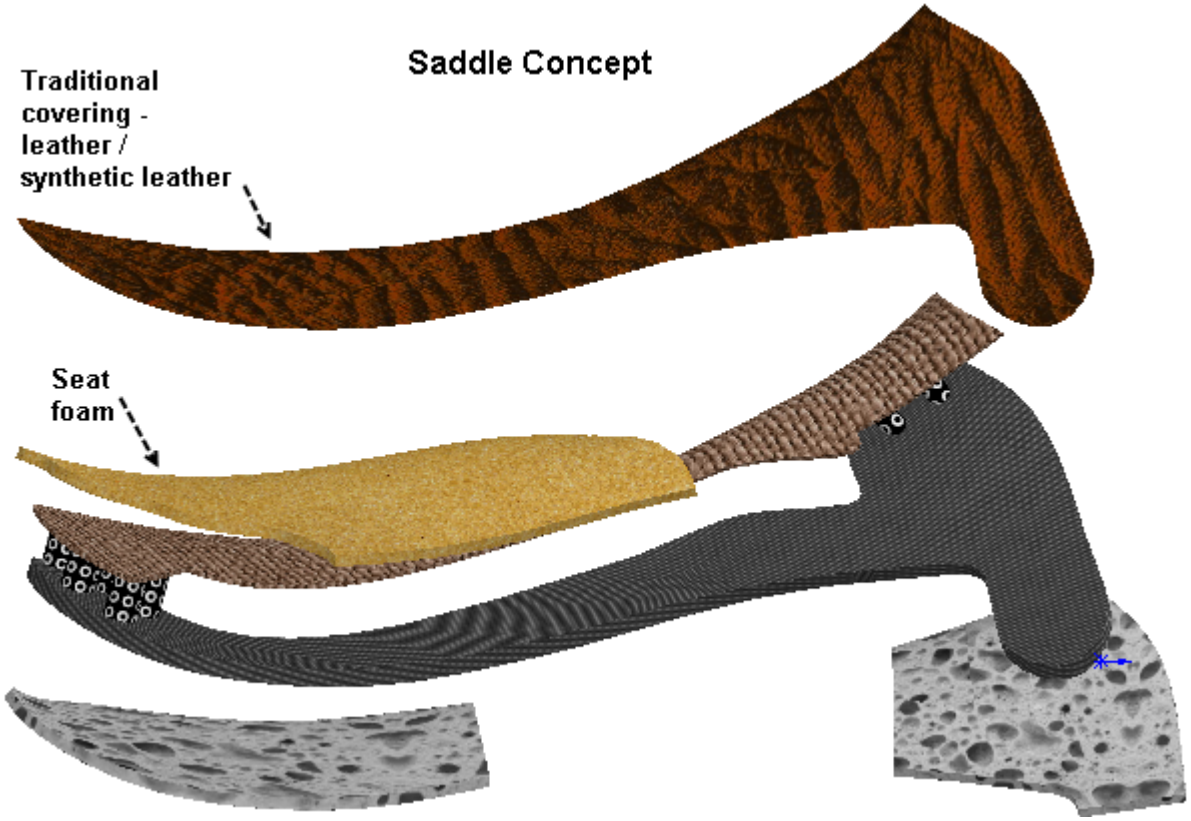

Figure 8.5.3 Side view of the concept

8.6 SUMMARY

With a clear understanding of the functional requirements of the product (Rao and Patel, 2010), an analytical approach (Karana, et al., 2010) was applied to explore potential candidate materials with specific properties which can guarantee optimal performance (Khabbaz, et al., 2009) by satisfying the defined objectives and constraints (Karana, et al., 2010; Khabbaz, et al., 2009).

Three material indices M_1, M_2, and M_3 were defined for minimizing stiffness, minimizing mass, and maximizing stored elastic energy. The mechanical properties considered in the selection process include the stiffness, flexural strength, density (Chatterjee, et al., 2009), and the Young's modulus. While M_1 ranked rubber with the highest performance in minimizing stiffness, M_2 ranked alumina whiskers with the highest performance in minimizing mass. A combination and intersection of M_1 and M_2 resulted in a set of materials with very low material index values for the functional objective of minimizing stiffness. In comparison with M_1 and M_2 of birch and beech wood, the author was of the opinion that the trade-off did not satisfactorily meet the stiffness objective. To minimize the stiffness of the saddletree without bending failure under a rider's load, elastomers presented the best choice. M_3 also ranked elastomers with the highest performance in maximizing stored elastic energy.

Finally, a concept presenting an innovation process exploring new methods while retaining some traditional methods is presented.

CHAPTER NINE

CONCLUSIONS AND FUTURE WORK

9.1 CONCLUSIONS

This research presents pioneering work in the area of saddletree design; to date there are no scholarly publications in this area of study. The underlying philosophy of the research (as illustrated in figure 1.6.1) was to apply innovative tools and technologies to acquire knowledge on the performance of the saddletree thereby providing a foundation to support future product development. It has been demonstrated that science and engineering tools can be applied in the development of saddletrees, which were hitherto developed applying traditional crafts and skills. To both academia and industry practitioners, this is crucial in repositioning the industry to retain its market share by providing high performance saddlery products at an affordable cost.

The major conclusions drawn from this research include the following:

1. Through the development of numerical models, the response of the saddletree to loads has been evaluated and quantified in terms of its bending stiffness. The findings are as follows:

- Cantilever set-up -
    - The stiffness of the solid wood saddletree was determined to be 4.37N/mm (point load) and 3.63 N/mm (UDL).
    - The stiffness of the laminated wood saddletree was determined to be 4.68 N/mm (point load) and 3.87 N/mm (UDL).

- Simply supported set-up –
    - The stiffness of the solid wood saddletree was determined to be 596.16 N/mm.
    - The stiffness of the laminated wood saddletree was determined to be 526.62 N/mm.
    - Varying the laminate stacking sequence between 20 % of 90^0 and 80% of 0^0, and 80 % of 90^0 and 20 % of 0^0, the stiffness of the laminated wood saddletree ranged between 347.02 N/mm and 824.96 N/mm.

2. In comparison with the mean stiffness of the dorsoventral movement of the thoracolumbar spine, 2.093 N/mm (Schlacher, et al., 2004), it was evident that there is a stiffness mismatch between the saddletree and the thoracolumbar spine. This led us to arrive at a most important conclusion that the saddletree has to conform to the movements of the horseback to avoid the consequences of a mismatch.

3. It was established that the steel reinforcement plates (pair of spring steel inclusive) increased the stiffnesses of the cantilevered solid wood and laminated wood saddletree models by 85.81 % and 76.50 % (point load) respectively; and, by 131.68 % and 121.71 % (UDL) respectively. Simply supported, the stiffnesses of the solid wood and laminated wood saddletree models were increased by 365.75 % and 447.40 % respectively.

4. It was further established that the steel reinforcement plates (without the pair of spring steel) increased the stiffnesses of the cantilevered solid wood and laminated

wood saddletree models by 32.72 % and 20.30 % (point load) respectively; and, by 66.12 % and 51.16 % (UDL) respectively. Simply supported, the stiffnesses of the solid wood and laminated wood saddletree models were increased by 260.37 % and 386.77 % respectively.

5. Furthermore, it was established that the stiffness of the saddletree is sensitive to geometrical variations. A thickness reduction of the reinforced saddletree (pair of spring steel inclusive) from 7.5 mm to 6.0 mm resulted in a stiffness reduction of up to 20.70 % (point load) and up to 20.05 % (UDL) while a similar thickness reduction without the pair of spring steel resulted in a stiffness reduction of up to 30.37 % (point load) and up to 30.09 % (UDL).

6. Through the development of dynamic transient simulations, the response of the pommel to impact was evaluated. The stress strain curves illustrated yield at impact velocities of 7 m/s, 8.5 m/s, and 10 m/s. In addition, the nodal history plots demonstrated that the cap and lipped gullet plates dampened the oscillations in the pommel after impact.

7. Controlled physical experiments were performed to validate and support the findings of the numerical models. The findings include:

- The stiffnesses of the 3 cantilever saddletree specimens were determined to be 3.79 N/mm, 4.63 N/mm, and 4.85 N/mm.
- The stiffnesses of the 3 steel reinforced (pair of spring steel inclusive) cantilever saddletree specimens were determined to be 7.38 N/mm, 12.31 N/mm, and 7.93 N/mm.

- Interface pressure mat results exhibited pressure hot spots and uneven load distribution underneath the saddletree. Peak and average pressures were 82.7 KPa and 15.4 KPa respectively, representing 16.2 % and 10.0 % error in comparison with the estimated contact stresses obtained from the numerical models.
- The compression-flexure tests showed that delamination was the dominant failure mechanism in the wooden pommel.
- Furthermore, the compression-flexure tests showed that though the cap and lipped gullet plates protected the pommel from delamination, the reinforced structure failed in flexure.

8. This led to another important conclusion that the use of the steel reinforcement plates in the design and construction of the English jumping saddletree is not recommended. They stiffen the saddletree and do not protect it from failing.

9. Three material indices were defined in a materials selection process. The outcomes are as follows:

- Minimizing stiffness – elastomers were ranked with the highest performance with unfilled, natural rubber having a material index M_1 of 10.
- Minimizing mass - ranked alumina whiskers with the highest performance having a material index M_2 of 6.06.
- Maximizing stored elastic energy - elastomers were ranked with the highest performance with unfilled, natural rubber having a material index M_3 of 15.

10. Based on acquired knowledge and experience, design concepts leading to optimal saddle design were developed.

9.2 FUTURE WORK

1. Progression of concept

Further work is required to test, and improve the concepts leading to the development of a detailed design which will be patented, prototyped and manufactured. Most importantly, the damper and spring system in addition to jointing methods require further concept development and detailing. In addition, it is essential to explore and determine appropriate modern manufacturing techniques ensuring improved accuracy, symmetry, and mass customisation.

2. Developing understanding of different saddles

The skills, tools and methodology applied in developing a better understanding of the jumping saddletree and the knowledge gained from this research resulting in the development of the English jumping saddle can be transferred to other saddle types particularly the dressage and the eventing saddles. In addition, knowledge and understanding gained can be applied in updating relevant British Standards.

3. Bespoke design

Traditionally, the involvement of higher educational institutions in equestrianism has concentrated on veterinary research (Wood and Newbold, 2004). From this research, it is apparent that there are significant opportunities in developing performance saddlery products based on a combination of findings from veterinary research and engineering design research. There is an opportunity to develop a methodology for

determining the stiffness of a horseback and applying the data in developing bespoke saddletrees.

REFERENCES

Aceves, C. M., et al., (2008). Design selection methodology for composite structures. Materials and Design. 29: 418-426.

Adali, S. and Verijenko, V. E., (2001). Optimum stacking sequence design of symmetric hybrid laminates undergoing free vibrations. Composite structures. 54: 131 – 138.

Adams, D. F., et al., (2002). Experimental Characterization of Advanced Composite Materials. 3rd ed. CRC Press.

Adams, V., (2006). How To Manage Finite Element Analysis in the Design Process. Glasgow: NAFEMS Ltd.

Adams, V., (2008). A Designer's Guide to Simulation with Finite Element Analysis. Glasgow: NAFEMS Ltd.

Akbulut, M., and Sonmez, F. O., (2008). Optimum design of composites laminates for minimum thickness. Computers and Structures. 86: 1974-1982.

Allen, R. D., et al., (2005). Design of experiments for the qualification of EVA expansion characteristics. Robotics and Computer-Integrated Manufacturing. 21: 412-420.

Al-Qureshi, H. A., (2001). Automobile leaf springs from composite materials. Journal of Materials Processing Technology. 118: 58-61.

Amin, A. F. M. S., et al., (2002). An improved hyperelasticity relation in modeling viscoelasticity response of natural and high damping rubbers in compression: experiments, parameter identification and numerical verification. Mechanics of Materials. 34: 75-95.

Andersson, K., et al., (2007). Development of a harmonized method for the profiling of amphetamines VI: Evaluation of methods for comparison of amphetamine. Forensic science international. 169: 86 – 99.

Ashby, M. F., (2005). Materials selection in mechanical design. 3rd ed. Butterworth-Heinemann. Oxford.

Ashby, M., and Johnson, K., (2002). Materials and Design: the art and science of material selection in product design. Butterworth-Heinemann. Oxford.

Ashby, M. F., and Jones, D. R. H., (2005). Engineering materials 1: An introduction to properties, applications, and design. 3rd ed. Butterworth-Heinemann. Oxford.

Ashby, M. F., et al., (2007). Materials: engineering science processing and design. Butterworth-Heinemann. Oxford.

Ashby, M. F., et al., (2004). Selection strategies for materials and processes. Materials and Design. 25: 51-67.

Astley, R. J., et al., (1997). Mechanical modeling of wood microstructure, an engineering approach. IPENZ Transactions. 24(1)/EMCh:21-29.

Audigie, F., et al., (1999). Kinematics of the equine back: flexion-extension movements in sound trotting horses. Equine Veterinary Journal. Supplement 30: 210-213.

Bachus, K. N., et al., (2006). Measuring contact area, force and pressure for bioengineering applications: Using Fuji Film and Tekscan systems. Medical Engineering and Physics. 28: 483-488.

Back, W. and Clayton, H. M., (2001). Equine Locomotion. (2001). London, UK: Harcourt Publishers Ltd.

Bagci, E., (2009). Reverse engineering applications for recovery of broken or worn parts and re-manufacturing: Three case studies. Advances in Engineering Software. 40: 407-418.

Bailetti, A. J., and Litva, P. F., (1995). Integrating customer requirements into product designs. J PROD INNOV MANAG. 12: 3-15.

Baker, B., (2009). Re-inventing the ride. The Engineer. 15-28. June 22-23. 2009.

Balendra, G., et al., (2007). Injuries in amateur horse racing (point to point racing) in Great Britain and Ireland during 1993-2006. Br. J. Sports Med. 41:162-166. doi:10.1136/bjsm.2006.033894. http://bjsm.bmj.com/content/41/3/162.full (Accessed February 13, 2009).

Bardell, R., et al., (2003). Accuracy analysis of 3D data collection and free-form modelling methods. Journal of Materials Processing Technology. 133: 26-33.

Barnsby (n.d.)., Xtreem Jumping Saddle. http://www.barnsby.com/products/saddles-xtreem-jumping-saddle/default.asp (Accessed 14 October 2010).

Barton v. Irish, The 2002 Minnesota Court of Appeals, Unpublished. WL 51056920.

Basciftci, et al., (2004). Biomechanical evaluation of mandibular midline distraction osteogenesis by using the finite element method. American Journal of Orthodontics and Dentofacial Orthopedics. 125 (6): 706-715.

Bates, R. G., (1976). Saddle tree. Australia, Bates R. G. AU Patent 7135374: 1-8.

Baxter, M. R., (1995). Product Design: Practical methods for the systematic development of new products. CRC Press.

Bayliss, H. J., (1958). Improvements relating to wooden saddle trees. United Kingdom, George Sheldon Walsall Ltd. GB Patent 796301: 1-6.

Beatie, R. H., (1981). Saddles. Norman, University of Oklahoma Press.

Beebee, J., and Beebee, B., (1908). Improvements in or connected with Saddle Trees. United Kingdom, Beebee John and Beebee Benjamin. GB Patent

190820213: 1-2.

Beekman, W. J., et al., (2003). Failure mechanism determination for industrial granules using a repeated compression test. Powder Technology. 130: 367 – 376.

Belton, G. P., (2006). Tree for a saddle, an insert for a saddle tree and a saddle tree body. United States of America. U.S. Patent 2006179799: 1-11.

Benzley, S. E., et al., (1995). Pre- and post-processing for the finite element method. Finite Elements in Analysis and Design. 19: 243 – 260.

Berenberg, B. J., (1989). Composite Materials. In Young, W. C., and Budynas, R. G., 7th ed. Roark's Formulas for Stress and Strain. (2001) pp 827 – 840. McGraw-Hill: New York, USA. (Online) Available at: http://site.ebrary.com/lib/wolverhampton/docDetail.action?docID=10180048 (Accessed 02 June 2009).

Biewener, A. A., and Taylor, C. R. (1986). Bone strain: a determinant of gait and speed? J. Exp. Biol. 123: 383 – 400.

Billington, G., (2006). Saddle Fitting Essentials. 2nd Ed. Lorien Stable Press.

Blouet, E. and Beaumont, I., (2004). The Conservation of a 16th-century War Saddle. In Gilmour L. A. ed. *In the Saddle: An exploration of the saddle through history*. Archetype Publications, London, 2004, pp. 43-52.

Bobbert, M. F., et al., (2005). Can jumping capacity of adult show jumping horses be predicted on the basis of submaximal free jumps at foal age? A longitudinal study. The Veterinary Journal. 170:212-221.

Bonet, J., and Wood, R. D. (1997). Nonlinear continuum mechanics for finite element analysis. Cambridge university press: United Kingdom.

Bressel, E., and Cronin, J., (2005). Bicycle seat interface pressure: reliability, validity, and influence of hand position and workload. Journal of Biomechanics 38: 1325-1331.

Bretos, J., et al., (1999). Finite element analysis and experimental measurements of natural eigenmodes and random responses of wooden bars used in musical instruments. Applied Acoustics. 56(3): 141-156.

Brezovic, M., et al., (2003). Bending Properties of Carbon Fiber Reinforced Plywood. Wood Research (Bratislava). 48(4): 13-24.

British Horse Industry Confederation (BHIC) (2005). Strategy for the Horse Industry in England and Wales, The Department for Environment, Food and Rural Affairs (Defra).

British Standards Institution BSi (1996). Specification for saddle trees made from synthetic materials BS 7875:1996. Retrieved August 2, 2006, from the British Standards Online database, Standards policy and strategy committee.

British Standards Institution BSi (2003). Manufacture of saddle trees made from wood - Specification BS 6635:2003. Retrieved August 2, 2006, from the British Standards Online database, Standards policy and strategy committee.

British Standards Institution BSi (2009). Synthetic saddle trees – Specification BS 7875:2009. Retrieved February 28, 2010, from the British Standards Online database, Standards policy and strategy committee.

British Standard European Norm BS EN (2005). High performance helmets for equestrian activities. BS EN 14572:2005. Retrieved July, 19, 2007, from the British Standards Online database, Standards policy and strategy committee.

Brunnermeier, S. B., and Martin, S. A., (1999). Interoperability Cost Analysis of the U.S. Automotive Supply Chain. Research Triangle Institute (7007-03). (Online) Available at: http://www.rti.org/pubs/US_Automotive.pdf (Accessed 02 June 2009).

Bryan, W. J., (1999). Introduction to Finite Element Methods. Instructor's Guide. American Society of Mechanical Engineers, Career Development Series "Education for Growth". (Online) Available at: http://files.asme.org/MyASME/CareerSeries/18456.pdf (Accessed 08 August 2009).

Budak, I., et al., (2005). Development of a programme system for data-point pre-processing in Reverse Engineering. Journal of Materials Processing Technology. 162-163: 730-735.

Burgess, S. C., (1998). The modern Olympic vaulting pole. Materials and Design. 19: 197-204.

Buriol, T. M., and Scheer, S., (2008). CAD and CAE Integration Through Scientific Visualization Techniques for Illumination Design. Tsinghua Science and Technology. 13(S1): 26-33.

Butler, D. M., (1967). Saddletrees. United kingdom, Aulton & Butler Ltd. GB Patent 1063708: 1-3.

Butler, J. H., (1909). Improvements in Saddle Trees. United Kingdom, Butler John Henry. GB Patent 190904509: 1-6.

Butler, R. J., et al., (2003). Lower extremity stiffness: implications for performance and injury. Clinical Biomechanics. 18: 511-517.

Caceres, C. H., (2009). Transient environmental effects of light alloy substitutions in transport vehicles. Materials and Design. 30: 2813-2822.

Carcone, S. M., and Keir, P. J., (2007). Effects of backrest design on biomechanics and comfort during seated work. Applied Ergonomics 38(6): 755-764.

Carfagni, M., et al., (2007). Comfort assessment of motorcycle saddles: a methodology based on virtual prototypes. Int J Interact Des Manuf. 1(3):155-167.

Carrillo, E. H., et al., (2007). Traumatic injuries associated with horseback riding. Scandinavian Journal of Surgery 96: 79-82.

Casciati, S., and Domaneschi, M., (2007). Random imperfection fields to model the size effect in laboratory wood specimens. Structural safety. 29: 308 – 321.

Cauchick-Miguel, P. A., and King, T. G., (1998). Factors which influence CMM touch trigger probe performance. Int. J. Mach. Tools Manufact. 38 (4): 363-374.

CES EduPack 2005. The Cambridge Engineering Selector, Granta Design, Cambridge.

Chang, C-L., and Yang, S-H., (2009). Simulation of wheel impact test using finite element method. Engineering Failure Analysis. 16: 1711-1719.

Chatiri, M., et al., (2009). An assessment of the new LS-DYNA layered solid element: basics, patch simulation and its potential for thick composite structure analysis. 7th European LS-DYNA Conference. (Online) Available at: http://www.dynamore.de/documents/papers/euro2009/B-IV-01.pdf (Accessed 03 July 2009).

Cheng, F-T., and Perng, D-B., (1999). A systematic approach for developing a foot size information system for shoe last design. International Journal of Industrial Ergonomics. 25: 171-185.

Cheng, Z. Q., et al., (2001). Experiences in reverse-engineering of a finite element automobile crash model. Finite Elements in Analysis and Design. 37: 843-860.

Cheung, G., et al., (2004). Finite element analysis of a femoral retrograde intramedullary nail subject to gait loading. Medical Engineering & Physics. 26: 93-108.

Childs, P. R. N., (2004). Mechanical Design. 2nd ed. Elsevier Butterworth-Heinemann. Oxford.

Chiu, C-H., et al., (2007). An experimental investigation into the mechanical behaviors of helical composite springs. Composite Structures. 77: 331-340.

Cho, Y-B., and Averill, R. C., (1997). An improved theory and finite-element model for laminated composite and sandwich beams using first-order zig-zag sublaminate approximations. Composite Structures. 37: 281-298.

Chong, et al., (2007). Automatic mesh-healing technique for model repair and finite element model generation. Finite Elements in Analysis and Design. 43: 1109-1119.

Clayton, H. M., et al., (2010). Pressure on the horse's withers with three styles of blanket. The Veterinary Journal. 184: 52-55.

Clough, R. W., (1980). The finite element method after twenty-five years: a personal view. Computers & Structures. 12 (4): 361 – 370.

Chatterjee, P., et al., (2009). Selection of materials using compromise ranking and outranking methods. Materials and Design. 30: 4043-4053.

Chivate, P. N., and Jablokow, A. G., (1995). Review of surface representations and fitting for reverse engineering. Computer Integrated Manufacturing Systems. 8 (3): 193-204.

Colomb, F., et al., (2008). Seismic retrofit of reinforced concrete short columns by CFRP materials. Composite Structures. 82: 475-487.

Cottone, A., et al., (2007). Delamination study of through-thickness reinforced composite laminates via two-phase interface model. Composites: Part A. 38: 1985-1995.

Davalos, J. F., and Qiao, P., (1999). A computational approach for analysis and optimal design of FRP beams. Computers and Structures. 70: 169-183.

Davis, C., (2007). Gaining a competitive edge. Materials Today. 10(1-2): 60.

Davis, S., (1898). Improvements in the construction of saddle trees. United kingdom, Davis Samuel. GB Patent 189722272: 1-3.

Dawson, J. M., et al. (1999). Analysis of the structural behavior of the pelvis during lateral impact using the finite element method. Accident analysis and prevention. 31: 109 – 119.

De Cocq, P., et al., (2004). Effects of girth, saddle and weight on movements of the horse. Equine Vet Journal 36 (8): 758 – 763.

De Cocq, P., et al., (2006). Saddle pressure measuring: Validity, reliability and power to discriminate between saddle-fits. The Veterinary Journal 172: 265-273

De Cocq, P. et al., (2008). Usability of normal force distribution measurements to evaluate asymmetrical loading of the back of the horse and different rider positions on a standing horse. The Veterinary Journal. Doi:10.1016/j.tvjl.2008.03.002.

De Cocq, P., et al., (2010). Vertical forces on the horse's back in sitting and rising trot. Journal of Biomechanics. 43: 627-631.

De Moura, M. F. S. F., et al., (2009). Numerical analysis of the Edge Crack Torsion test for mode III interlaminar fracture of composite laminates. Engineering Fracture Mechanics. 76: 469 – 478.

Deng, Y. –M., and Edwards, K. L., (2007). The role of materials identification and selection in engineering design. Materials and Design. 28: 131-139.

Denoix, J. M., and Audigie, F., (2001). The Neck and Back. In Back, W., and Clayton, H. M., ed. Equine Locomotion, W. B. Saunders, pp. 167-191.

Department of Defense and the Federal Aviation Administration, (1999). The Composite Materials Handbook – MIL 17 Volume 3: Materials Usage, Design, and Analysis. Technomic Publishing Company, Inc. and Materials Sciences Corporation, American Society for Testing and Materials.

Dobosz, M., and Wozniak, A., (2005). CMM touch trigger probes testing using a reference axis. Precision Engineering. 29: 281-289.

Doyle, B. J. et al., (2009). Experimental modelling of aortic aneurysms: Novel applications of silicone rubbers. Medical Engineering & Physics. 31: 1002-1012.

Drewniak, E. I., et al., (2007). Accuracy of circular contact area measurements with thin-film pressure sensors. Journal of Biomechanics. doi: 10.1016/j.jbiomech.2006.12.002.

Dutta, A., and Talukdar, S., (2004). Damage detection in bridges using accurate modal parameters. Finite Elements in Analysis and Design. 40: 287-304.

Eagar, P., et al., (2001). A method for quantifying the anterior load-displacement behavior of the human knee in both the low and high stiffness regions. Journal of Biomechanics. 34: 1655 – 1660.

Edwards, E. H., (1990). The Saddle. J. A. Allen & Company Ltd.

Edwards, E. H., (1994). Encyclopedia of the horse. London: Dorling Kindersley Limited.

Edwards, K. L., (1998). A designers' guide to engineering polymer technology. Materials and Design. 19: 57-67.

Edwards, K. L., and Deng, Y. –M., (2007). Supporting design decision-making when applying materials in combination. Materials and Design. 28: 1288-1297.

Eitzen, I., (2004). Pressure mapping in seating: A frequency analysis approach. Archives of physical medicine and rehabilitation 85(7): 1136-1140.

Ekh, J., and Schon, J., (2008). Finite element modeling and optimization of load transfer in multi-fastener joint using structural elements. Composite Structures. 82: 245-256.

Eugene, R. I., (1999). Stiffness and Damping in Mechanical Design. Marcel Dekker Inc. New York.

Evans, J. W., et al. (1990). The Horse. New York: W. H. Freeman and Company.

Evans, D. L., et al., (1995). Performance-related Problems and Exercise Physiology. In Higgins, A. J. and Wright, I. M. ed. The Equine Manual, 1995, W. B.

Saunders Company Ltd, pp. 921-966.

Faber, M., et al. (2001). Three dimensional kinematics of the equine spine during canter. Equine veterinary journal. Supplement . 33: 145-149.

Fam, A., and Son, J-K., (2008). Finite element modeling of hollow and concrete-filled fiber composite tubes in flexure: Optimization of partial filling and a design method for poles. Engineering Structures. 30 (10): 2667-2676.

Fan, L. Q., et al., (2008). Development of a distributed collaborative design framework within peer-to-peer environment. Computer-Aided Design. 40: 891-904.

Fatt, M. S. H., and Ouyang, X., (2007). Integral-based constitutive equation for rubber at high strain rates. International Journal of Solids and Structures. 44: 6491-6506.

Fatt, M. S. H., and Ouyang, X., (2008). Three-dimensional constitutive equations for Styrene Butadiene Rubber at high strain rates. Mechanics of Materials. 40: 1-16.

Fernandez, A. I., et al., (2010). Selection of materials with potential in sensible thermal energy storage. Solar Energy Materials & Solar Cells. 94: 1723-1729.

Finnish Forest Industries Federation, (2002). Handbook of Finnish Plywood. Finnish Forest Industries Federation, Finland. ISBN 952-9506-63-5.

Forero Rueda, M. A., et al. (2009). Optimisation of energy absorbing liner for equestrian helmets. Part 1: Layered foam liner. Materials and Design. 30: 3405-3413.

Forest Products Laboratory (1999). Wood handbook – Wood as an engineering material. General Technical Report FPL-GTR-113. (Online) Available at: http://www.fpl.fs.fed.us/documnts/fplgtr/fplgtr113/fplgtr113.pdf (Accessed 17 April 2009).

Foucault, G., et al., (2008). Adaptation of CAD model topology for finite element analysis. Computer-Aided Design. 40: 176-196.

Fruehwirth, B., et al. (2004). Evaluation of pressure distribution under an English saddle at walk, trot and canter. Equine Veterinary Journal 36 (8): 754-757.Gilmour L. (2004). Saddles of the Stuart Period. In Gilmour L. A. ed. In: The Saddle: An exploration of the saddle through history. London: Archetype Publications, 2004, pp. 67-82.

Fuchs, E. R. H., et al., (2008). Strategic materials election in the automobile body: Economic opportunities for polymer composite design. Composites Science and Technology. 68: 1989-2002.

Galicki, J., and Czech, M., (2005). Tensile strength of softwood in LR orthotropy plane. Mechanics of Materials. 37: 677-686.

Garimella, R. V., (2002). Mesh Data Structure Selection for Mesh Generation and FEA Applications. International Journal of Numerical Methods in Engineering. 55(4): 451-478.

Garratt, G. A., (1931). The Mechanical Properties of Wood: Including a Discussion of the Factors Affecting the Mechanical Properties, Working Stresses for Structural Timber, and Methods of Timber Testing. London: Chapman & Hall Limited.

Gibson, R. F. (1994). Principles of Composite Material Mechanics. International editions. New York: McGraw-Hill, Inc.

Gilardi, G., and Sharf, I., (2002). Literature survey of contact dynamics modelling. Mechanism and machine theory. 37: 1213-1239.

Gilmour, L. (2004). Saddles of the Stuart Period. In Gilmour L. A. ed. In the Saddle: An exploration of the saddle through history. Archetype Publications, London, 2004, pp. 67-82.

Gomis-Bellmunt, O. and Campanile, L. F., (2010). Design Rules for Actuators in Active Mechanical Systems. London. Springer-Verlag.

Gordon, J., (2001). The Horse Industry - Contributing to the Australian Economy, Rural Industries Research and Development Corporation.

Groenwold, A. A., and Haftka, R. T., (2006). Optimization with non-homogenous failure criteria like Tsai-Wu for composites lainates.

Gurdal, Z. et al., (1999). Design and optimization of laminated composite materials. John Wiley & Sons.

Hadland, T., (2009). The spaceframe Moultons. LIT VERLAG, Dr. W. Hopf Berlin.

Hall, J. L., et al. (2009). Second generation prototype design and testing for a high altitude Venus balloon. Advances in Space Research. 44: 93-105.

Hammond, W. B., and Peltier, J. M., (1988). Scientific Computation. In Sibilia, J. P., ed. (1988). A Guide to Materials Characterization and Chemical Analysis. 2nd ed. Verlag GmbH: Wiley-VCH, pp. 353-376.

Hardwick, J. E., (1936). Improvements in and relating to saddles. United Kingdom, John Edward Hardwick. GB Patent 449159: 1-2.

Hariharan, K., and Balaji, C., (2009). Material optimization: A case study using sheet metal-forming analysis. Journal of Materials Processing Technology. 209: 324-331.

Harman, J., (2009). Integrative therapies in the treatment of back pain. In Henson F. M. D., ed. Equine back pathology: diagnosis and treatment. 2009, Blackwell Publishing Ltd. West Sussex: United Kingdom, pp. 235-248.

Harman, J. C. (1995). Practical Saddle Fitting, part 2. The Equine Athlete. 8(3): 14-17.

Harman, J. C., et. al., (2004). The Horse's Pain-free Back and Saddle-fit Book. Illustrated Ed. Trafalgar Square BooksHayes M. H., (2008). Riding And Hunting. Hoar Press.

Hausberger, M., et al., (2008). A review of the human-horse relationship. Applied Animal Behaviour Science. 109: 1-24.

Hawileh, R. A., et al., (2010). Nonlinear finite element analysis and modeling of a precast hybrid beam-column connection subjected to cyclic loads. Applied mathematical modeling. 34: 2562 – 2583.

Hayes, M. H., (2008). Riding And Hunting. Read books.

Heidenfelder, J., et al., (2006). Mechanical properties of different midsole materials in running shoes. Journal of Biomechanics. 39 (Suppl 1): S550.

Hellen, T., (2003). How To Use Elements Effectively. Glasgow: NAFEMS Ltd.

Henley Centre (2004). A report of research on the horse industry in Great Britain, Department for Environment, Food and Rural Affairs.

Her, S-C., and Liang, Y-C., (2004). The finite element analysis of composite laminates and shell structures subjected to low velocity impact. Composite Structures. 66: 277-285.

Herencia, J. E., et al., (2008). Initial sizing optimisation of anisotropic composite panels with T-shaped stiffeners. Thin-Walled Structures. 46: 399-412.

Hickling, L. (2004). The Saddle of Henry V at Westminster Abbey Library. In Gilmour L. A. ed. In the Saddle: An exploration of the saddle through history. Archetype Publications, London, 2004, 39-41.

Hitchen, J. (2006). Adjustable saddle tree. United Kingdom, Jabez Cliff & Company Ltd. GB Patent 2423230: 1-24.

Hodges, P. W., et al., (2005). Intra-abdominal pressure increases stiffness of the lumbar spine. Journal of Biomechanics. 38: 1873 – 1880.

Hole, S. L., et al., (2002). A note on the linear and temporal stride kinematics of Olympic show jumping horses between two fences. Applied Animal Behaviour Science. 75: 317-323.

Holmes, M., and Jeffcott, L., (2010). Editorial – Equitation science, rider effects, saddle and back problems in horses: Can technology provide the answer? The Veterinary Journal. 184: 5-6.

Hopkins, P., (2005). Benchmarks for Membrane and Bending Analysis of Laminated Shells. Part 1: Stiffness Matrix and Thermal Characteristics. Glasgow:

NAFEMS Ltd.

Hostens, I., et al. (2001). Buttock and back pressure distribution tests on seats of mobile agricultural machinery. Applied Ergonomics 32(4): 347-355.

Hughes, D, A., (1992). Analysis of bird impact on fan blade leading edges. Ph.D. St. Hugh's College, Oxford.

Humphries, K., (1998). Saddle Fitting. Illustrated Ed. J. A. Allen.

Iba K. et al. (2001). Horse-related injuries in a thoroughbred stabling area in Japan. Arch Orthop Trauma Surg 121: 501-504.

Ivanyi, P., and Ivanyi, M. Jr., (2009). On the simulation of failure mechanisms in steel structures. Advances in engineering software. 40: 871 – 882.

Jain, L. K., and Mai, Y-W., (1995). Determination of Mode II Delamination Toughness of Stitched Laminated Composites. Composites Science and Technology. 55: 241-253.

Jaksic, N., and Nilsson, K. F., (2009). Finite element modelling of the one meter drop test on a steel bar for CASTOR cask. Nuclear Engineering and Design. 239: 201:213.

Javidrad, F., and Rahmati, R., (2009). An integrated re-engineering plan for the manufacturing of aerospace components. Materials and Design. 30: 1524-1532.

Jeffcott, L. B., (1975). (2) The Diagnosis of Diseases of the Horse's Back. Equine Veterinary Journal. 7 (2): 69-78.

Jeffcott, L. B., (1979). Back Problems in the Horse – A look at past, present and future progress. Equine Veterinary Journal 11 (3): 129 – 136.

Jeffcott, L. B., and Dalin, G., (1980). Natural rigidity of the horse's backbone. Equine Veterinary Journal. 12(3): 101-108.

Jeffcott, L. B., et al., (1999). Validity of saddle pressure measuremnts using force-sensing array technology - Preliminary studies. The Veterinary Journal 158(2): 113-119.

Jeffcott, L. B., (2009). The normal anatomy of the osseous structure of the back and pelvis. In Henson F. M. D., ed. Equine back pathology: diagnosis and treatment. 2009, Blackwell Publishing Ltd. West Sussex: United Kingdom, pp. 3-15.

Johnson, A. F., et al., (2001). Computational methods for predicting impact damage in composite structures. Composites Science and Technology. 61: 2183-2192.

Johnston, C., et al., (2004). Kinematic evaluation of the back in fully functioning riding horses. Equine Veterinary Journal. 36 (6): 495-498.

Karana, E., et al., (2010). A tool for meaning driven materials selection. Materials and Design. 31: 2932-2941.

Karger, L., et al., (2007). Rapid simulation of impacts on composite sandwich panels inducing barely visible damage. Composite Structures. 79: 577-534.

Karger, L., et al., (2008). Efficient simulation of low-velocity impacts on composite sandwich panels. Computers and Structures. 86: 988-996.

Karger, L., et al., (2009). Evaluation of impact assessment methodologies. Part I: Applied methods. Composites: Part B. 40: 65-70.

Karlsson, et al., (1998). Black box engineering: Redefining the role of product specifications. J PROD INNOV MANAG. 15: 534-549.

Karvinen, K. G., and Pegg, N. G., (2006). A simplified method for nonlinear failure analysis of stiffened plates. Marine structures. 19: 97 – 109.

Keefer, S. L., (1996). Hwaer Cwom Mearh? The Horse in Anglo-Saxon England. Journal of Medieval History. 22 (2): 115 - 134.

Khabbaz, R. S., et al., (2009). A simplified fuzzy logic approach for materials selection in mechanical engineering design. Materials and Design. 30: 687-697.

Khanal, M., et al., (2008). Compression and impact loading experiments of high strength spherical composites. Int. J. Miner. Process. 86: 104 – 113.

Khashaba, U. A., et al., (2006). Effect of washer size and tightening torque on the performance of bolted joints in composite structures. Composite Structures. 73: 310 – 317.

Khoei, A. R., (2002). An integrated software environment for finite element simulation of powder compaction processes. Journal of Materials Processing Technology. 130 – 131: 168 – 174.

Kim, Y., et al., (1997). Delamination buckling of FRP layer in laminated wood beams. Composite Structures. 37 (3/4): 311-320.

Korochkina, T. V., et al., (2008). Experimental and numerical investigation into nonlinear deformation of silicone rubber pads during ink transfer process. Polymer Testing. 27: 778 – 791.

Koc, M., et al., (2000). The use of FEA and design of experiments to establish design guidelines for simple hydroformed parts. International Journal of Machine Tools and Manufacture. 40: 2249-2266.

Kollmann, F. F. P., et al., (1975). Principles of Wood Science and Technology II. Springer Verlag.

Kong, X. Q., and Wu, C. W., (2009). Measurement and prediction of insertion force for the mosquito fascicle penetrating into human skin. Journal of Bionic

Engineering. 6: 143 – 152.

Kouchakzadeh, M., A and Sekine H., (2000). Compressive buckling analysis of rectangular composite laminates containing multiple delaminations. Composite Structures. 50:249-255.

Kramer, M., et al., (2005). Laboratory experiments on low-crested breakwaters. Coastal engineering. 52: 867 – 885.

Krishnamurthy, K. S., et al., (2001). A parametric study of the impact response and damage of laminated cylindrical composite shells. Composites Science and Technology. 61: 1655-1669.

Krishnamurthy, K. S., et al., (2003). Impact response and damage in laminated composite cylindrical shells. Composite Structures. 59: 15-36.

Kurtoglu, T., and Campbell, M. I., (2009). An experimental study on the effects of a computational design tool on concept generation. Design Studies. 30: 676-703.

Kweon, S., and Medeiros, D. J., (1998). Part orientations for CMM inspection using dimensioned visibility maps. Computer-Aided Design. 30 (9): 741-749.

Kyung, G., and Nusbaum, M. A., (2008). Driver sitting comfort and discomfort (part II): Relationships with and prediction from interface pressure. International Journal of Industrial Ergonomics. 38: 526-538.

Lacoste, M., et al., (2006). Assessment of Seated Postural Control in Children: Comparison of a Force Platform Versus a Pressure Mapping System. Arch Phys Med Rehabil. 87: 1623-1629.

Lai, C. H. Y., and Li-Tsang, C. W. P., (2009). Validation of the Pliance X System in measuring interface pressure generated by pressure garment. BURNS. 35: 845-851.

Lakshmininarayana, H., (2004). Finite Elements Analysis: Procedures in Engineering. Orient Blackswan.

Lam, F., et al., (2004). Structural performance of wood-based stair stringers. Forest Products Journal. 54(4): 39-44.

Lang, E. M., and Fodor, T., (2002). Finite Element Analysis of Cross-Halved Joints for Structural Composites. Wood and Fiber Science. 34(2): 251-265.

Lappan, A., (1904). Improvements in riding saddles. United Kingdom, Lappan Adam. GB Patent 190324919: 1-3.

Lawry, M. H., (2003). I-Deas Student Guide. 2nd edition. Electronic Data Systems Corporation, EDS. McGraw-Hill.

Lee, C-H., and Chang, K-H., (2009). A computational procedure for evaluating the J-integral for mode I crack in welds: A 3-D finite element analysis.

Computational Materials Science. 46(1): 186-192.

Lena, P. D., and Margara, L., (2010). Optimal global alignment of signals by maximization of Pearson correlation. Information processing letters. 110: 679 – 686.

Leski, A., (2007). Implementation of the virtual crack closure technique in engineering FE calculations. Finite Elements in Analysis and Design. 43: 261-268.

Li, X., et al., (2009). On surface reconstruction: A priority driven approach. Computer-Aided Design. 41(9): 626-640.

Liang, C-C., et al., (2005). Optimum design of dome contour for filament-wound composite pressure vessels based on a shape factor. Composite Structures. 58: 469-482.

Licka, T., et al., (2001). Range of back movement at trot in horses without back pain. Equine Veterinary Journal Supplement. 33: 150-153.

Licka, T. and Peham, C., (1998). An objective method for evaluating the flexibility of the back of standing horses. Equine Veterinary Journal 30(5): 412-415.

Lin, A. C., et al., (1998). Automated sequence arrangement of 3D point data for surface fitting in reverse engineering. Computers in Industry. 35:149-173.

Lin, B-T., and Kuo, C-C., (2009). Application of an integrated RE/RP/CAD/CAE/CAM system for magnesium alloy shell of mobile phone. Journal of Materials Processing Technology. 209(6): 2818-2830.

Lin, C-L., et al., (2008). Multi-factorial analysis of a cusp-replacing adhesive premolar restoration: A finite element study. Journal of Dentistry. 36: 194-203.

Lin, D., et al., (2009). Dental implant induced bone remodeling and associated algorithms. Journal of the Mechanical Behavior of Biomedical Materials. 2(5): 410-432.

Liswaniso, D., (2001). A study of pressure patterns beneath the saddle of riding horses using force sensing array (FSA) technology. Fitzwilliam College, Cambridge. PhD.

Liu, Y., et al., (2009). Comparing drop impact test method using strain gauge measurements. Microelectronics Reliability. 49: 1299-1303.

Livingston, E. H., (2003). Who was Student and why do we care so much about his *t*-Test?. Journal of surgical research. 118: 58 – 65.

Lopes, C. S., et al., (2009). Low-velocity impact damage on dispersed stacking sequence laminates. Part I: Experiments. Composites science and technology. 69: 926-936.

Luo, R. K., and Wu, W. X., (2006). Fatigue failure analysis of anti-vibration rubber spring. Engineering Failure Analysis. 13: 110-116.

Lopes, C. S., et al., (2009). Low-velocity impact damage on dispersed stacking sequence laminates. Part II: Numerical simulations. Composites Science and Technology. 69: 937-947.

Madenci, E., and Guven, I., (2006). The Finite Element Method and Applications in Engineering Using ANSYS®. New York. Springer Science+Business Media, LLC.

Mackerle, J., (2005). Finite element analysis in wood research: a bibliography. Wood Science and Technology 39(7): 579-600.

MacLoed, I. A., (2005). Modern structural analysis: modeling process and guidance. Thomas Telford.

Mahdi, E., et al., (2006). Light composite elliptic springs for vehicle suspension. Composite Structures. 75: 24-28.

Malinowski, K., and Luba, N., (2004). The Equine Industry - Economic and Societal Impact. In: Scanes C. G. and Miranowski J. A., ed. Perspectives in World Food and Agriculture 2004. Iowa State Press, 2004, pp. 187-203.

Maniya, K., and Bhatt, M. G., (2010). A selection of material using a novel type decision-making method: Preference selection index method. Materials and Design. 31: 1785-1789.

Mankame, N. D., and Ananthasuresh, G. K., (2004). Topology optimization for synthesis of contact-aided compliant mechanics using regularized contact modeling. Computers and Structures. 82: 1267 – 1290.

Mao, S., et al., (2010). Off-highway heavy-duty truck under-hood thermal analysis. Applied thermal engineering. 30: 1726 – 1733.

MaoHong, Y., (2004). Unified strength theory and its applications. Berlin; London: Springer-Verlag.

Mars, W. V., and Fatemi, A., (2002). A literature survey on fatigue analysis approaches for rubber. International Journal of Fatigue. 24: 949-961.

Marsden, W., and Irving, D., (2002). How To Analyse Composites. Glasgow: NAFEMS Ltd.

Matejicek, J., et al., (2004). Residual stresses in cold-coiled helical compression springs for automotive suspensions measured by neutron diffraction. Materials Science and Engineering: A. 367: 306-311.

Maxim, R. E., et al., (2006). Predicting dynamic failure of dense granules from static compression tests. Int. J. Miner. Process. 79: 188-197.

McCarthy, M. A., et al., (2005). Three-dimensional finite element analysis of single-bolt, single-lap composite joints: part I – model development and validation. Composite Structures. 71: 140 – 158.

McLester, J., and St. Pierre, P., (2008). Applied Biomechanics: Concepts and Connections. Thomson Wadsworth. Canada.

Mehta C., and Patel, N. R., (1996). SPSS Exact Tests™ for Windows®. SPSS Inc. Chicago, USA.

Menq, C., and Chen, F. L., (1996). Curve and surface approximation from CMM measurement data. Computers Ind. Engng. 30 (2): 211-225.

Meschan, E. M, et al., (2007). The influence of the width of the saddle tree on the forces and the pressure distribution under the saddle. The Veterinary Journal. 173(3): 578-584.

Miller, K., et al., (2000). Mechanical properties of brain tissue in-vivo: experiment and computer simulation. Journal of Biomechanics. 33: 1369-1376.

Miller, W. S., et al., (2000). Recent development in aluminium alloys for the automotive industry. Materials Science and Engineering: A. 280: 37-49.

Mohsenimanesh, A., et al., (2009). Stress analysis of a multi-laminated tractor tyre using non-linear 3D finite element analysis. Materials and Design. 30: 1124-1132.

Morio, C., et al. (2009). The influence of footware on foot motion during walking and running. Journal of Biomechanics. 42: 2081-2088.

Moses, D. M., and Prion, H. G. L., (2004). Stress and failure analysis of wood composites: a new model. Composites Part B: Engineering 35(3): 251-261.

Moss, P. M., et al. (2002). A changing pattern of injuries to horse riders. Emergency Medicine Journal. 19: 412-414.

MSC.Software, (2000). MSC.Marc New Features Guide, Version 2000. MSC.Software Corporation.

MSC.Software, (2004). MSC.Marc Volume B: Element Library. Version 2005. MSC.Software Corporation.

MSC.Software, (2004). MSC.Marc Volume C: Program Input. Version 2005. MSC.Software Corporation.

MSC.Software, (2005). MSC.Patran 2005 r2 Reference Manual. Part 3: Finite Element Modelling. MSC.Software Corporation.

MSC.Software, (2007). Marc 2007 r1. Volume B: Element Library. MSC.Software Corporation.

MSC.Software, (2008). MD Nastran R3 Explicit Nonlinear (SOL 700) User's Guide. Volume 1. MSC.Software Corporation.

MSC.Software, (2008a). MSC.Laminate Modeler, Version 2008, User's Guide. MSC.Software Corporation.

MSC.Software, (2008b). Marc 2008 r1. Volume B: Element Library. MSC.Software Corporation.

MSC.Software, (2008). Marc 2008 r1. Volume C: Program Input. MSC.Software Corporation.

MSC.Software, (2008). Marc® 2008 r1. User's guide. Volume 1. MSC.Software Corporation.

MSC.Software, (2010). Marc 2010 Volume E: Demonstration problems. MSC.Software Corporation.

Muller, U., et al., (2003). Effects of cell anatomy on t he plastic and elastic behaviour of different wood species loaded perpendicular to grain. IAWA Journal. 24(2):117-128.

Naik, G. N., and Murty, A. V. K., (1999). A failure mechanism-based approach for design of composite laminates. Composite Structures. 45: 71-80.

Naik, N. K., and Meduri, S., (2001). Polymer-matrix composites subjected to low-velocity impact: effect of laminate configuration. Composites Science and Technology. 61: 1429-1436.

Naveiro, R. M., and Pereira, R. C., (2008). Design education in Brazil. Design Studies. 29: 304-312.

Ness, J. R. (2006). A Device For A Saddle Tree. W. I. P. Organisation, Suldal Hestesenter and Ness John Ragnvald. WO Patent 2006083174: 1-16.

Nguyen, V. B., et al., (2009). Mechanical properties of single alginate microspheres determined by microcompression and finite element modelling. Chemical Engineering Science. 64: 821-829.

Nicholls, F. (1935). Improvements in trees of riding saddles. United Kingdom, Frank Nicholls. GB Patent 426580.

Ning, H., et al., (2007). Thermoplastic sandwich structure design and manufacturing for the body panel of mass transit vehicle. Composite Structures. 80: 82-91.

Ning, H., et al., (2009). Design and development of thermoplastic composite roof door for mass transit bus. Materials and Design. 30: 983-991.

Noels, L., et al., (2002). Automatic time stepping algorithms for implicit numerical simulations of non-linear dynamics. Advances in Engineering Software. 33: 589 – 603.

Nohut, S., and Schneider, G. A., (2009). Failure probability of ceramic coil springs. Journal of the European Ceramic Society. 29: 1013-1019.

Ochola, R. O., et al., (2004). Mechanical behaviour of glass and carbon fibre reinforced composites at varying strain rates. Composite Structures. 63: 455-467.

Oleson, M., et al., (2005). A comparison of forefoot stiffness in running and running shoe bending stiffness. Journal of Biomechanics. 38: 1886-1894.

Olsson, R. (2003). Closed form prediction of peak load and delamination onset under small mass impact. Composite Structures. 59: 341-349.

Omkar, S. N., et al., (2008a). Artificial immune system for multi-objective design optimization of composite structures. Engineering Applications of Artificial Intelligence. 21: 1416-1429.

Omkar, S. N., et al., (2008b). Vector evaluated particle swarm optimization (VEPSO) for multi-objective design optimization of composite structures. Computers and Structures. 86: 1-14.

Orifici, A. C., et al., (2008). Compression and post-buckling damage growth and collapse analysis of flat composite stiffened panels. Composites Science and Technology. 68: 3150-3160.

Osawa, S., et al., (2002). Development of a ball step-gauge and an interferometric stepper used for ball-plate calibration. Journal of the International Societies for Precision Engineering and Nanotechnology. 26: 214-221.

Osnes, H., and McGeorge, D., (2009). Experimental and analytical strength analysis of double-lap joints for marine applications. Composites: Part B. 40: 29-40.

Otto, K. N., and Wood K. L., (1996). A reverse engineering and redesign methodology for product evolution. ASME Design Engineering Technical Conferences and Design Theory and Methodology Conference, 96-DETC/DTM-1523. Irvine, California.

Otto, K. N., and Wood K. L., (1998). Product evolution: A reverse engineering and redesign methodology. Research in Engineering Design. 10: 226-243.

Padhi, G. S., et al., (2002). BOLJAT: a tool for designing composite bolted joints using three-dimensional finite element analysis. Composites: Part A. 33: 1573-1584.

Palani Rajan, et al., (2005). An empirical foundation for product flexibility. Design Studies. 26 (4): 405-438.

Palazotto, A. N., et al., (2000). Finite element analysis of low-velocity impact on composite sandwich plates. Composite Structures 49: 209-227.

Pavia, A., and Posnikoff, J. M., (2005). Horses for dummies. 2nd Ed. Wiley Publishing.

Peham, C., et al., (2004). Influence of the rider on the variability of the equine gait. Human Movement Science 23(5): 663-671.

Peham, C., and Schobesberger, H., (2004). Influence of the load of a rider or of a region with increased stiffness on the equine back: a modelling study. Equine Veterinary Journal 36(8): 703-705.

Peham, C., and Schobesberger, H., (2006). A novel method to estimate the stiffness of the equine back. Journal of Biomechanics Volume 39(15): 2845-2849.

Peham, C., et al., (2010). A comparison of forces acting on the horse's back and the stability of the rider's seat in different positions at the trot. The Veterinary Journal. 184: 56-59.

Pellissetti, M. F., and Schueller, G. I., (2009). Scalable uncertainty and reliability analysis by integration of advanced Monte Carlo simulation and generic finite element solvers. Computers and Structures. 87: 930 – 947.

Phatak, N. S., et al., (2009). Strain measurement in the left ventricle during systole with deformable image registration. Medical Image Analysis. 13: 354-361.

Piao, C., et al., (2005). Finite Element Analysis of Wood Laminated Composite Poles. Wood and Fiber Science. 37(3): 535-541.

Powers, P. N. R., and Harrison, A. J., (2000). A study on the techniques used by untrained horses during loose jumping. Journal of equine veterinary science. 20(12): 845-850.

Pokharel, N., and Mahendran, M., (2002). Numerical modelling of sandwich panels subject to local buckling. In Loo, Y-C., et al., ed. Advances in Mechanics of Structures and Materials: Proceedings of the 17th Australasian Conference (ACMSM17), Queensland, Australia, 12-14 June 2002. Taylor & Francis, 2002, pp. 513-520.

Prasad, R. B. K., and Kumar, P. D., (2008). Analysis of composite ENF specimen using higher order beam theories. Thin-Walled Structures. 46: 676-688.

Putti, A. B., et al., (2008). Normal pressure values and repeatability of the Emed® ST4 system. Gait and Posture. 27: 501-505.

Qian, J., and Zhao, Y-P., (2002). Materials selection in mechanical design for microsensors and microactuators. Materials and Design. 23: 619-625.

Qiao, et al., (1998). Modeling and optimal design of composite-reinforced wood railroad crosstie. Composite structures. 41:87-96.

Quantum (n.d.). http://www.quantumsaddle.com/why_quantum/the_saddle (Accessed 14 October 2010).

Qui, K. Q., and Ren, Y. L., (2006). Fabrication and mechanical properties of glassy coil springs. Materials Letters. 60: 1851-1853.

Qureshi, A., et al., (2006). Principles of product flexibility. Proceedings of IDETC/CIE 2006. ASME 2006 International Design Engineering Technical Conferences & Computers and Information in Engineering Conference, DETC 2006-99583. Philadelphia, Pennsylvania.

Ragan, R., et al., (2002). Seat-Interface Pressures on Various Thicknesses of Foam Wheelchair Cushions: A Finite Modeling Approach. Arch Phys Med Rehabil. 83:872-875.

Raju, et al., (2010). Top hat stiffeners: A study on keel failures. Ocean Engineering. 37: 1180-1192.

Ramalhete, P. S., et al., (2010). Digital tools for material selection in product design. Materials and Design. 31: 2275-2287.

Rao, R. V., and Patel, B. K., (2010). A subjective and objective integrated multiple attribute decision making method for material election. Materials and Design. 31: 4738-4747.

Rao, S. S. (1999). The Finite Element Method in Engineering. 3rd ed. Boston (USA). Butterworth Heinemann.

Rao, S. S. (2005). The Finite Element Method in Engineering. 4th ed. Boston (USA). Butterworth Heinemann.

Reddy, G. P. and Gupta, N., (2010). Material selection for microelectronic heat sinks: An application of the Ashby approach. Materials and Design. 31: 113-117.

Reddy, J. N., (2004). Mechanics of Laminated Composite Plates and Shells: Theory and Analysis. 2nd edition. USA: CRC Press.

Riahi, A., and Curran, J. H., (2009). Full 3D finite element Cosserat formulation with application in layered structures. Applied Mathematical Modelling. 33: 3450-3464.

Ribeiro, A. S. et al., (2009). Study of strengthening solutions for glued-laminated wood beams of maritime pinewood. Construction and Building Materials. 23(8): 2738-2745.

Robinson, G. (2001). Horse supply in the English civil war, 1642-1646. The University of Reading. PhD.

Rodman, U., et al., (2008). Exact buckling analysis of composite elastic columns including multiple delamination and transverse shear. Engineering Structures. 30: 1500-1514.

Roe, J. P. et al (2003). Spinal and spinal cord injuries in horse riding: The New South Wales experience 1976-1996. ANZ J. Surg. 73: 331-334.

Roy, R., (2004). Block 3: Creativity and concept design – T211 Design and Designing. The open University, Milton Keynes.

Sapuan, S. M., (2001). A knowledge-based system for materials selection in mechanical engineering design. Materials and Design. 22: 687-695.

Schlacher, C., et al., (2004). Determination of the stiffness of the equine spine. Equine Veterinary Journal. 36 (8): 699-702.

Schmidt, J., and Kaliske, M., (2009). Models of numerical failure analysis of wooden structures. Engineering Structures. 31: 571-579.

Schneller, J., and Subic A.J. (2000). Design of an equestrian stirrup with a bi-directional release mechanism. In Subic A. J. and Haake S., ed. The Engineering of Sport Research, Development and Innovation, 2000, Blackwell Science Ltd, pp. 139-149.

Serrano, E., (2001). Glued-in rods for timber structures – a 3D model and finite element parameter studies. International Journal of Adhession & Adhessives. 21: 115-127.

Setoodeh, A. R., et al., (2009). Low velocity impact analysis of laminated composite plates using a 3D elasticity based layerwise FEM. Journal of Materials and Design. 30(9): 3795-3801.

Shanian, A. and Savadogo, O., (2006). A material selection model based on the concept of multiple attribute decision making. Materials and Design. 27: 329-337.

Shanian, A. and Savadogo, O., (2009). A methodological concept for material selection of highly sensitive components based on multiple criteria decision analysis. Expert Systems with Applications. 36: 1362-1370.

Shelton, F., and Lott, J. W., (2003). Conducting and interpreting interface pressure evaluations of clinical support surfaces. Geriatric Nursing. 24 (4): 222-227.

Silva, M. A. L., et al., (2006). Numerical analysis of the ENF test for mode II wood fracture. Composites: Part A 37: 1334-1344.

Smith, I., et al., (2003). Fracture and fatigue in Wood. John Wiley & Sons, Ltd.

Snodgrass, S. J., et al., (2008). Measuring the posteroanterior stiffness of the cervical spine. Manual Therapy. 13: 520 - 528.

Sokovic, M., and Kopac. J., (2006). RE (reverse engineering) as necessary phase by rapid product development. Journal of Materials Processing Technology. 175: 398-403.

Son, J-K., and Fam, A., (2008). Finite element modeling of hollow and concrete-filled fiber composite tubes in flexure: Model development, verification and investigation of tube parameters. Engineering Structures. 30 (10): 2656-2666.

Son, Y. S., and Baek, J., (2008). A modified correlation coefficient based similarity measure for clustering time-course gene expression data. Pattern recognition letters. 29: 232 – 242.

Spears, I. R., and Miller-Young, J. E., (2006). The effect of heel-pad thickness and loading protocol on measured heel-pad stiffness and a standardized protocol for inter-subject comparability. Clinical Biomechanics. 21: 204 – 212.

Stanton, T. R., and Kawchuk, G. N., (2009). Reliability of assisted indentation in measuring lumbar spinal stiffness. Manual Therapy. 14: 197 – 205.

Stewart, T., et al., (2009). Strong and light plaster casts? Injury-International Journal of The Care of The Injured. 40: 890 - 893.

Stinson, M. D., et al. (2003). Seat-interface pressure: a pilot study of the relationship to gender, body mass index, and seating position. Archives of Physical Medicine and Rehabilitation 84(3): 405-409.

Stump, R. L. et al., (2002). Managing seller-buyer new product development relationships for customized products: a contingency model based on transaction cost analysis and empirical test. The Journal of Product Innovation Management. 19:439-454.

Sun, et al., (2000). Comparison of implicit and explicit finite element methods for dynamic problems. Journal of Materials Processing Technology. 105: 110 – 118.

Sun, E. Q., (2006). Shear Locking and Hourglassing in MSC Nastran, ABAQUS, and ANSYS. MSCSoftware North American Virtual Product Development Conference. California, United States of America 16-19 July 2006. (Online) Available at: http://www.mscsoftware.com/events/vpd2006/na/presentations/tech_papers/27.pdf (Accessed on 05 July 2009).

Swain, B. P., (2002). Saddle tree. United States of America, Mondial Ind. Ltd. U.S. Patent 6363698: 1-7.

Synder-Smith, D., and Bauer, D., (2006). The Classic Western Rider. John Wiley and Sons.

Tabiei, A., and Wu, J., (2000). Three-dimensional nonlinear orthotropic finite element material model for wood. Composite Structures. 50: 143-149.

Tam, E. W., et al., (2003). Pelvic movement and interface pressure distribution during manual wheelchair propulsion. Archives of Physical Medicine and Rehabilitation. 84:1466-1472

Tao, J., and Jiyong, K., (2007). A 3-D point sets registration method in reverse engineering. Computers and Industrial Engineering. 53: 270-276.

Thacker, J. G., et al., (1998). Experiences during development of a dynamic crash response automobile model. Finite Elements in Analysis and Design. 30: 279-295.

Thakker, A., et al., (2008). A novel approach to materials selection strategy case study: Wave energy extraction impulse turbine blade. Materials and Design.

29: 1973-1980.

Theofanous, M., et al., (2009). Flexural behaviour of stainless steel oval hollow sections. Thin-Walled Structures. 47: 776-787.

Tiberkak, R. et al., (2008). Damage prediction in composite plates subjected to low velocity impact. Composite Structures. 83: 73-82.

Townsend, H. G. G, et al., (1983). Kinematics of the equine thoracolumbar spine. Equine Veterinary Journal. 15(2): 117-122.

Tsai, Y-J., and Powers, C. M., (2009). Increased shoe sole hardness results in compensatory changes in the utilized coefficient of friction during walking. Gait & Posture. 30: 303-306.

Tu, C. Y., and Chao, C. C., (1999). Three-dimensional contact dynamics of laminated plates: Part 2. Oblique impact with friction. Composites: Part B. 30: 23-41.

Ubeyli, M., et al., (2007). On the comparison of the ballistic performance of steel and laminated composite armours. Materials and Design. 28: 1257-1262.

U. S. Department of Defense (DoD), Technomic, (1999). Composite Materials Handbook - Mil 17, Volume 2: Polymer Matrix Composites: Materials Properties. CRC Press.

U. S. Department of Transportation, Federal Highway Administration (2007). Manual for LS-DYNA: Wood Material Model 143 (FHWA-HRT-04-097). (Online) Available at: http://www.tfhrc.gov/safety/pubs/04097/04097.pdf (Accessed 18 April 2009).

Van der Putten, E. P., and Snijders, C. J., (2001). Shoe design for prevention of injuries in sport climbing. Applied Ergonomics. 32: 379-387.

Van Kesteren, I. E. H. (2008). Product designers' information needs in materials selection. Materials and Design. 29: 133-145.

Van Weeren, P. R., (2009). Kinematics of the equine back. In Henson F. M. D., ed. Equine Back Pathology: Diagnosis and Treatment. Wiley-Blackwell. Pp. 39-60.

Varady, T., et al., (1997). Reverse engineering of geometric models—an introduction. Computer Aided Design. 29(4): 255-268.

Varvani-Farahani, A., et al., (2007). An energy-based fatigue damage parameter for off-axis unidirectional FRP composites. Composite Structures. 79: 381-389.

Veryzer, R. W., (1998). Discontinuous innovation and the new product development process. J PROD INNOV MANAG. 15: 304-321.

Viceconti, M., et al. (2006). Primary stability of an anatomical cementless hip stem: A statistical analysis. Journal of biomechanics. 39: 1169 – 1179.

Von Peinen K., et al., (2009). Relationship between the forces acting on the horse's back and the movements of the rider and horse while walking on a treadmill. Equine Veterinary Journal. 41(3): 285-291.

Walker, R. D., 1995. Patents as scientific and technical literature. Metuchen, NJ, & London: The Scarecrow Press, Inc.

Wallden, M., (2010). Shifting paradigms. Journal of Bodywork & Movement Therapies. 14: 185-194.

Walther, M., et al., (2008). Children sport shoes – A systematic review of current literature. Foot and Ankle Surgery. 14: 180-189.

Wang, Y., et al., (2006). Modeling and simulation for a drop-impact analysis of multi-layered printed circuit boards. Microelectronics Reliability. 46: 558-573.

Wang, Y. Y., et al., (2005). Simulation of drop/impact reliability for electronic devices. Finite Elements in Analysis and Design. 41: 667-680.

Waterer, J. W., (1975). A history of saddles in Europe, The Museum of Leathercraft.

Weaver, M. P., and Jeffcott, L. B., (2003). Orthopaedics 4. The vertebral column. In Mair, T., et al., ed. Equine Medicine, Surgery and Reproduction, 2003, Saunders, Elsevier Science Limited, pp. 387-397.

White., R. E., and Lightfoot, R. O., (1975). Saddle trees and saddles. United States of America, White Polytechniques Ltd. U.S. Patent 3888070: 1-6.

White, R. E., and Lightfoot, R. O., (1976). Improvements relating to saddle trees and to saddles. United Kingdom, White Polytechniques Ltd. GB Patent 1439761: 1-7.

Wijesinghe, K. R. C., et al., (2005). Towards object-oriented finite element pre-processors exploiting modern computer technology. Journal of Materials Processing Technology. 161: 247 – 252.

Wilcox, R. K., (2006). (i) An introduction to basic mechanics. Current Orthopaedics. 20 (1): 1-8.

Williams, B., (2000). What all engineers need to know before using finite element analysis. ALGOR Centre for Mechanical Simulation Technology Finite Element Analysis, Simulation and Design Optimization. (Online) Available at: http://www.algor.com/news_pub/tech_reports/2000/need2know/Need2Know.asp (Accessed 02 June 2009).

Wilson, D. C., et al., (2006). Accuracy and repeatability of a new method for measuring facet loads in the lumbar spine. Journal of Biomechanics. 39: 348-353.

Witte, K., et al., (2009). Motion pattern analysis of gait in horseback riding by means of Principal Component Analysis. Human Movement Science. 28: 394-405.

Wolf, S., et al., (2008). Foot motion in children shoes – A comparison of barefoot walking with shod walking in conventional and flexible shoes. Gait & Posture. 27: 51-59.

Wood, B., and Newbold, R., (2004). The character of East Midlands equestrianism in the 21st century. A survey of the equestrian sector in the East Midlands with and assessment of wider linkages and recommendations on future policy. East Midlands Equestrianism. (Online) Available at: http://www.lboro.ac.uk/departments/mm/research/equestrian/eastmidlandsequestrianismorg/ (Accessed 16 July 2010).

Wozniak, A., and Dobosz, M., (2003). Metrological feasibilities of CMM touch trigger probes. Part I: 3D theoretical model of probe pretravel. Measurment. 34: 273-286.

Wright, C. E., and Leckie, J., (1906). Improvements connected with saddle trees. United Kingdom, Wright Charles Edward and Leckie John. GB Patent 190604345: 1-4.

Wright, C. E., and Wedge, D., (1922). Improvements in and connected with gig saddle trees. United Kingdom, Charles Edward Wright and Daniel Wedge. GB Patent 184042: 1-6.

Wu, X., et al., (1999). Distribution of human-seat interface pressure on a soft automotive seat under vertical vibration. International Journal of Industrial Ergonomics. 24: 545-557.

Xu, B. H., et al., (2009). Numersical 3D finite element modelling and experimental tests for dowel-type timber joints. Construction and Building Materials. 23: 3043 – 3052.

Yague, J-A., et al., (2009). A new out-of-machine calibration technique for passive contact analog probes. Measurement. 42: 346-357.

Yan, J., and Strenkowski, J. S., (2006). A finite element analysis of orthogonal rubber cutting. Journal of Materials Processing Technology. 174: 102 – 108.

Yang, D. W., et al., (1995). Comparative investigation into implicit, explicit, and iterative implicit/explicit schemes for the simulation of sheet-metal forming processes. Journal of Materials Processing Technology. 50: 39 – 53.

Yang, J., et al., (1997). Stiffness of trabecular bone of the tibial plateau in patients with rheumatoid arthritis of the knee. The Journal of Arthroplasty. 12 (7): 798 – 803.

Yang, J., and Han, S., (2006). Repairing CAD model errors based on the design history. Computer-Aided Design. 38: 627-640.

Yang, Q., and Reidsema, C., (2008). Integrated Design System: An Information Processing Approach for Knowledge-Based Product Development. In Gunasekaran, A., ed. Techniques and Tools for the Design and Implementation of Enterprise Information Systems, 2008, Idea Group Inc (IGI), pp. 86-121.

Yau, H-T., and Menq, C-H., (1995). Automated CMM path planning for dimensional inspection of dies and molds having complex surfaces. Int. J. Mach. Tools Manufact. 35 (6): 861-876.

Yau, H-T., (1997). Reverse engineering of engine intake ports by digitization and surface approximation. Int. J. Mach. Tools Manufact. 37(6): 855-871.

Ye, X., et al., (2008). Reverse innovative design – an integrated product design methodology. Computer-Aided Design. 40: 812-827.

Yonezu, et al., (2009). Indentation induced lateral crack in ceramics with surface Hardening. Materials Science and Engineering A. 507: 226-235.

Yoshihara, H., (2005). Mode II initiation fracture toughness analysis for wood obtained by 3-ENF test. Composites Science and Technology. 65: 2198-2207.

Yoshihara, H., et al., (1995). Relationship between the Strength and Grain Orientation of Wood – Examination and modification of the Hankinson's formula. Bull. Tokyo Univ. For. 93: 1-5.

Zhang, X., et al., (2010). Stress and failure analysis of laminated composites based on layerwise B-spline finite strip method. Composites Structures. 92: 3020-3030.

Zhang, Y., (2003). Research into the engineering application of reverse engineering technology. Journal of Materials Processing Technology. 139: 472-475.

Zi, G., et al., (2008). The static behaviour of a modular foam-filled GFRP bridge deck with a strong web-flange joint. Composite Structures. 85: 155-163.

APPENDIX A

SWOT

Strengths	Weaknesses
• Known brands • Market segments • Sales and distribution chains • Marketing channels • Small business enterprises	• Family businesses with little or no professional managers • Limited access to finance • Resistance to change • Obsolete methods • Paucity of new products
Opportunities	**Threats**
• Research capacity and interest of locally based HEI • Government grants and support for SMEs • Collaborative alliances	• Dwindling exports • Increased imports • Declining employment trend

THREATS

Global exports from the United Kingdom

Table A1.1 Saddlery & harness global exports from the United Kingdom

Year	Exports (£ million)
1999	27.29
2000	26.06
2001	27.12
2002	26.76
2003	24.82
2004	24.26

Values in millions of £

(Source of data: the UK Trade Info http://www.uktradeinfo.com/index.cfm)

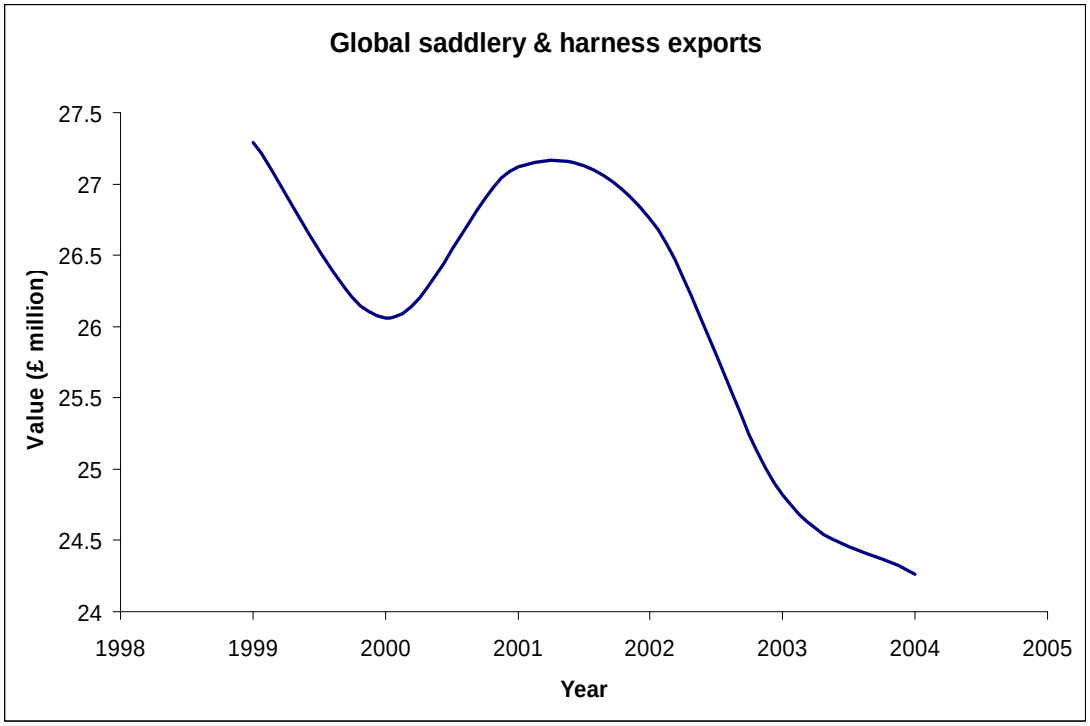

Figure A1.1 Saddlery & harness global exports from the United Kingdom

Exports to the United States of America

Table A1.2 Leather, saddlery & harness exports from 17 countries to the United States of America

	1996	1997	1998	1999	2000	2001	2002	2003	2004
Argentina	44.37	12.34	12.83	12.89	11.09	7.21	15.45	11.70	12.91
Australia	1.16	0.68	1.16	0.69	0.9	1.07	0.79	0.74	0.88
Brazil	7.05	1.90	2.72	2.27	2.25	2.19	1.90	2.77	3.32
Canada	8.71	12.17	13.31	12.25	15.43	17.41	15.48	15.70	16.70
China	31.21	31.43	36.68	45.85	61.41	76.62	92.75	140.31	180.12
Germany	12.54	13.45	15.10	15.41	15.24	18.19	21.01	25.88	26.19
France	4.30	3.96	3.93	4.90	7.29	8.07	8.13	9.27	11.61
Hong Kong	2.07	1.47	1.08	2.03	3.35	3.23	4.18	3.81	2.99
India	12.17	13.54	13.29	15.29	22.06	23.96	30.42	33.16	37.96
Italy	6.97	7.67	9.35	8.64	9.30	17.93	13.98	16.43	11.16
Japan	2.40	1.98	1.54	1.34	1.28	0.99	0.68	0.77	0.68
Korea	2.20	1.80	2.27	2.94	3.33	3.88	3.21	1.58	1.46
Mexico	43.27	38.62	32.17	35.53	39.76	30.40	35.78	30.17	28.11
Switzerland	2.22	1.89	2.61	2.85	2.76	2.30	2.36	3.04	3.18
Taiwan	19.64	20.49	16.22	19.09	20.64	20.17	20.82	24.60	23.63
Thailand	10.93	5.94	2.87	3.13	5.17	4.42	5.49	7.99	9.13
United Kingdom	14.77	15.70	15.92	16.76	15.82	13.01	11.98	13.64	13.51
% of total exports to US	90.45%	89.36%	89.71%	91.55%	92.95%	93.46%	92.98%	92.72%	93.83%

Values in millions of US dollars.
(Source of data: the U.S. International Trade Statistics hosted by the U.S. Census Bureau http://censtats.census.gov/sitc/sitc.shtml)

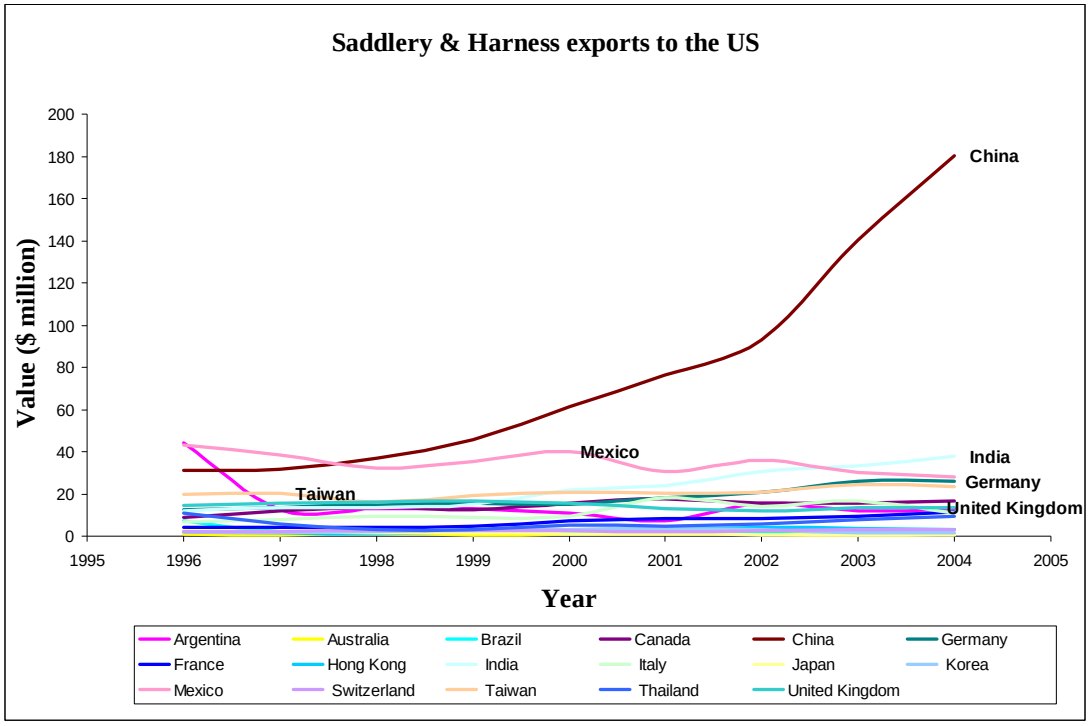

Figure A1.2 Leather, saddlery & harness from 17 countries to the United States of America

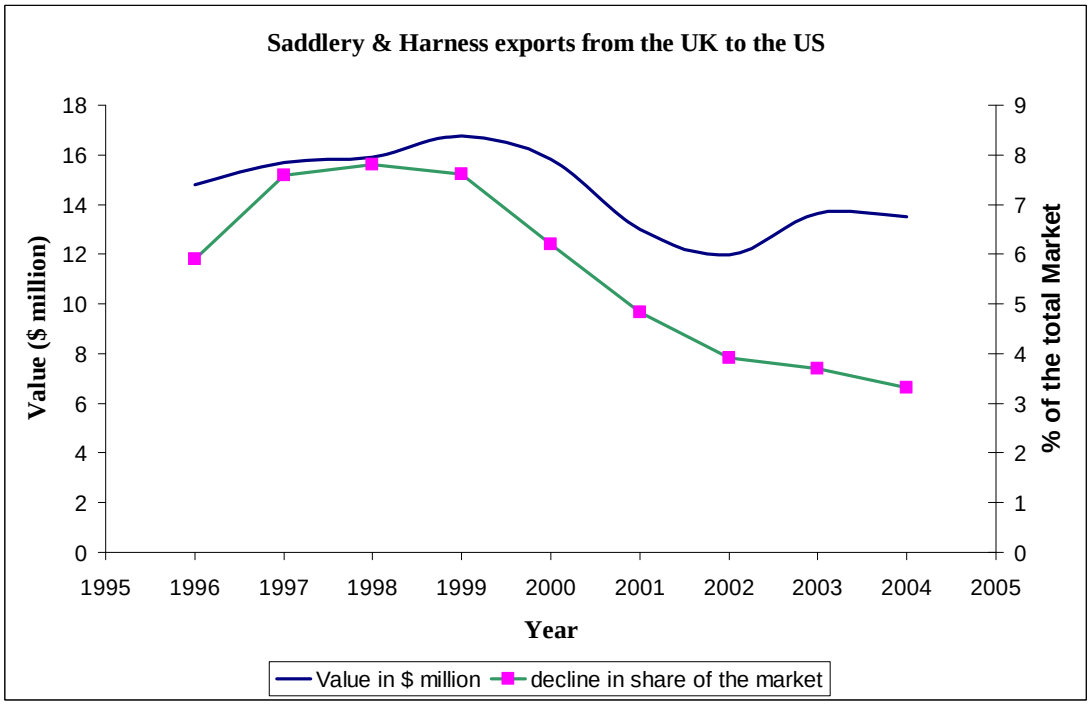

Figure A1.3 The values and market share of UK leather, saddlery & harness to the United States of America

Global imports into the United Kingdom

Table A1.3 Saddlery & harness global imports into the United Kingdom

Year	Imports (£ million)
1999	15.52
2000	19.22
2001	21.55
2002	24.55
2003	25.97
2004	30.24

Values in millions of £

(Source of data: the UK Trade Info http://www.uktradeinfo.com/index.cfm)

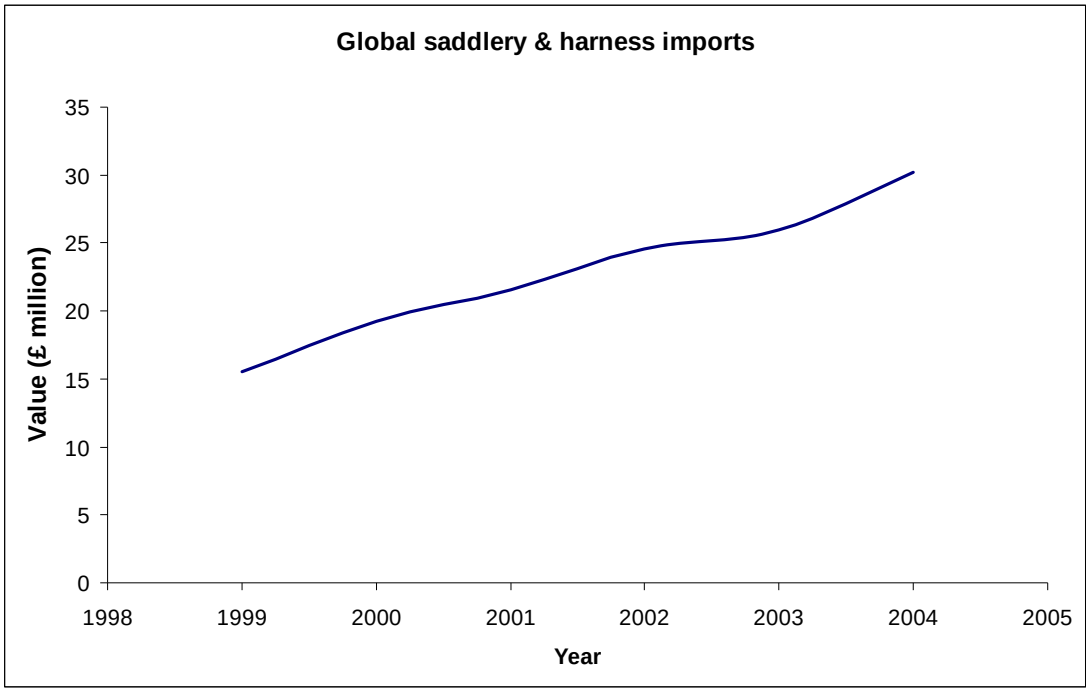

Figure A1.4 Saddlery & harness global imports into the United Kingdom

Employment trend

Table A1.4 Walsall employment figures – leather products industry

Year	Walsall Employment no
1993	1674
1995	1454
1996	1492
1997	1519
1998	1389
1999	1320
2000	954
2001	1139
2002	818
2003	782

(Source of data: office of National Statistics)

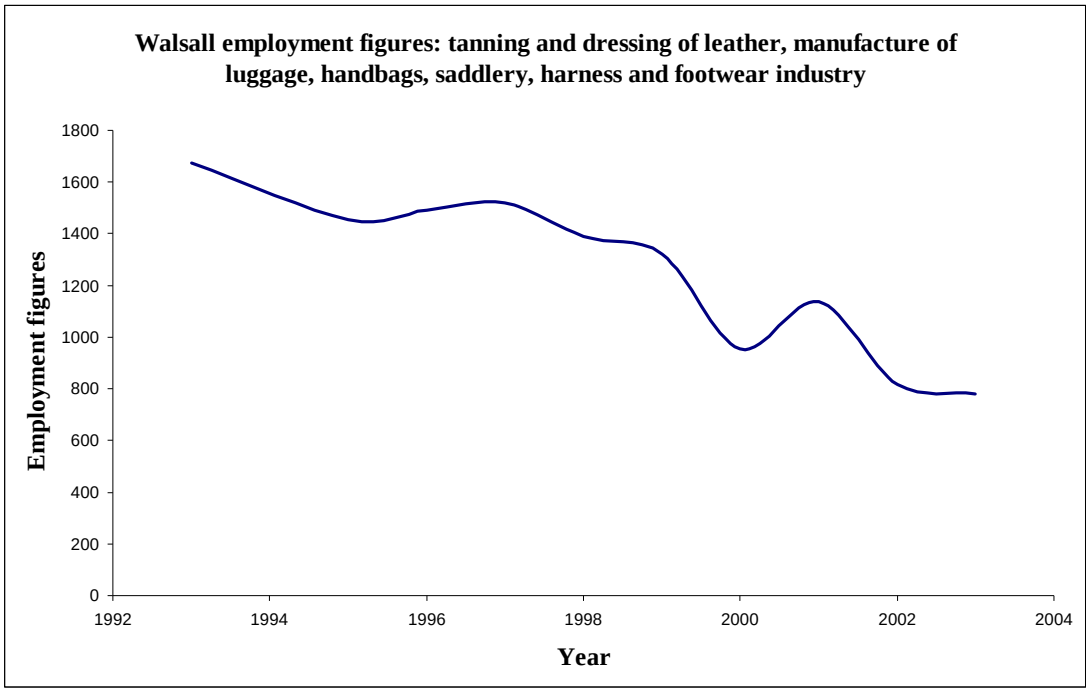

Figure A1.5 Employment figures in the leather, saddlery & harness, and footwear industry based in Walsall.

REFERENCES

HM Revenue & Customs (n. d). UK World Trade SITC. UK Trade Info. Available at: http://www.uktradeinfo.com/index.cfm. (Accessed 12 May 2005).

U.S. Census Bureau. U.S. International Trade Statistics. Available at: http://censtats.census.gov/sitc/sitc.shtml (Accessed 27 June 2005).